NEW MEXICO INSTITUTE OF MINING AND TECHNOLOGY

THE KINETICS OF MINERAL DISSOLUTION IN AQUIFERS AND THEIR USE FOR HYDROLOGIC INVESTIGATIONS

by

Abraham Mercado

Submitted to the Faculty of the
New Mexico Institute of Mining & Technology
in partial fulfillment of the requirements
for the degree of Doctor of Philosophy in
Geoscience (Geochemistry)

October 1972

ACKNOWLEDGEMENTS

The present work was done at the Geoscience Department of the New Mexico Institute of Mining & Technology, Socorro, New Mexico, under the supervision of Dr. G. K. Billings, with Dr. G. W. Gross, Dr. W. Brutsaert, and Dr. R. Beane, acting as advisors.

This study was financed in large part by the Water Resources Research Institute of New Mexico, under contract No. WRRI-3109/140.

It is a pleasure to express my thanks to Dr. G. K. Billings, and members of my advisory committee, who devoted much of their precious time to criticize and revise this work; to the Graduate School of New Mexico Tech for the graduate assistantship; and to the Water Resources Research Institute of New Mexico, for their financial assistantship in carrying out this work.

This list would not be complete without the mention of: Dr. de Josselin de Jong, who was extremely demanding, yet friendly and helpful in guiding me through subtle mathematical principles; Dr. W. Back, Dr. B. B. Hanshaw, Dr. F. A. Kohout, Mr. E. Welder of the U.S. Geological Survey, and Mr. F. H. Henninghausen of the New Mexico State Engineer Office, for supplying most of the field data used in this dissertation; Dr. J. Bear, vice president of the Technion in Haifa, Dr. M. Wilkening, Dean of the NMT Graduate School, Dr. G. W. Gross, and Dr. D. Rabinowitz of the NMT Geoscience Department, for helping me all the way from Israel to New Mexico; Mr. R. W. Stallman of the U.S.G.S. in Denver, Colorado, and Mr. R. Schneidder of the Water Resources Research Institute in Washington, D. C., for their friendly encouragement and moral support,

offered at the very beginning of this study; Mr. John Sonderegger for his friendship, and the continuous challenging and inspiring criticism; Dr. Ralph McGehee, and Dr. Chester McKee for guiding me through the fascinating labyrinth of computer science; Mrs. Lynn L. Brandvold for lending her equipment, and giving me a free hand in carrying out my chemical analyses. Mr. Pui-San (Charlie), for his precise silicate analyses; Mrs. Helen Richardson for smoothing over administrative difficulties; Miss Rosie Trujillo and Miss Martha Cinelli who were extremely patient and efficient in typing this dissertation; Mr. Robert Wood, Mr. Michael Woolridge, and Mr. William E. Arnold, for preparing the drawings; Mrs. Jackie Trujillo and Mr. Charles Treseder who prepared the photocopies; and the staff of the Geoscience Department of the NMT for their friendly support and professional assistance during the various stages of this study.

It is not an easy task to transform a respectable hydrologist into an experimental hydrogeochemist. Insofar as this has been accomplished it is due to the combined efforts of my advisor Dr. G. K. Billings and the individuals mentioned above. To all of them I wish to express my sincere thanks.

All errors are exclusively mine.

Finally, I wish to express my deep gratitude to my wife, children and family for their moral support and understanding. Their gratification at the completion of this work, is my greatest reward.

ABSTRACT

In this dissertation, a kinetic model for the dissolution of multimineral assemblages in porous media is derived, with a special emphasis on the simultaneous dissolution of calcite, dolomite, and gypsum in carbonate aquifers. Observed supersaturation of groundwater samples, with respect to calcite and dolomite, is explained by kinetic competition among dissolving minerals. The validity of the kinetic model was verified by laboratory experiments involving the dissolution of calcite, gypsum, and calcite + gypsum.

The applicability of a computerized version of this model is demonstrated by the evaluation of hydrogeochemical data for the limestone aquifer of central Florida. The kinetic model is calibrated with the aid of available hydrologic age estimates and chemical data for part of the aquifer. Chemical-age estimates for the remaining part of the aquifer are obtained by using the calibrated concentration-time relationships of aqueous species. Available ^{14}C data in this aquifer are then compared and shown to deviate significantly from hydrologic estimates. This deviation is explained on the basis of dissolution-precipitation kinetics.

A general differential equation, describing the dissolution of minerals and the transport of their products in porous media, is derived and simplified. The numerical solution of the equation, which represents the hydrogeochemical model of a given aquifer, is based on the transformation of aquifer, space coordinates into time coordinates of "tracing-points" moving along groundwater streamlines, followed by an inverse

transformation which yields theoretical water quality maps. The applicability of the model for integrating hydrologic and geochemical data in aquifers is demonstrated for the limestone aquifer of Roswell, New Mexico.

TABLE OF CONTENTS

LIST OF FIGURES

Figures | Page

LIST OF TABLES

LIST OF SYMBOLS

A_s - surface area of mineral (cm^2)

a - chemical activity (-)

b - aquifer thickness (m, ft)

C - concentration (ppm), or molarity (moles per liter; abbreviated by m)

D - dispersion coefficient (cm^2/min; cm^2/yr); diffusion coefficient (cm^2/sec)

d - average grain size (mm, cm)

ΔG_r - free-energy change of reaction (calories per mole)

H - hydraulic potential (m, ft)

ΔH° - Standard enthalpy of formation (calories per mole)

I - ionic strength (M)

i - number of species; index number of a rectangular grid system, along x-axis

J - gradient of the hydraulic potential (-)

j - number of minerals in the dissolving system; index number of a rectangular grid system, along the y-axis

K, K_{eq} - equilibrium constant of reaction (-)

k - rate constant for chemically controlled reactions with constant reactants (M/min; M/yr)

$\tilde{k}$ - specific rate constant for a chemically-controlled reactions with constant reactants (m-cm/min)

k^* - rate constant for the $\beta(t)$ approximation (min^{-1})

$\tilde{k}^*$ - specific rate constant for the $\beta(t)$ approximation (cm/min)

k_d - rate constant for transport controlled reactions (M/min; M/yr)

k_1 - specific rate constant for the logarithmic rate law (M-cm)

k_p - specific rate constant for the parabolic rate law ($M\text{-cm/min}^{\frac{1}{2}}$)

M - moles per liter

m - molar concentration (M)

n - porosity (-)

p 0 index for products

P - pressure (Atm.; mm Hg)

pK - $-\log_{10}$ (K)

Q - discharge rate (cc/min)

$\bar{R}$ - harmonic mean radius of grains (mm, cm, m)

R - reaction rate (M/min; M/yr); the gas constant (=1.98719 cal/mole)

r - index for reactants

S° - standard entropy (cal/mole/ K)

S - distance along streamlines

t - time

T - temperature (°C, °K); transmissivity (gpd/ft; ft^2/day; m^2/day)

v - seepage velocity (m/yr; ft/yr)

V - volume

W - mineral weight (gram)

x,y,z - distance along Cartesian coordinates

α - fraction of dissolving mineral in porous medium (-)

β - reaction ratio (-)

γ - activity coefficient (M^{-1})

δ - transport distance (cm); the difference between the equivalent molar concentrations of non-participating cations and anions (M)

ε - time weighted average deviation between theoretical and measured values (ppm, pH)

ν - stoichiometric coefficients (-)

τ_1 - hydraulic residence-time (min)

τ_2 -chemical residence-time (min)

1. INTRODUCTION

The aim of the present work is to develop some quantitative relationships between hydrologic and geochemical processes in groundwater aquifers, and to develop the necessary tools for using groundwater quality data as tracers for hydrologic studies. The application of tracers in groundwater hydrology is discussed below.

1.1 Tracer Techniques in Groundwater Hydrology

The hydrologist's approach to groundwater utilization is described in terms of a few hydrological characteristics; namely the occurrence and origin of water, the physical properties of the aquifer and the fluid such as permeability, porosity, viscosity, the direction and velocity of water flow and the water dispersion and mixing pattern. Those characteristics are usually determined through a combination of detailed geological mapping, climatological surveys, measurements of water levels, and pumping tests. The growing need for and continuing emphasis on the development of groundwater resources, often within a rather limited time schedule, has stimulated the development of several time saving techniques in groundwater investigations; some are based on the application of tracers.

In essence, the concept of a tracer to follow the movement of groundwater is very simple and straightforward. Methods, using dyes and salts, have been applied for many years even back to Roman times.

The breakthrough in nuclear technology for peaceful use in the middle 50's, provided the possibility of using radioactive substances as tracers (Feely, 1961). Since that time a prolific expansion of these methods and a refinement of analytical tools took place. A treatise on

the development of some tracer methods between 1960 and 1965 is given by Nir (1965). The place of the various tracer methods in hydrologic investigation programs is discussed by Harpaz et al. (1963), and by Gat, et al. (1971).

Most tracer methods are based on the rather severe and limiting assumption that there is no chemical or physical interaction between the tracer solution and the aquifer. The performance of tracers is usually judged by their ability to follow as exactly as possible the flow pattern of the water molecules themselves. For this reason, tritium, deuterium, and ^{18}O are supposed to be very close to the "ideal tracer" definition, while ^{90}Sr, for example, being strongly absorbed in most natural porous media, is judged a relatively poor tracer. In cases where the "ideal tracer" assumption is not justified, which is for example the case with ^{14}C dating, elaborate techniques are applied for determining appropriate correction factors (Pearson, 1965; Pearson and Hanshaw, 1970; Wendt, et al. 1966).

1.2 Geochemical Tracers

More than 60 constituents and properties (Hem, 1970) are included in some water analyses though only about 10 are frequently measured and reported - the six major ions (Ca^{++}, Mg^{++}, Na^{+}, Cl^{-}, HCO_3^{-}, and $SO_4^{=}$), electrical conductivity, pH, TDS (total dissolved solids), and temperature. These properties are sufficient for studying the volumetrically-major geochemical processes in most carbonate aquifers. The use of these data is rather limited, at least as far as the study of the dynamic behavior of groundwater systems is concerned.

Natural waters acquire their chemical characteristics through chemical reactions with solids, liquids and gases with which they have come into contact during the various stages of the hydrologic cycle. While the reactions with liquids and gases can be regarded as almost instantaneous on the hydrologic time scale, the dissolution process of most minerals can be shown to be a distinct function of time. It is expected, therefore, that certain quantitative relationships may be obtained between the concentration of the various aqueous species and the residence time of the groundwater in the aquifer. These relationships should be rather similar in essence, to those used by tritium and ^{14}C dating methods.

If the groundwater solution remains stagnant, such that no flow exists in the aquifer, equilibrium among the minerals and the aqueous species will be attained after some time and no concentration-distance gradient would be observed from water quality maps. On the other hand, under flow conditions, the concentration-distance gradient will be some function of flow velocity, the distance from the recharge boundaries of the aquifer where the concentration of the various species will be at a minimum, and the kinetics of reactions between the water mass and minerals of the aquifer.

The idea of using the concentration-time curve of dissolved aqueous species, as a dating technique, contradicts entirely the concept of the "ideal tracer" mentioned above. Instead of using a tracer which is free from interactions with the solid matrix of the aquifer, the consequences of such interactions are proposed here to be used as a dating method.

The idea that the kinetic relationships between the hydrologic and geochemical systems can be used for both geochemical and hydrologic studies is not entirely new. It has been emphasized by several investigators (Schoeller, 1962; Hem, 1970; Helgeson, 1970; Back and Hanshaw, 1971; Deju, et al., 1969; Deju, 1971) that the kinetics of mineral weathering in aquifers and the flow pattern in them are highly interrelated. The basic assumption of this work is that the study of the dissolution processes in aquifers, based on appropriate interpretation of the natural variations in the chemical composition of their water, may provide valuable information on the characteristics of the groundwater flow.

1.3 Equilibrium and Kinetic Models

The conventional approach to understanding the chemistry of natural environments, is based on the comparison of the composition of natural waters with the equilibrium composition of model systems. Pioneer work in this direction was done by Garrels and Christ (1965), Helgeson (1968), and Helgeson, et al., (1969).

The equilibrium composition of these systems provides, however, very little insight into their actual chemical evolution as a function of time. Moreover, as far as the geochemical tracer techniques are concerned, they are useless when chemical equilibrium is reached. This is analogous, for example, to the "dead" radioactivity of ^{14}C after 30-50 thousand years of residence time in the aquifer.

Kinetic models can overcome this difficulty. During their evolution, groundwaters may be undersaturated with respect to some minerals with which they have been in contact, and supersaturated or equilibrated

with respect to other minerals. The chemical path, and the final composition of the equilibrated groundwater solution, will depend, therefore, upon the kinetic properties of each mineral reacting in the system. The study of the actual chemical path as a function of time may provide the analytical tools for examining the link between the geochemical and hydrologic systems.

Theoretical mass transfer models were developed by Helgeson and his co-workers (Helgeson, 1968; Helgeson et al., 1969; Helgeson et al., 1970), however the systems are described in terms of nondimensional reaction progress and the predicted reaction paths can not be related directly to time.

Plummer (1972) has analyzed several kinetic mechanisms for the dissolution of single-phase solids in aqueous solutions. Analytical expressions have been derived by Plummer for congruent dissolution reactions controlled by transport processes, chemical kinetics, and reactions controlled simultaneously by chemical and transport processes. Plummer did not consider the dissolution of multimineral assemblages in open water systems, which is the real situation in most groundwater aquifers, and which is the proper extension of his work.

Natural water systems are systems which are open to their surroundings. Such factors as influx of aqueous species, diffusion, and dispersion may alter completely the situation predicted on the basis of water system models (Morgan, 1967). The dissolution of minerals in open systems can be represented by simple superposition of the kinetic equations describing the dissolution in closed systems, with the mass-transfer equations describing the spread of an ideal tracer in open

systems; i.e.,

$$\frac{\partial C_i}{\partial t} = \text{div } (\underline{\underline{D}} \text{ grad } C_i) - \text{div } (\underline{v}\, C_i) + \sum_j F_{ij} \qquad (1.1)$$

where: C_i - the concentration of the i-th aqueous species.

t - the time.

$\underline{\underline{D}}$ - the dispersion tensor.

$\underline{v}$ - the velocity vector.

F_{ij} - the kinetic function for the dissolution of the i-th species, with respect to the j-th mineral.

Various kinetic functions (F) are derived and discussed in the following chapter. The mass transfer equation and the validity of the proposed superposition are discussed in Chapter 6.

1.4 Objectives and Scope of Study

Only limited work has been done toward the use of geochemical data for hydrologic investigations; moreover, very little is known about the actual kinetics of dissolution processes in aquifers. The ultimate objective of this study is the derivation of a model which integrates both hydrologic and geochemical properties of a groundwater system in order to reproduce water quality maps measured in the field. After calibration of the model with a controlled portion of the aquifer, water quality data of the remaining portion can be used to refine existing information concerning the flow pattern in the aquifer.

Investigations are carried out in the following sequence: (a) consideration of various kinetic models for dissolution of multimineral assemblages in aqueous solutions; (b) dissolution experiments for calcite,

gypsum and calcite + gypsum in aqueous solutions; (c) development and demonstration of a computer simulated hydrogeochemical model for studying field problems.

2. KINETIC MODELS FOR DISSOLUTION OF MINERALS IN CLOSED SYSTEMS

2.1 General Description of Kinetic Models

Five distinct processes may occur in reactions between liquids and solids (Plummer, 1972):

(a) Transport of reactants from the bulk solution to the mineral-solution interface.

(b) Adsorption of the reactants on the surface.

(c) Chemical reaction on the surface.

(d) Desorption of the products from the surface.

(e) Transport of the products from the interface into the bulk solution.

Processes (a) and (e) can be defined as transport-controlled, while the remaining are controlled by the chemical properties of the solid-liquid interface (including surface electrostatic effects). Any one of the processes listed above may be rate determining.

The distinction between transport and chemically controlled reactions allows their classification into three main groups according to the rate limiting step (Moelwyn-Hughes, 1947; Frank-Kamenitskii, 1955; Plummer, 1972):

(a) Transport-controlled reactions.

(b) Chemically-controlled reactions.

(c) Reactions controlled simultaneously by both processes.

These classes of heterogeneous reactions are described schematically in Figure 2.1.

The following discussion is limited to the transport-controlled

Figure 2.1 - Schematic description of heterogeneous reactions controlled by: transport processes (A), chemical kinetics (C), and both processes (B). C(t) is the concentration of the bulk solution as a function of time, $C_m(t)$ is the concentration at the liquid-solid interface as a function of time, and C_s is the concentration under equilibrium conditions, as $t \to \infty$. (From Plummer 1972).

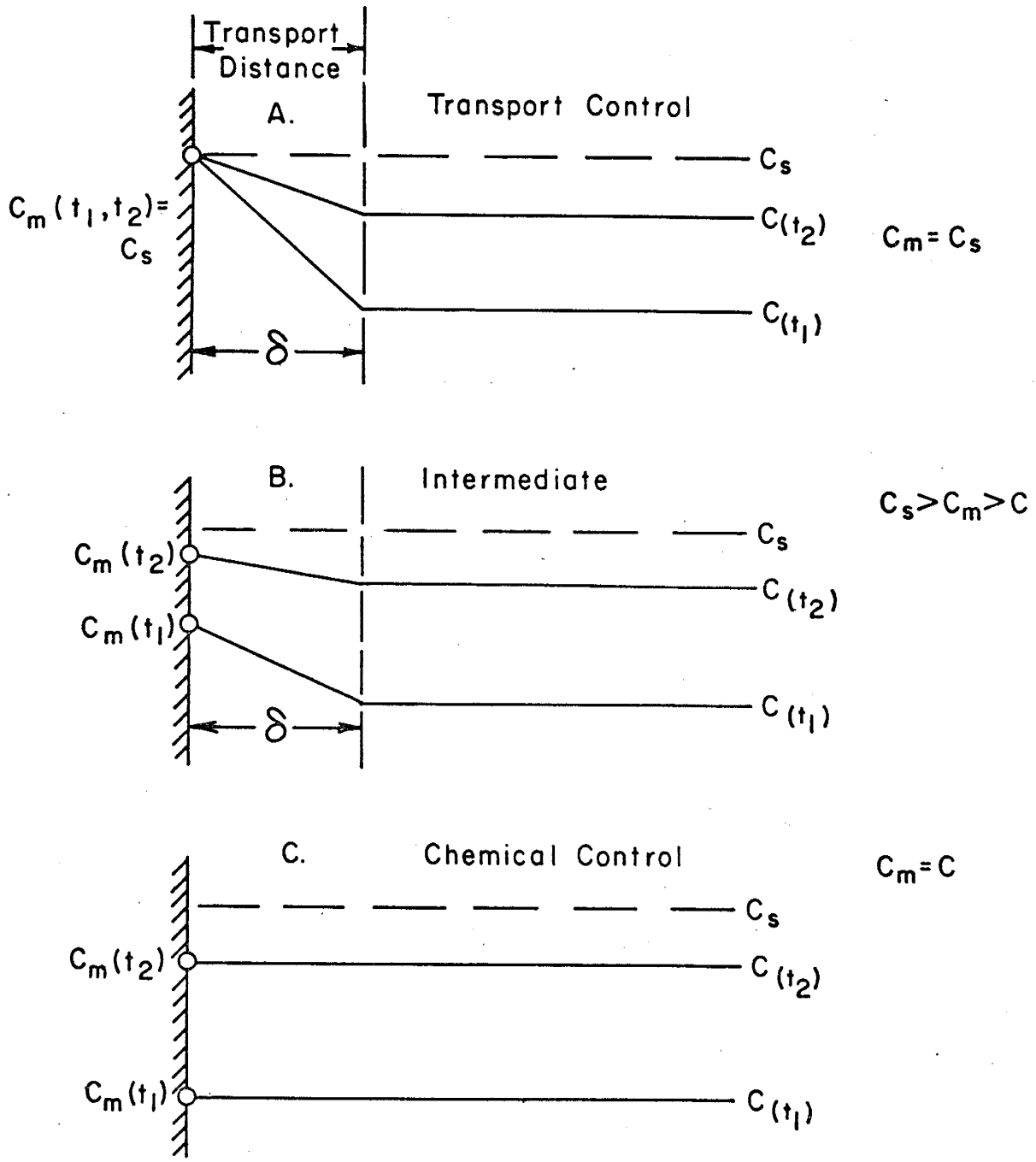
Transport Distance
A.
Transport Control
$C_m(t_1,t_2)=C_s$
C_s
$C_{(t_2)}$
$C_{(t_1)}$
δ
$C_m=C_s$
B.
Intermediate
$C_s>C_m>C$
$C_m(t_2)$
$C_m(t_1)$
C_s
$C_{(t_2)}$
$C_{(t_1)}$
δ
C.
Chemical Control
$C_m=C$
$C_m(t_2)$
$C_m(t_1)$
C_s
$C_{(t_2)}$
$C_{(t_1)}$

and chemically-controlled processes as they are the two extremes of possible reaction mechanisms (a and b above, respectively). Kinetic models will be studied first for single minerals. Results will be then extended to the general case of multimineral assemblages in closed systems.

2.2 Transport-Controlled Reactions

(a) Nernst Equation - Mineral dissolution reactions are frequently regarded as being transport-controlled (Weyl, 1958; Sung-Tsuen and Nancollas, 1971; Plummer, 1972). Transport-controlled processes are governed by first order differential equation with respect to reactant or product concentrations (Frank-Kamenitskii, 1955), such as the Nernst equation (Nernst, 1904), which is described briefly below.

Let the concentration of the bulk solution be C, and the concentration on the mineral surface, where the chemical reaction takes place, be designated as C_m (Fig. 2.1). Let the rate of the reaction at the surface be expressed by some function $f(C_m)$, which represents the actual chemical kinetics on the surface. The amount of reactants or products supplied and transformed from the surface is limited by the specific diffusion flux J across the transport distance - δ (Fig. 2.1) as determined by Fick's first law of diffusion:

$$J = -D \frac{dC}{dx} \qquad (2.1)$$

where D is the molecular diffusion coefficient, and x is the distance.

Following the basic assumptions made by Nernst (1904), when formulating his general theory for heterogeneous reactions, the diffusional flux J can be approximated by:

$$J \cong \frac{D}{\delta} (C_s - C) \qquad (2.2)$$

where C_s is the concentration at saturation.

Because a mineral can dissolve no faster than reactants and products can be supplied or removed from the mineral surface equation (2.2) can be used to determine the upper limit of the reaction rate. A mass-balance over a solution volume V in contact with a surface area A_s of the dissolving mineral gives:

$$V \frac{dC}{dt} = JA_s = \frac{DA_s}{\delta} (C_s - C)$$

or:

$$\frac{dC}{dt} = k_d (C_s - C) \qquad (2.3)$$

where k_d is the diffusional rate constant given by:

$$k_d = DA_s/\delta V \qquad (2.4)$$

The rate constant k_d is independent of the actual kinetic function $f(C_m)$, as it depends only upon the diffusion coefficient D, the transport length δ, and the geometric factor A_s/V.

The solution to equation (2.3), subject to the initial condition of C=0 at t=0, yields then:

$$C(t) = C_s(1-e^{-k_d t}) \qquad (2.5)$$

Arbitrarily selecting $C/C_s = 0.95$, to indicate a state of near equilibrium between the bulk solution and the dissolving mineral, the time required to attain this ratio will be an inverse function of the

rate constant k_d:

$$t_{(C/C_s = 0.95)} = 2.976/k_d \qquad (2.6)$$

The value of t predicted by equation (2.6) is constant for any dissolution reaction provided that transport is the rate-limiting factor (i.e. k_d is a single constant).

It is interesting to estimate the order of magnitude of $(t)_{C/C_s = 0.95}$ for typical limestone aquifers predicted by transport theory. Computed values of the transport distance δ for a wide variety of substances dissolving under laboratory conditions are close to $\delta = 3 \times 10^{-3}$ cm (Plummer, 1972). The diffusion coefficient D is approximately 10^{-5} cm^2/sec, or about 1 cm^2/day for a variety of aqueous species (Garrels, et al., 1949).

The ratio A_s/V for a given porous medium can be estimated from the expression (Appendix A):

$$A_s/V \cong \frac{3}{\overline{R}} \left(\frac{1-n}{n}\right) \qquad (2.7)$$

where n is the porosity, and $\overline{R}$ is the harmonic mean radius of the grains. Considering the case of a fissured limestone, a gross porosity of about 3% (Halevy and Nir, 1962) may serve as a representative value. Estimating the mean "grain" size of a limestone aquifer is rather difficult; the range of R=1 cm to 1000 cm will probably cover all the possibilities. The computed value of A_s/V will vary then between 100 and 0.1 cm^{-1} for radii of 1 and 1000 cm respectively. Using equation (2.4) with the parameters estimated above, the computed value of k_d will be within the limits of 0.33×10^2 to 0.33×10^5 day^{-1}, and $(t)_{C/C_s = 0.95}$, as computed from

equation (2.6) will be 10^{-4} to 10^{-1} days. The maximum value of $(t)_{C/C_s} = 0.95$ corresponds to the rather exaggerated equivalent radius of 1000 cm. More refined calculations, made by Weyl (1958) and Plummer (1972) yield values of the same order of magnitude.

Limited field data indicate that no dissolution process in groundwater aquifers occurs as fast as predicted above. Based on data for the limestone aquifer of central Florida (Hanshaw, et al., 1965, Back and Hanshaw, 1971) calcite equilibrium is attained after 4000 years (based on ^{14}C dating), while dolomite equilibrium is attained after more than 15,000 years.

This gap between field data and the values predicted above, as well as the fact that different minerals even with the same geometric factors do not dissolve at the same rate, leads to the conclusion that dissolution of minerals in aquifers is not controlled by transport processes.

This conclusion may be complicated, however, by coating of the mineral surface with low-porosity product layers. Such layers are produced, for example, during the incongruent dissolution of some silicate minerals (Helgeson, 1971). The effect of such coating will be two-fold: increase of the transport distance δ and a decrease of the molecular diffusion coefficient D. The overall effect may decrease the ratio D/δ by several orders of magnitude, increasing proportionately $(t)_{C/C_s} = 0.95$.

Nevertheless, computed k_d values, computed from laboratory dissolution experiments with calcite and gypsum (Ch. 4), were lower by 3 and 5 orders of magnitude, respectively, than predicted by transport theory. This gap can not be explained by coating, or other proposed field-effects,

so, transport-controlled kinetics as a rate-equation to explain field and experimental data is therefore rejected.

(b) The kt^{ω} Expression - According to Helgeson (1971) dissolution reaction reactions follow the general relation:

$$\frac{dC_i}{dt} = k_i t^{\omega} \tag{2.8}$$

where C_i is the molarity of the i-th dissolving species, k_i the rate constant, t the time, and the exponent ω depends on the kinetic characteristics of the reaction. The term ω may take the value of -1, -1/2, or 0, which yields logarithmic, parabolic or linear functions respectively. It should be mentioned here that the value of k_i, in both logarithmic and parabolic laws, depends strongly on the initial conditions; i.e. C_i at t=0. The value of k_i is defined for a constant volume and surface area of the dissolving mineral.

The parabolic rate law was justified theoretically for the case of incongruent reactions (Helgeson, 1971), where the reaction rate is controlled by slow diffusion transport through a growing low-porosity product layer on the mineral surface.

Considering first the parabolic law:

$$\frac{dC_i}{dt} = k_p / t^{1/2} \tag{2.9}$$

and solving for the initial conditions of $C_i=0$ at $t=t_o$, we get the parabolic concentration-time curve:

$$C_i(t) = 2k_p\left(t^{1/2} - t_o^{1/2}\right) \tag{2.10}$$

Similarily for the logarithmic rate law:

$$C_i(t) = k_1 \ln\left(\frac{t}{t_o}\right) \tag{2.11}$$

The basis for selecting these particular rate laws is not thermodynamic but empirical. Both parabolic and logarithmic rate laws predict that the net rate of reaction will decrease with time; however, $C_i(t) \rightarrow \infty$ as $t \rightarrow \infty$ which is unrealistic for the congruent reactions considered in this dissertation; hence they are deleted here from further field and laboratory applications. One could propose limiting the expression at equilibrium by stating $C_i(t) \rightarrow$ a constant as $t \rightarrow t_{equilibrium}$. Treating the experimental data, discussed later, with the parabolic law lead to more error than the kinetic law finally selected. This was an additional reason for deletion.

2.3 Chemically Controlled Reactions

The general mathematical treatment of chemically controlled reactions can be exceedingly complicated. The stoichiometric equation for a given reaction represents only the final relationship between reactants and products, while frequently the reaction may take a devious route, as governed by the principle of minimum expenditure of energy (Walas, 1959). Nevertheless, the principle is maintained that the stoichiometric chemical equations are close approximation for some reversible elementary reactions, therefore, the Law of Mass-Action, can be applied to describe the kinetics of the reaction (Gardiner, 1969). The dissolution of some abundant minerals, such as calcite and gypsum obey the kinetic interpretation of the Law of Mass-Action, as discussed below.

(a) The Kinetics of Mineral Dissolution Based on the Law of Mass-Action - The Law of Mass-Action, derived originally by Guldberg and Waage between 1864 and 1867, is a powerful tool for determining the equilibrium concentration of chemical species. The Law of Mass-Action states that: "the rate of chemical reaction is proportional to the active masses of participants" (Gardiner, 1969, page 22). Mathematically, the forward dissolution rate R_f is given by:

$$R_f = k_f \prod_r (a_r)^{-\nu_r} \tag{2.12}$$

and the backward precipitation rate R_b by:

$$R_b = k_b \prod_p (a_p)^{\nu_p} \tag{2.13}$$

where a_p and a_r are the chemical activities of the product and reactant species respectively, and ν_p or ν_r their respective stoichiometric reaction coefficients; k_f and k_b are the forward and backward rate constants per unit volume and unit surface area of the dissolving mineral.

Molar concentrations C_i are related to chemical activities a_i by:

$$C_i = a_i/\gamma_i \tag{2.14}$$

where γ_i is the activity coefficient of the i-th species, determined in dilute solutions with the aid of the Debye-Hückel equation (See Ch. 3).

Under equilibrium conditions $R_f = R_b$ such that:

$$k_f \prod_r (a_r)_{eq}^{-\nu_r} = k_b \prod_p (a_p)_{eq}^{\nu_p} \tag{2.15}$$

which yields:

$$[\Pi_p(a_p)^{\nu_p}/\Pi_r(a_r)^{-\nu_r}] = k_f/k_b = K_{eq}(T,P) \tag{2.15}$$

or:

$$[\Pi_i(a_i)^{\nu_i}]_{eq} = k_f/k_b = K_{eq}(T,P) \tag{2.16}$$

a_i represents now the activities of both reactants and products, and ν_i their respective stoichiometric coefficients; ν_i is negative for reactants, and positive for products by convention. $K_{eq}(T,P)$ is the temperature and pressure dependent equilibrium constant, equivalent to the ratio k_f/k_b. The validity of this identity was verified experimentally on numerous occasions (Moelwyn-Hughes, 1947, p. 163; Denbigh, 1955, p. 440). The fact that reaction rates have been successfully predicted by the collision theory for ideal gases and solutions, as well as the similarity between Arrhenius and van't Hoff (revised form) equations (Moelwyn-Hughes, 1947), is additional support for the kinetic interpretation of the Law of Mass-Action.

The net dissolution rate R_{net} is determined by the difference between the forward and backward rates:

$$R_{net} = R_f - R_b \tag{2.17}$$

The rate of increase and decrease of the product and reactant concentrations, respectively, is related to the reaction rate by (Gardiner, 1969):

$$\frac{1}{\nu_r}\frac{dC_r}{dt} - \frac{1}{\nu_p}\frac{dC_p}{dt} = R_{net} \tag{2.18}$$

where C_p and C_r are the concentrations of product and reactant species respectively. Notice that the stoichiometric reaction coefficients of reactants are negative.

From equations (2.12), (2.13), (2.16), (2.17), and (2.18):

$$\frac{1}{\nu_i}\frac{dC_i}{dt} = k_f \prod_r (a_r)^{-\nu_r} \left(1 - \frac{\prod_i (a_i)^{\nu_i}}{K_{eq}}\right) \tag{2.19}$$

or:

$$\frac{1}{\nu_i}\frac{dC_i}{dt} = k_f \prod_r (a_r)^{-\nu_r} [1 - \beta(t)] \tag{2.20}$$

where $\beta(t)$ is denoted as the reaction ratio at time t, defined by:

$$\beta(t) = \frac{1}{K_{eq}} \prod_t [a_i(t)]^{\nu_i} \tag{2.21}$$

As $t \to \infty$:

$$\lim_{t\to\infty} \beta = \lim_{t\to\infty} \frac{1}{K_{eq}} \prod_i (a_i)^{\nu_i} = \frac{1}{K_{eq}} \left[\prod_i (a_i)^{\nu_i}\right]_{eq} = 1 \tag{2.22}$$

For the special case in which the only reactant species are solids (for example, the dissolution of gypsum), the activity product of reactants equals unity, such that:

$$R_f = k_f \tag{2.23}$$

Similarily, when reactant aqueous species remain constant, or nearly so, during the reaction (for example, the dissolution of calcite in a buffered acid solution), the activity product of reactants is constant, such that:

$$R_f = k_f[\prod_r (a_r)^{-\nu_r}]_{const} = \tilde{k}' \tag{2.24}$$

In both cases equation (2.20) is simplified by:

$$\frac{1}{\nu_i}\frac{dC_i}{dt} = \tilde{k}[1 - \beta(t)] \tag{2.25}$$

where i now represents only product species.

The reaction rate in equation (2.25) is determined for unit volume and unit surface area. For a specific solution volume V, being in contact with a surface area A_s of the dissolving mineral, the mass balance of the dissolved species requires that:

$$V\left(\frac{1}{\nu_i}\frac{dC_i}{dt}\right) = \tilde{k}A_s[1 - \beta(t)]$$

which gives:

$$\frac{1}{\nu_i}\frac{dC_i}{dt} = k[1 - \beta(t)] \tag{2.26}$$

where the combined rate constant k is given by:

$$k = \tilde{k}A_s/V = \tilde{k}\left(\frac{3\alpha}{\overline{R}}\frac{1-n}{n}\right) \tag{2.27}$$

where n is the porosity, $\overline{R}$ is the harmonic mean grain radius, and α is the fraction of the dissolving mineral in the porous medium. The expression above, for the ratio A_s/V, is derived in Appendix A.

Equation (2.26) was selected as the primary rate equation for the interpretation of laboratory and field data, as discussed later. The variation of reactants (mainly hydrogen ion), observed during the study, was rather limited. This permitted the use of the product term approximation

above (Eq. 2.24). The fact that experimental dissolution curves (see later chapters) have been successfully reconstructed, supports the validity of the use of this approximation. A more general statement of the rate equation finally used is equation 2.20. It was not considered further because of time limitations.

Equation (2.20) or equation (2.26) represents a system of i (= number of species in the reaction) differential equations. These systems can can be solved numerically for any specified set of initial concentrations $(C_i)_o$, rate constant, temperature, pressure, and time intervals Δt, to obtain a discrete function $C_i(t)$.

(b) Thermodynamic Representation of the Rate Equation - The reaction rate equation derived above (Eq. 2.26) is actually a function of the Gibbs free energy of reaction (ΔG_r). At any stage of the reaction ΔG_r is determined from (for example, Krauskopf, 1967):

$$\Delta G_r(T,P) = -RT \ln K_{eq} + RT \ln [\Pi(a_i)^{\nu_i}] \qquad (2.28)$$

where R is the gas constant, and T the absolute temperature. Recalling the definition of β (Eq. 2.21), the equation above can be rewritten:

$$\Delta G_r(T,P) = RT \ln\beta \qquad (2.29)$$

Notice that ΔG_r is a negative quantity for $\beta < 1$. Equation (2.29) yields an expression for β as a function of free energy, temperature and pressure:

$$\beta = \exp(\Delta G_r/RT) \qquad (2.30)$$

and the approximate rate law (Eq. 2.26) can be rewritten in its thermo-

dynamic form by:

$$\frac{1}{\nu_i}\frac{dC_i}{dt} = k[1 - \exp(\Delta G_r/RT)] \tag{2.31}$$

For small values of $\Delta G_r/RT$, the exponential term in the equation above can be approximated by the first two terms of the Taylor's series expansion for e^x:

$$\exp(\Delta G/RT) \cong 1 + \Delta G/RT \tag{2.32}$$

Equation (2.31) is then approximated by:

$$\frac{1}{\nu_i}\frac{dC_i}{dt} \cong k(-\Delta G/RT) \tag{2.33}$$

(c) Approximate Solution for $\beta(t)$ - To this point, the variable of interest has been $C_i(t)$. One might also make use of the function $\beta(t)$. In order to consider $\beta(t)$ in following sections of the dissertation an approximate analytical solution, which can be used for rough estimates, is derived below. This approximation is also developed because the previous equations such as (Eq. 2.26):

$$\frac{dC_i}{dt} = k[1 - \beta(t)]$$

can only be solved numerically. It is desirable to have some tools for analytical approximation in addition to numerical solutions. Such analytical expressions may provide a deeper insight into the overall kinetic process.

The differentiation of $\beta(t)$, given by equation (2.21) with respect to t yields:

$$\frac{d\beta}{dt} = \frac{1}{K_{eq}} \sum_{j} \left[\prod_{\substack{i \\ i \neq j}} (a_i)^{\nu_i} \; \nu_j (a_i)^{\nu_j - 1} \; \frac{da_j}{dt} \right]$$

or:

$$\frac{d\beta}{dt} = \frac{1}{K_{eq}} \prod_{i} (a_i)^{\nu_i} \sum_{i} \frac{\nu_i}{[a_i]} \frac{da_i}{dt} \tag{2.34}$$

Substituting β and da_i/dt from equations (2.21) and (2.26) respectively, assuming that the solution is very dilute such that $\gamma_i \approx 1$, and rearranging the terms, we get:

$$\frac{d\beta}{dt} = k(1 - \beta)\beta \sum_{i} \left(\frac{\nu_i^2}{a_i} \right) \tag{2.35}$$

Equation (2.35) is a nonlinear equation with respect to β; its solution can be obtained only by numerical methods. The only way to solve this equation analytically is to assume that the variable product $\beta \sum_{i} \frac{\nu_i^2}{a_i}$ can be approximated by some mean value, to be determined later, such that:

$$k^* = k \left[\overline{\beta \sum_{i} \frac{\nu_i^2}{a_i}} \right] \tag{2.36}$$

The fact that this variable product approaches a constant for large t supports this assumption that the product term above can be approximated by a constant and (Eq. 2.35) is approximated by:

$$\frac{d\beta}{dt} \approx k^*(1 - \beta) \tag{2.37}$$

The solution of equation (2.37), with the initial conditions of $\beta = \beta_o$ at t=0, yields:

$$(1 - \beta)/(1 - \beta_o) = \exp\,[-k^*t] \tag{2.38}$$

which express the relative deviation from equilibrium as a function of time. The equation above is similar to the exponential law describing the decay of radioactive substances.

Substituting the approximate expression for $(1 - \beta)$ into equation (2.26) under the condition $\gamma = 1$, and solving for the initial conditions of $a_i = (a_i)_o$ at t=0, gives:

$$a_i(t) = a_i(o) + \nu_i \frac{k}{k^*} (1 - \beta_o)[1 - \exp(-k^*t)] \tag{2.39}$$

The value of k^* can be determined now from the condition that $a_i(\infty) \rightarrow (a_i)_{eq}$, which yields:

$$k^* = \nu_i k\ (1 - \beta_o)/[(a_i)_{eq} - (a_i)_o] \tag{2.40}$$

The value of $(a_i)_{eq}$ is determined by considering both the Law of Mass Action and the stoichiometric equation for equilibrium conditions:

$$\Pi[(a_i)_o + \nu_i x]^{\nu_i} = K_{eq} \tag{2.41}$$

The value of the concentration change due to (x) can be determined by any standard method for solving nonlinear equations (for example: the secant method). From equation (2.40) the representative mean value of the variable product is given by:

$$\overline{\beta[\Sigma_i \frac{\nu_i^2}{a_i}]} = \nu_i(1 - \beta_o)/[(a_i)_{eq} - (a_i)_o] \qquad (2.42)$$

There is no analytical method to estimate the error involved in this approximation. It is necessary to compare the results of numerical solutions (relatively "exact") with the corresponding analytical approximations.

Figure 2.2 shows the computed reaction ratios and the variable product $\beta\Sigma \frac{\nu_i^2}{a_i}$ as a function of time for the hypothetical reaction $AB \rightleftarrows A+B$, as determined from equation (2.38). Arbitrarily selecting equilibrium constant as $K_{eq} = 10^{-8}$; the initial activities of the A and B aqueous species as 10^{-4} and 10^{-8} respectively; the initial reaction ratio β_o is: $10^{-4} \times 10^{-8}/10^{-8} = 10^{-4}$; the activity of the pure solid phase is unity by convention. Assuming the change of the ionic strength caused by the progressing reaction is negligible, γ remains about unity. The rate constant is $k = 10^{-5}$ M/min. By applying the secant method (for example, Conte, 1965) for solving equation (2.41), the equilibrium activities of A and B were computed to be 1.618×10^{-4} and 6.18×10^{-5}, respectively, that is equal to the molar concentration for $\gamma \approx 1$. At these activities:

$$[(A) \cdot (B)]_{eq} = (1.618 \times 10^{-4}) \times (6.181 \times 10^{-5}) = 10^{-8} = K_{eq}$$

The mean value of the product $\beta\Sigma_i \frac{\nu_i^2}{a_i}$ (eq. 2.41) is:

$$\overline{\beta[\Sigma \frac{\nu_i^2}{a_i}]} = \nu_i(1 - \beta_o)/[(a_i)_{eq} - (a_i)_o]$$

$$= 1 \times (1 - 10^{-4})/[10^{-4}(1.618 - 1.0)]$$

$$= 1 \times (1 - 10^{-4})/[10^{-4}(0.618 - 10^{-4})]$$

$$= 1.618 \times 10^4$$

Figure 2.2 - Comparison between numerical integration of the rate equation (2.26) and approximate analytical solution (Eq. 2.38) of the $\beta(t)$ function for the hypothetical reaction $AB \rightleftarrows A + B$; $K_{eq} = 10^{-8}$; initial activities of A and B are 10^{-4} and 10^{-8} respectively. The ionic strength is approximately zero; activity coefficients remain about unity through the reaction. For deriving the analytical approximate solution, the product $\beta(t) \sum_i \frac{\nu_i^2}{a_i}$, which varies in this example between 1.0×10^4 and 2.24×10^4, was replaced by the average 1.618×10^4, determined from equation (2.42). The rate constant is $k = 10^{-5}$ M/min, yielding $k^* = 0.1618$ min^{-1}.

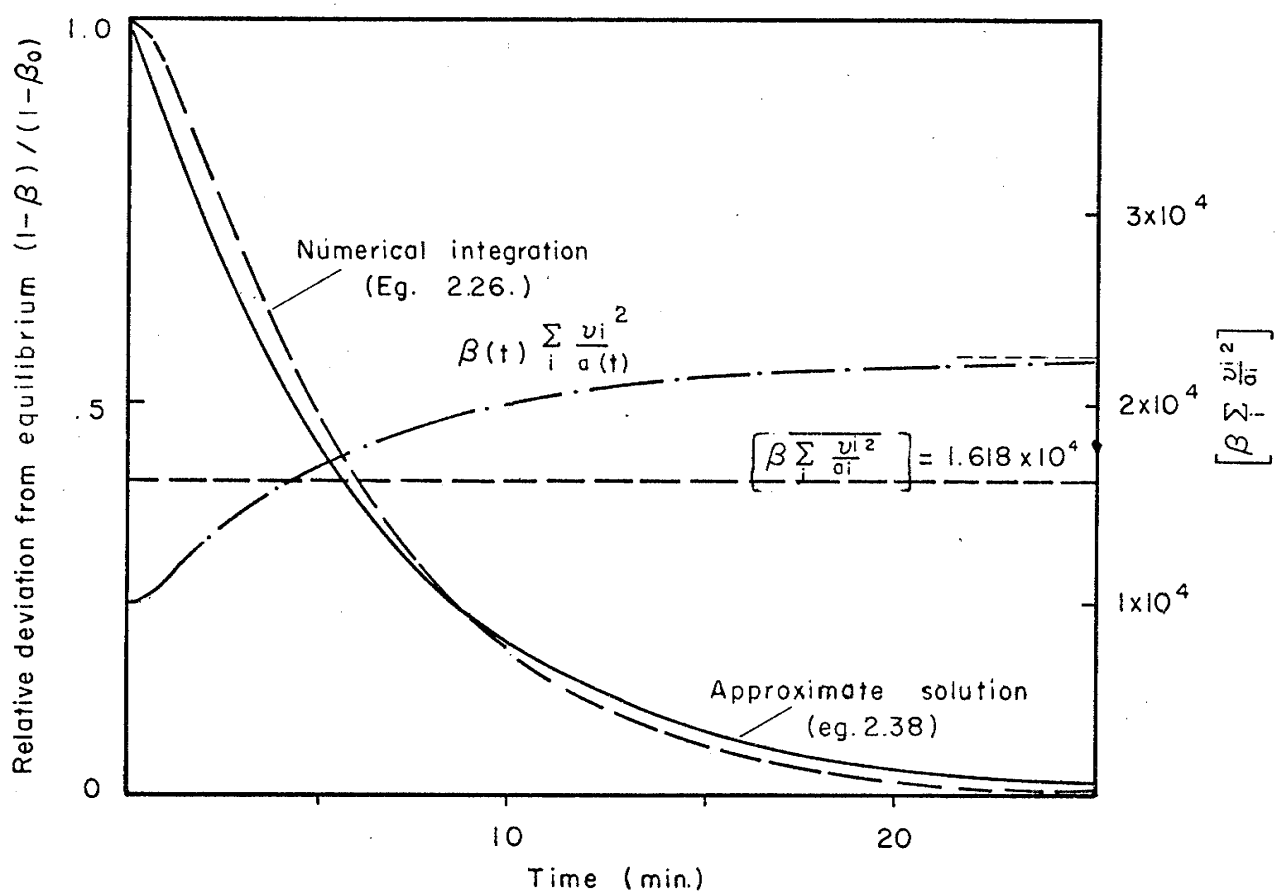
1.0
.5
0
Relative deviation from equilibrium (1−β) / (1−β₀)
Numerical integration
(Eg. 2.26.)
β(t) Σ νi² / a(t)
Approximate solution
(eg. 2.38)
[β Σ νi²/ai] = 1.618 x 10⁴
3x10⁴
2x10⁴
1x10⁴
[β Σ νi²/ai]
10
20
Time (min.)

and the value of k^* is then:

$$k^* = k[\beta\Sigma_i \frac{\nu_i^2}{a_i}] = 10^{-5} \times 1.618 \times 10^4 = 0.1618$$

Figure 2.2 shows the comparison between the $\beta(t)$ approximation (Eq. 2.37), based on the value of k^* computed above and the numerical solution of $\beta(t)$ based on the explicit integration of equation (2.25). The computed product $\beta\Sigma_i \frac{\nu_i^2}{a_i}$ varies between 1.00×10^4 at $t = 0$ and 2.24×10^4 near equilibrium; or $1.618 \times 10^4 \pm 38\%$. This deviation, which affects the rate $d\beta/dt$ by the same amount of error is smoothed during the integration of the rate equation. As a result (Fig. 2.2) equation (2.38) is a close approximation of $\beta(t)$ for the specific reaction and initial concentrations considered above. Computation of $\beta\Sigma_i \frac{\nu_i^2}{i}$ for the experimental data of Chapter 4 yield a similar degree of error.

Based on other computer runs similar to that shown by (Fig. 2.2) the accuracy of the approximate solution presented above will decrease for higher orders of reaction, lower initial concentrations, lower initial reaction ratios, and significant variations of the activity coefficients during the reaction.

2.4 Selection of the Reaction-Rate Equations

Six rate equations (Table 2.1) were considered above for describing the dissolution of single-phase solids in aqueous solutions. The first four are based on the Law of Mass-Action, which represents in this work the kinetics of chemically-controlled dissolution processes. Of these equations, only one was selected to be used further (Eq. 2.26):

TABLE 2.1 - LIST OF KINETIC RATE EQUATIONS CONSIDERED IN THIS WORK

Kinetic Statement	Rate Equation	Validity Limitations	Remarks
Chemically-Controlled Kinetics:			
Law of Mass-Action (exact)	$\frac{1}{\nu_i}\frac{dC_i}{dt} = k_f[\prod_r (a_r)^{\nu_i}](1 - \beta)$	Stoichiometric reactions.	Not used in this work.
Law of Mass-Action (approx.)	$\frac{1}{\nu_i}\frac{dC_i}{dt} \cong k(1 - \beta)$	Stoichiometric reactions. Constant activities of reactants.	Accepted as the primary rate equation for this work.
Free Energy-Rate Relationships	$\frac{1}{\nu_i}\frac{dC_i}{dt} \cong k(-\Delta G_r/RT)$	$\beta(t = 0) >> 0$; constant activities of reactants. $\Delta G/RT$ is small.	Not used in this work.
$\beta(t)$ Approximation	$\frac{d\beta}{dt} \approx k^*(1 - \beta)$ $\frac{1 - \beta}{1 - \beta_o} = \exp(-k^*t)$	Low order reactions. Constant ionic strength.	Accepted as a tool for rough estimates of the overall process.
Transport-Controlled Kinetics:			
Nernst Equation	$\frac{dC_i}{dt} = k_d(C_s - C_i)$	Predicts the uppermost limit of reaction rates; nonrealistic for field conditions and laboratory experiments considered in this work.	Not used.
Helgeson Equations	$\frac{dC_i}{dt} = kt^w$ $(w = -1, 1/2, 0)$	$C << C_s (C_i \to \infty$ for $t \to \infty)$ unless a limit is set for t.	Not used. Greater error than that of accepted statement.

$$\frac{dC_i}{dt} \cong k(1 - \beta)$$

In addition, the $\beta(t)$ approximation (Eq. 2.38), and its corresponding analytical solution (Eq. 2.39) were chosen as approximate analytical tools for obtaining rate estimates of the overall dissolution process.

The kinetic equations based on transport theory (Table 2.1) were rejected as discussed in previous sections of this chapter. Nevertheless, the interpretation of dissolution experiments here reported indicates that as far as the performance of kinetic models is judged by their ability to reproduce experimental data within a reasonable accuracy, all models, except the logarithmic regression (Eq. 2.11) are suitable for this purpose.

2.5 The General Case of Multimineral Assemblages Dissolving in Closed Aqueous Systems

The kinetic model chosen above, equation (2.26):

$$\frac{1}{\nu_i}\frac{dC_i}{dt} \cong k(1 - \beta)$$

was derived for the dissolution of a single minerals and for $R_f \cong k$. It can be extended, however, to describe the dissolution of multimineral assemblages. The variation of the concentration C_i of a given species (i) with respect to time t, will be the sum of the variations contributed by each mineral (j).

Considering equation (2.26) the overall variation of concentration of the i-th species with time is given by:

$$\frac{dC_i}{dt} = \sum_j [\nu_{ij} k_j (1 - \beta_j)] \qquad (2.44)$$

where: ν_{ij} - the stoichiometric coefficient of the i-th species with respect to the j-th mineral.

k_j - the dissolution rate constant of the j-th mineral.

β_j - the reaction ratio of the bulk solution at time t, with respect to the j-th mineral.

The equation above represents kinetic competition among various dissolving minerals. For example, under the condition:

$$\nu_i^{(1)} k^{(1)} (1 - \beta^{(1)}) >> \nu_i^{(2)} k^{(2)} (1 - \beta^{(2)})$$

the rapid rate of dissolution of mineral (1), may cause a temporary supersaturation of the bulk solution with respect to mineral (2), such that $\beta^{(2)} > 1$. In this case, simultaneous dissolution of mineral (1) and precipitation of mineral (2) occur in an attempt by the system to reach overall equilibrium.

3. DISSOLUTION OF CALCITE, DOLOMITE AND GYPSUM IN AQUEOUS SOLUTIONS

In this chapter the dissolution of minerals in carbonate aquifers is briefly discussed, emphasizing first the equilibrium state. The simultaneous dissolution of major minerals is then presented as a kinetic process.

As the major minerals forming carbonate aquifers, one may list calcite, aragonite, dolomite, gypsum, anhydrite, and minor silicates (Hanshaw and Back, 1965a). However, only calcite, dolomite and gypsum are considered in this dissertation.

The relatively rapid rates of dissolution and precipitation of some of these minerals under surface condition have encouraged geochemists to study the correlations between field observations, laboratory experiments, and thermochemical data. Most of these studies are oriented toward equilibrium models and deal with the dissolution of carbonate minerals. The effect of sulphate minerals, and the kinetic competition between the various minerals has not been considered by most investigators (Hanshaw and Back, 1965a; Hostetler, 1964; Langmuir, 1971).

3.1 Equilibrium Considerations

(a) Calcite - The dissolution of calcite takes place by the following steps (Garrels and Christ, 1965): (i) The dissolution of calcite into calcium and carbonate ions:

$$CaCO_3 \rightleftarrows Ca^{++} + CO_3^{=} \quad ; \; pK(25°C) = 8.35 \qquad (3.1)$$

where $pK(=-\log_{10}K)$ represents the equilibrium constant for the dissolution of calcite at 25°C and 1 atmosphere; (ii) Hydrolysis of carbonate ions to form bicarbonate and H_2CO_3. This step is actually the result of

four separate equilibria:

$$HCO_3^- \rightleftarrows H^+ + CO_3^= \quad ; \; pK(25°C) = 10.33 \tag{3.2}$$

$$H_2CO_3 \rightleftarrows H^+ + HCO_3^- \quad ; \; pK(25°C) = 6.35 \tag{3.3}$$

$$H_2O \rightleftarrows H^+ + OH^- \quad ; \; pK(25°C) = 14.0 \tag{3.4}$$

$$CO_2 + H_2O \rightleftarrows H_2CO_3 \quad ; \; pK(25°C) = 1.47 \tag{3.5}$$

The reaction ratio with respect to the calcite dissolution β_c, as an example, is determined from:

$$\beta_c = [(\gamma_{Ca^{2+}} \cdot C_{Ca^{2+}}) \cdot (\gamma_{CO_3^{2-}} \cdot C_{CO_3^{2-}})]/K_c(T,P) \tag{3.6}$$

where $K_c(T,P)$ is the temperature and pressure dependent equilibrium constant for the stoichiometric dissolution of calcite; γ and C denote activity coefficients and molar concentrations, respectively, and the activity of the solid phase is assigned a value of unity.

Within the pH range of most aquifer water, the major constituent among carbonate species is bicarbonate; it is necessary to calculate $C_{CO_3^=}$ from the equilibrium relationships between carbonate species, assuming that equilibrium is attained among these species. From equation (3.2):

$$C_{CO_3^=} = \frac{1}{\gamma_{CO_3^=}} [K_{HCO_3^-}(T,P) \; \gamma_{HCO_3^-} \; C_{HCO_3^-}/\gamma_{H^+} \; C_{H^+}] \tag{3.7}$$

The values of $C_{CO_3^=}$ computed from the equation above are highly sensitive to pH measurements, as the pH is defined by:

$$pH = - \log_{10}(\gamma_{H+}\ C_{H+}) \qquad (3.8)$$

(b) Dolomite - The dissolution of dolomite is congruent at ordinary temperatures (Krauskopf 1967, p. 87) and it should occur in steps similar to those of calcite; i.e. - (i) The dissolution of dolomite into calcium, magnesium, and carbonate ions:

$$CaMg(CO_3)_2 \rightleftarrows Ca^{++} + Mg^{++} + 2CO_3^{=} \ ; \ pK(25°C) = 16.5 \qquad (3.9)$$

and (ii) Hydrolysis of carbonate ions to form bicarbonates, governed by the relationships given previously.

The reaction ratio β_d with respect to the dolomite dissolution reaction is stated in a manner similar to that of calcite.

The value of pK for dolomite is controversial because the dolomite has not been experimentally precipitated under aquifer conditions. Estimates for $pK_d(25°C)$ vary between 16.5 and 19.5 (Stumm and Morgan, 1970). Interpretation of field data (Hsu, 1963; Barnes and Back, 1964) indicates, however, that the range of 16.5 to 16.7 is most acceptable. In a subsequent chapter of this work the value of $pK_d = 16.5$ will be defended.

(c) Gypsum - The dissolution of gypsum is represented by:

$$CaSO_4 \cdot 2H_2O \rightleftarrows Ca^{++} + SO_4^{=} + 2H_2O \ ; \ pK(25°C) = 4.61 \qquad (3.10)$$

Because the activities of both solid gypsum and water can be assigned a value of unity, the reaction ratio β_g with respect to gypsum is given by:

$$\beta_g = [(\gamma_{Ca^{2+}} \cdot C_{Ca^{2+}}) \cdot (\gamma_{SO_4{}^{2-}} \cdot C_{SO_4{}^{2-}})]/K_g(T,P) \qquad (3.11)$$

3.2 Thermochemical Data

Equilibrium constants of chemical reactions are a function of temperature and pressure. The effects of pressure, however, are often disregarded (Garrels and Christ, 1965; p. 343) because the volume changes for reactions in aqueous solutions are commonly small and the pressure corrections are thus often smaller than the uncertainty in the experimental data (Helgeson, 1969).

The dependence of equilibrium constants on temperatures can be obtained experimentally or derived from available thermochemical data. Values of the equilibrium constants used in this work are summarized in Table 3.1. Experimental data and values from thermodynamic equations (App. B) (Table 3.1) of pK(T) were regressed with respect to the temperature T using a quadratic polynomial of the form:

$$pK(T) = a + 10^{-4}\, b(T - T_r) + 10^{-6}\, c(T - T_r)^2 \qquad (3.12)$$

where a, b, and c are the polynomial coefficients, based on the data used in this dissertation (Appendix B); T is the temperature and T_r is the reference temperature of the polynomial regression, both in °C. A more detailed discussion on the derivation of pK(T) is given in Appendix B.

3.3 Activity Coefficients and Corrections for Ion-Pairs and Complexes

The Law of Mass-Action applies to activities rather than molar concentrations. Techniques are available for measuring the activities of certain ions. If a direct measurement of the ion activity is impossible a correction factor γ_i should be used such that (Eq. 2.14):

$$a_i = \gamma_i C_i$$

TABLE 3.1 - pK(= -log K) As a Function of Temperature***

Dissolution or dissociation reaction	pK at 25°C	Coefficients of the pK expansion (ep. 3.14)*				Temp. range (°C)	Reference
		a	b	c	T_r(°C)		
Calcite	8.34	8.34	123.33	-22.22	25	10 - 40	GC
Dolomite	16.50	16.29	185.00	250.00	15	5 - 25	L
Gypsum	4.61	4.61	- 7.00	75.33	25	10 - 40	HB + KEQ
CO_2	1.47	1.47	123.00	-66.70	25	10 - 40	GC
H_2CO_3	6.35	6.35	-52.50	175.00	25	15 - 35	GC
HCO_3^-	10.33	10.33	-90.00	111.11	25	10 - 40	GC
H_2O **	1.008 **	1.008	876.00	2656.00	25	10 - 40	GC

Notes: (*) $pK(T) = a + 10^{-4}\, b(T - T_r) + 10^{-6}\, C(T - T_r)^2$

(**) $\partial_w(T) = K_w(T)/10^{-14}$

$= a + 10^{-4}\, b(T - T_r) + 10^{-6} C(T - T_r)^2$

(***) See also Appendix "B"

References: GC - Garrels and Christ 1965

HB - Hanshaw et al 1965a

KEQ- Based on computer program KEQ (Appendix B)

L - Langmuir (1971); pK(25°C) of Langmuir was shifted downwards with 0.5 pK unit.

where a_i is the activity and C_i the measured molarity of the i-th ion.

Activity coefficients of single ions can be computed with the aid of the Debye-Hückel equation. This equation is based on the observation that charged ions, even in very dilute solutions exert long-range electrostatic forces upon one another, with the result that the chemical activities of the participants in the reaction are changed.

Various forms of the Debye-Hückel equation exist in the literature. The form used here is (Garrels and Christ, 1965; Hem, 1970):

$$-\log \gamma_i = \frac{A(T) z_i^2 \, I^{1/2}}{1 + B(T) a_i^{o} \, I^{1/2}} \tag{3.13}$$

where: A(T) - a constant related to the solvent, dependent on temperature.

z_i - the ionic charge.

B(T) - another temperature-dependent constant related to the solvent.

a_i^{o} - a constant related to the "effective diameter" of the ion in the solution.

I - the ionic strength of the solution, defined by:

$$I = 1/2 \sum_i C_i z_i^2 \tag{3.14}$$

The tabulated values of A(T) and B(T) for water as a solvent (Garrels and Christ, 1965; Table 2.6) were regressed to the linear relationships:

$$A(T) = 0.4850 + 0.000920T \tag{3.15}$$

$$B(T) = 0.3241 + 0.000162T \tag{3.16}$$

where T is the temperature in degrees C for the interval 0 - 60°C. The values of the effective diameter a_i^o for the major ions were adapted from Hem (1970; Table 5).

The validity of the Debye-Hückel equation is restricted to solutions in which ionic strength does not exceed 0.05 (Garrels and Christ, 1965) to 0.10 (Back and Hanshaw, 1965; Hem, 1970). The range of the ionic strength for field samples considered in this work is in the range of 3×10^{-3} to 5×10^{-2}. Ionic strength and the corresponding activity coefficients were computed here by the ACTCF subroutine* (Appendix G).

In dilute solutions, charged, dissolved species can be regarded as individual free ions and their activity coefficients (γ_i) can be derived directly from the Debye-Hückel equation. As the ionic strength of the solution increases the difference between measured activities and those predicted by the Debye-Hückel equation becomes larger. This deviation is explained under certain conditions by short-range interactions between adjacent ions forming ion-pairs or complexes.

The list of all possible ion-pairs that might occur in natural water systems is rather large (Garrels and Christ, 1965); however, only $CaSO_4^o$, $MgSO_4^o$, and $MgHCO_3^+$, are considered to be of significant importance in carbonate aquifers (Langmuir, 1971). The dissociation of these complexes is described by:

---

* Note - The computer programs and subroutines, used in this dissertation, are available on request from the: Geoscience Dept., New Mexico Institute of Mining and Technology, Socorro, New Mexico 87801

$$CaSO_4^o \rightleftarrows Ca^{++} + SO_4^= \tag{3.17}$$

$$MgSO_4^o \rightleftarrows Mg^{++} + SO_4^= \tag{3.18}$$

$$MgHCO_3^+ \rightleftarrows Mg^{++} + HCO_3^- \tag{3.19}$$

Assuming that equilibrium is attained among all aqueous species in solution, the following equilibrium relationships should prevail:

$$\frac{\gamma_{Ca^{++}} \cdot C_{Ca^{++}} \cdot \gamma_{SO_4^=} \cdot C_{SO_4^=}}{C_{CaSO_4^o}} = K_{CaSO_4}(T) \tag{3.20}$$

$$\frac{\gamma_{Mg^{++}} \cdot C_{Mg^{++}} \cdot \gamma_{SO_4^=} \cdot C_{SO_4^=}}{C_{MgSO_4^o}} = K_{MgSO_4^o}(T) \tag{3.21}$$

$$\frac{\gamma_{Mg^{++}} \cdot C_{Mg^{++}} \cdot \gamma_{HCO_3^-} \cdot C_{HCO_3^-}}{\gamma_{MgHCO_3^+} \quad C_{MgHCO_3^+}} = K_{MgHCO_3^+}(T) \tag{3.22}$$

In the equations above the activity coefficients of the noncharged species were assigned an activity coefficient of unity (Garrels and Thompson, 1962). The activity coefficient of $MgHCO_3^+$ was approximated by the corresponding coefficient of HCO_3^- (ibid).

The dependence of the equilibrium constants given above on the temperature T(°C) is given by Langmuir (1971):

$$pK_{CaSO_4^o} = 2.20 + 0.0044T \tag{3.23}$$

$$pK_{MgSO_4^o} = 2.03 + 0.0132T \tag{3.24}$$

$$pK_{MgHCO_3^+} \cong 0.95 \qquad (3.25)$$

Chemical analyses, reported in terms of individual ions, represent the sum of both free and complexed ions, while only the free ions are considered in the calculation of the reaction ratios described above. Chemical data considered in this dissertation have been corrected for complexing and ion-pairs by numerical iteration (Subroutine COMPLX, Appendix G) to yield the molarities and activities of free ions, based on the corrected ionic strength.

3.4 Simultaneous Dissolution of Calcite, Dolomite, and Gypsum

The simultaneous dissolution of the three major minerals forming carbonate aquifers may serve as an example of the kinetic competition discussed previously. The solubility product of gypsum (pK = 4.61) is higher by almost 4 and 12 orders of magnitude respectively than the solubility products of calcite (pK = 8.35) and dolomite (pK = 16.5). This difference between the solubility products forces the dissolution reaction of gypsum to proceed, even when the solution is supersaturated with respect to calcite or dolomite.

(a) The Dissolution Process - The progress of the simultaneous dissolution of calcite, dolomite and gypsum can be expressed by the time-dependent concentrations of calcium, magnesium, sulphate, carbonate species and hydrogen.

The concentrations of calcium, magnesium and sulphate are determined by integrating the following rate equations (Eq. 2.44):

$$\frac{dC_{Ca^{++}}}{dt} = k_c(1 - \beta_c) + k_d(1 - \beta_d) + k_g(1 - \beta_g) \tag{3.26}$$

$$\frac{dC_{Mg^{++}}}{dt} = k_d(1 - \beta_d) \tag{3.27}$$

$$\frac{dC_{SO_4^{=}}}{dt} = k_g(1 - \beta_g) \tag{3.28}$$

where k_c, k_d, and k_g are the rate constants of the chemically-controlled dissolution processes for calcite, dolomite, and gypsum respectively; β_c, β_d, and β_g are the reaction ratios of the solution with respect to these minerals.

In equations (3.26) and (3.27) β_c and β_d depend on the pH and the equilibrium distribution of carbonate species which can be determined in carbonate aquifers by considering one of the following boundary conditions related to partial pressure of CO_2: (i) The system is equilibrated with a given partial pressure of CO_2 (either constant or varying with time) governed by external processes; (ii) The system is originally equilibrated with an external CO_2 source but then closed at $t=0^+$. It will be demonstrated later that the first boundary condition is more realistic.

Considering the first boundary condition (constant partial pressure of CO_2) electrical neutrality requires:

$$C_{HCO_3^-} + 2C_{CO_3^=} - C_{H^+} + C_{OH^-} = 2(C_{Ca^{++}} + C_{Mg^{++}} - C_{SO_4^=}) + \delta \tag{3.29}$$

where δ is an additional term introduced to correct for the existence of other, non-participating, ions in the solution. For most aquifers δ can be approximated by:

$$\delta \cong C_{Na^+} - C_{Cl^-} \tag{3.30}$$

For a pH of 7 - 8, which is the range of most aquifer water, the concentration of hydrogen and hydroxyl ions can be neglected, and equation (3.29) is approximated by:

$$C_{HCO_3^-} + 2C_{CO_3^=} \cong 2(C_{Ca^{++}} + C_{Mg^{++}} - C_{SO_4^=}) + \delta \tag{3.31}$$

Assuming equilibrium among carbonate species, the concentration of the bicarbonate ion is determined from the ratio between dissolved CO_2, and hydrogen (equations 3.3 and 3.5):

$$C_{HCO_3^-} = \frac{K_{CO_2} \cdot K_{H_2CO_3}}{\gamma_{HCO_3^-} \cdot \gamma_{H^+}} \cdot \frac{C_{CO_2}}{C_{H^+}} \tag{3.32}$$

and the concentrations of carbonates (Eq. 3.2) are expressed by:

$$C_{CO_3^=} = \frac{K_{CO_2} \cdot K_{H_2CO_3} \cdot K_{HCO_3^-}}{\gamma_{CO_3^=} \cdot \gamma^2_{H^+}} \cdot \frac{C_{CO_2}}{C^2_{H^+}} \tag{3.33}$$

Substitution of equations (3.32 and 3.33) into equation (3.31) yields a non-linear equation with respect to the molarity of the hydrogen ion (C_{H^+}):

$$\frac{A/(\gamma_{HCO_3^-} \ \gamma_{H^+})}{C_{H^+}} + 2\,\frac{B/[\gamma_{CO_3^=} \gamma^2_{H^+}]}{C^2_{H^+}} - D = 0 \tag{3.34}$$

where A, B, and D are constants given by:

$$A = K_{CO_2} \cdot K_{H_2CO_3} \cdot C_{CO_2} \tag{3.35}$$

$$B = K_{CO_2} \cdot K_{H_2CO_3} \cdot K_{HCO_3^-} \cdot C_{CO_2} \tag{3.36}$$

$$C = 2(C_{Ca^{++}} + C_{Mg^{++}} - C_{SO_4^=}) + \delta \tag{3.37}$$

Equation (3.33) can be solved by means of standard numerical techniques (Subroutine DISTRD in Appendix G). The activity coefficients (γ) were not included in the constants because they may change during the numerical iteration on C_{H^+}.

Within the pH range of most aquifer water the major carbonate species is the bicarbonate ion; thus, $C_{HCO_3^-}$ can be determined directly from the electrical neutrality condition (Eq. 3.31):

$$C_{HCO_3^-} \cong 2(C_{Ca^{++}} + C_{Mg^{++}} - C_{SO_4^=}) + \delta \tag{3.38}$$

The pH is determined from the equilibrium relationships among carbonate species (Eq. 3.32):

$$pH = -\log_{10}\left(\frac{K_{CO_2} \cdot K_{H_2CO_3}}{\gamma_{HCO_3^-}} \cdot \frac{C_{CO_2}}{C_{HCO_3^-}} \right) \tag{3.39}$$

where $C_{HCO_3^-}$ is determined from equation (3.34).

In the case of the second boundary condition (partial pressure of CO_2 varying with time as governed by the dissolution process), the carbonate mass balance should be considered in addition to the equations given above. At any time t the carbonate balance requires:

$$C_{CO_2} + C_{H_2CO_3} + C_{HCO_3^-} + C_{CO_3^=} = C_C \tag{3.40}$$

where C_C is the total molarity of carbon species at time t. The total carbonate species are determined through the stoichiometric relationships of the calcite and dolomite dissolution reactions (equations 3.26 and 3.27):

$$\frac{dC_C}{dt} = k_c(1 - \beta_c) + 2k_d(1 - \beta_d) \tag{3.41}$$

Assuming that the resulting pH under these boundary conditions would be well above 8, (Garrels and Christ, 1965, p. 86 - case 5) the major carbonate species will be $CO_3^{=}$ and HCO_3^{-}, such that equation (3.40) can be approximated by:

$$C_{HCO_3^-} + C_{CO_3^=} \cong C_C \tag{3.42}$$

In dilute solutions and in this pH range, the concentrations of the hydroxyl ions can not be neglected and equation (3.29) is approximated by:

$$C_{HCO_3^-} + 2CO_3^{=} + C_{OH^-} \cong 2(Ca^{++} + C_{Mg^{++}} - C_{SO_4^=}) + \delta \tag{3.43}$$

Multiplying equation (3.42) by 2 and subtracting equation (3.43) from the resulting equation gives:

$$C_{HCO_3^-} - C_{OH^-} = 2C_C - 2(C_{Ca^{++}} + C_{Mg} - C_{SO_4^=} + \delta/2) \tag{3.44}$$

From the combination of equations (3.2, 3.4, 3.42, and 3.44):

$$(2C_C - D)\left[1 + \left(\frac{\gamma_{HCO_3^-} K_{HCO_3^-}}{\gamma_{CO_3^-} \gamma_{H^+}} \frac{1}{C_{H^+}}\right)\right] = C_C(t) + \frac{K_w}{\gamma_{OH^-} \gamma_{H^+} C_{H^+}} \tag{3.45}$$

which yields:

$$pH = -\log \left(\frac{\gamma_{HCO_3^-} K_{HCO_3^-}}{\gamma_{CO_3^=} H^+} - \frac{K_w}{(2C_C - D)\gamma_{OH^-} \gamma_{H^+}} \right) \Big/ \left(\frac{C_C}{(2C_C - D)} - 1 \right) \quad (3.46)$$

Actually, equation (3.45) is most easily solved numerically, since the resulting pH may change the activity coefficients slightly, and a few iterations are required to get accurate results.

(b) Computation Procedures - A computer program, names CARMOD-B, (Appendix G), was developed for treating kinetics of dissolution reactions. The rate equations in this program are restricted to the dissolution of calcite, dolomite, and gypsum described above. The steps taken for computing the concentration-time relationships, governed by the progress of the dissolution process are:

(1) Read initial concentrations (Ca^{++}, Mg^{++}, $SO_4^=$, HCO_3^-, pH), boundary conditions (temperature, P_{CO_2}, Cl^-, Na^+), and rate constants (k_c, k_d, and k_g).

(2) Correct for ion-pairs and complex ions and determine activities of free ions in solution (Subroutine COMLX1).

(3) Determine reaction ratios with respect to calcite (β_c), dolomite (β_d), and gypsum (β_g).

(4) Integrate explicitely equations (3.26) to (3.28) from t to $t + \Delta t$, to obtain the new concentrations of the calcium, magnesium, and sulphate ions, as well as the resulting variation of the total carbon (C_C). Ensure stability of the numerical integration by comparing relative variation of species concentration with a given tolerance. Use this

comparison to increase or decrease the next time step (Δt). The use of a simplified version of the "Predictor-Corrector" numerical technique for solving a system of differential equations (Carnahan, et al., 1969) enables considerable increase of the individual time-steps, without affecting the stability of the numerical solution. This step is carried out by Subroutine SINTG2.

(5) Determine the new distribution of carbonate species and pH, by considering one of the two CO_2 boundary conditions discussed previously.

(6) Repeat steps (2) to (5). Terminate integration when elapsed time is equal to or larger than a given limit, or when a practical specified equilibrium with respect to the dissolving minerals is attained.

(c) Hypothetical Example - The following example in which calcite, dolomite, and gypsum were allowed to dissolve under constant CO_2 pressure demonstrates the dissolution in a hypothetical carbonate aquifer. Figure 3.1 shows the concentration-time relationships using the CARMOD-B computer program, following the steps outlined previously.

The comparison between the curves for the simultaneous dissolution and those for each mineral dissolving separately demonstrates the effects of kinetic competition on reaction paths and the final composition of the solution.

Relatively rapid dissolution of gypsum causes the solution to become saturated with respect to calcite and near-equilibrium is reached with respect to dolomite in the early stages of reaction. As a result

calcite precipitates removing both calcium and carbonate from the solution. Gypsum continues to dissolve increasing the $SO_4^=$ and Ca^{++} content of the solution and leading to supersaturation of carbonate minerals. The depletion of HCO_3^- caused by calcite precipitation is followed by a decrease in pH. The pH of the solution is governed by the ratio between the constant CO_2 pressure and the concentration of the bicarbonate ion (Eq. 3.39). The increase of Mg^{2+} partially compensates for the excess negative charge added by the $SO_4^=$ ions; as a result, the concentration of both pH and HCO_3^- stabilizes.

An important feature of the hypothetical simultaneous process is the increase in time requires to attain overall equilibrium; 90% (= β) of the separate reactions were completed after about 600, 75, and 8000 years for calcite, dolomite, and gypsum respectively, as compared to more than 16,000 years required for gypsum to attain 90% of equilibrium under the conditions of simultaneous dissolution. These values of time are all for the hypothetical case shown in Figure 3.1.

Figure 3.1 - Hypothetical chemically controlled simultaneous dissolution of calcite, dolomite, and gypsum under constant CO_2 pressure. Solid curves represent the progress of the simultaneous reaction; dashed curves represent the dissolution of each mineral separately, other minerals being absent. The theoretical curves were computed by the CARMOD-B computer program for $k_c = 5.0 \times 10^{-6}$ M/yr, $k_d = 2.5 \times 10^{-5}$ M/yr, $k_g = 2.5 \times 10^{-6}$ M/yr, $pK_d = 16.5$ for a temperature of 25°C, and $pCO_2 = 2.0$ ($pCO_2 = -\log_{10}$ CO_2 concentration). The concentration of all species, except hydrogen and bicarbonates, was initially zero. No correction is made here for ion-pairs and complexes. The term β is given in % of the value of saturation, i.e., one. This also is true for subsequent figures.

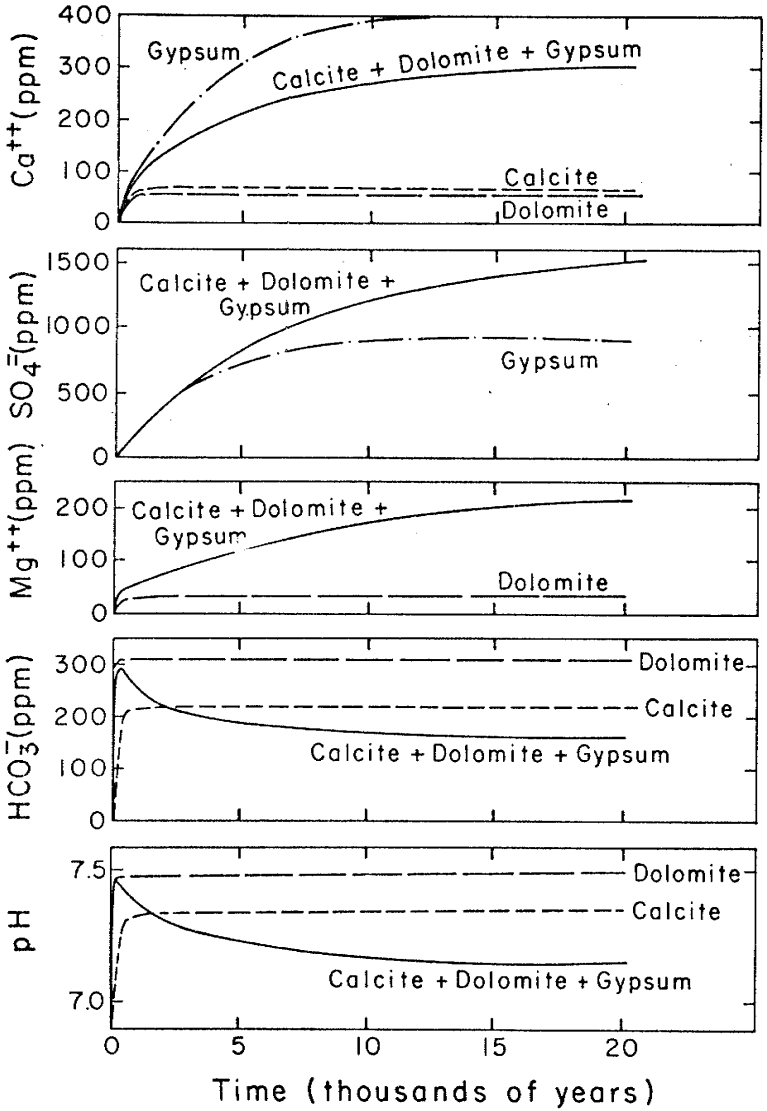

(a.) Chemical Composition

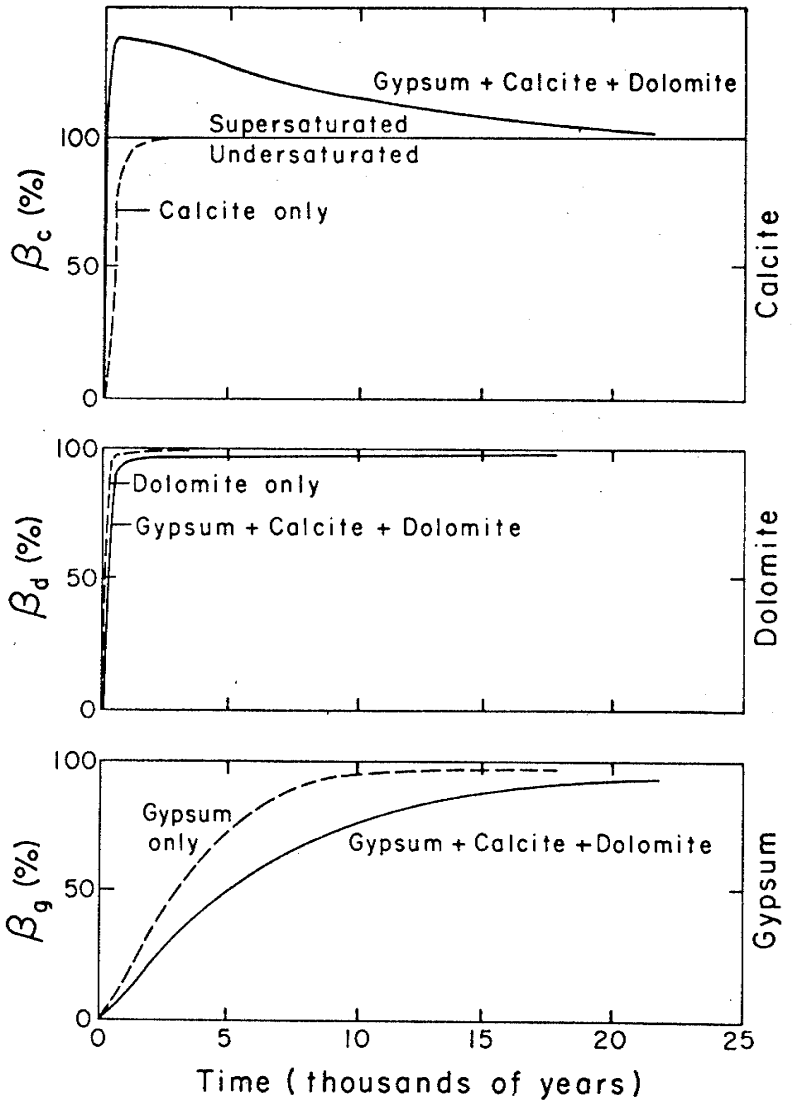

(b.) Reaction Ratio

4. LABORATORY EXPERIMENTS - DISSOLUTION OF CALCITE AND GYPSUM IN AQUEOUS SOLUTIONS

Laboratory experiments were carried out in order to test the theoretical approaches presented previously as well as to estimate the magnitude of the dissolution rates for calcite and gypsum. The major portion of the experiments reported below deal with the dissolution of calcite under various conditions, testing the kinetic approach for the dissolution of single minerals. The aim of the remaining experiments was to demonstrate the kinetic competition between calcite and gypsum when they are allowed to dissolve simultaneously.

4.1 Experimental Procedures

The laboratory experiments consisted of two types - the stagnant and the flow experiments.

In the stagnant experiments (Fig. 4.1) a measured weight of mineral, having a certain grain size interval, was stirred with a magnetic stirrer in a plastic bottle containing a measured volume of distilled water. The bottle was left open, allowing the solution to equilibrate with atmospheric CO_2. Samples (10-100 cc) were taken regularly from the bottle for chemical analyses. Following each sampling, the bottle was refilled with distilled water to its initial volume, thus diluting the remaining solution.

In the second type of experiments, denoted as the flow experiments, water flowed from bottom to top (Fig. 4.1) at a certain flow rate. Complete mixing was assured by rotational flow and continuous stirring. Dynamic stability is attained after prolonged time, as determined by the

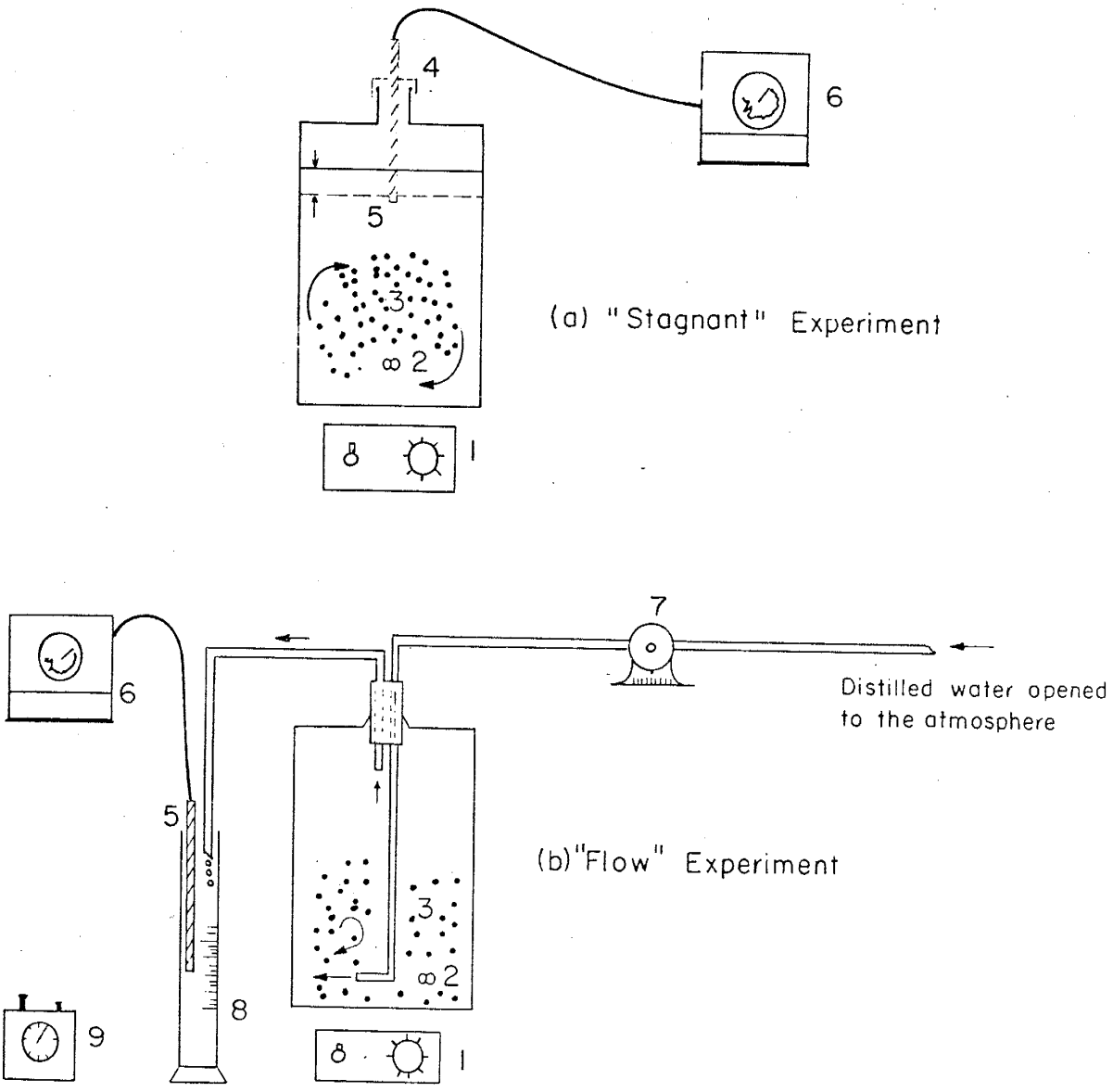

LEGEND

1. Magnetic stirrer
2. Stirring rod
3. Mineral suspension
4. Perforated foil
5. Thermometer
6. Temperature recorder
7. Metering pump
8. Graduated cylinder
9. Stop watch

Figure 4.1 - Experimental Design

relationship between the reaction rate of the dissolving mineral and the residence time of the solution. The volume of the container in this case was 1025 cc; samples were collected regularly at the bottle outlet avoiding the dilution practices in the stagnant experiments. Inflow water was equilibrated with atmospheric CO_2.

The calcite used here was collected at a manganese mine located about 5 miles south of Socorro, N.M. The calcite crystals, yellowish in color, were separated manually from the remaining manganese ore. The calcite was then crushed, milled, and sieved. Potential ferrous contaminants were extracted with a magnet.

Fluid samples were analyzed for electrical conductivity, pH, HCO_3^-, and Ca^{++} ions; $SO_4^=$ was measured when necessary. Solution temperature was monitored continuously with a Fischer & Porter temperature recorder. After pH was measured, samples were filtered through ashless #40 filter paper for the remaining chemical analyses.

Conductivity was measured with a standard conductivity cell having cell constants of k = 0.95 and 0.2; conductivity cells were calibrated against standard KCl solutions. Measured conductivities were converted into 25°C standard conductivities with the aid of common conversion tables. The accuracy of conductivity measurements is believed to be within ± 5 to 10%.

The pH was measured with Beckman glass and reference electrodes, connected to a Corning-Model 12 laboratory pH meter. The accuracy of pH measurements was within ± 0.02 pH units. However, sampling procedures as well as the unbuffered nature of the dilute samples may have increased this error to ± 0.05 pH units.

Total carbonates and alkalinity (HCO_3^- + $CO_3^=$) were determined by titrating 25-50 ml of the filtered samples with 0.005N H_2SO_4, using a titrating pipette of 0.05 cc division. The titration end point was determined by applying the trial and error procedure outlined by Golterman (1969). The division between bicarbonate and carbonate ions was facilitated by the SCELEXP and SCEL1 computer programs written for processing and interpretation of experimental data (Appendix G). The carbonate alkalinity was measured with probable accuracy of ± 10^{-2} millimoles per liter or an equivalent of ± 0.6 ppm HCO_3^-.

The concentration of the calcium ion was measured with a Perkin-Elmer 303 atomic absorption spectrophotometer. Accuracy was within the limits of 0.05 to 0.10 ppm and over the range 0 - 20 ppm.

The concentration of the sulphate ion was determined by a turbidimetric method (Golterman, 1969). The light extinction was measured by a Bausch & Lomb colorimeter using a wave length of 400 mμ. Accuracy was no better than ± 10%. Sulphate measurements were checked by conductivity and by theoretical concentrations determined from electrical neutrality conditions; whenever necessary, chemical analyses were repeated.

The reaction ratio β was computed with the aid of the SCELEX and SCEL1 computer programs, which provides the necessary corrections for temperature variations, activity coefficients, and ion-pairing. The accuracy of the computed values with respect to calcite and gypsum, was determined to be ± 10%.

The experimental conditions are summarized in Table 4.1. The plots of two typical experiments are given in Figure 4.2. The computer printout of all experimental results is given in Appendix D.

4.2 The Diffusion of CO_2 as a Rate Limiting Factor

A comparison between the computed partial pressure of CO_2 during the experiments and the atmospheric P_{CO_2} in Socorro (= $10^{-3.57}$ Atm.) shows that equilibrium between the liquid and gas phases is attained only after the solution is substantially equilibrated with respect to the dissolving calcite. Pressure of dissolved CO_2 usually dropped at the beginning down to about 10^{-5} - 10^{-6} Atm., and then increased gradually up to about the CO_2 pressure at Socorro. This deviation indicates that the dissolution rate of calcite, in this case, was much higher than the diffusion rate of CO_2 through the air-liquid interface. Thus diffusion of CO_2 was the rate limiting step. Apparently, the dissolution process, as monitored in the stagnant experiments, should be treated as some transition case between the closed and open systems. discussed by Garrels and Christ (1965).

In Appendix C, the two cases analogous to closed and open systems are considered: (i) The dissolution of calcite in pure water, being equilibrated with a constant external CO_2 pressure, and (ii) The dissolution of calcite in pure water, originally equilibrated with the same CO_2 source, but then closed before the addition of calcite. For both cases, the concentration of the aqueous species, as a function of the reaction ratio β, was determined at the atmospheric P_{CO_2} in Socorro (Appendix C). The functions $Ca^{++}(\beta)$, $HCO_3^-(\beta)$, $pH(\beta)$, and $pCO_2(\beta)$, both theoretical and experimental, are plotted in Figure 4.3. As can be seen from this figure, the observed concentrations of the various species monitored during the stagnant experiments are a significant function of

TABLE 4.1 - SUMMARY OF EXPERIMENTAL CONDITIONS

RUN	Duration (min)	Mesh Interval	Mineral Weight (gr)	Av. Temp. (°C)	Type*	Flow Rate (cc/min)	Mineral**
B1	6030	200-270	17.6	24.6	S	0.0	C
B2	2460	200-270	17.6	25.2	F	3.7	C
B3	3376	200-270	17.6	25.5	S	0.0	C
B4	3009	200-270	17.6	25.3	F	16.1	C
D1	12988	65-100	14.8	24.8	S	0.0	C
D2	1330	65-100	14.8	24.8	F	11.5	C
D3	1629	65-100	14.8	25.3	S	0.0	C
D4	2968	65-100	14.8	26.2	F	6.4	C
D5	5385	65-100	14.8	26.3	S	0.0	C
D6	4920	65+100	67.8	26.3	S	0.0	C
D7	3048	65-100	67.8	25.8	F	7.2	C
E1	3194	100-150	31.4	25.8	S	0.0	C
E2	2871	100-150	31.4	25.7	F	5.4	C
H1	60	150-270	15.0	24.7	S	0.0	G
I1	6880	100-150*** 150-270	155.0*** 15.0	27.4	S	0.0	C+G

Notes: (*) S-"Stagnant"; F-"Flow"

(**) C-Calcite; G-Gypsum

(***) The upper figures for calcite; the lower for gypsum.

Figure 4.2 - Results of two typical stagnant (a) and flow (b) calcite dissolution experiments. Theoretical curves for β are based on the $\beta(t)$ approximation. Discontinuities of theoretical curves represents the dilution caused by sampling procedures; the dilution ratio is 100/875.

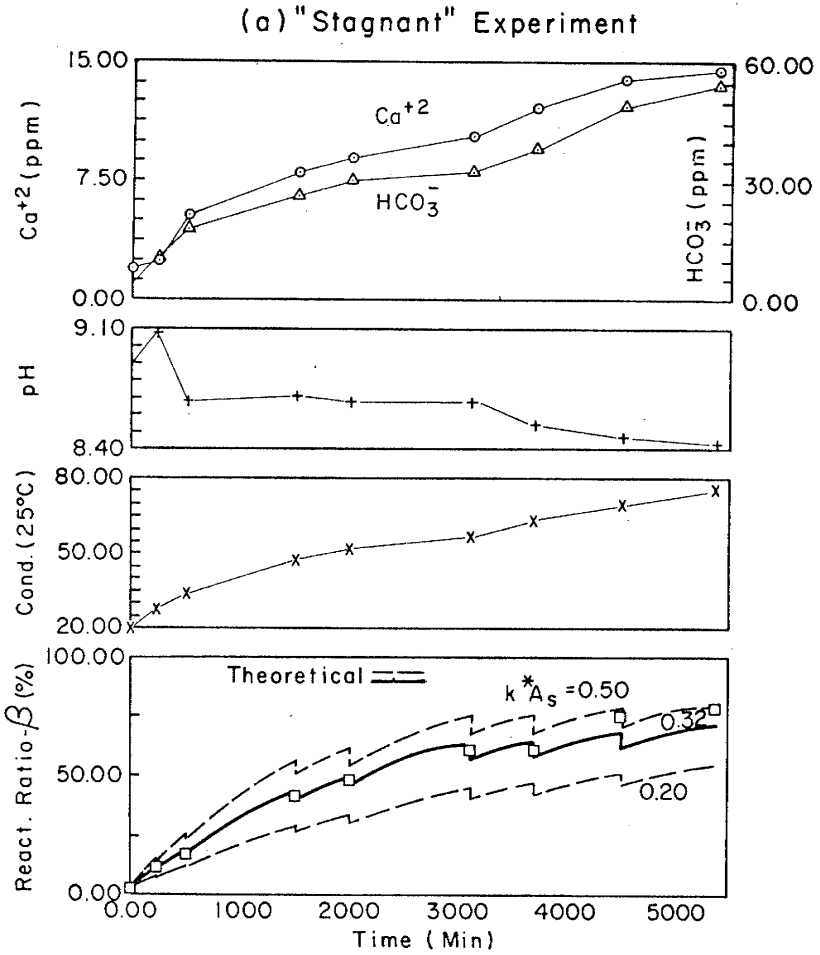
(a) "Stagnant" Experiment
15.00
7.50
0.00
Ca^{+2} (ppm)
Ca^{+2}
HCO_3^-
60.00
30.00
0.00
HCO_3^- (ppm)
9.10
8.40
pH
80.00
50.00
20.00
Cond. (25°C)
100.00
50.00
0.00
React. Ratio-β (%)
Theoretical
k^*A_s =0.50
0.32
0.20
0.00
1000
2000
3000
4000
5000
Time (Min)

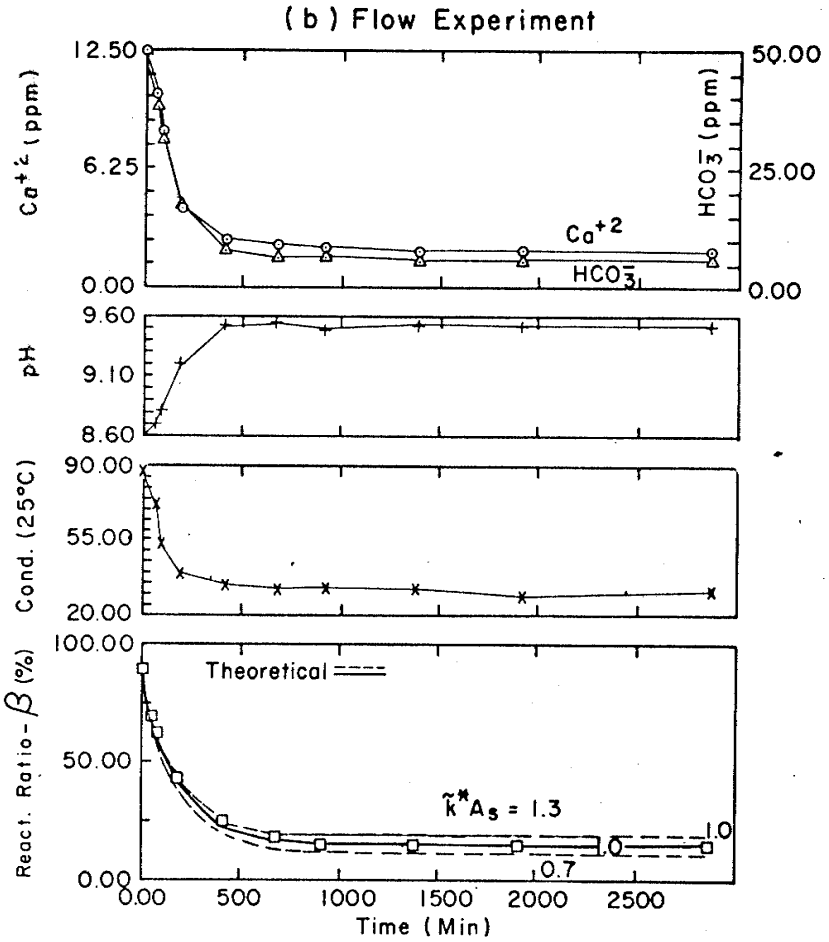
(b) Flow Experiment
12.50
6.25
0.00
Ca^{+2} (ppm)
Ca^{+2}
HCO_3^-
50.00
25.00
0.00
HCO_3^- (ppm)
9.60
9.10
8.60
pH
90.00
55.00
20.00
Cond. (25°C)
100.00
50.00
0.00
React. Ratio-β (%)
Theoretical
$\tilde{k}^*A_s$ = 1.3
1.0
0.7
0.00
500
1000
1500
2000
2500
Time (Min)

Figure 4.3 - Comparison between theoretical and measured concentrations as a function of β, for both closed and open systems. Dashed curves represent the general trend of measured concentrations for the stagnant experiments (runs D3 and D5 are excluded. The term β is given in % of the value at saturation, i.e., one.

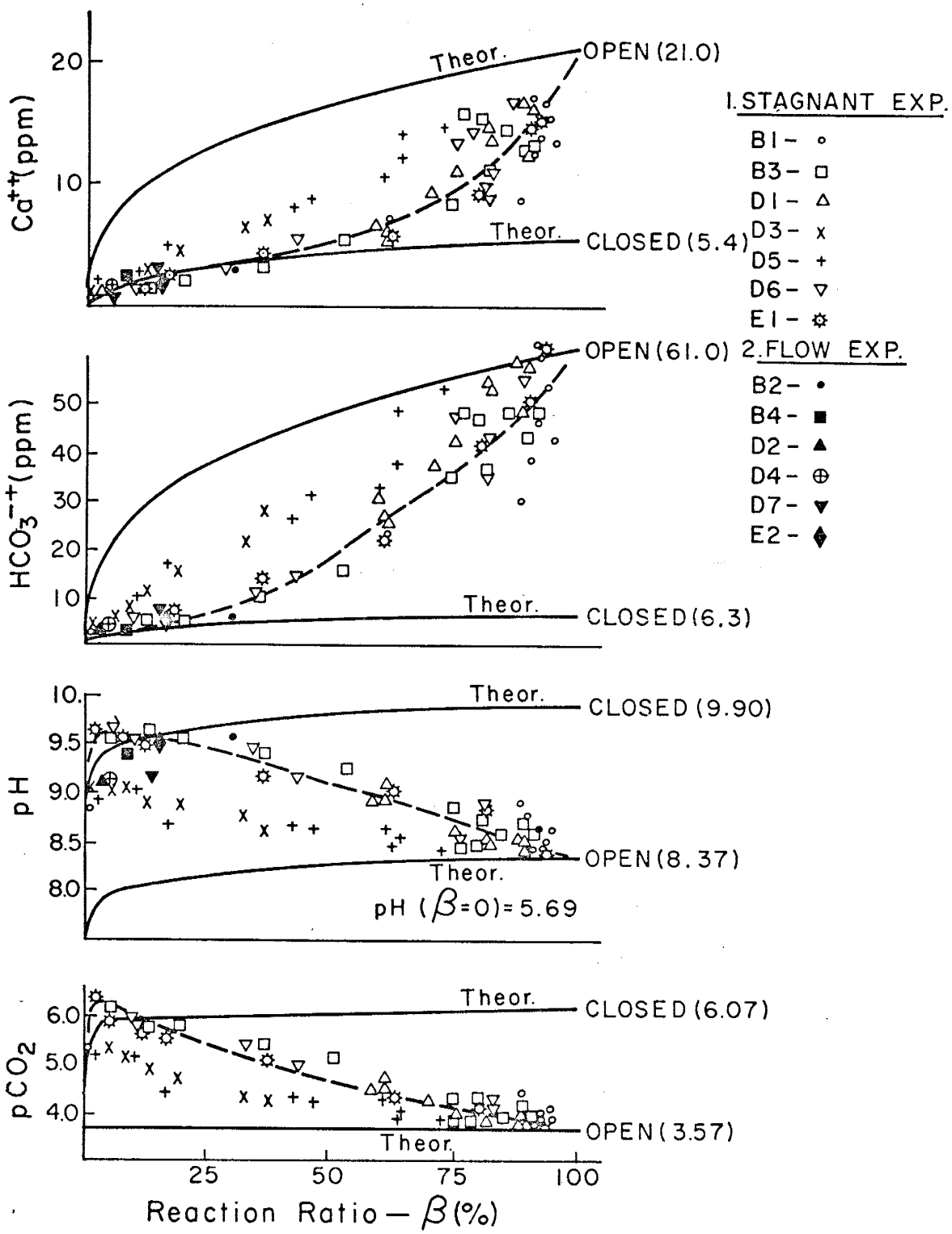
Ca++(ppm)
20
10
Theor.
OPEN (21.0)
Theor.
CLOSED (5.4)
HCO3−+(ppm)
50
40
30
20
10
OPEN (61.0)
Theor.
CLOSED (6.3)
pH
10.
9.5
9.0
8.5
8.0
Theor.
CLOSED (9.90)
OPEN (8.37)
Theor.
pH (β=0)= 5.69
pCO2
6.0
5.0
4.0
Theor.
CLOSED (6.07)
OPEN (3.57)
Theor.
25
50
75
100
Reaction Ratio — β (%)
1. STAGNANT EXP.
B1 - ○
B3 - □
D1 - △
D3 - x
D5 - +
D6 - ▽
E1 - ☼
2. FLOW EXP.
B2 - •
B4 - ■
D2 - ▲
D4 - ⊕
D7 - ▼
E2 - ♦

pCO_2 (= -log CO_2 concentration) and therefore of β. The dashed curves represent the general trend of the observed data. From these curves, it is seen that the open system, should be regarded as closed up to $\beta \leq 25\%$, which corresponds to a pCO_2 (= -log CO_2 concentration) of about 5.4. On the other hand, the observed concentration of the flow type experiments (Fig. 4.3) are in relatively good agreement with the theoretical curves for closed systems, supporting the interpretation of CO_2 diffusion as a rate-limiting step.

4.3 Comparison Between Theoretical Models and Experimental Results

(a) Theoretical Considerations - Two kinetic models are considered for interpreting experimental results: (i) Chemically controlled dissolution, approximated for single-phase solids by (Eq. 2.26):

$$\frac{1}{\nu_i}\frac{dC_i}{dt} \cong k(1 - \beta)$$

or for multimineral assemblages by (Eq. 2.44):

$$\frac{dC_i}{dt} \cong \sum_j [\nu_{ij} k_j (1 - \beta_j)]$$

(ii) The approximate rate equation with respect to the reaction ratio β (Eq. 2.38) valid solely for the dissolution of single phase solids:

$$\frac{d\beta}{dt} \simeq k^*(1 - \beta)$$

which yields (Eq. 2.39):

$$(1 - \beta)/(1 - \beta_o) = \exp[-k^* t]$$

The rate constants of these models were determined for each experiment by scanning for the best fit between computed and measured data; for this purpose the SCEL1 and SCELEX computer programs were used.

The SCEL1 program is similar to the CARMOD-B computer program described previously, adjusted for interpreting the laboratory experiments. Since the dissolution process was governed by the CO_2 exchange through the air-liquid interface the measured, linearily interpolated $CO_2(t)$ function, served as a boundary condition for reconstructing the calcite dissolution experiments.

The SCELEX computer program computes the $\beta(t)$ approximation only. The derivation of formulas used in the SCELEX program is given briefly below:

Consider a perfectly mixed dissolution cell (Fig. 4.4), similar to the experimental set-up of Figure 4.1, having a volume of V, mineral surface area of A_s. A flow rate Q is maintained through the dissolution cell. The reaction rate constant for the $\beta(t)$ approximation is k^*. The reaction ratio of the water entering the cell is β_{in}, and the reaction ratio of the water leaving the cell is $\beta_{out}(t)$. Assuming a perfect mixing, $\beta_{out}(t)$ equals the reaction ratio of the water in the cell $\beta(t)$. It was shown previously that the function can be treated approximately as a tracer.

The "mass" balance for the reaction ratio β requires (Fig. 4.4);

$$V \frac{d\beta}{dt} = Q\beta_{in} + \tilde{k}^* A_s (1 - \beta) - Q\beta \qquad (4.1)$$

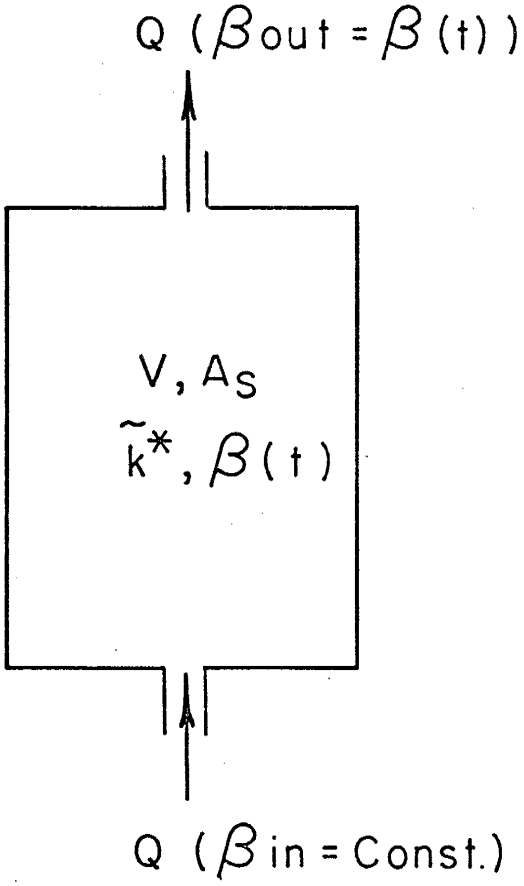

V – Cell volume

A_S – Surface area of the dissolving mineral

$\tilde{k}^*$ – "Corrected" forward reaction rate coefficient

Q – Flow rate through the cell

β – Reaction ratio

t – Time

Figure 4.4 - Perfectly-mixed dissolution cell

where $\tilde{k}^*$ is the specific rate constant per unit volume V and surface area A_s. Defining τ_1 and τ_2 as the hydraulic and chemical residence time respectively, given by:

$$\tau_1 = \frac{V}{Q} \; ; \; \tau_2 = \frac{V}{\tilde{k}^* A_s} = \frac{1}{k^*} \tag{4.2}$$

Substituting τ_1 and τ_2 into equation (4.1) and rearranging the terms we have:

$$\frac{d\beta}{dt} = \frac{\beta_{in}}{\tau_1} + \frac{1}{\tau_2} - \beta \left(\frac{1}{\tau_1} + \frac{1}{\tau_2}\right) \tag{4.3}$$

The solution of equation (4.3) for the initial conditions of $\beta = \beta_o$ at $t = 0$, will be:

$$\beta(t) = \frac{1}{\tau_1+\tau_2} \left[\tau_1+\tau_2\beta_{in} - (\tau_1+\tau_2\beta_{in} - (\tau_1+\tau_2)\beta_o)\exp\left(\frac{\tau_1+\tau_2}{\tau_1\tau_2}t\right)\right] \tag{4.4}$$

For $\beta_{in} = 0$ (distilled water) equation (4.4) becomes:

$$\beta(t) = \frac{1}{\tau_1+\tau_2} \left[\tau_1 - (\tau_1 - (\tau_1+\tau_2)\beta_o)\exp\left(-\frac{\tau_1+\tau_2}{\tau_1\tau_2}t\right)\right] \tag{4.5}$$

After prolonged time ($t \to \infty$), a new reaction ratio, dynamically stable, is attained:

$$\beta(\infty) = \frac{\tau_1}{\tau_1+\tau_2} \tag{4.6}$$

Equations (4.5 and 4.6) serve as the basis for the interpretation of the flow experiments. For measured functions of $\beta(t)$, and for $\beta(\infty)$, one can determine, by trial and error, the chemical residence time τ_2; Knowing

the cell volume V, we can determine the value of $\tilde{k}^*A_s$ from equation (4.2). The surface area A_s of the dissolving mineral, can also be determined from its weight, density, and grain size. The best fit between theoretical and experimental curves was carried out by a computer program, named SCELEXP, which was programmed for this purpose.

For the case of Q = 0 (stagnant experiments) equation (4.3) reduces to the form:

$$V \frac{d\beta}{dt} = \tilde{k}^*A_s(1 - \beta) \tag{4.7}$$

The solution of the equation above for the same initial conditions yields;

$$\beta(t) = 1 - (1 - \beta_o)\exp\left(-\frac{t}{\tau_2}\right) \tag{4.8}$$

Equation (4.8) serves as the basis for interpreting the results of the stagnant type experiments. Again, for a measured function of $\beta(t)$ one determines the value of τ_2 by trial and error, using the SCELEXP program.

(b) Determination of the Rate Constants - The best-fit values of the rate constants, for each one of the experimental runs, was determined by trial and error procedure, facilitated by the two computer programs. Best-fit values were chosen as those having the minimum time weighted averages of simple, absolute, and square-root errors with respect to the measured data, as defined by:

$$\varepsilon_{\underline{simple}} = \frac{\sum_{i=1}^{n} (C_t^i - C_m^i)\Delta t_i}{\sum_{i=1}^{n} \Delta t_i} \tag{4.9}$$

$$\varepsilon_{\underline{\text{absolute}}} = \frac{\sum_{i=1}^{n} \left| C_t^i - C_m^i \right| \Delta t_i}{\sum_{i=1}^{n} \Delta t_i} \qquad (4.10)$$

$$\varepsilon_{\underline{\text{sq. rt}}} = \left(\frac{\sum_{i=1}^{n} (C_t^i - C_m^i)^2 \Delta t_i}{\sum_{i=1}^{n} \Delta t_i} \right)^{1/2} \qquad (4.11)$$

where C_t^i and C_m^i are the theoretical and measured concentrations of the i-th sample respectively; Δt_i is the weighting time interval defined by: $\Delta t_i = 1/2(t_{i+1} - t_{i-1})$; n is the number of samples in the specific run. The same criteria was used also with respect to the β function. Fig. 4.5 shows the results of a typical scan for the best-fit value of $\tilde{k}^* A_s$ related to the β function. The sensitivity of the error curves permits to determine $\tilde{k}^* A_s$ as 1.4 ± 0.1 cc/min; at this value, both absolute and square root errors of β attain their minimum.

Tables 4.2 through 4.4 summarize the best-fit values of $\tilde{k}$, and $\tilde{k}^*$ as determined by the trial and error procedure outlined above. In Figures 4.2, 4.6, 4.7, and 4.8 a comparison is shown between measured and computed results. As can be seen from these figures, the measured data are in relatively good agreement with both theoretical models.

In order to determine the specific rate constants $\tilde{k}$ from the experimental $k = \tilde{k} A_s / V$ product, an estimate of the surface area A_s is made, based on the unit cell of the calcite crystal as a rhombohedron. The shape of the uncleaved crystal can be approximated by a cube, with

Figure 4.5 - Error analysis for the best-fit between experimental results (run B1) and theoretical curves, based on the $\beta(t)$ approximation. The smallest deviation was obtained for $\tilde{k}^* A_s = 1.4 \pm 0.1$ cc/min, where simple (●), absolute (□), and square root (◇) errors attain their minimum.

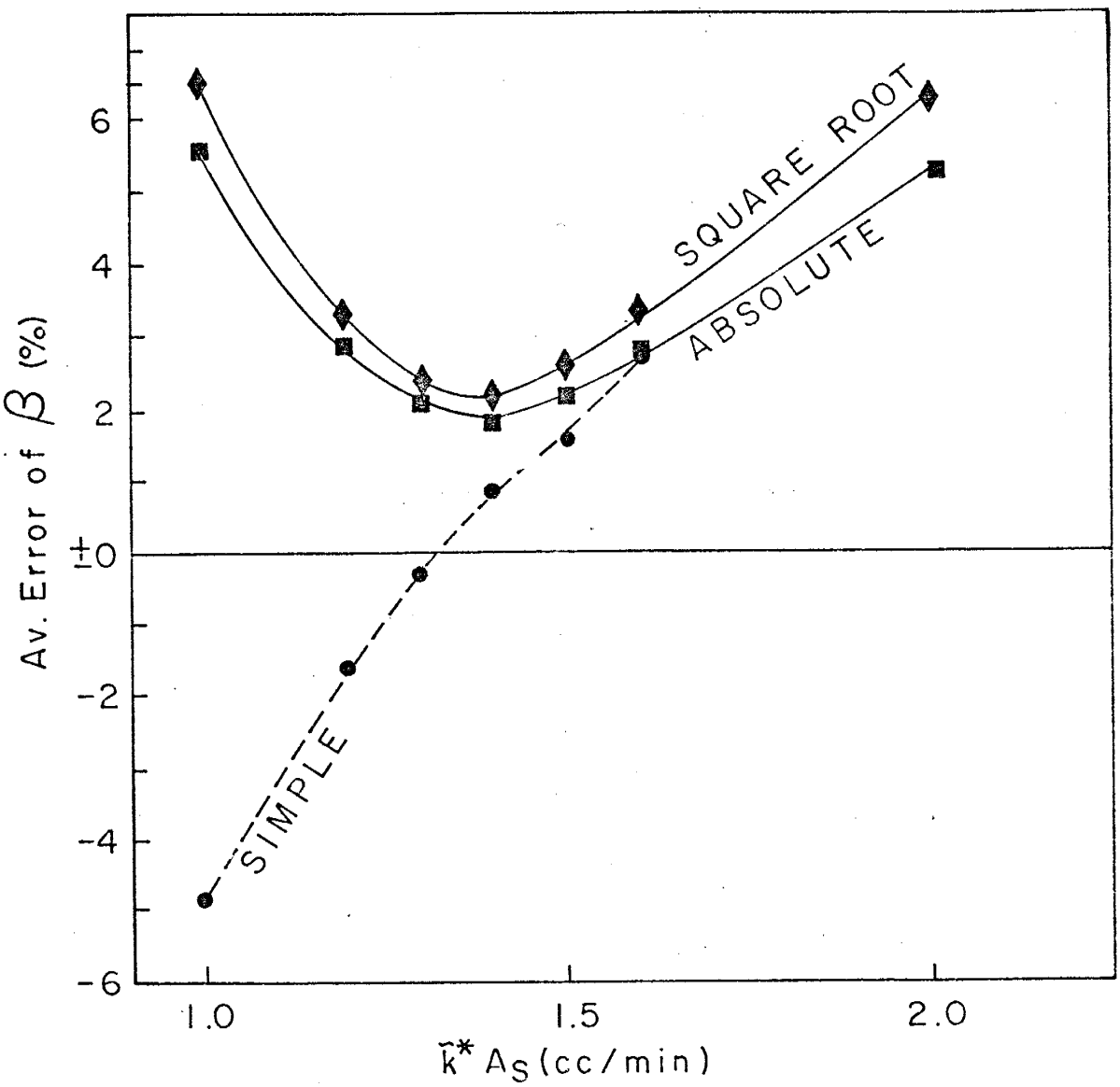
SQUARE ROOT
ABSOLUTE
SIMPLE
Av. Error of β (%)
6
4
2
±0
-2
-4
-6
1.0
1.5
2.0
k̃* As (cc/min)

TABLE 4.2 - DETERMINATION OF k and $\tilde{k}(= k\ V/A_s)$
FOR THE STAGNANT EXPERIMENTS (CHEMICALLY-CONTROLLED PROCESS)

Run	Mineral[1]	d	W	A_s[2]	V	$kx10^7$	$\tilde{k}x10^8$	$(\tilde{k}A_s/W)x10^6$
		mm	gram	cm^2	cc	M/min	M-cm/min	M-cc/min/gr
BI	C	0.0635	17.6	8650	875	3.70	3.74	18.4
B3	C	0.0635	17.6	8650	875	3.75	3.78	18.6
D1	C	0.1775	14.3	2600	875	0.90	3.01	5.3
D3	C	0.1775	14.8	2600	875	1.83	6.20 ?	10.8 ?
D5	C	0.1775	14.8	2600	875	1.48	4.99	8.75
D6	C	0.1775	67.8	1900	875	3.20	2.69	4.14
E1	C	0.1255	31.4	7800	875	2.35	2.64	6.55
H1	G	0.0780	15.0	6000	1750	7745.	22,600.	90,000.
I1	C+G	0.1255 / 0.0780 [3]	155.0 / 15.0 [3]			5.80 / 7745. [4,3]		

Notes - (1) C = calcite; G = gypsum (2) Determined from equation (4.14)

(3) The upper figure for calcite; the lower for gypsum.

(4) Based on the values of $(\tilde{k}A_s/W)$ for Runs E1 and H1.

TABLE 4.3 - DETERMINATION OF $\tilde{k}^*A_s$ - FOR THE STAGNANT EXPERIMENTS

(The β Approximation)

Run	Grain Size d	Weight W	$\tilde{k}^*A_s$	A_s (1)	$\tilde{k}^*$ (1)
	(mm)	(gr)	(cc/min)	(cm^2)	(cm/min $\times 10^4$)
B1	0.0635	17.6	1.4	8650	1.62
B3	0.0635	17.6	1.3	8650	1.50
C1	0.0635	17.6	1.1	8650	1.28
D1	0.1775	14.8	0.32	2600	1.23
D3	0.1775	14.8	0.32	2600	1.23
D5	0.1775	14.8	0.32	2600	1.23
D6	0.1775	67.8	1.0	11900	.84
E1	0.1255	31.4	1.0	7800	1.28

Note: (1) Based on eq. (4.14)

TABLE 4.4 - DETERMINATION OF $\tilde{k}^*$ FOR THE FLOW EXPERIMENTS

(The β Approximation)

RUN	Grain Size d	Weight W	Q	τ_1	$\beta_{(\infty)}$	$\tilde{k}^* A_s$	A_s	$\tilde{k}^*$
	(mm)	(gr)	(cc/min)	(min)	(%)	(cc/min)	(cm^2) 10^{-3}	(cm/min) 10^4
B2	0.063	17.6	3.7	278	28	1.5	8.65	1.73
B4	0.063	17.6	16.1	64	8	1.5	8.65	1.73
D2	0.1775	14.8	11.5	89	3	0.35	2.60	1.35
D4	0.1775	14.8	6.4	160	5	0.40	2.60	1.54
D7	0.1775	67.8	7.2	143	14	1.20	11.9	1.00
E2	0.1255	31.6	5.4	190	15	1.00	7.8	1.28

Figure 4.6 - Comparison between experimental results (Run D5) and theoretical curves, for $k_c = 1.48 \times 10^{-7}$ M-min^{-1}, the discontinuity of theoretical curves represents the dilution caused by sampling. Stagnant experiment for calcite.

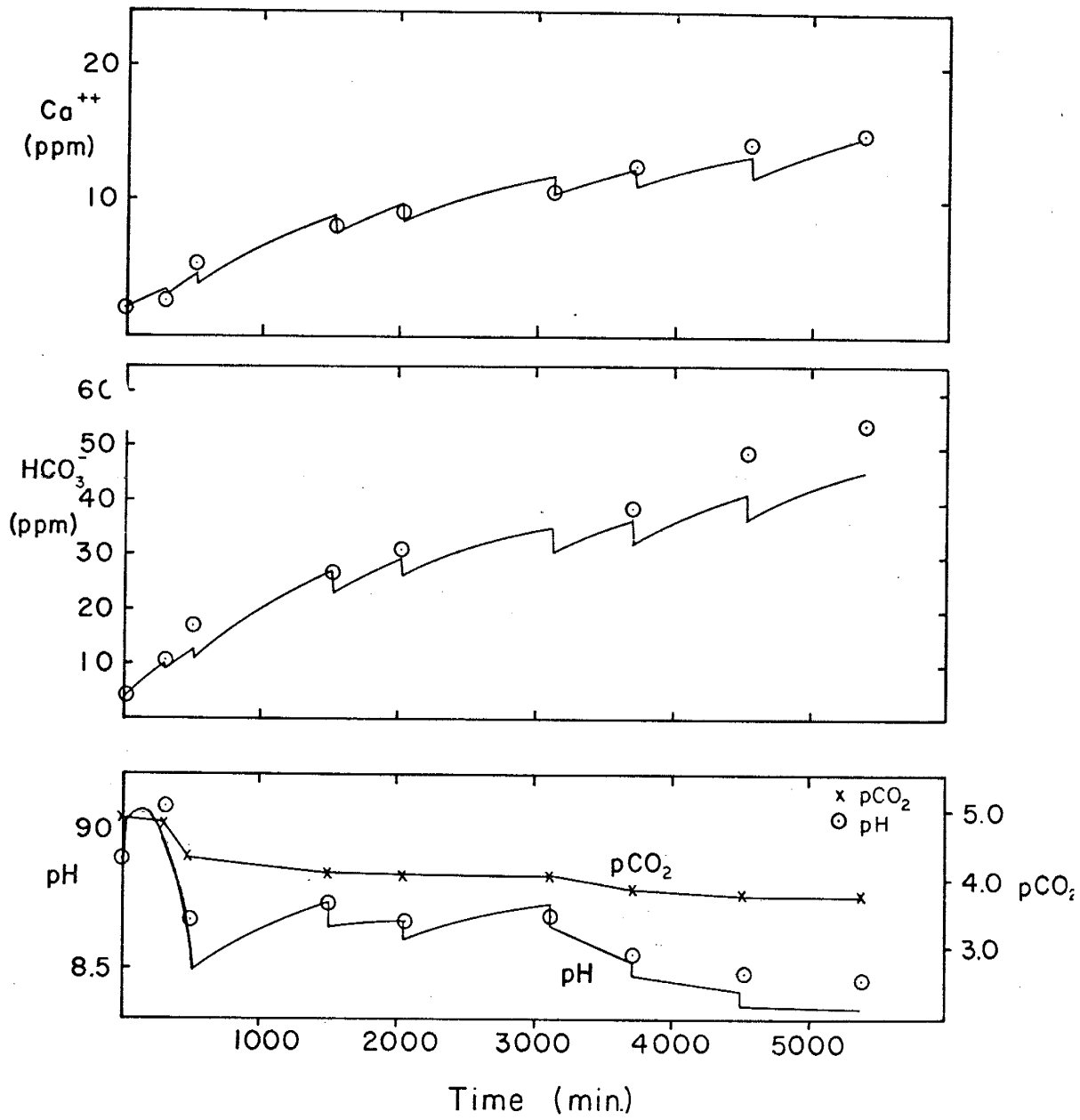
20
Ca^{++}
(ppm)
10
60
HCO_3^-
50
40
(ppm)
30
20
10
90
pH
8.5
x pCO_2
⊙ pH
pCO_2
pH
5.0
4.0
3.0
pCO_2
1000
2000
3000
4000
5000
Time (min.)

Figure 4.7 - Comparison between experimental results (Run H1) and theoretical curves (k_g = 7.745 x 10^{-4} M-min^{-1}) for the dissolution of gypsum. The model fails to reproduce the first two minutes of the reaction, which suggests that a different model is needed at the beginning of reaction, or experimental problems.

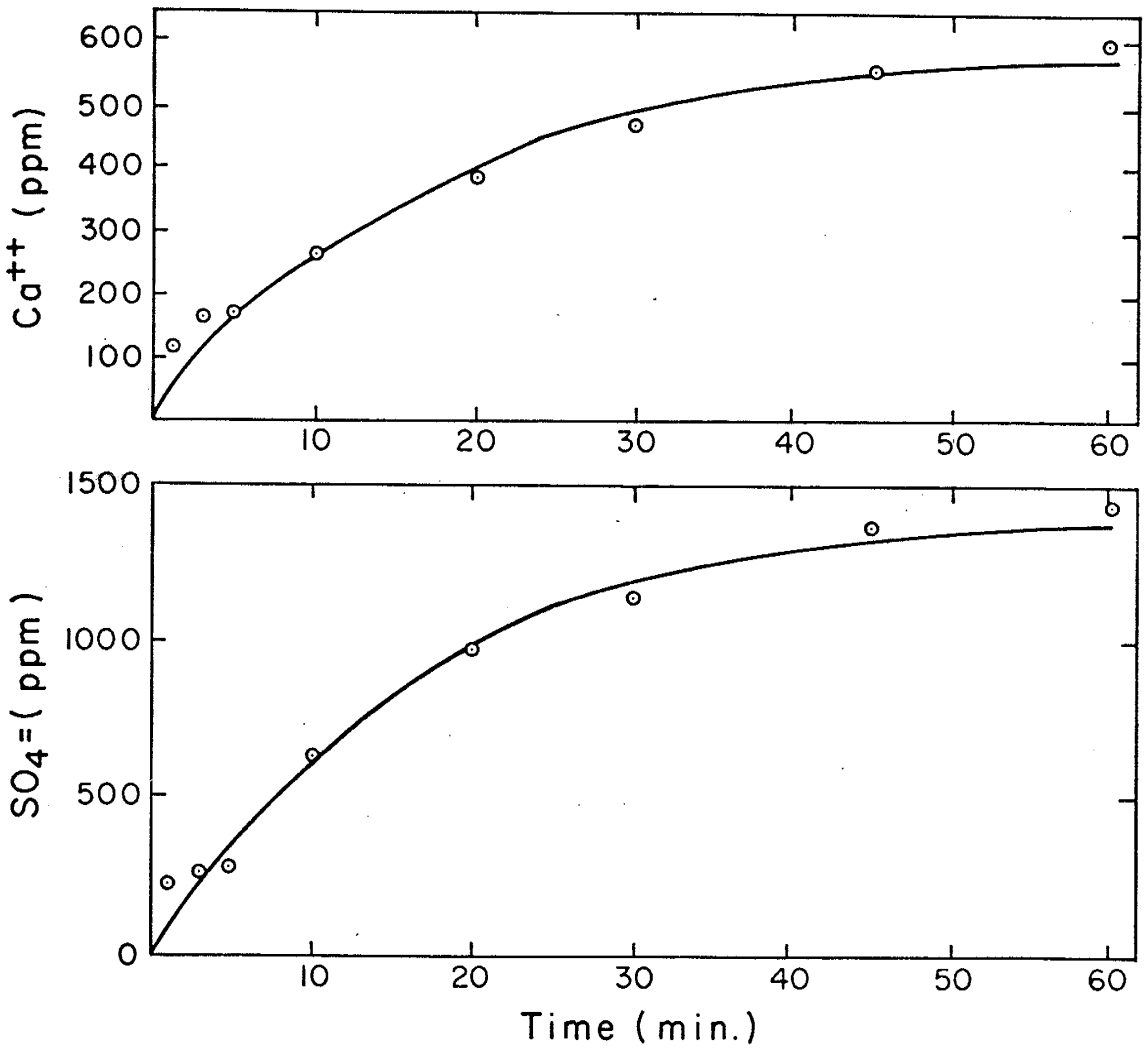
600
500
400
300
200
100
Ca^{++} (ppm)
10
20
30
40
50
60
1500
1000
500
0
$SO_4^=$ (ppm)
10
20
30
40
50
60
Time (min.)

Figure 4.8 - Comparison between experimental results (Run I1) and theoretical curves for the simultaneous dissolution of calcite and gypsum. Theoretical curves were determined for $k_c = 5.8 \times 10^{-7}$ M-min^{-1}, and $k_g = 7.75 \times 10^{-4}$ M-min^{-1}. The rate constants for both minerals are based on the experimental results of runs H1 and E1 (see Tables 4.2 and 4.3). The supersaturation with respect to calcite is explained by kinetic competition between the two dissolving minerals. Notice the change in time-scale between 200 and 500 min. pCO_2 = (-log CO_2 concentration).

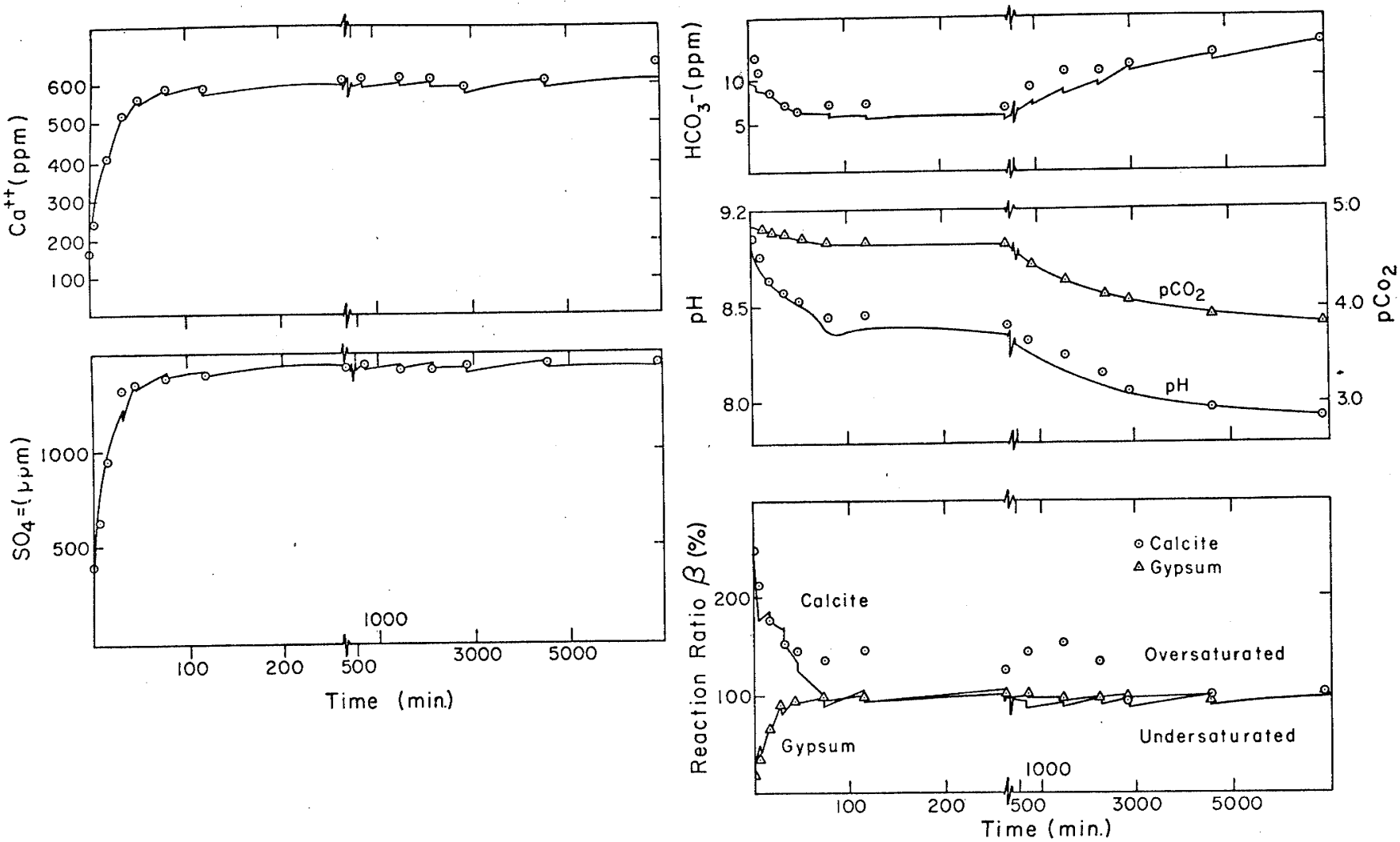
Ca++(ppm)
600
500
400
300
200
100
SO4=(μm)
1000
500
100
200
500
1000
3000
5000
Time (min.)
HCO3-(ppm)
10
5
9.2
8.5
8.0
pH
pCO2
5.0
4.0
3.0
Reaction Ratio β (%)
200
100
Calcite
Gypsum
Oversaturated
Undersaturated
Time (min.)

diagonal being equal to the average seive opening d. The volume V_o of a single particle will be then:

$$V_o = (d/\sqrt{2})^3$$

The surface area of a single particle is:

$$(A_s)_o = 6(d/\sqrt{2})^2$$

Considering the density of calcite to be 2.72 cc, the number of particles N per gram of calcite will be determined by:

$$N = 1/[2.72\ x(d/\sqrt{2})^3]$$

The specific surface area $\tilde{A}_s$ per gram will be then:

$$\tilde{A}_s = N(A_s)_o = 3.12/d$$

and finally, the surface area in cm^2 of W grams of calcite, having the average grain size of d (cm) is given by:

$$A_s = 3.12\ W/d \qquad (4.14)$$

It should be emphasized, however, that although the relative dimension of the calcite crystal may be well known, the cleavage caused by crushing the milling procedures might increase the specific area considerably.

The computed values of A_s, and the specific rate constants are summarized in Tables 4.2 through 4.4; the computed values of $\tilde{k}$ and $\tilde{k}^*$ for calcite vary within the limits of $2.64 - 6.20 \times 10^{-8}$ M-cm/min

and 0.84 - 1.73 x 10^{-4} cm/min, respectively; the respective average values are: (3.86 ± 1.21) x 10^{-8} M-cm/min, and (1.35 ± 1.25) x 10^{-4} cm/min. The computed specific rate constant $\tilde{k}$ of the gypsum dissolution experiment (Run H1) is 2.26 x 10^{-4} M-cm/min. The computed rate constants for both gypsum and calcite were used to determine the theoretical curves for the simultaneous dissolution experiment (Run I1).

In Figures 4.9 the specific reactivity ($\tilde{k}A_s/W$) of calcite is plotted against the average grain size d; W is the calcite weight. As expected, the plot can be approximated by a hyperbolic function with respect to d (Equation 4.14). The theoretical curves plotted in these curves are based on the average values given above, and on equation (4.14) which relates the specific surface area A_s/W to the average grain size d.

4.4 The Performance of Kinetic Models

The performance of the two kinetic equations (2.36 and 2.38) should be judged by considering three main criteria: (i) The ability to reproduce experimental data within a reasonable accuracy, using a single rate constant for each experimental run, (ii) the consistency of the computed rate constants under varying experimental conditions, and (iii) the computed rate constants should agree with relevant physical and chemical data, whenever available.

Both the approximate form of the Law of Mass-Action (Eq. 2.26), and the $\beta(t)$ approximation (Eq. 2.38), are suitable for the purpose of the single mineral dissolution experiments (Runs B1 to H1). Only the first model (Eq. 2.44) can be used for describing the dissolution of multimineral assemblages. It should be mentioned, however, that as far

Figure 4.9 - Specific chemical reactivities $\tilde{k}A_s/W$, and $\tilde{k}^*A_s/W$, as a function of the average grain size d, computed for chemically-controlled kinetics (a) and the $\beta(t)$ approximation (b) respectively.

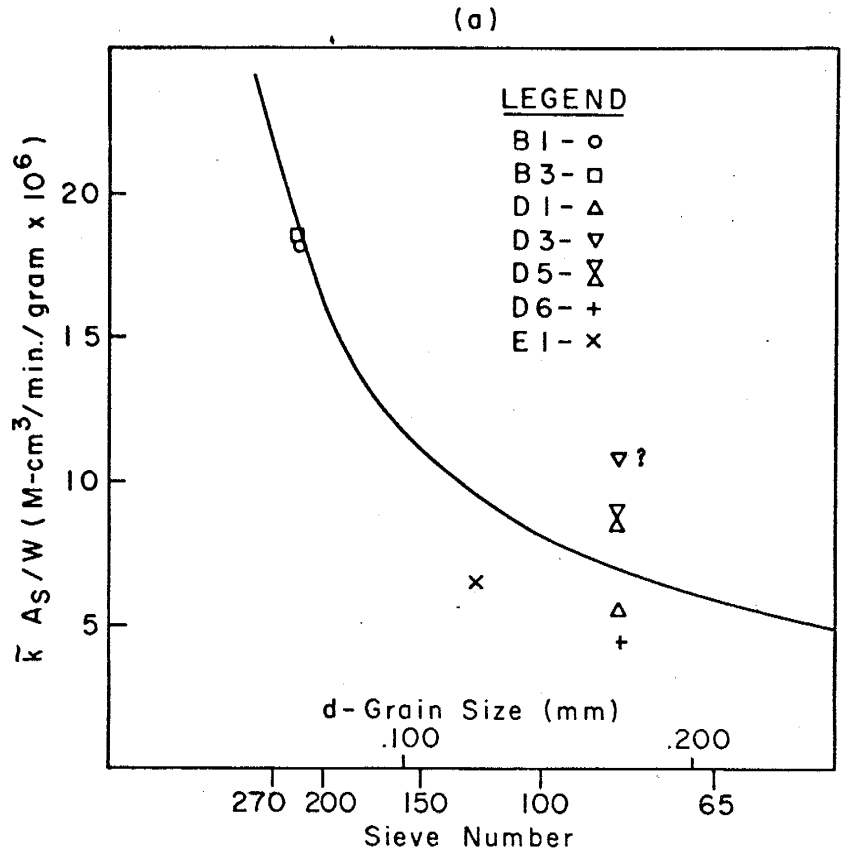
(a)
LEGEND
B1 - o
B3 - □
D1 - △
D3 - ▽
D5 - ⧖
D6 - +
E1 - ×
▽?
$\bar{k}$ A_S/W (M-cm^3/min./gram x 10^6)
20
15
10
5
d-Grain Size (mm)
.100
.200
270 200 150 100 65
Sieve Number

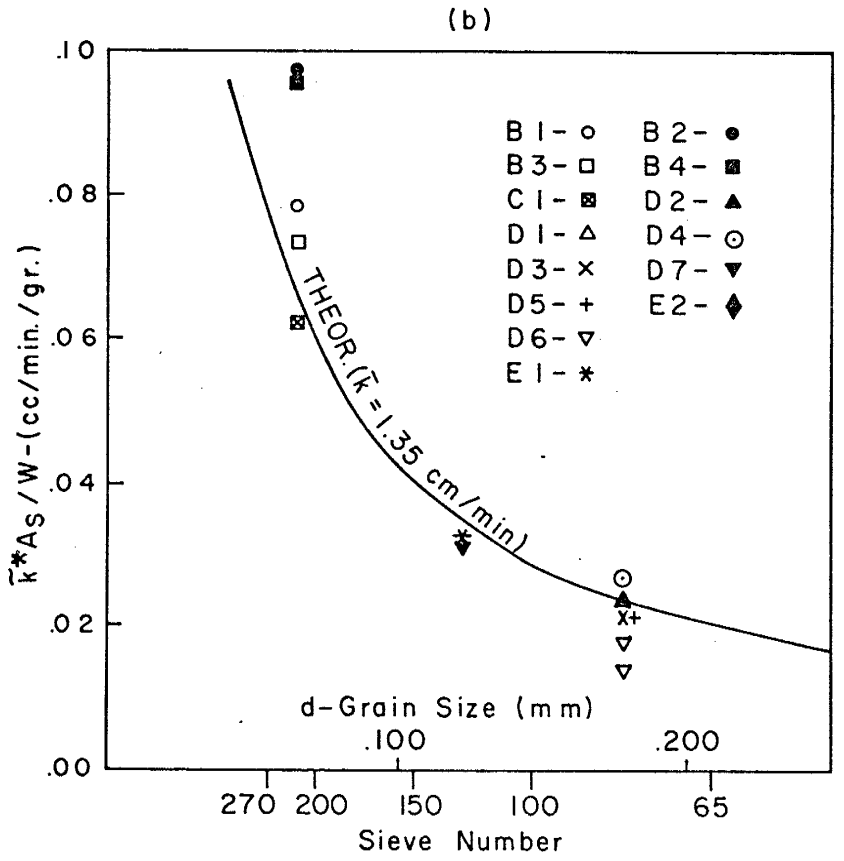
(b)
B1 - o
B2 - ●
B3 - □
B4 - ■
C1 - ⊠
D2 - ▲
D1 - △
D4 - ⊙
D3 - ×
D7 - ▼
D5 - +
E2 - ◆
D6 - ▽
E1 - *
THEOR. ($\bar{k}$ = 1.35 cm/min)
$\bar{k}$*A_S/W-(cc/min./gr.)
.10
.08
.06
.04
.02
.00
d-Grain Size (mm)
.100
.200
270 200 150 100 65
Sieve Number

as the first criterion is considered, all reaction rate equations discussed in Chapter 2, except the logarithmic regression were suitable for the reproduction of experimental data for single minerals.

The consistency of the remaining two equations (2.26 and 2.38) can be rated according to the relative spread of their computed rate constants (i.e., the standard deviation of computed values divided by the mean). Following this rule, the best performing model for describing the dissolution of single minerals is the $\beta(t)$ approximation; its relative spread is about 18%, as compared to 31% for the approximation based on the Law of Mass Action. The relative spread for the Nernst equation and the parabolic regressions, rejected in Chapter 2, is 37% and 50%, respectively.

It is rather surprising that the rough approximation for the $\beta(t)$ function yielded the best performing model. This is partially explained by the fact that the calcite dissolution was governed in these experiments by the rate of CO_2 diffusion through the air-liquid interface. The diffusion rate, according to Fick's first law is a first order process with respect to the differences between the CO_2 partial pressure in the atmosphere and in the solution; this may reduce the rather complicated kinetics of the calcite dissolution to a first order reaction, and as mentioned before, the $\beta(t)$ function is the exact solution for the case of a first order reaction.

5. EVALUATION OF FIELD DATA - (I) THE LIMESTONE AQUIFER OF CENTRAL FLORIDA

The limestone aquifer of central Florida was chosen as an example of evaluating kinetic aspects of field data in order to estimate chemical residence times. This aquifer has the advantage of being relatively large in areal extent (roughly-half million km^2), and relatively homogeneous on that scale. Carbonate equilibria and the ^{14}C distribution, as related to the groundwater flow pattern have been studied (Back et al., 1967; Back and Hanshaw, 1970, 1971; Hanshaw et al., 1965a, 1965b, 1965c). Groundwater ages were presented based on both hydrological and ^{14}C data. The availability of age estimates and water quality data allows the study of the dissolution process in the field by using the kinetic approach used in previous chapters for closed water systems.

This field test is to compare the kinetic model developed in earlier chapters against spatially distributed chemical data. This is done by using residence time based on hydrologic data. The age of samples is then plotted against their chemical composition after correcting for interionic effects. A curve is fit to these data. The curve is the kinetic expression and the rate constant is adjusted for best-fit. Thus, a calibration of chemical composition against time is achieved. This, if small error results, demonstrates the validity of the form of the kinetic model, and develops the field rate constant. Calibrating on the basis of a few samples and then calculating the chemical residence time for the rest of the aquifer is the aim of the Florida field test. After the chemical residence time has been calculated for all available samples, this residence time or age is compared to ages of samples based on ^{14}C.

5.1 Hydrogeological Background

The principal aquifer consists of limestones of Tertiary age, which contain minor amounts of dolomite, gypsum, and disseminated quartz sand (Hanshaw, et al., 1965a). The principal aquifer is overlain by confining beds of Miocene age, chiefly clay of the Hawthorn Formation (Back and Hanshaw, 1970, Fig. 4). To the north the confining layers are thin to non-existent allowing major recharge in this area. The flow pattern within the aquifer is dominated by two groundwater mounds (Fig. 5.1). The natural outlets of the aquifer system are the Atlantic Ocean and the Gulf of Mexico, as well as some springs in the northern part of the area. The average gradient of the potentiometric surface is about 1 meter per kilometer (Hanshaw, et al., 1965b). The transmissivity of the aquifer is about 3000 m^2 per day or about 250,000 gal/day/ft. The average porosity is 10% and the thickness 300 m. Based on these estimates, the groundwater velocity is roughly 10 cm per day or 100 ft per year.

Sea-water underlies the entire Florida peninsula, from near sea-level at some parts of the coast, to about 700 m below sea-level in central Florida. The interface between salt-water and fresh-water forms one of the boundaries of the aquifer, both hydrologically and geochemically.

5.2 Chemical Characteristics of Groundwater

The published data (Hanshaw et al., 1965a, Hanshaw and Back, 1970) used for this study are 20 chemical analyses (Appendix E) collected from 18 wells (Fig. 5.1). Figure 5.2 shows the areal distribution of Ca, Mg, SO_4, HCO_3, pH, and pCO_2 in the aquifer. The distribution of the reaction ratios β_c, β_d, and β_g with respect to calcite, dolomite, and gypsum

Figure 5.1 - Potentiometric map of central Florida showing location of sampling points, areas of major recharge, and general pattern of flow (dashed arrows). Circled points represent wells used for the calibration of the kinetic model. Notice the relative stagnancy of groundwater in the vicinity of wells 7N and 6N (Map from Back and Hanshaw, 1970, 1971).

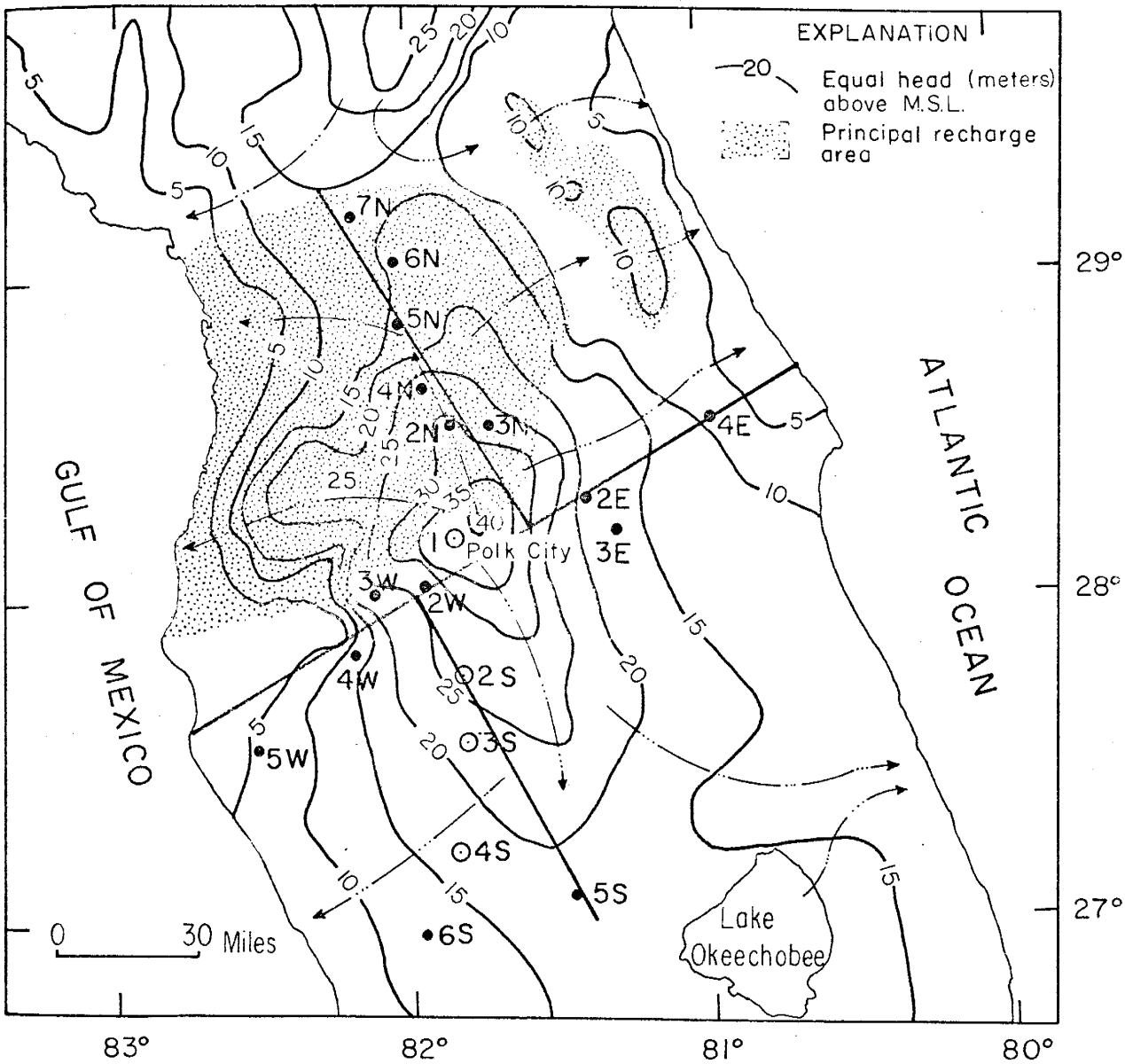
EXPLANATION
20
Equal head (meters) above M.S.L.
Principal recharge area
GULF OF MEXICO
ATLANTIC OCEAN
7N
6N
5N
4N
3N
2N
4E
2E
3E
1O
Polk City
3W
2W
4W
2S
3S
4S
5S
5W
6S
Lake Okeechobee
0
30 Miles
29°
28°
27°
83°
82°
81°
80°

respectively, as computed by the FILDAT computer program (Appendix G) are shown in Fig. 5.3. Most of the samples are supersaturated with respect to calcite. Computation of the dolomite reaction ratio for pK (25°C) = 17.0, instead of 16.5 would cause the samples to be oversaturated with respect to dolomite.

The supersaturation with respect to calcite was related by Back and Hanshaw (1971) to the entropy produced from chemical and physical processes taking place in the groundwater system. This phenomenon will be related here to kinetic competition between gypsum, dolomite and calcite.

The distribution of aqueous species (Fig. 5.2) reflects the general pattern of groundwater flow in the aquifer. The minimum concentration of dissolved species is attained on the crest of the principal groundwater mound. The concentration increases in the direction of flow, thus being some function of the residence time of the groundwater in the aquifer.

Figure 5.4 is a modified Piper's diagram. The dissolution process does not alter the dominancy of calcium and magnesium among cations. The sulphate content increases more rapidly than carbon species. As a result groundwater is transformed gradually from bicarbonate to sulphate water. Samples 5S, 6S and 4E are contaminated by sea-water (Fig. 5.4) and are excluded from the dissolution study.

The increase of dissolved CO_2 concentration in the direction of flow suggests consideration of CO_2 formation in addition to atmospheric and soil CO_2 contributions in the recharge area. Under ultimately closed conditions, where CO_2 variations are governed by the dissolution

Figure 5.2 - Calcium, magnesium, sulphate, bicarbonate, pH, and computed pCO_2 (=-log CO_2 concentration) maps of the limestone aquifer in central Florida. All values, except pH and pCO_2, are in ppm. Circled points indicate samples used for the calibration of the kinetic model. Values within brackets indicate mixtures with saline water, excluded from the dissolution study. Derived from data published by Back and Hanshaw (1970, 1971). Chemical data are summarized in Appendix E. Dashed arrows indicate the general pattern of groundwater flow. Contours were drawn by hand based solely on saw field data.

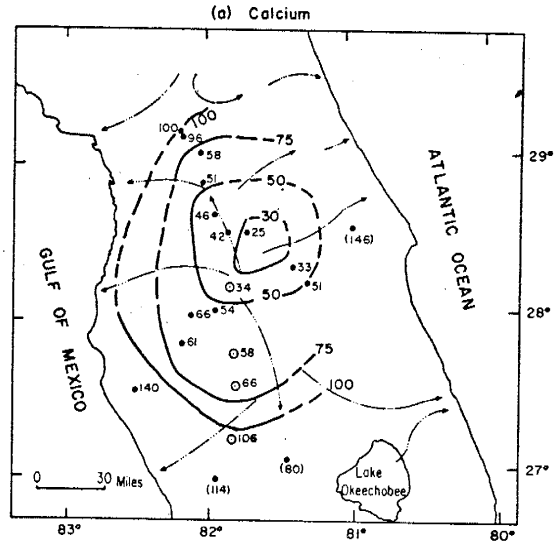
(a) Calcium
GULF OF MEXICO
ATLANTIC OCEAN
Lake Okeechobee
0 30 Miles
83°
82°
81°
80°
29°
28°
27°

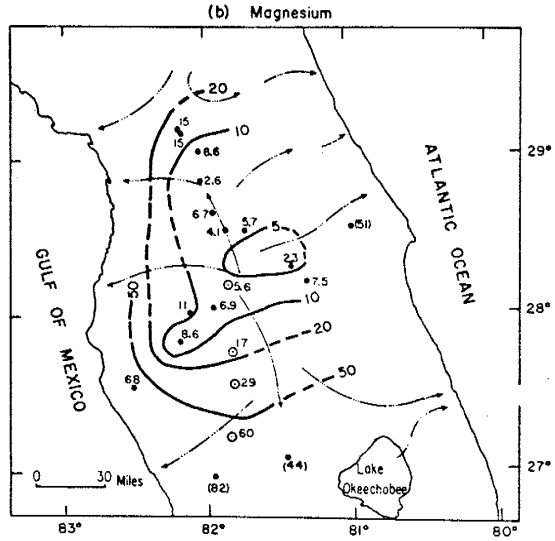
(b) Magnesium
GULF OF MEXICO
ATLANTIC OCEAN
Lake Okeechobee
0 30 Miles
83°
82°
81°
80°
29°
28°
27°

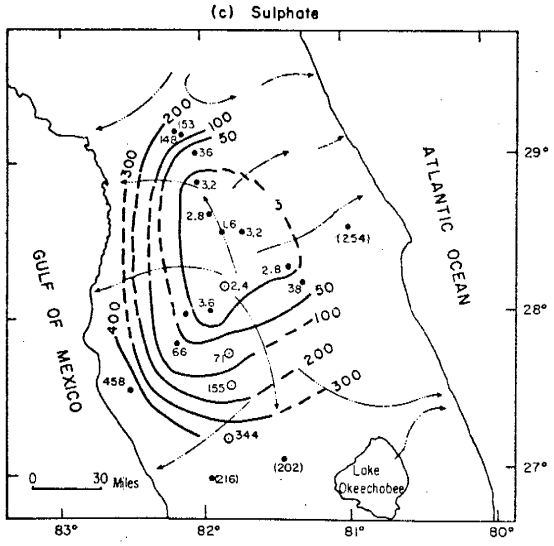
(c) Sulphate
GULF OF MEXICO
ATLANTIC OCEAN
Lake Okeechobee
0 30 Miles
83°
82°
81°
80°
29°
28°
27°

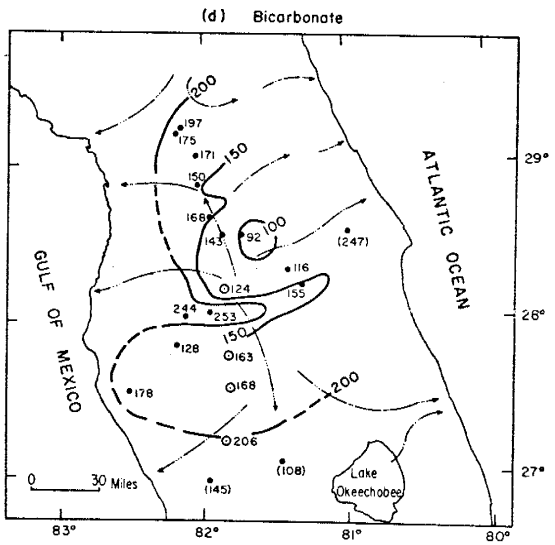
(d) Bicarbonate
GULF OF MEXICO
ATLANTIC OCEAN
Lake Okeechobee
0 30 Miles
83°
82°
81°
80°
29°
28°
27°

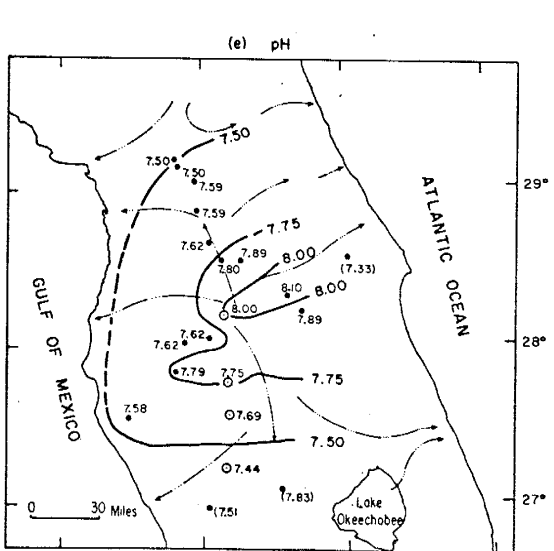
(e) pH
GULF OF MEXICO
ATLANTIC OCEAN
Lake Okeechobee
0 30 Miles
83°
82°
81°
80°
29°
28°
27°

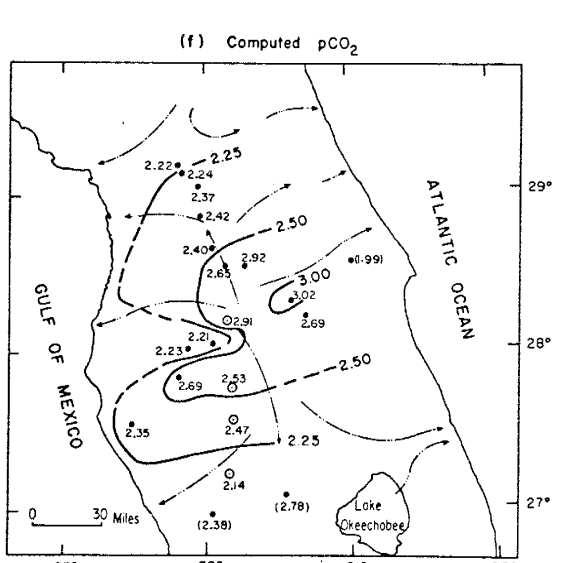
(f) Computed pCO_2
GULF OF MEXICO
ATLANTIC OCEAN
Lake Okeechobee
0 30 Miles
83°
82°
81°
80°
29°
28°
27°

Figure 5.3 - Computed reaction ratios with respect to calcite, dolomite and gypsum. Reaction ratios with respect to dolomite are based on pK_d (25°C) = 16.5, which is 0.5 pK lower than the conventional value. Circled points indicates samples used for the calibration of the kinetic model. Values within brackets indicate mixtures with saline water. Notice the rise and decline of β_c, the reaction ratio with respect to calcite, along the north-south streamline. The same trend is predicted by the kinetic model. Values for β are in % of saturation value (i.e., one).

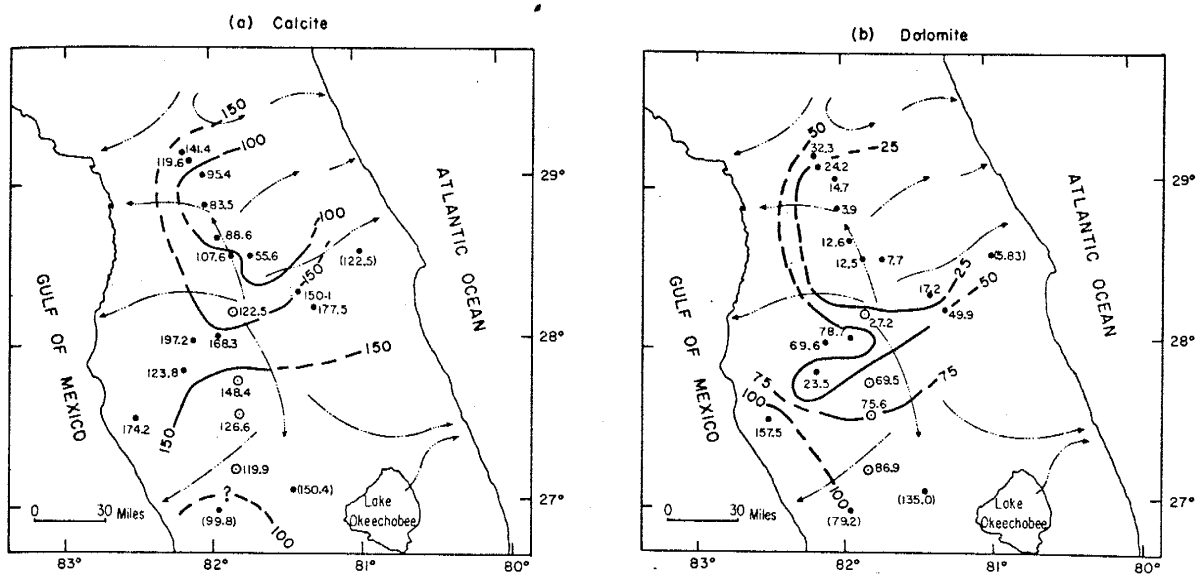
(a) Calcite
(b) Dolomite
GULF OF MEXICO
ATLANTIC OCEAN
Lake Okeechobee
0 30 Miles
83°
82°
81°
80°
29°
28°
27°

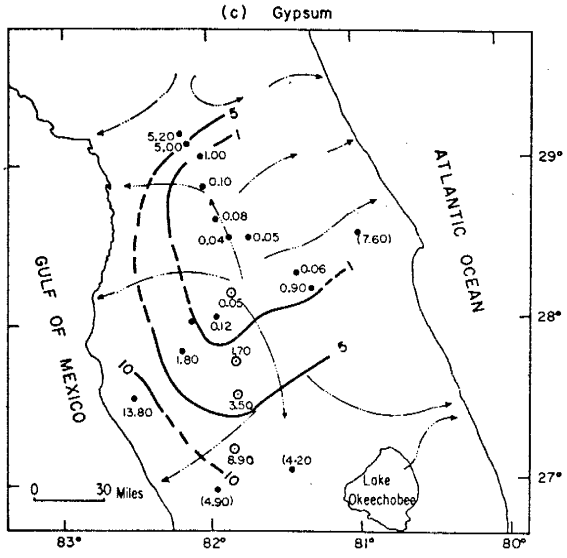
(c) Gypsum
GULF OF MEXICO
ATLANTIC OCEAN
Lake Okeechobee
0 30 Miles
83°
82°
81°
80°
29°
28°
27°

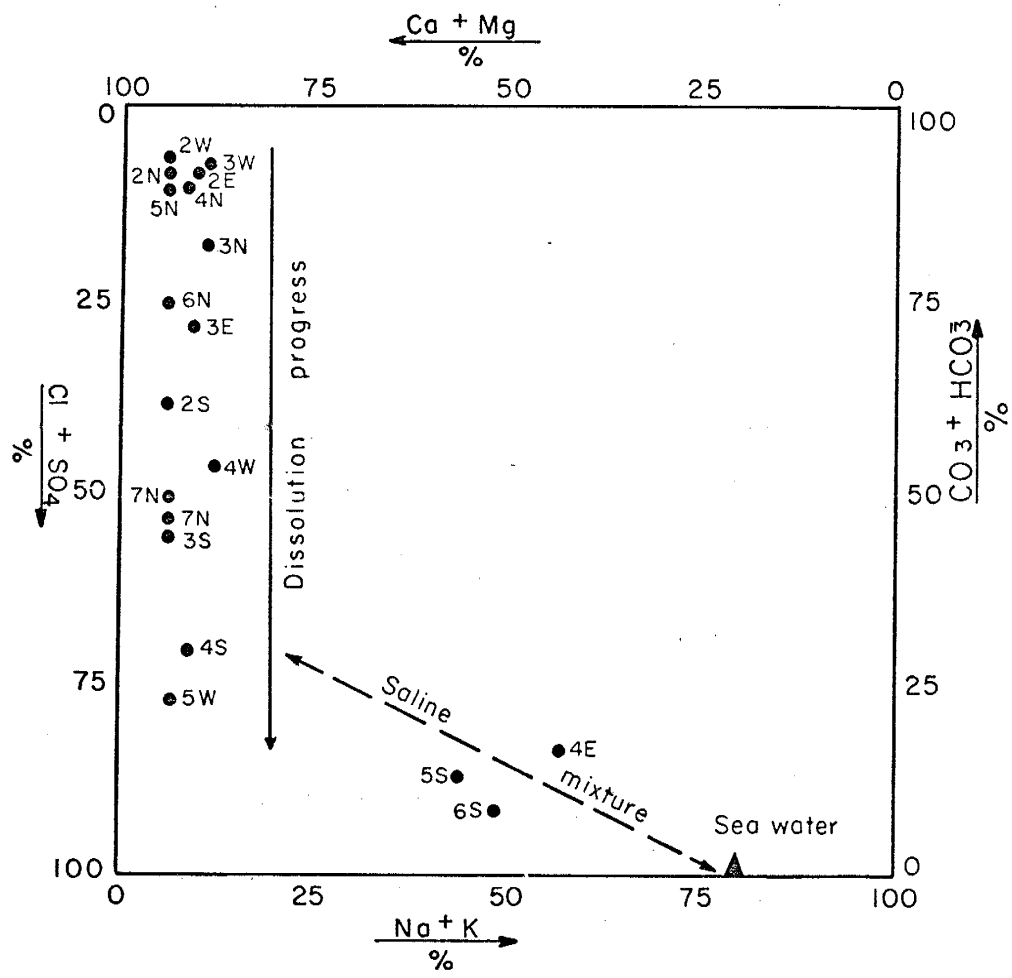

Figure 5.4 - Chemical characteristics of the Florida groundwater (modified Piper diagram). Units are % total cation or anion in millequivalents.

process of calcite only, one should expect the decrease dissolved CO_2 concentration with the progress of the dissolution process (Appendix C).

5.3 Calibration of the Kinetic Model

Age estimates, both hydrologic and ^{14}C, are available for 4 groundwater samples (Hanshaw et al., 1965a) collected along the north-south streamline (Fig. 5.1). These estimates allow a test of the kinetic model, simulated by the CARMOD-B computer program (Appendiz G) under field conditions. The age estimates, based on hydrologic data only and the corresponding chemical data are summarized in Table 5.1.

The kinetic model was calibrated by obtaining the best-fit between computed and measured data for the four samples of Table 5.1. Concentration-time curves were computed by following the steps listed in Chapter 3. Computed pCO_2, as well as the measured temperature and the chloride and sodium concentration serves as a time-varying boundary conditions for the dissolution process. Due to absence of better information, the time varying boundary conditions listed above, were interpolated linearily, with respect to the estimated residence time between each two adjacent wells. The best-fit kinetic rate constants were determined by curve fittings, with the aid of the CARMOD-B computer program to be $k_c = 6.5 \times 10^{-7}$, $k_d = 1 \times 10^{-6}$, and $k_g = 2.25 \times 10^{-7}$ moles per liter per year, for calcite, dolomite, and gypsum, respectively. Best-fit values were chosen as those having the minimum time-weighted average errors with respect to the measured data (see Chapter 4).

Figure 5.5 and Table 5.2 compare the measured and computed data. Most errors (Table 5.2) are within the precision of conventional chem-

TABLE 5.1 - CHEMICAL COMPOSITION OF GROUNDWATER AND RESIDENCE TIME IN THE LIMESTONE AQUIFER OF FLORIDA[1]

Well	Distance between wells[1] (km)	Groundwater velocity[2] (m/yr)	Residence time (years)	Chemical Data[1]						
				Ca (ppm)	Mg (ppm)	SO_4 (ppm)	HCO_3 (ppm)	pH	pCO_2	Temp. (°C)
1 - Polk City			0	34.	5.6	2.6	124	8.00	2.91	23.8
	45.0	10.								
2S - Fort Meade			4500	56.	17.	71.	163	7.75	2.53	26.6
	22.5	7.								
3S - Wauchulla			7700	66.	29.	155.	168	7.69	2.47	25.4
	37.0	5.								
4S - Arcadia			15100	106.	60.	344.	206	7.44	2.14	26.3

Notes: (1) Derived from data published by Hanshaw et al (1965a, 1965b)

(2) Estimated by Hanshaw et al (1965a)

ical analyses. Figure 5.6 shows the results of a sensitivity test of the calibrated model with respect to the deviations between measured and computed concentrations. In this test the deviations of the calibrated model are compared to the corresponding deviations, caused by varying each one of the calibrated rate constants separately. A consistent increase of errors, caused by these variations will indicate that the calibrated rate constants are rather close to their optimal combination. The results of this test can serve also as a qualitative basis for rating the accuracy of the computed constants; high sensitivity will indicate high accuracy and vice-versa. Applying this criterion for the Florida aquifer, the gypsum rate constant seems to be the most accurate followed by the calcite and dolomite rate constants.

Figure 5.7 shows the results of the sensitivity test with respect to the dolomite equilibrium constant. The increase of the equilibrium constant from the conventional value of $10^{-17.0}$ to $10^{-16.5}$ was necessary in order to reproduce the observed magnesium concentrations. The results of the sensitivity test supports the use of $K_{dol}(25°C) = 10^{-16.5}$.

The theoretical curves shown in Figure 5.5 were computed by assuming the carbonate species are equilibrated with a CO_2 source other than the dissolution of carbonate minerals, varying in concentration with time.

A computer analysis based on the assumption the groundwater is disconnected from any CO_2 sources after leaving the recharge area, resulted in decrease of dissolved CO_2 concentration and decrease in pH, as well as a decrease of calcium and magnesium ions, which contradicts field measurements. This contradiction supports the previous assumption

Figure 5.5 - Comparison between field data (points) and theoretical curves, as computed for $k_c = 6.5 \times 10^{-7}$, $k_d = 10^{-6}$, and $k_g = 2.25 \times 10^{-7}$ M/yr. The computed dissolved CO_2 concentration as determined from pH and HCO_3^- field measurements, serves as a boundary condition. The calibration of the kinetic model is based on four wells along the north-south streamline (Fig. 5.1), for which both hydrologic residence-time and detailed chemical data are available (Hanshaw, et al., 1965). Notice the theoretical rise and decline of the calcite reaction ratio β_c, confirmed also by field data (Fig. 5.3). The term β is in % of the value at saturation, i.e., one.

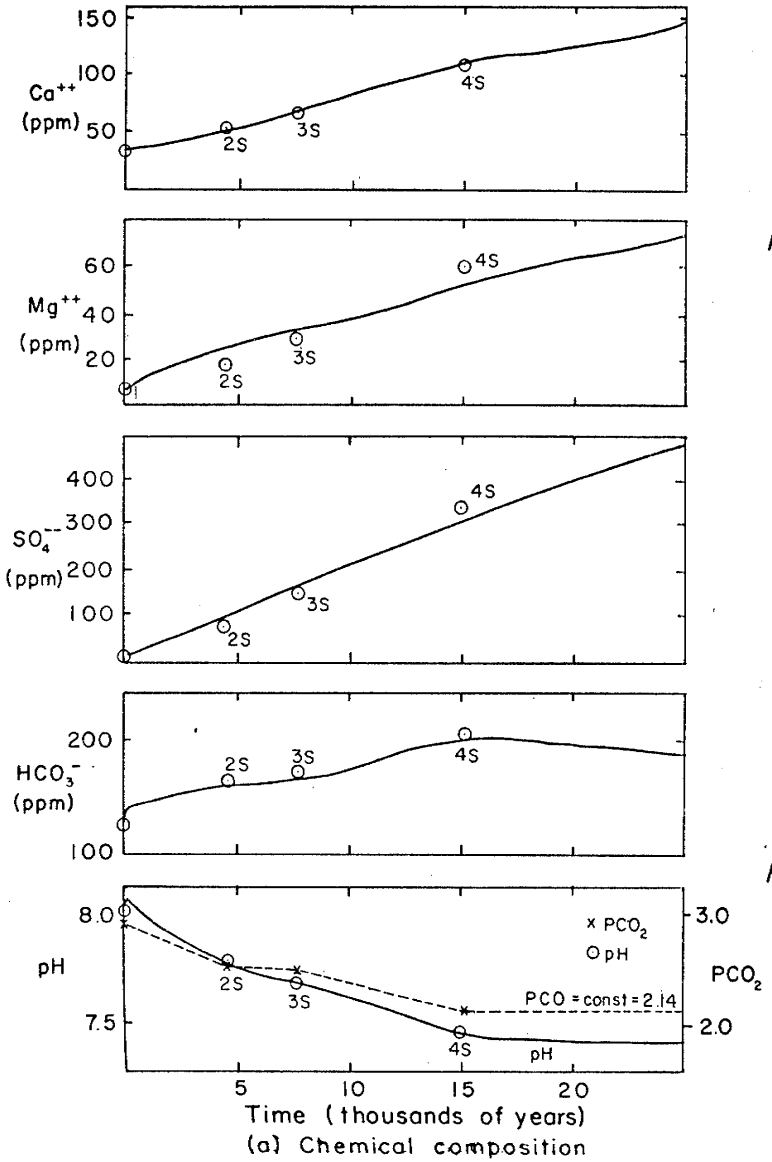
150
100
50
Ca++ (ppm)
2S
3S
4S
60
40
20
Mg++ (ppm)
400
300
200
100
SO4-- (ppm)
200
100
HCO3- (ppm)
8.0
7.5
pH
x PCO2
O pH
PCO = const = 2.14
3.0
2.0
PCO2
5
10
15
20
Time (thousands of years)
(a) Chemical composition

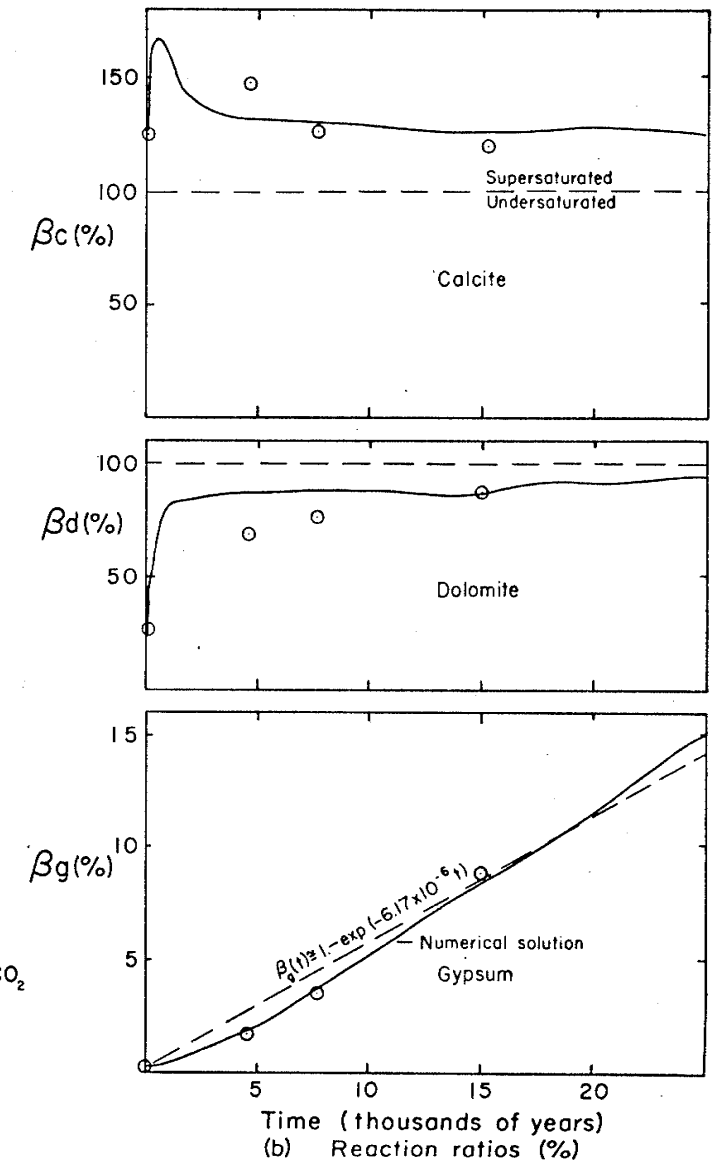
150
100
50
βc (%)
Supersaturated
Undersaturated
Calcite
100
50
βd (%)
Dolomite
15
10
5
βg (%)
Numerical solution
Gypsum
5
10
15
20
Time (thousands of years)
(b) Reaction ratios (%)

TABLE 5.2

THE FLORIDA LIMESTONE AQUIFER

COMPARISON BETWEEN COMPUTED AND MEASURED DATA

MASS ACTION KINETICS

REACTION RATE CONSTANTS (MOLE PER YR)

CALCITE = 0.650000E-06
DOLOMITE = 0.100000E-05
GYPSUM = 0.225000E-06

SAMPLE NO	TIME (YS)	MEASURED DATA CA	MG	SO4	HCO3	PH	COMPUTED DATA CA	MG	SO4	HCO3	PH
1	0.0	34.0	5.6	2.4	124.0	8.00	34.0	5.6	2.4	124.0	8.00
2S	0.4500E 04	56.0	17.0	71.0	163.0	7.75	53.8	24.5	96.5	164.2	7.75
3S	0.7700E 04	66.0	29.0	155.0	168.0	7.69	68.6	33.0	161.9	168.6	7.69
4S	0.1510E 05	106.0	60.0	344.0	206.0	7.44	108.4	53.8	309.2	207.5	7.44
TIME AV. SIMPLE ERROR(PPM)							1.1	2.1	0.4	1.0	0.00
TIME AV. ABSOL. ERROR(PPM)							2.4	5.7	20.5	1.0	0.00
TIME AV. SQ.RT. ERROR(PPM)							2.4	5.9	23.7	1.1	0.00

Figure 5.6 - Sensitivity of the time-weighted average absolute (+) and simple (⊙) errors ε to variations of the (a) calcite, (b) dolomite, and (c) gypsum rate constants. Variations of rate constants are expressed as fractions of the calibrated constant $(k_c)_o$. The error is defined here as: error = computed - measured. The error sensitivity is proportional to the relative deviation from equilibrium; the average reaction ratios with respect to calcite, dolomite, and gypsum are about 130%, 85%, and 5% respectively.

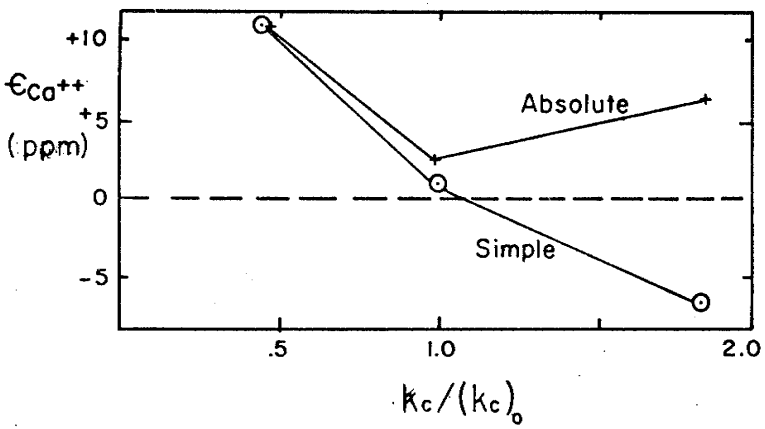

(a) Calcite

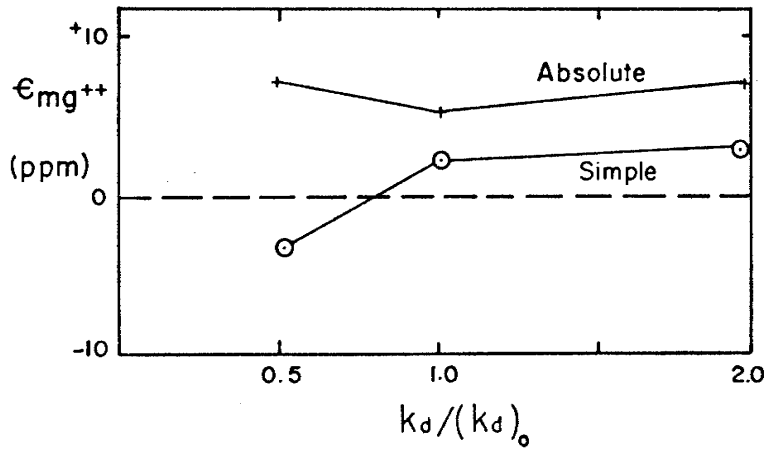

(b) Dolomite

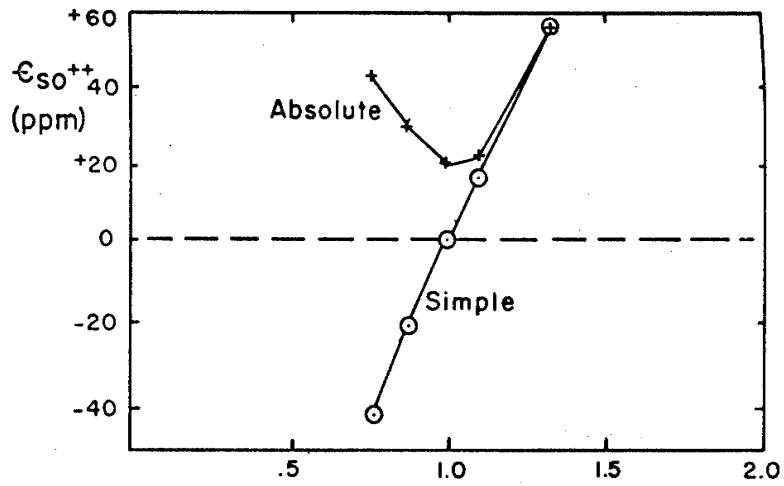

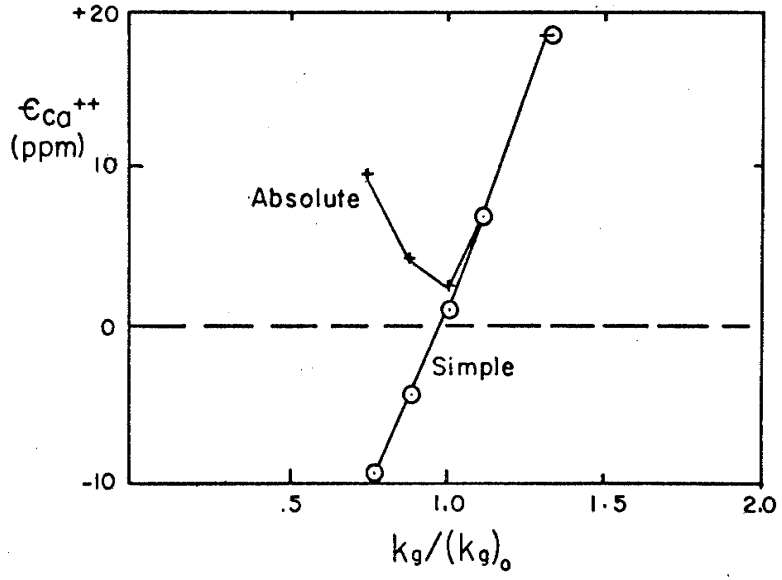

(c) Gypsum

Figure 5.7 - Sensitivity of the time-weighted average absolute (+) and simple (⊙) errors ε to variations of the dolomite equilibrium constant. The suggested expression of pK(=-log K) for dolomite as a function of temperature is: $\bar{p}K_d(T) = 16.29 + 185 \times 10^{-4} (T - 15) + 250 \times 10^{-6} (T - 15)^2$, where T is the temperature in °C. From this expression $pK_d(25°C) = 16.5$ instead of the conventional value of 17.0 ± 0.3 (Langmuir, 1971). Variations are made with respect to this value. The error is defined here as: error = computed - measured.

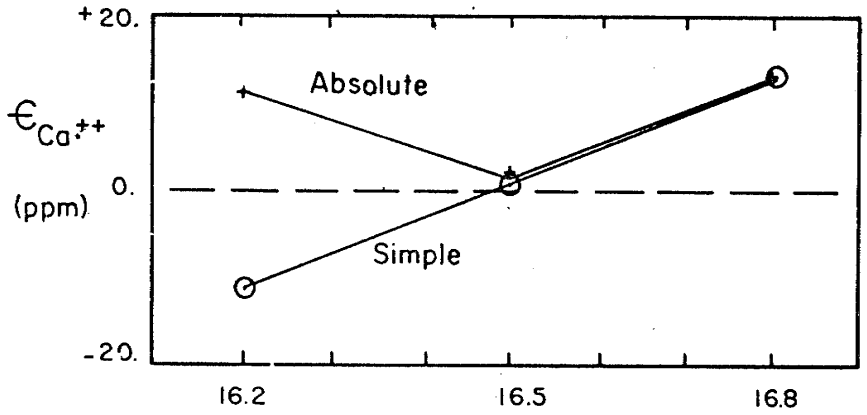

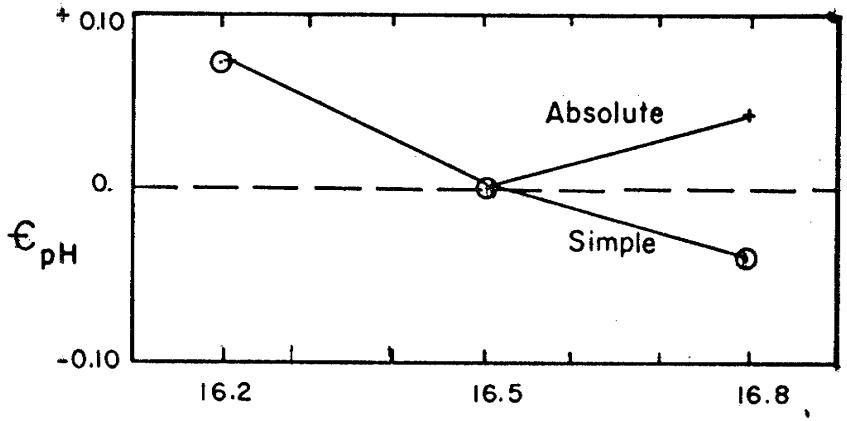

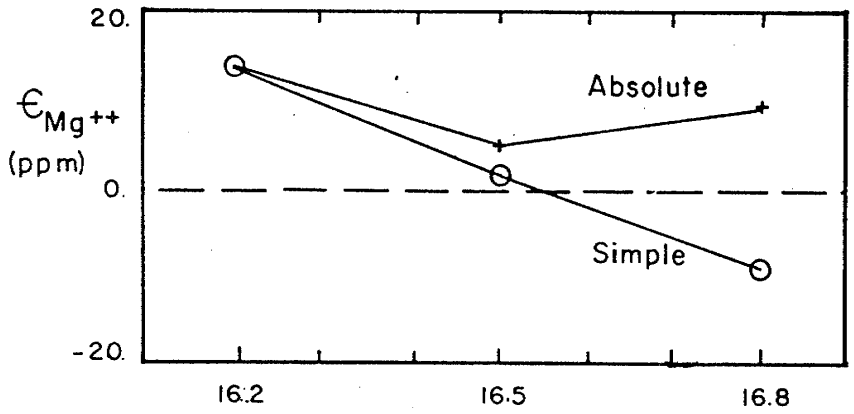

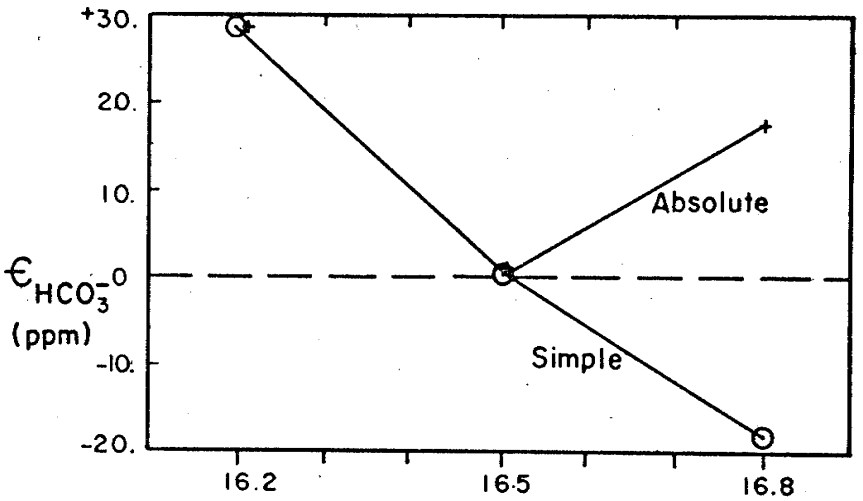

PK_d (25°C)

PK_d (25°C)

that CO_2 is contributed by other than carbonate mineral dissolution, rather than being produced solely through the calcite dissolution process.

The dashed curve in the reaction ratio plot with respect to gypsum (Figure 5.5b), represents the approximate solution of the $\beta(t)$ function (Eq. 2.39). As can be seen, the $\beta(t)$ approximation may be rather useful, even in simultaneous dissolution processes, provided that the reaction is dominated by one mineral only.

5.4 The Residence-Time Distribution of Groundwater in the Aquifer

(a) Age Estimates - The resulting curves of the calibrated model (Figure 5.5) may serve now as a useful tool for estimating the residence-time distribution in the aquifer, relative to the recharge area. This technique makes use of other groundwater samples, not included in the calibration process of the kinetic model.

Residence-time estimates can be obtained from the concentration-time relationship $C_i(t)$ of any individual species (i). Since each individual curve may yield a different value, an average estimate $\bar{t}$ should be used:

$$\bar{t} = \sum_i w_i t_i / \sum_i w_i \qquad (5.1)$$

where t_i is the residence-time estimate based on the theoretical variation of the i-th species, or β - property of the solution, and w_i is some weighting factor. The selection of the value w_i is rather subjective; however, it should be related to the ratio between the slope of the function and the precision of the individual chemical analysis or precision of the β - computation. The weighting factor w_i should be larger for

accurate chemical analyses, and large variations of species concentration with time.

In this dissertation, the average residence time $\bar{t}$ was estimated from:

$$\bar{t} = 1/4\ (t_{Ca} + t_{Mg} + t_{SO_4} + t_{\beta_g}) \qquad (5.2)$$

where t_{Ca}, t_{Mg}, t_{SO_4}, and t_{β_g} represents the residence time estimated from the plots of calcium, magnesium, sulphate, and β_g respectively (Fig. 5.5). Bicarbonate and pH are not included in the expression above, because their variation with time seems to be too small compared to the precision of their measurement in the field. The same applies to β_c and β_d. The four individual estimates in equation (5.2) were assigned an equal weighting factor of w = 1. The comparison between chemical and available hydrological residence-time estimates is shown in Figure 5.8. The distribution of the residence-times in the aquifer, based on chemical data is shown in Figure 5.9.

Table 5.3 summarizes the chemical data of samples, their corresponding residence-time estimates, computed from equation (5.2), and residence times based on hydrologic parameters and ^{14}C. The hydrologic and ^{14}C residence times are from published data (Hanshaw, et al., 1965a; Back and Hanshaw, 1971). The relative spread of estimates of individual species around t_{chem} seems to be inversely proportional to the residence time. This relationship probably reflects the mineralogical heterogeneity of the aquifer. Older water has covered larger distances. Therefore the chemical data reflects the average mineralogical composition of the

Figure 5.8 - Comparison of geochemical and ^{14}C age estimates with hydrologic estimates along the north-south streamline. The progressive deviation of ^{14}C data from hydrologic estimates may be explained by the precipitation of calcite. The spread of geochemical estimates only indicates the calibration accuracy of the kinetic model.

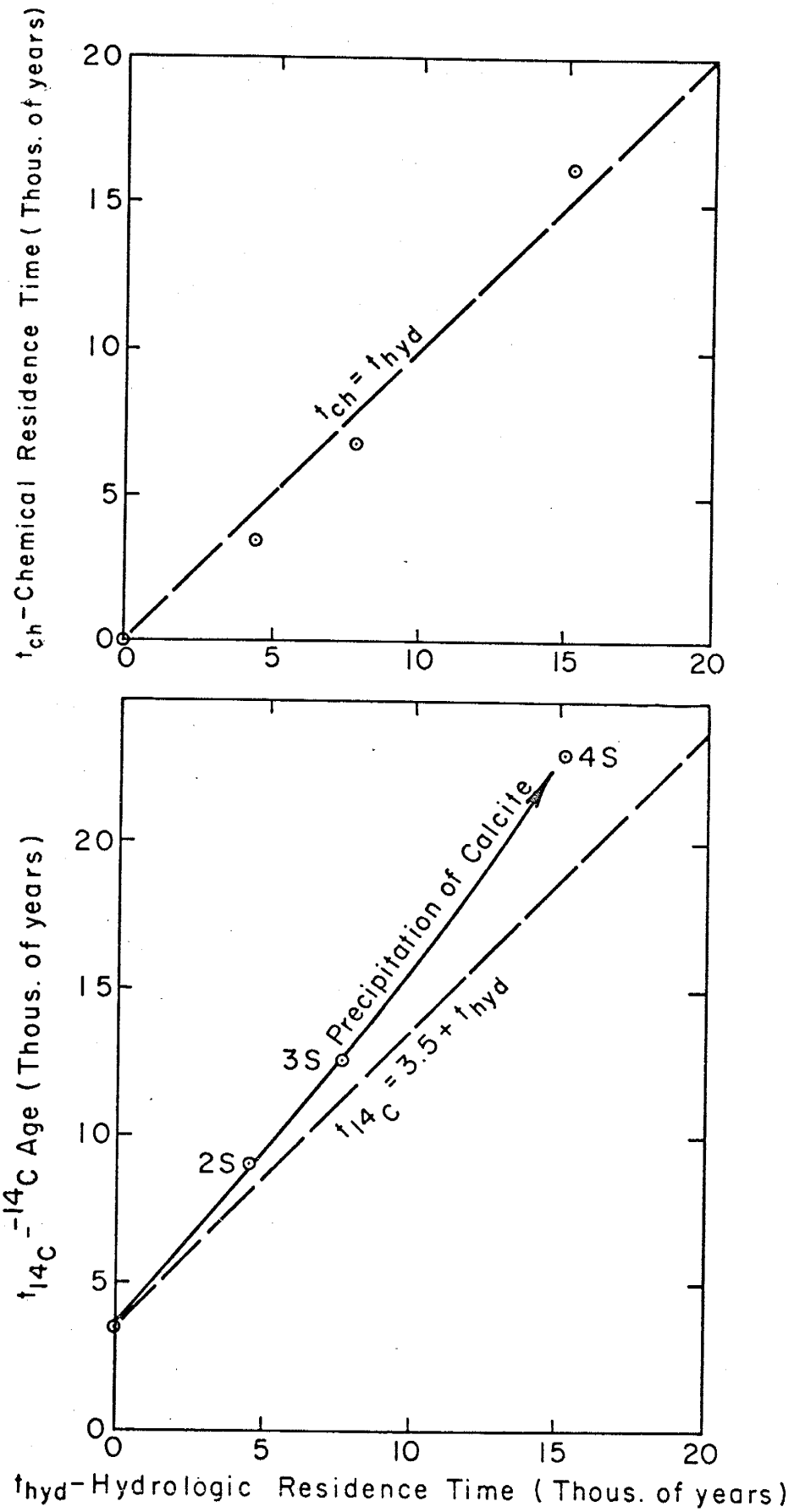
t_{ch}-Chemical Residence Time (Thous. of years)
$t_{ch} = t_{hyd}$
t_{14C}-^{14}C Age (Thous. of years)
4S
3S Precipitation of Calcite
2S
$t_{14C} = 3.5 + t_{hyd}$
t_{hyd}-Hydrologic Residence Time (Thous. of years)
0
5
10
15
20

Figure 5.9 - Comparison between geochemical (heavy solid and dashed lines) and ^{14}C (light dashed lines) age distributions. Age estimates are given in thousands of years. For comparison purposes the ^{14}C estimated age of Polk City (about 3500 years) was added to all geochemical estimates to yield a common base for all types of age estimates. Numbers indicate the geochemical age estimate of samples (Table 5.3) + 3500 years. The ^{14}C map is from Back and Hanshaw (1971). Circled points were used for calibrating the kinetic model.

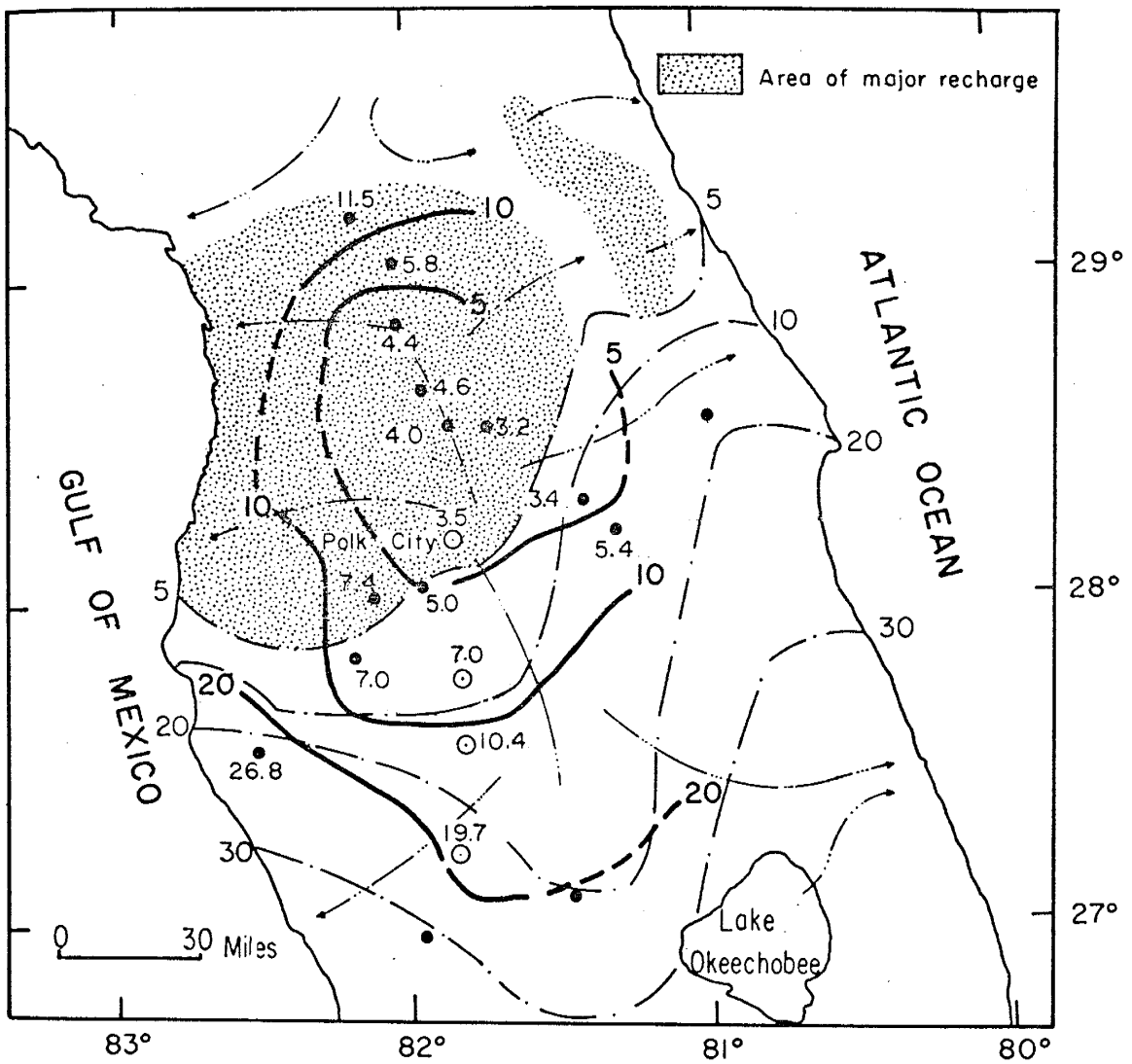
Area of major recharge
GULF OF MEXICO
ATLANTIC OCEAN
Polk City
Lake Okeechobee
0 30 Miles
11.5
5.8
4.4
4.6
4.0
3.2
3.5
3.4
5.4
7.4
5.0
7.0
7.0
10.4
26.8
19.7
10
5
20
30
29°
28°
27°
83°
82°
81°
80°

TABLE 5.3 - RESIDENCE TIME ESTIMATES BASED ON CHEMICAL, HYDROLOGIC AND ^{14}C DATA *

Well	Chemical Data				Residence Time (thousands of years)							Area(1)
	Ca (ppm)	Mg (ppm)	SO_4 (ppm)	β_g %	t_{Ca}	t_{Mg}	t_{SO_4}	t_{β_g}	t_{chem}(2)	t_{hyd}(3)	$t_{^{14}C}$	
1	34.	5.6	2.4	0.05	0	0	0	0	0	0	3.5	R
2S	56.	17.0	71.	1.7	4.95	2.2	3.2	3.8	3.5	4.5	9.0	C
3S	66.	29.	155.	3.5	7.1	6.1	7.3	7.2*	6.9	7.7	12.7	C
4S	106.	60.	344.	8.9	14.7	17.7	16.7	15.5	16.2	15.1	23.0	C
2W	54.	14.	3.6	0.12	4.4	1.4	0.06	0.12	4.8	-	5.0	C
3W	66.	11.	-	-	7.1	0.75	-	-	3.92	-	-	C ?
4W	61.	8.6	66.	1.8	5.9	0.28	3.1	4.4	3.42	-	6.5	C ?
5W	140.	68.	458.	13.8	24.0	22.2	23.4	23.7	23.30	-	21.0	C
2E	33.	2.3	0.06	0.0	-0.27	0.02	-0.05	0.02	-0.05	-	14.2	C
3E	51.	7.5	38.	0.9	3.9	0.12	1.65	1.87	1.88	-	11.2	C
2N	42.	4.1	1.6	0.04	1.98	-0.08	-0.04	0.02	0.46	-	3.6(4)	R
3N	25.	5.7	3.2	0.05	-1.5	0.1	0.04	0.0	-0.34	-	-	R
4N	46.	6.7	2.8	0.08	2.9	0.65	0.2	0.5	1.06	-	-	R
5N	51.	2.6	3.2	0.10	3.9	-0.25	0.04	0.08	0.94	-	1.5(4)	R
6N	58.	8.6	36.	1.00	5.3	0.25	1.60	2.00	2.28	-	-	R
7N	100.	15.	153.	5.20	13.5	1.75	7.3	9.30	7.96	-	3.7(4)	R

Notes. (1) R - Area of major recharge
C - Covered by clay
(2) based on equation (5.2)
(3) Derived from Table 1 in Hanshaw et al (1965b)
(4) Derived from Table 2 Hanshaw et al (1965a)
* Chemical and hydrologic residence times are relative to Polk City (well #1).

aquifer on the regional scale. Chemical composition of young water may still be governed by local inhomogeneities. In addition, fresh water is contributed over all of the northern part of the aquifer. Mixtures with fresh water will have different characteristics than those predicted by the dissolution model for closed systems. It should be mentioned that the contribution of fresh water prevented Hanshaw et al., (1965a) from using their ^{14}C data in this area for hydrological estimates.

(b) Comparison Between Chemical, Hydrologic and ^{14}C Age Estimates

To this point the kinetic model has been calibrated with the aid of available hydrologic estimates for part of the aquifer (samples 1, 2S, 3S, 4S). The resulting chemical-age estimates for the remaining part of the aquifer are based on this calibration, and no use was made of ^{14}C data (Hanshaw et al., 1965a, Back and Hanshaw, 1971) available for most of the covered part of the aquifer (Fig. 5.1). It is of interest, therefore, to compare the chemical and ^{14}C estimates, as they were derived independently. The deviations between the two may be explained on the basis of the dissolution-precipitation kinetics discussed previously.

Both estimates are compared to the available hydrologic estimates, assumed to be relatively "exact" (Fig. 5.8). Hydrologic and chemical age estimates are relative to groundwater in the recharge area, assigned a reference age of zero. ^{14}C age estimates are absolute, as they are relative to the date of rainfall infiltration. The ^{14}C age estimate for the recharge area (Polk City well) is about 3500 years (based on the comparison between Table 2, Hanshaw, et al., 1965a, and Fig. 3, Back and Hanshaw, 1971). For the purpose of comparison, an age of 3500 years was

added to both hydrologic and chemical estimates (Figures 5.8, 5.9 and 5.10). From this comparison (Fig. 5.8) ^{14}C data seems to deviate significantly from hydrologic estimates. The deviation increases with the estimated hydrologic residence time. An explanation for this trend is porposed later in this chapter. Chemical estimates in Figure 5.8 are based on the calibration of the kinetic model with the available hydrologic data, and the spread of points around the 45° line reflects only the accuracy of the calibrated model.

Chemical and ^{14}C estimates are compared in Figures 5.9 and 5.10. In general, the trend of the two estimates is in reasonable agreement. Some of the significant deviations, however, calls for further discussion.

The ^{14}C age of samples 2E and 3E (Fig. 5.8) seems to be rather exaggerated with respect to reasonable hydrological estimates. From Figure 5.1, the average hydraulic gradient in the west to east direction is about twice that in the north to south direction; the distance between Polk City and wells 2E and 3E is shorter by a factor of 50% than the distance to well 3S. It follows that, for equal permeability and porosity, the residence time of the water in wells 2E and 3E should be shorter by a factor of 3 than the residence time of 3S; according to ^{14}C estimates the residence time for both locations is about equal. Assuming that the age of the groundwater in well 3S is exact, the age of the water in 2E and 3E should of the order of magnitude of 4000 years rather than an average of 12,000 years, indicated by ^{14}C measurements. This shift of the ^{14}C age will bring these two points rather close to the ideal 45° line (Fig. 5.10). The same applies to samples 3S and 4S; their deviation from hydrologic estimates is shown in Figure 5.8.

Figure 5.10 - Comparison between ^{14}C and geochemical age estimates. The ^{14}C age of the full (●) and circled (⊙) points was interpolated from the ^{14}C map in Fig. 5.9. The ^{14}C age of triangle (Δ) points with respect to Polk City is from data published by Hanshaw, et al. (1965a; Table 2). The geochemical age of the circled points (⊙) coincides with hydrologic estimates, as those wells were used for the calibration of the kinetic model. Arrows indicate direction of the corrections discussed in the text.

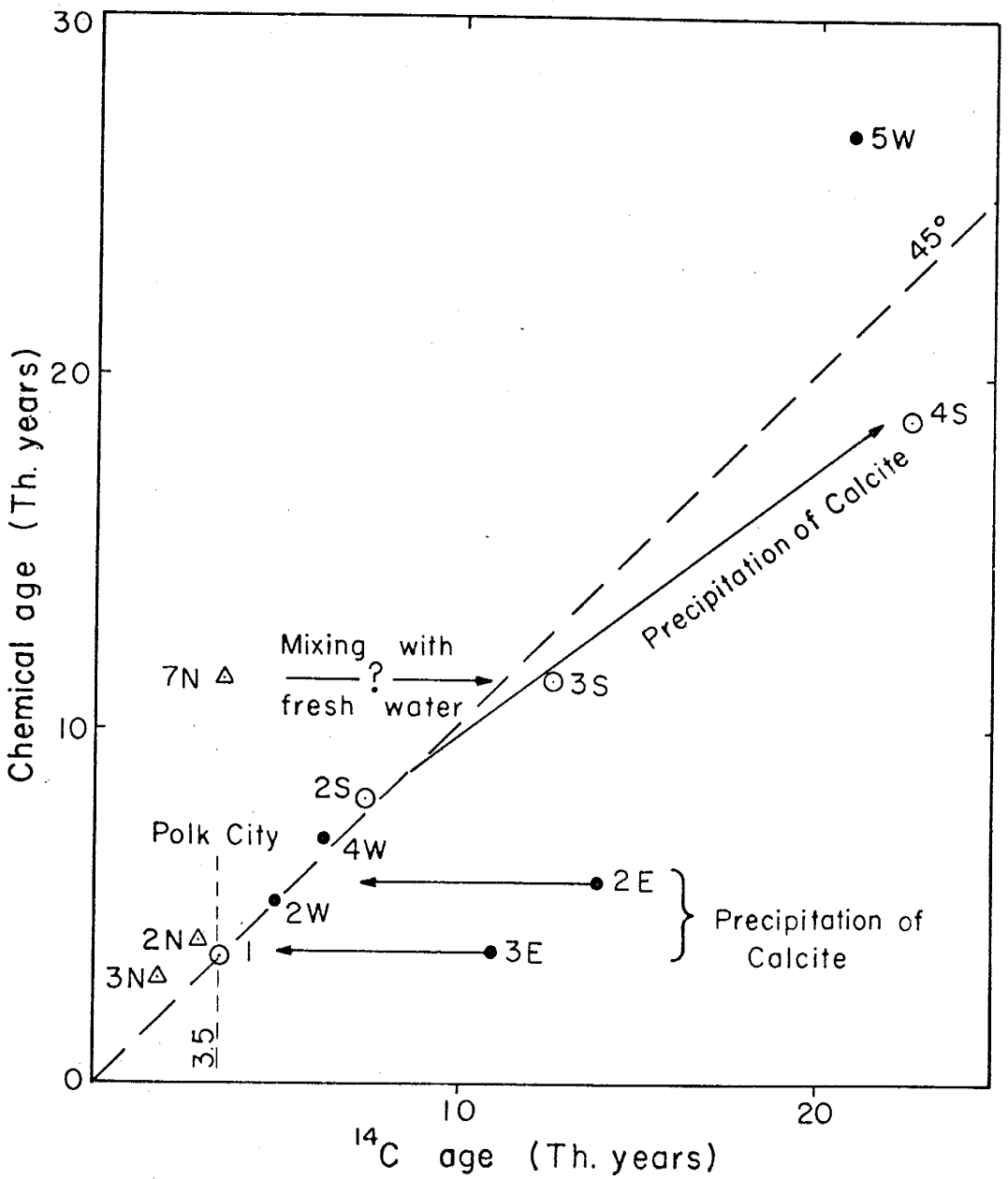
30
20
10
0
10
20
Chemical age (Th. years)
^{14}C age (Th. years)
5W
45°
4S
Precipitation of Calcite
Mixing with
fresh water
?
7N
3S
2S
Polk City
4W
2W
2N
1
3N
2E
3E
Precipitation of
Calcite
3.5

In addition, mixing of relatively old groundwater with fresh water in the recharge area (Fig. 5.9) will decrease the apparent groundwater age; this applies to both ^{14}C and chemical dating methods. However, the radioactivity decay curve of ^{14}C is exponential whereas the curve of concentration-time relationships is reasonably linear (Fig. 5.5). As a result the deviation caused by dilution of ^{14}C and chemical species will be larger for ^{14}C estimates than for chemical estimates; this may explain the shift of sample 7N from the 45° (Fig. 5.10).

Generally, precalibrated chemical estimates seem to be more accurate than the ^{14}C estimates based on comparison to hydrologic conditions. Some of the observed deviations between the ^{14}C and hydrologic age estimates can be explained by dissolution-precipitation kinetics, as discussed below.

(c) Some Remarks on the Deviations of ^{14}C Data

The ^{14}C dating method is based essentially on the decay of the ^{14}C radioactivity, where the active dateable carbon is derived from plants. Active carbon is diluted, however, by ^{14}C free carbon species, such as the dissolution products of limestone, dolomite, and the reaction products of petroleum-derived CO_2 gas with carbonate minerals. The measured radioactivity should thus be corrected for dissolution in order to determine the correct residence time of the water in the aquifer.

The correction factors used (Pearson, 1965), are based on the assumption that the only diluent is limestone. Using the significant difference of the $\delta^{13}C$ values between plant and limestone derived carbon, the measured $\delta^{13}C_{sm}$ of the groundwater sample should reflect the dilution ratio P of the active carbon (Pearson, 1965):

$$\delta^{13}C_{sm} = \left(\frac{pl}{pl+ls}\right) \delta^{13}C_{pl} + \left(\frac{ls}{pl+ls}\right) \delta^{13}C_{ls} \qquad (5.3)$$

where pl and ls stands for plant-derived and limestone-derived carbon fractions respectively. The dilution ratio (P) is defined by:

$$P = \frac{pl}{pl+ls} \qquad (5.4)$$

From equations (5.3) and (5.4):

$$P = \frac{\delta^{13}C_{sm} - \delta^{13}C_{ls}}{\delta^{13}C_{pl} - \delta^{13}C_{ls}} \qquad (5.5)$$

Using the average values of $\delta^{13}C_{pl} = -25$ °/oo , and $\delta^{13}C_{ls} = 0.0$ °/oo , equation (5.5) is simplified to (Pearson, 1965):

$$P = \delta^{13}C_{sm}/-25. \qquad (5.6)$$

The value of P is usually smaller than 1. The measured radioactivity A* is corrected finally by:

$$A = A^*/P \qquad (5.7)$$

The age t is determined from the ratio between the corrected radioactivity A and the ^{14}C radioactivity of rain water A_o:

$$t = \frac{2.3t_{1/2}}{0.693} \log (A/A_o) \qquad (5.8)$$

where $t_{1/2}$ is the half-life of ^{14}C. Notice that for the same measured radioactivity A*, large values of P will yield older ages than for small ones.

The major error in the interpretation of ^{14}C measurements stems from the improper evaluation of the correction factor P. No allowance is made in the equations above for possible fractionation of carbon isotope species by dissolution. One may expect (Rankama, 1954) that the light isotope (^{12}C) will be preferred in dissolution compared to the heavy isotope (^{13}C). As a result the dilution of ^{14}C would be larger than predicted by equation (5.6), yielding older apparent ^{14}C ages. In addition, most groundwater samples are supersaturated with respect to calcite, indicating that calcite is precipitating rather than dissolving. During precipitation the heavy isotopes are preferred in the solid over the abundant ^{12}C isotopes (ibid). Precipitation will thus cause a depletion of both ^{13}C and ^{14}C, reducing the ^{14}C radioactivity A^* and making $\delta^{13}C$ more negative. Again, the corrected ^{14}C age, based on equations (5.6), (5.7), and (5.8), will be older than anticipated. This qualitative discussion could explain the major part of the deviations between the hydrologic and ^{14}C estimates discussed above (Fig. 5.8); particularly when there are variations in the degree of supersaturation. For example see Figure 5.5 and 5.3.

In addition, the possibility that limestone-derived carbon is not the dominant diluent, may introduce serious difficulties in determining a correction factor. Proper interpretation of ^{14}C data seems to require more investigation of the effects of dissolution and precipitation processes.

6. THE HYDROGEOCHEMICAL MODEL

The distribution of aqueous species in aquifers is the combined result of two processes: (i) The dissolution process, depending on the intrinsic physical and chemical properties of the mineral assemblages forming the porous medium; and (ii) the mass transfer of the dissolved aqueous species due to both convection and dispersion in porous media.

Dissolution processes of multimineral assemblages in closed aqueous systems were examined, both analytically and experimentally, in previous chapters. The mass transfer process of dissolved species is discussed below. The combined process will be defined later in this Chapter in terms of a general differential equation, which governs the dissolution-convection-dispersion combined process.

6.1 Mass Transfer in Porous Media

Mass transport of a nonreactive tracer in porous media can be described macroscopically by the superposition of two basic transport modes: (Ogata, 1958, 1970): (i) convection, and (ii) dispersion. The combined process is termed generally hydrodynamic dispersion in porous media (Bear, 1965).

The convection mode, which obeys Darcy's law for flow in porous media, can be considered as a rather satisfactory approximation of transport in aquifers (Nir, 1964). It will occur if all fluid particles move with the same velocity. As a result, a sharp interface between the invaded and original fluids in the porous medium exists.

Experience shows, however, that the interface between the two liquids is not sharp, and actually a transition zone exist between the two miscible fluids, in which the concentration varies gradually from

the concentration of one fluid to the concentration of the other. The existence of the transition zone instead of a sharp front is related to the dispersion phenomenon, which is the second basic mode of transport in porous media. Dispersion describes the spread of moving particles caused by microscopic variations of fluid velocities within a pore and molecular diffusion.

The hydrodynamic dispersion (convection + dispersion) of an ideal tracer in steady saturated flow through homogeneous and isotropic porous media is described by (Bachmat and Bear, 1964):

$$\frac{\partial C}{\partial t} = \text{div}(\underline{\underline{D}} \text{ grad } C) - \text{div}(\underline{v}C) \qquad (6.1)$$

where: C - concentration of the dispersing tracer at time t.

$\underline{v}$ - the seepage velocity vector

$\underline{\underline{D}}$ - the dispersion coefficient, a second rank symmetric tensor.

The dispersion and convection modes of transport are represented by the first and second terms, respectively, of the right-hand side of the equation above.

The equation above was solved and verified experimentally for simple flow regimes only (Rifai et al., 1956; de Josselin de Jong, 1958; Lau et al., 1959; Bear and Todd, 1960; Ogata and Banks, 1961; Mercado and Bear, 1966; Mercado, 1967; Passioura and Rose, 1970). More complicated cases were solved by numerical methods (Shamir and Harleman, 1966; Reddel, 1969; Nalluswami, 1971).

6.2 The General Differential Equation of Dissolution and Mass-Transfer in Porous Media

The combination of mass-transfer and dissolution modes can be represented by:

$$\frac{\partial C}{\partial t} = \left(\frac{\partial C}{\partial t}\right)_{\substack{\text{mass}\\ \text{transfer}}} + \left(\frac{\partial C}{\partial t}\right)_{\text{dissolution}} \tag{6.2}$$

or by a combination of equations 2.44 and 6.1:

$$\frac{\partial C_i}{\partial t} = \text{div}(\underline{\underline{D}} \text{ grad } C_i) - \text{div}(\underline{v} C_i) + \sum_j [\nu_{ij} k_j (1 - \beta_j(t))] \tag{6.3}$$

where: C_i - the concentration of the i-th species

t - the time

$\underline{\underline{D}}$ - the dispersion tensor

$\underline{v}$ - the velocity vector

ν_{ij} - the stoichiometric coefficient of the i-th species with respect to the dissolution reaction of the j-th mineral

k_j - the kinetic rate constant with respect to the j-th mineral

β_j - the reaction ratio of the bulk solution with respect to the j-th mineral at time t

The solution of the equation above, subject to the field boundary conditions, should yield the distribution of aqueous species in a given groundwater system, at any time t. This equation will be regarded

hereafter, as the hydrogeochemical model.

Equation (6.3) represents the general differential equation of the combined dissolution-convection-dispersion process. However, under many regional field conditions, this equation can be simplified, as discussed below.

Nir (1964) has compared the exact solution of the hydrodynamic dispersion equation for one-dimensional flow with solutions based on a "piston-flow" model (mass-transfer by convection only) and has shown that "... the piston flow solution is a satisfactory approximation to this equation under many encountered conditions ...". For most regional field studies the dispersion term in the equation above can thus be neglected, and the spread of dissolved species can be approximated by:

$$\frac{\partial C_i}{\partial t} \cong \sum_j \nu_{ij} k_j (1 - \beta_j) - \mathrm{div}(\underline{v} C_i) \qquad (6.4)$$

Furthermore, when a steady flow prevails in the aquifer for a sufficiently long time, depending on the ratio between flow and dissolution rates, a steady nonequilibrium state is established such that the convection of aqueous species by water flowing through the aquifer is equal to the net rate of their production by dissolution. Under these conditions, $\frac{\partial C_i}{\partial t} \cong 0$, and:

$$\sum_j \nu_{ij} k_j (1 - \beta_j) \cong \mathrm{div}(\underline{v} C_i) \qquad (6.5)$$

The development of groundwater resources in the last 50 - 100 years, has changed the steady flow rates in aquifers. As a result the present distribution of aqueous species is changing gradually toward

a new steady, nonequilibrium state. However, considering the low dissolution rates in aquifers (see Chapter 5), it is expected that the present water quality maps still reflect the historical flow conditions under which the equation above is valid.

Equation (6.5) is used in this dissertation as a simplified version of the general hydrogeochemical model (Eq. 6.3) in order to study the hydrogeochemical processes in aquifers under steady flow conditions. A numerical method for solving Eq. (6.5) is derived below.

6.3 The Numerical Method

Theoretically, the simplified hydrochemical model, described by equation (6.5), can be solved numerically by writing both terms in their finite difference form (Fig. 6.1). For a three-dimensional flow problem, this will require the solution of N = i x j x r x s x t equations with N unknowns, where i is the number of species, j the number of minerals, and r, s, and t are index numers of the grid points along the x, y, and z axes. Considering, for example, a moderate size grid of 30 x 30 x 10, three minerals (calcite, dolomite, and gypsum), and five aqueous species (calcium, magnesium, sulphate, bicarbonate and hydrogen) the number of equations to be solved simultaneously is:

$$N = 5 \times 3 \times 30 \times 30 \times 10 = \underline{135{,}000 \text{ equations}}$$

In addition, the non-linear corrections for activity coefficients, ion-pairs, and complex ions will require a considerable number of iterations to obtain an accurate solution. The straightforward solution of equation (6.5) requires a vast amount of computer time and storage and was therefore rejected.

(a) Transformation from Space to Time Coordinates - The numerical method actually used is based on the transformation of equation (6.5) from Cartesian space coordinates (x, y, x) into time coordinates of imaginary "tracing points" moving along the groundwater streamlines. By using this transformation, the complicated dissolution-convection process is reduced to the case of dissolution in closed water systems, studied in previous chapters.

For this transformation, $\phi - \psi$ coordinates (ϕ - potentials, and Ψ - streamlines) are used instead of Cartesian coordinates. Since the velocity is tangent to the lines of ψ = constant, equation (6.5), in $\phi - \psi$ coordinates will have only one convection term, whereas in Cartesian coordinates a convective terms exists in each of the coordinate directions. Similar transformation was used by Shamir and Harleman (1967) for simplifying the numerical solution of the dispersion equation.

Using the property of the $\phi - \psi$ coordinates, equation (6.5) is rewritten as a one-dimensional differential equation with respect to the distance S along streamlines:

$$\sum_j [\nu_{ij} k_j (1 - \beta_j)] = \frac{d}{dS} (v_s C_i) \tag{6.6}$$

where v_s is the velocity of the tracing-point along the streamline (S). Equation (6.6) can be written also as:

$$\sum_j [\nu_{ij} k_j (1 - \beta_j)] = C_i \frac{dv_s}{dS} + v_s \frac{dC_i}{dS} \tag{6.7}$$

For constant velocity $\left(\frac{dv_s}{dS} = 0\right)$ or when $v_s \frac{dC_i}{dS} >> C_i \frac{dv_s}{dS}$ the

first term on the right hand side of equation 6.7 can be neglected. The error caused by neglecting this term is absorbed by the field rate constant. In order to simplify the present model, the assumption of $\frac{dv_s}{dS} = 0$ was made in the field example of the Roswell aquifer discussed in the next chapter. The above inequality is not true for the Roswell basin although the simplification was used. It should be realized that neglecting this term $\left(C_i \frac{dv_s}{dS}\right)$ adds another parameter to the field rate constant. This is undesirable and future research should make use of equation 6.7 without simplification.

By setting $dv_s/dS = 0$ and $v_s = dS/dt$, equation 6.7 is reduced to:

$$\sum_j [\nu_{ij} k_j (1 - \beta_j)] \cong v_s \frac{dC_i}{dS} \cong \frac{dC_i}{dt} \tag{6.8}$$

The equation above is identical with the kinetic function (Eq. 2.44), derived for the dissolution of minerals in closed water systems. This identity is explained by the fact that the kinetic dissolution rates of the minerals are independent of flow velocity although the determined field kinetic rate is not. Flow rates will, however, govern the distribution of species in space coordinates.

The equation above is integrated with respect to time from t to $t + \Delta t$ (see computation procedures in Chapter 3) where Δt is the residence time of the tracing point moving along the streamline, obtained by integration, from S to $S+ \Delta S$ at a constant velocity. The velocity v_s is changed at each new step ΔS, according to the given velocity field. The integration yields the steady non-equilibrium concentration of species at new point $S+ \Delta S$.

The computed concentration-time relationships are transformed back into space coordinates using the computed coordinates of the tracing points as a function of time. This numerical scheme, which is based essentially on two separate steps, yields theoretical water quality maps of the aquifer for steady uniform flow conditions or under the conditions discussed with respect to equation 6.7, and at a steady non-equilibrium state with respect to the dissolving minerals. The accuracy of the theoretical maps depends on the number of tracing points used in the computation.

(b) Movement of Tracing Points Along Streamlines - In the method described above a determination of the seepage velocities and the consequent displacement along streamlines is necessary for relocating the moving points after each time step. To accomplish this a central grid cell and the six adjacent cells are used (Fig. 6.1) for two-dimensional flow problems. The measured hydraulic potential at each grid point should be known. However, if necessary, the steady flow equation can be solved for a given set of boundary conditions and hydrologic constants, using standard techniques, in order to determine the potential distribution.

Tracing points are located in one of the four sub-squares of the central cell (Fig. 6.1). Using the given potentials and the location of the tracing point in the central grid cell, the seepage velocity in the x and y directions is determined with the aid of Darcy's law. Consider for example, the horizontal velocity at point (x,y) located at the upper left-most square of the central cell (Fig. 6.1). The two parallel gradients $(J_j)_x$ and $(J_{j+1})_x$ are given by:

Figure 6.1 - Grid system used to determine the displacement of a tracing point from $(x,y)_t$ to $(x',y')_{t+1}$ during a time-interval of Δt. The circled node points are chosen according to the location of the tracing point prior to its displacement. Hydrologic, geochemical constants, and boundary conditions are assigned to each cell, as part of the input data.

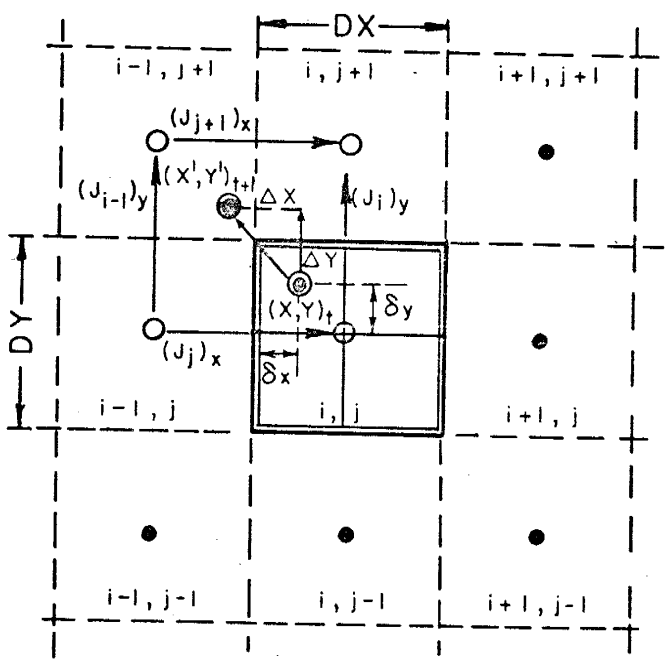
DX
DY
i-1, j+1
i, j+1
i+1, j+1
$(J_{j+1})_x$
$(X',Y')_{t+1}$
$(J_{i-1})_y$
ΔX
$(J_i)_y$
ΔY
$(X,Y)_t$
δ_y
$(J_j)_x$
δ_x
i-1, j
i, j
i+1, j
i-1, j-1
i, j-1
i+1, j-1

$$(J_j)_x = (H_{i-1,j} - H_{i,j})/Dx \tag{6.9}$$

$$(j_{j+1}) = (H_{i-1,\ j+1} - H_{i,\ j+1})/Dx \tag{6.10}$$

where H is the potential and Dx the grid spacing on the x-direction. The interpolated gradient at point (x,y) in the x-direction is given then by (Fig. 6.1):

$$(\bar{J}_{x,y})_x = \frac{\delta y - Dy/2}{Dy} [(J_j)_x - (J_{j+1})_x] + (J_{j+1})_x \tag{6.11}$$

and finally the velocity v_x at this point is:

$$v_x \cong \frac{T_{i,j}}{(bn)_{i,j}} (\bar{J}_{x,y})_x \tag{6.12}$$

where $T_{i,j}$ and $(bn)_{i,j}$ are the transmissivity and the effective thickness (total thickness, b, times porosity, n) of the aquifer at the grid cell (i,j). The velocity in the y-direction is determined in a similar way.

The displacements Δx and Δy, in the x and y directions respectively (Fig. 6.1), are determined from:

$$\Delta x = v_x \cdot \Delta t \tag{6.13}$$

and

$$\Delta y = v_y \cdot \Delta t \tag{6.14}$$

where Δt is the time-step interval.

In this dissertation no provision was made for returning "missed" tracing points; instead, the potential along the boundaries was set equal to the value of one of the adjacent grid nodes, such that the velocities

across these boundaries were zero. In addition, the transmissivity along boundaries was set equal to zero.

(c) Chemical Boundary Conditions and Distribution of Rate Constants

The integration of the kinetic equation with respect to time is subject to several boundary conditions. Those prevailing in carbonate aquifers are pCO_2, temperature, and sodium and chloride concentration. These properties were treated previously (Chapter 5) as being a function of time. They should be related actually to the space coordinates of their measurement in the field.

Appropriate chemical boundary conditions are assigned to each block in the grid system, according to their measured distribution in the aquifer. The computed coordinates of tracing points are then used to assign new boundary conditions for the dissolution process, following each step of their displacement along streamlines. The same adjustment could also be made for the dissolution rate constants if the abundance of the dissolving minerals varies drastically in space coordinates. The affect of various parameters on rate constants is discussed in Chapter 8.

6.4 Computation Procedures

A computer program HYDCEM (Appendix G), was developed for handling the numerical scheme described above. This program applies specially to carbonate aquifers and is based on the following steps:

(1) Read hydrological grid data: potentials, transmissivity, thickness of the aquifer, and its porosity.

(2) Read chemical grid data: pCO_2, temperature, sodium, chloride, and rate constants with respect to calcite, dolomite, and gypsum.

(3) Read location (x,y,z) and chemical composition (Ca, Mg, SO_4, HCO_3, pH) of tracing points along recharge boundaries.

(4) Balance for electrical neutrality of the given chemical analyses (subroutine BALANC). The electrical balance of analyses is necessary at this point, as the initial concentrations, or part of them, might be assigned on the basis of water quality contour maps.

(5) Locate tracing points on grid system (subroutine PLOC).

(6) Assign each tracing point the chemical boundary conditions corresponding to its location in the grid system.

(7) Determine seepage velocities v_x and v_y at the location of tracing points and displace them according to a predetermined time step Δt. The displacement of tracing points will follow the path of streamlines. Increase, or decrease, the next time-step by comparing the maximum displacement with a given tolerance. The tolerance used in this dissertation was 10% of the grid spacing. This step is carried out by the PMOVE subroutine.

(8) Integrate the rate equation from 0 to Δt, subject to the boundary conditions prevailing at the grid block of the pre-displaced tracing point. The integration procedure of this step is described in Chapter 3. This step is carried out by the CARMOD subroutine.

(9) Plot new location of tracing points and print their computed chemical composition (Ca^{++}, Mg^{++}, $SO_4^{=}$, HCO_3^{-}, and pH).

This step is carried out after a given number of iterations.

(10) Repeat steps (5) to (9). Terminate iteration when all tracing points have reached the aquifer boundaries, or when the elapsed time is larger than or equal to a given limit.

The flow chart of the HYDCEM computer program is given in Fig. 6.2.

6.5 Water Quality Maps

The final result of the integration procedure with respect to time are water quality maps in space coordinates. These maps are based on the assumption that the major geochemical process prevailing in the aquifer is the dissolution and precipitation of minerals. In addition, it is here assumed that the dissolving species are disconnected hydraulically from any other aqueous solutions originating from different sources or geochemical processes, in other words mixing is assumed to be absent. The geochemical interpretation of the chemical variations in hydraulically open systems, such as free surface aquifers replenished from above, requires further investigations, as it is considerably more complicated.

Knowing the areal distribution of the hydraulic constants and the groundwater chemical quality, the HYDCEM program can be used to evaluate the areal distribution of the geochemical parameters, and vice versa. The computation of water quality maps assumed values for certain kinetic and hydrologic parameters. If the resulting species distribution is not that of known water quality data, new kinetic, and/or, hydraulic parameters must be proposed. As is the case with any model, it must finally compare with reality (if known), or with other models based on hydrologic or geologic data. As mentioned before, the logical procedure of using

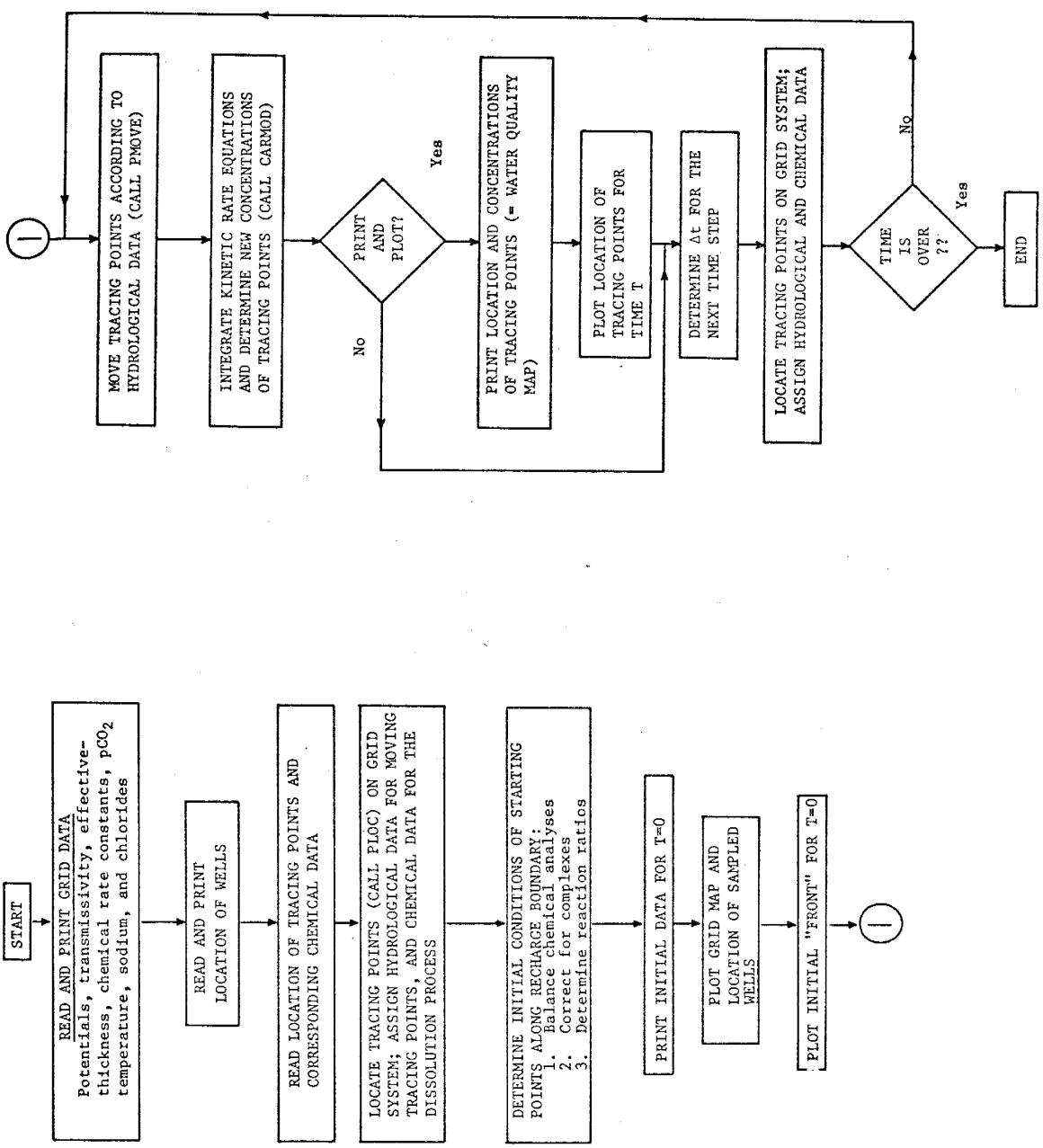

Figure 6.2 - Flow chart of the HYDCEM Computer Program.

this model should be to calibrate first the geochemical constants for a given controlled part of the aquifer, and then to use the water quality data of the reamining part for refining our knowledge on the flow pattern in the aquifer.

The analysis in the following chapter will demonstrate the interaction between hydrological and geochemical data, both insufficient, yielding as a result more refined information on both systems in the Roswell artesian aquifer in southeastern New Mexico.

7. EVALUATION OF FIELD DATA - (II) THE ROSWELL LIMESTONE AQUIFER; SOUTHEASTERN NEW MEXICO

The hydrogeochemical model developed in the preceding chapter is field tested by several steps. Using published data for transmissivity, water level, and effective thickness, the residence time is calculated. This is followed by computing average field rate constants using the chemical analyses and the calculated residence times. These field rate constants are then refined according to chemical boundary conditions (e.g., CO_2 concentration) and hydrologic parameters (e.g., transmissivity) existing at each sample point. This process of continually refining rate constants and hydrologic data until the model reproduces the distribution of chemical species is the test of the model. If a computed water quality map is reasonably similar to actual data, the form of the model is proper. If the map is not similar, this may point up the need for correction of input parameters.

The Roswell limestone aquifer (Fig. 7.1) was chosen as a field test of the hydrogeochemical model (Chapter 6). It is a complicated aquifer, and one might wish for a simpler test area. The presentation below should therefore be regarded as a demonstration of the proposed model rather than a detailed hydrogeochemical study of the basin.

The need for the rational exploitation of this aquifer has been a source of much concern in recent years. As a result, a large mass of hydrologic data for the basin and its recharge area are available (Hantush, 1955; Saleem and Jacob, 1971; Gisser and Mercado, 1972), but still not sufficient for detailed investigation. The Roswell

Figure 7.1 - Location of Roswell Basin, New Mexico.
(From Saleem and Jacob, 1971)

Figure 7.2 - General map of the investigated area showing: location of sampled wells in the pertinent aquifers [San Andres (●), San Andres + Grayburg (○), San Andres + Shallow (□)], recharge boundaries, and the grid-system used for the calibration of the hydrogeochemical model. Circled points (⊙) indicate location of sampled wells chosen as initial conditions along the recharge boundary. The intrusion of saline water is represented by the 1952 and 1968 500 ppm iso-chloride lines in the vicinity of Roswell.

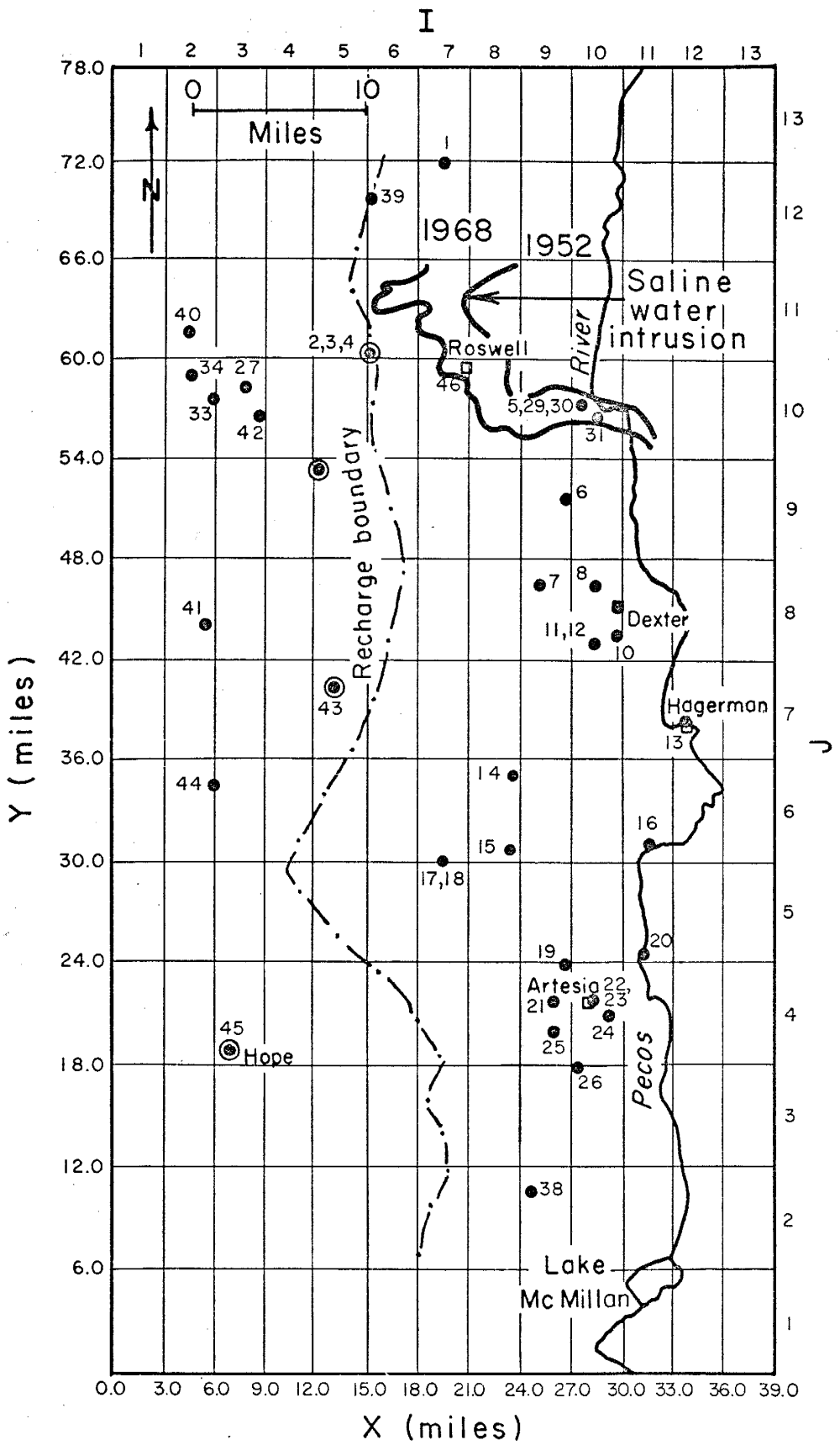
I
J
Y (miles)
X (miles)
0
10
Miles
N
1968
1952
Saline water intrusion
River
Pecos
Recharge boundary
Roswell
Dexter
Hagerman
Artesia
Hope
Lake Mc Millan
1
39
40
2,3,4
34
27
33
42
46
5,29,30
31
6
7
8
41
11,12
10
43
13
44
14
16
15
17,18
19
20
21
22,23
24
25
26
45
38

Figure 7.3 - Average east-west hydrogeological cross-section of the Roswell basin, showing general pattern of flow, location of major areas of recharge, evapotranspiration by phreatophytes, leakage between the two main aquifers, and the two alternative directions of saline water encroachment. Geological cross-section from Saleem and Jacob (1971).

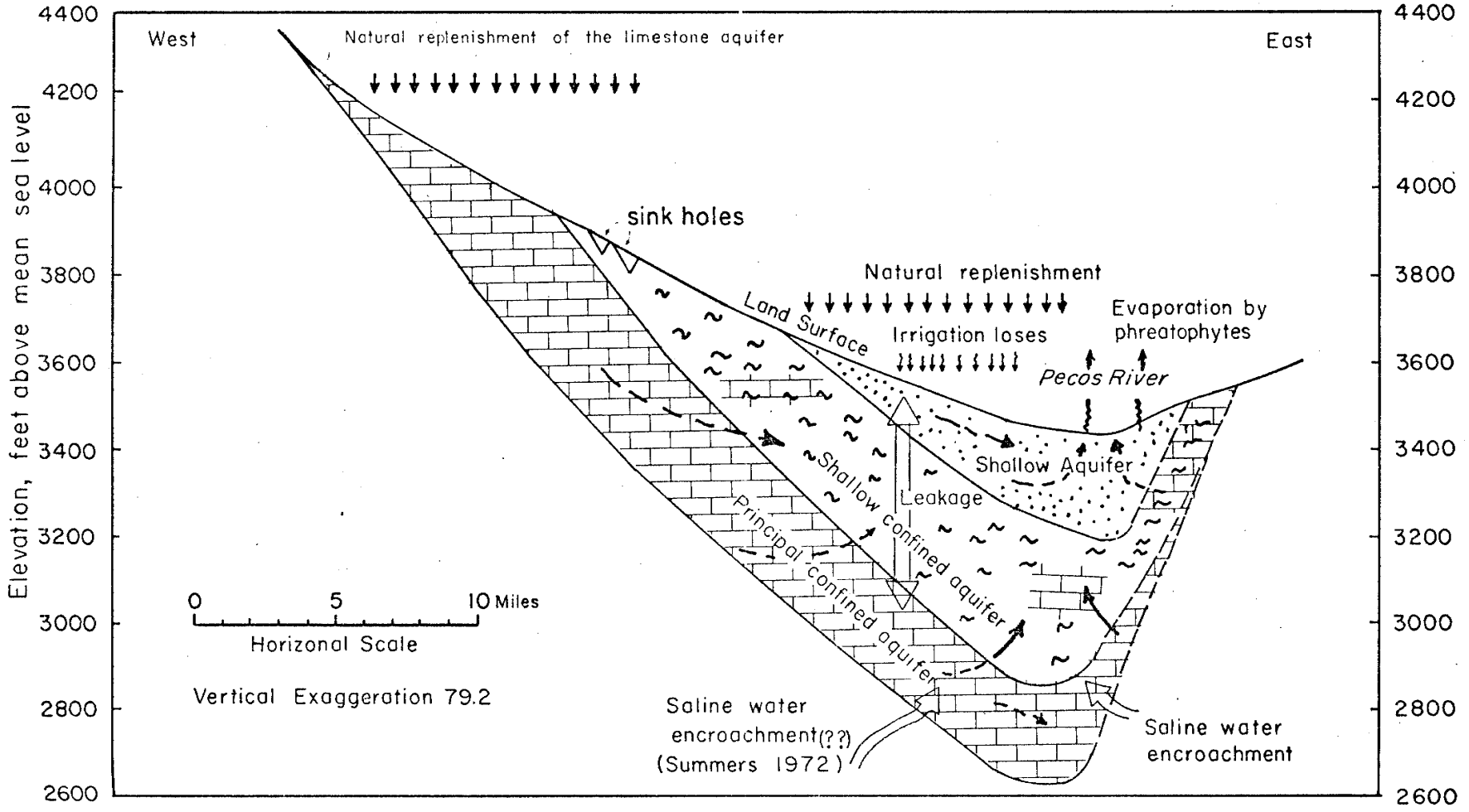
West
East
Natural replenishment of the limestone aquifer
sink holes
Natural replenishment
Land Surface
Irrigation loses
Evaporation by phreatophytes
Pecos River
Shallow Aquifer
Leakage
Shallow confined aquifer
Principal confined aquifer
Saline water encroachment(??) (Summers 1972)
Saline water encroachment
0 5 10 Miles
Horizonal Scale
Vertical Exaggeration 79.2
Elevation, feet above mean sea level
4400
4200
4000
3800
3600
3400
3200
3000
2800
2600

basin is also one of the few basins for which systematic tritium measurements have been carried out for a considerable number of wells since 1959 (Buttlar, 1959; Rabinowitz, 1972), providing valuable information on groundwater velocities in the basin. Chemical data of groundwater is available mostly for the eastern part of the area (Hood, 1959), where intrusion of saline water (Henninghausen, 1970) has caused significant problems for irrigation. Additional samples were collected and analyzed by the author (Fig. 7.2; Appendix E).

7.1 Hydrogeological Background and Data

(a) General - The groundwater system of the Roswell basin consists of two distinct aquifers (Fig. 7.3)--the San Andres limestone semi-confined aquifer of Permian age, and a shallow phreatic aquifer of Quaternary age, consisting of alluvial sand and gravels. The two aquifers are separated over much of the area by semi-confining beds of the low-permeability Artesia group, ranging in thickness from 0 to 600 ft. (Welder, 1972; Henninghausen, 1970). The work presented here is limited to the study of the dissolution processes taking place in the San Andres limestone aquifer. The San Andres formation is divided into three main units (Kelley, 1971), of which only the upper one (the Fourmile Draw member) is exploited by wells.

(b) The Aquifer System - The Roswell groundwater basin can be defined as a leaky-coupled system, in which the leakage occurs through the Artesia semi-confining beds (Fig. 7.3).

The main source of water in the basin is precipitation on the outcrops of the San Andres limestone aquifer in the west. The eastern boundary of the recharge area is located between the western boundaries

Figure 7.4 - Potentiometric surface contour map (January, 1926) of the San Andres Limestone aquifer (Saleem and Jacob, 1971), showing the general pattern of flow.

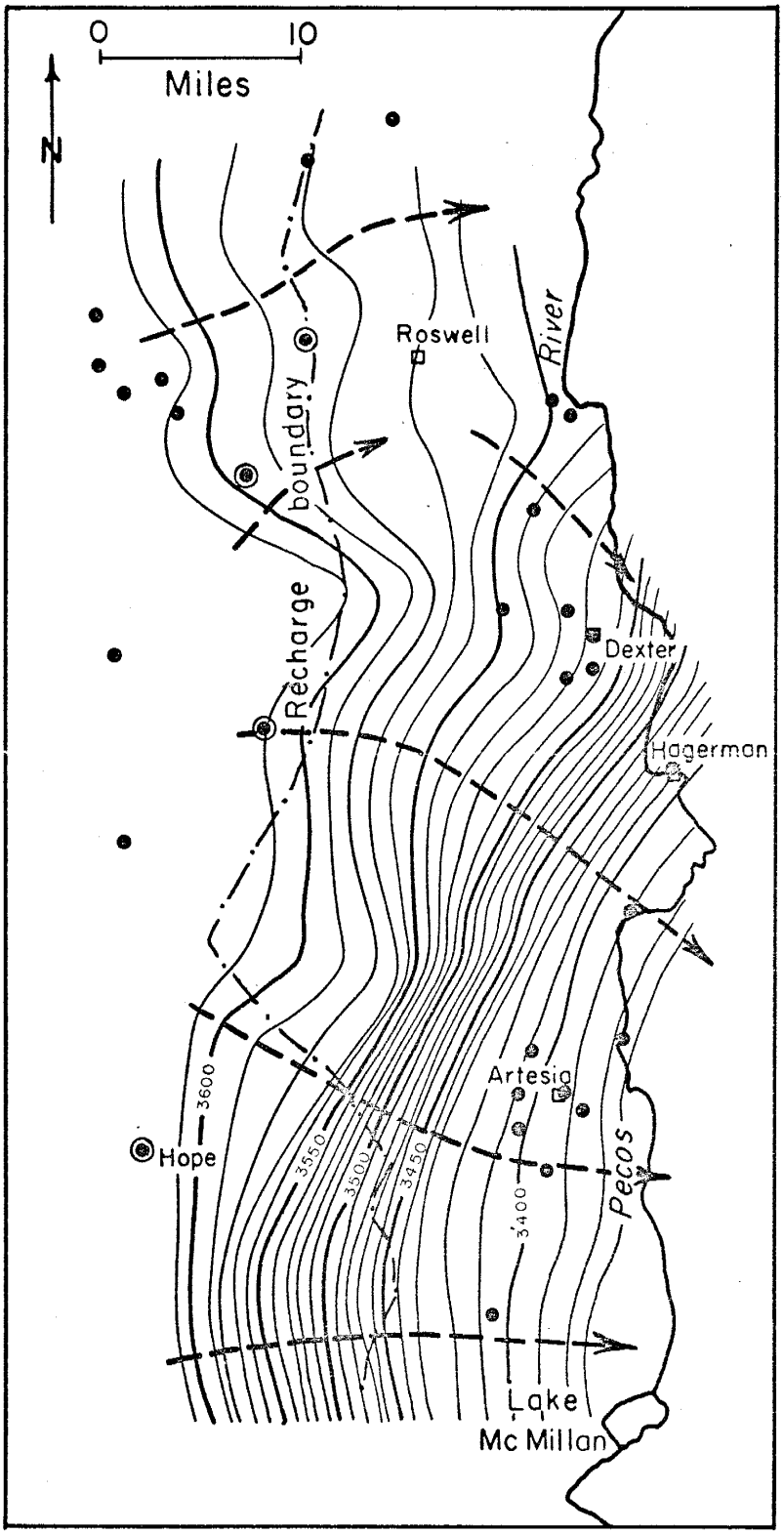
0
10
Miles
N
Roswell
River
boundary
Recharge
Dexter
Hagerman
Artesia
Hope
3600
3550
3500
3450
3400
Pecos
Lake
Mc Millan

of the shallow aquifer and the alluvium Quaternary beds (Fig. 7.3). Following the mapping of exposed sinkholes (Summers, 1972; Motts and Cushman, 1964), the recharge boundary was located along the eastern border of this zone sinkholes (Fig. 7.2). The average replenishment rate through the limestone outcrops was estimated at 240,000 acre-ft/yr (Hantush, 1955). The shallow aquifer is replenished partly by direct percolation of rainfall, as well as by considerable amounts of irrigation losses (about 25%).

The general direction of the groundwater flow in both aquifers is toward the east. Fig. 7.4 shows a typical water level map of the principal limestone aquifer. The general pattern of flow is described in Figures 7.3 and 7.4 .

The connection between the confined and shallow aquifers is by leakage through the semi-confining Artesia beds (Fig. 7.3). The direction of leakage is determined by the difference in hydraulic head between the two aquifers; the direction of flow is from the aquifer having the higher potential to the aquifer having the lower one. The most obvious direction of leakage in the undisturbed system is from the confined to the shallow aquifer. However, due to the intensive utilization of the confined limestone aquifer and the high return flow from irrigation to the shallow aquifer, the net direction of leakage is now from the shallow to the confined aquifer (Saleem and Jacob, 1971; Gisser and Mercado, 1972).

The natural outlet of the leaky-coupled system is the Pecos river, to which the shallow aquifer discharges either by direct seepage or through small springs located on its tributaries. The

TABLE 7.1 Average values of aquifer characteristics[1]

(From Saleem and Jacob 1971)

Area	Confined Aquifer				Shallow Aquifer		
	T* ($10^3 ft^2$/day)	S	K' /b' (per day)	B (10^3 ft)	T ($10^3 ft^2$/day)	S**	B (10^3 ft)
Roswell	187.0	1.0×10^{-5}	1.5×10^{-4}	35.0	13.4	0.10	9.5
Dexter	10.0	5.0×10^{-5}	8.2×10^{-6}	35.0	13.4	0.10	40.0
Artesia	20.1	5.0×10^{-5}	3.2×10^{-5}	25.0	13.4	0.10	20.0
Lakewood	8.8	1.0×10^{-4}	1.3×10^{-5}	26.0	13.4	0.10	36.0
Intake Area	10.0	5.0×10^{-2}					

1 After Hantush (1955).

* T, S, K' /b', and B denote transmissivity, storativity, leakance, and leakage factor, respectively.

** The ultimate average specific yield is believed to be about 20 percent.

evapotranspiration by salt cedars, located mainly along the Pecos river, may be considered another important component of the natural discharge from the shallow aquifer.

Groundwater is withdrawn mainly from the two principal aquifers. The average pumpage is about 400,000 acre-ft/yr (Mercado and Gisser, 1972). The deep aquifer accounts for about 60% of the pumpage volume.

(c) The Hydrologic Constants - The hydraulic characteristics of the aquifers, namely transmissivity, storativity, and leakance, were estimated through elaborate hydrological studies by Hantush (1955), Saleem and Jacob (1971), and Summers (1972). Table 7.1 summarizes the average values of these constants for the various parts of the Roswell basin. From this table the storativity and transmissivity of the shallow aquifer seems to be rather constant and homogeneous, whereas the transmissivities at various locations of the limestone aquifer vary by more than one order of magnitude, Figure 7.5 shows the transmissivity distribution in the limestone aquifer as evaluated from maps prepared by Summers (1972), and Motts and Cushman (1964).

7.2 Chemical Characteristics of Groundwater in the Roswell Basin

Figure 7.6 shows the areal distribution of the various aqueous species in the aquifer, based on both published data (Hood, 1959), and samples collected by the author (Appendix E). Figure 7.7 shows the distribution of computed $pCO_2 (=-\log CO_2)$, and measured temperature.

The distribution of aqueous species reflects the general pattern of flow in the aquifer (Fig. 7.4). The minimum concentration of species (except bicarbonates) is attained in the recharge area. The concentration of species increases in the direction of low, being proportional

Figure 7.5 - Transmissivity (thousands of gpd/foot) map of the Roswell limestone aquifer. The major part of the map is based on Summers (1972). The transmissivity of the southeastern part of the aquifer was reduced according to Motts and Cushman (1964). The calibration of the hydrogeochemical model, presented in this chapter, is based on this map.

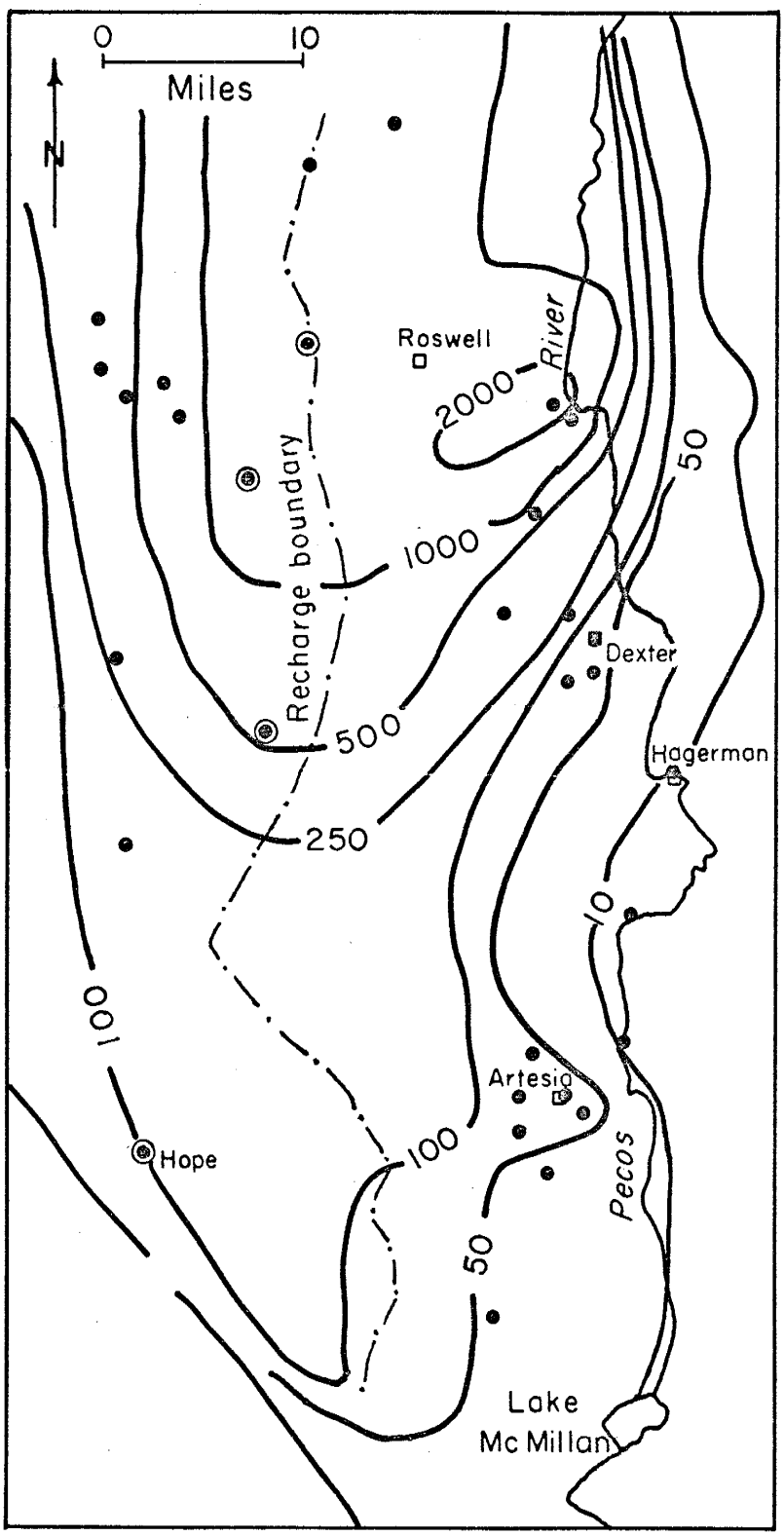
0
10
Miles
N
Roswell
River
2000
1000
500
250
100
50
10
100
50
Recharge boundary
Dexter
Hagerman
Artesia
Hope
Pecos
Lake
Mc Millan

Figure 7.6 - Calcium, magnesium, sulphate, bicarbonate, and pH maps of the Roswell limestone aquifer, showing both measured (figures beside sampling points) and computed (iso-concentration lines) concentrations of species. Computation of the iso-concentration lines is by use of the hydrogeochemical model and not simply interpolating the raw field data. Chemical analyses of circled sampling points (⊙) were used for estimating the initial concentrations of aqueous species along the recharge boundary. Theoretical concentrations were computed by the HYDCEM computer program for $k_c = 4.0 \times 10^{-4}$, $k_d = 4.5 \times 10^{-5}$, and $k_g = 5.85 \times 10^{-6}$ M/year, as discussed later in this chapter. The groundwater velocity field, as determined by the HYDCEM program, is based on the 1926 water level map and the transmissivity distribution described by Figures 7.4 and 7.5 respectively; the effective thickness (=bn) of the aquifer was estimated to be two feet (Rabinowitz, 1972). Numbers in regular parenthesis (pH map) indicate pH measurements made at the laboratory after prolonged time, and thus possibly worthless for geochemical interpretation.

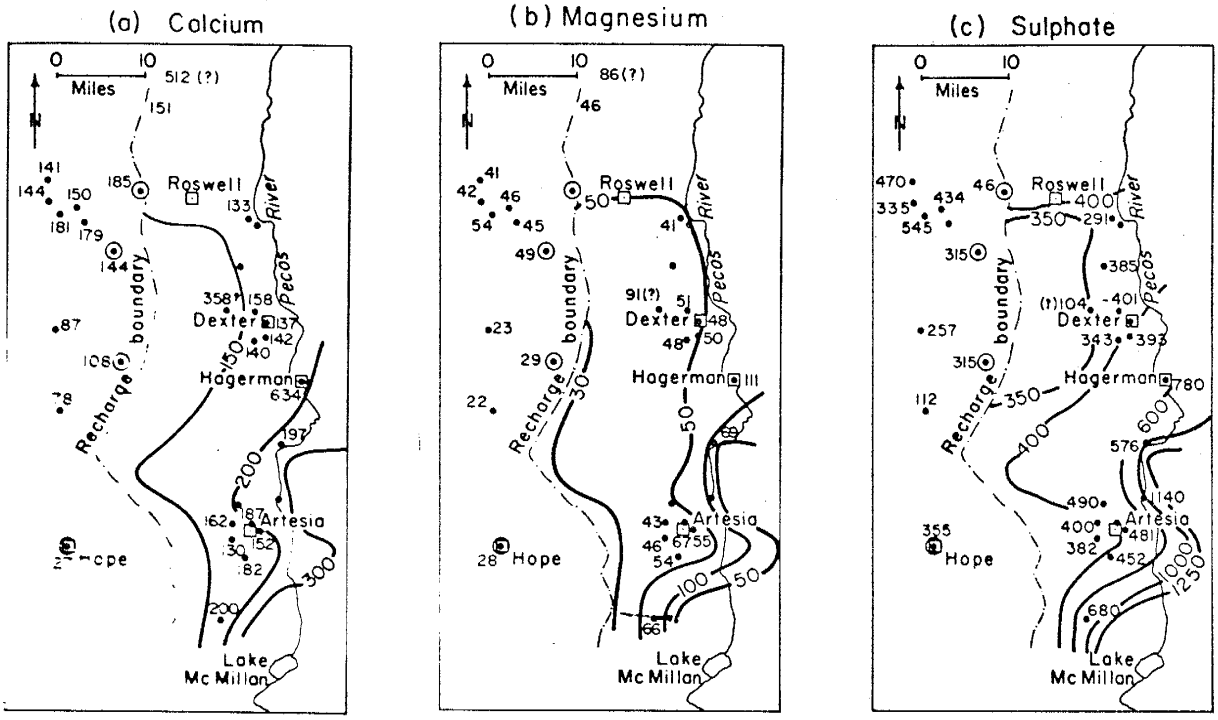
(a) Calcium
0 10
Miles
N
512 (?)
151
141
144
150
185
Roswell
133
River
Pecos
181
179
144
boundary
358
158
Dexter
137
142
87
140
150
Recharge
106
Hagerman
634
78
197
200
187
162
Artesia
152
30
182
300
200
Hope
Lake
Mc Millan
(b) Magnesium
0 10
Miles
N
86(?)
46
41
42
46
Roswell
50
River
54
45
41
49
91(?)
51
Pecos
boundary
Dexter
48
23
48
50
Recharge
29
Hagerman
111
30
22
50
68
43
Artesia
46
67
55
28
Hope
54
100
50
66
Lake
Mc Millan
(c) Sulphate
0 10
Miles
N
470
46
Roswell
400
River
434
335
350
291
545
315
385
Pecos
boundary
(?)104
401
Dexter
257
343
393
315
Recharge
Hagerman
780
350
112
600
400
576
490
1140
Artesia
400
481
355
382
452
1000
1250
Hope
680
Lake
Mc Millan
(d) Bicarbonate
0 10
Miles
N
150(?)
175
200
200
190
180
190
228
Roswell
River
195
397(?)
250
275
300
236
226
Pecos
boundary
224
239
Dexter
235
236
234
241
250
235
245
Hagerman
186
Recharge
354
225
226
235
182
240
Artesia
160
176
242
223
Hope
250
250
245
Lake
Mc Millan
(e) pH
0 10
Miles
N
7.65
7.6
7.4
7.15
7.60
(7.50)
Roswell
7.40
River
{7.49}
{7.60}
7.70
7.20
6.95
7.50
7.10
(7.40)
7.20
boundary
Pecos
Dexter
(7.80)
7.85
(7.15)
7.49
Hagerman
Recharge
7.45
7.40
7.30
7.10
(7.70)
(7.20)
(7.30)
Artesia
7.41
Hope
Legend
7.60 — Field pH
(7.40) — Lab. pH
{7.49} Lab. pH within 12 hours
[6.95] — Field pH of saline sample
7.17
7.15
Lake
Mc Millan

Figure 7.7 - Temperature (°C) and pCO_2(= -log CO_2 concentration) maps of the Roswell limestone aquifer. Both maps serve as boundary conditions for the dissolution process simulated by the HYDCEM computer program. One of the explanations for the steep temperature gradient along the Pecos river is the low groundwater velocity along the eastern boundary of the aquifer. Similarly, the low temperature area in the west-central part of the map may indicate an area of major recharge (?). Iso-pCO_2 lines are based on field pH measurements only.

(a) $pCO_2 = -\log(CO_2)$

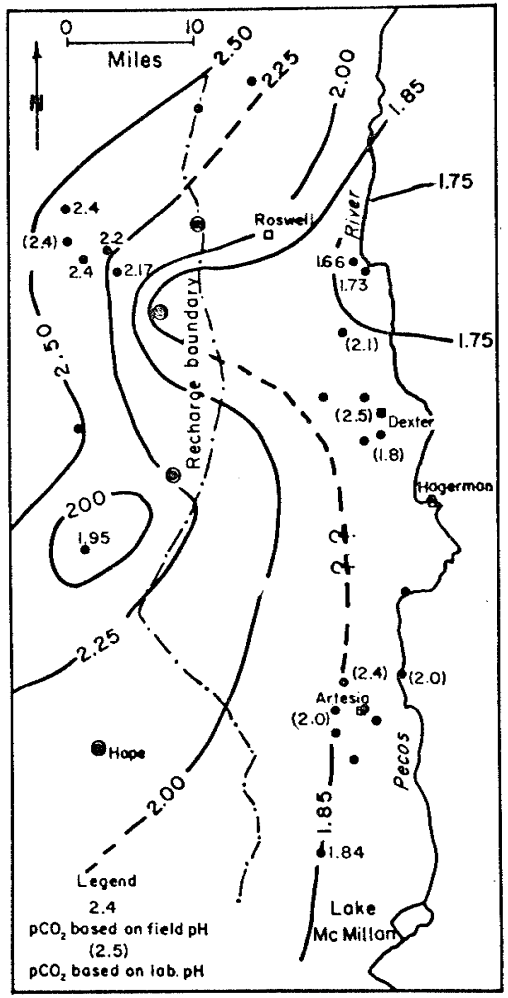

(b) Temperature

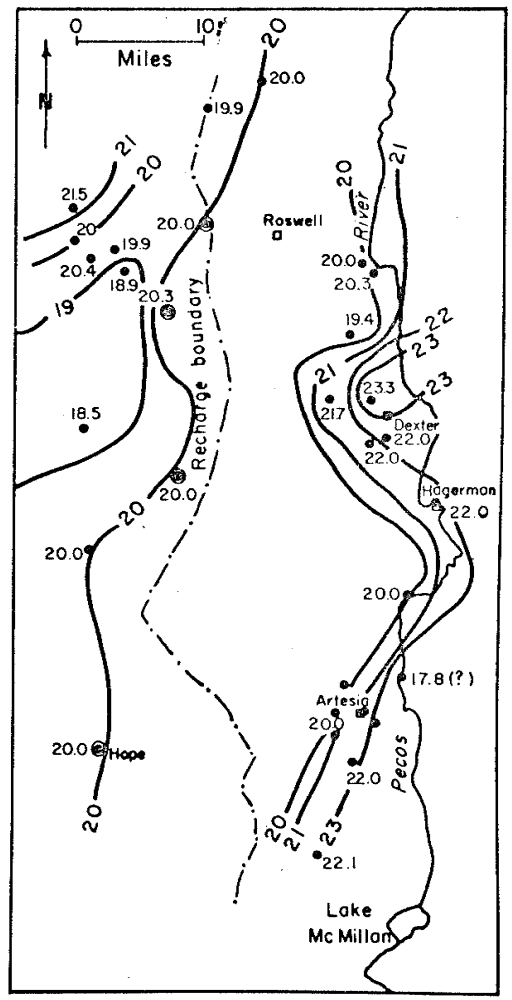

Figure 7.8 - Residence time (years) distribution of the groundwater solution in the Roswell limestone aquifer, computed with the aid of the HYDCEM program, and based on corrected transmissivity (see text). Ages are related to the recharge boundary isochrone, assigned a zero reference age. The dissolution process was simulated along the stream-lines indicated in the figure.

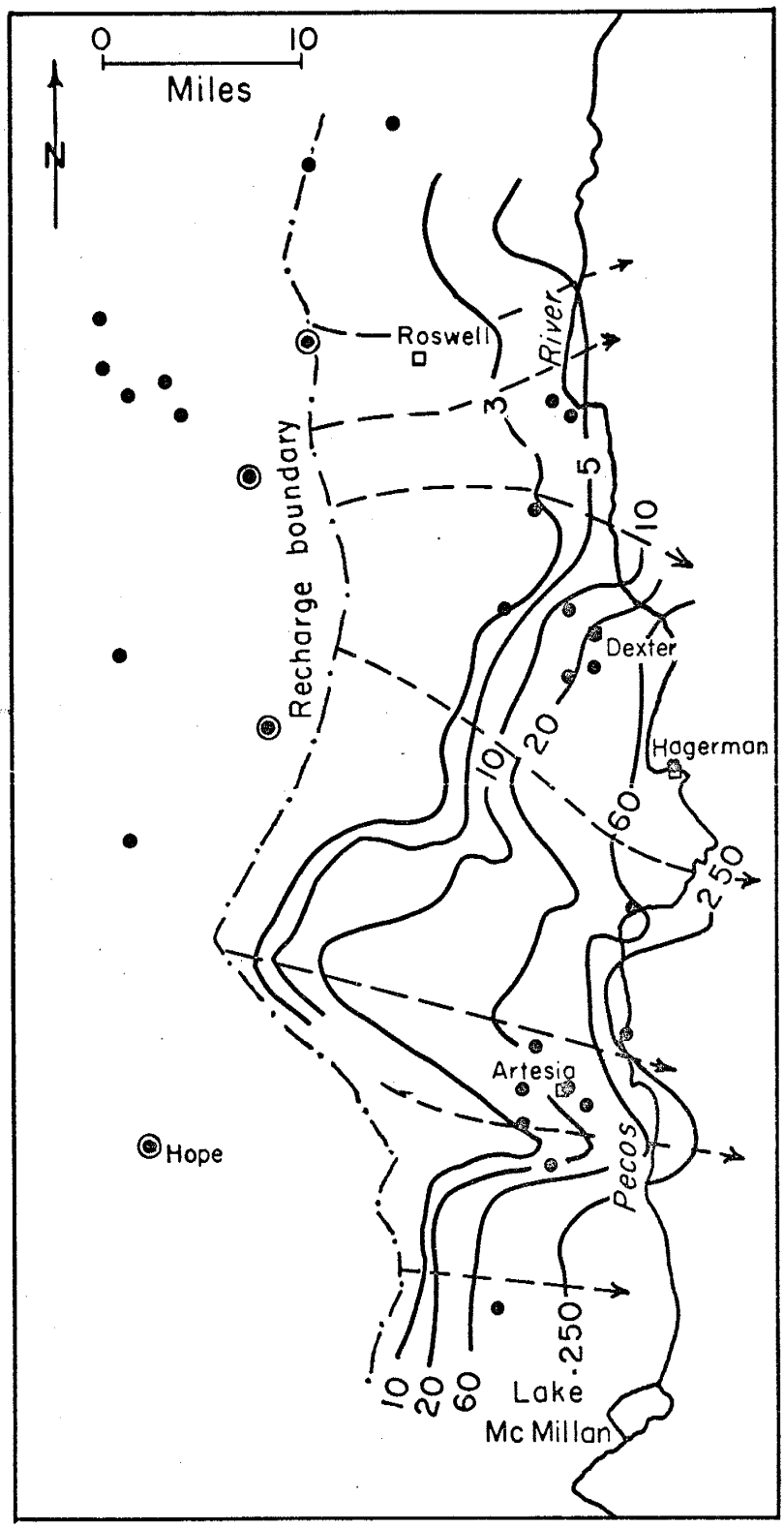
0
10
Miles
N
Roswell
Pecos River
Recharge boundary
3
5
10
Dexter
Hagerman
10
20
60
250
Artesia
Hope
10
20
60
250
Lake
Mc Millan

Figure 7.9 - Chemical characteristics of the Roswell limestone groundwater (modified Piper diagram) showing the changes caused by dissolution process and mixing with sodium-chloride brines. According to the plot there is no significant difference between "pure" San Andres water and mixtures of San Andres water with Grayburg (○) or shallow aquifer (⊕) waters. Units are % of total cations or anions in millequivalents.

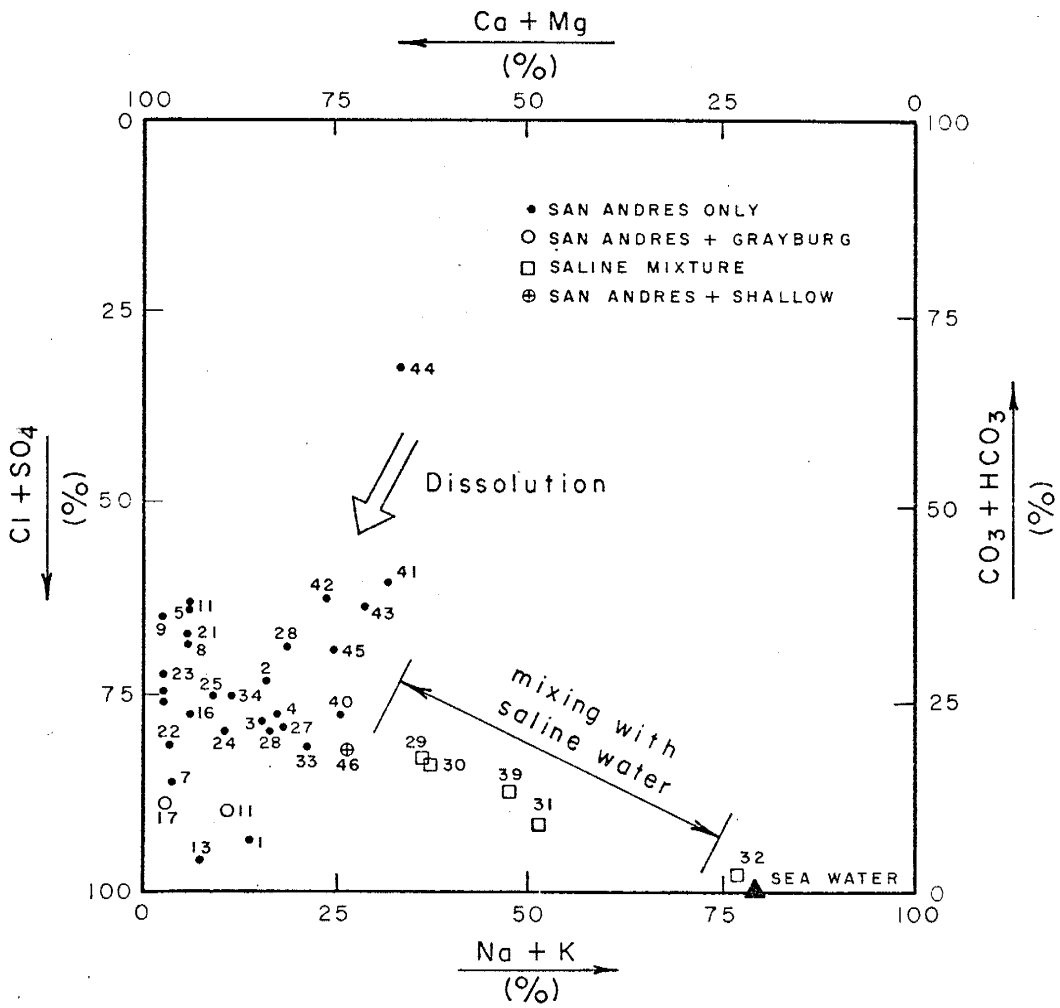
Ca + Mg
(%)
100
75
50
25
0
SAN ANDRES ONLY
SAN ANDRES + GRAYBURG
SALINE MIXTURE
SAN ANDRES + SHALLOW
Dissolution
mixing with saline water
SEA WATER
Cl + SO4
(%)
CO3 + HCO3
(%)
Na + K
(%)

to the residence-time of groundwater (Fig. 7.8).

A modified Piper diagram of the available chemical analyses is given in Fig. 7.9, showing essentially the same trends observed in the Florida limestone aquifer (Fig. 5.4). Samples 29, 30, 31, 32, and 39 were excluded from subsequent study, as they are significantly mixed with saline water intruding along the northeastern boundaries of the aquifer (Fig. 7.2).

The computed pCO_2 ($=-\log CO_2$) of groundwater in the limestone aquifer varies between 1.66 and 2.54 (Fig. 7.7), which is well above the atmospheric pCO_2 (=3.5). This may indicate that CO_2 is produced or supplied within the aquifer system, downstream of the recharge boundaries.

The existence of high dissolved CO_2 concentrations, regardless of their origin, causes additional dissolution of both calcite and dolomite, increasing the permeability and porosity of the aquifer. A positive correlation between dissolved CO_2 concentration and transmissivity (=permeability x thickness) is shown in Fig. 7.10 . The validity of this correlation is limited to the northeastern part of the aquifer. The lack of correlation in the southern portion of the aquifer may reflect varistions in mineralogy. The dissolution of gypsum is pH and pCO_2 independent.

The high permeability of the northern portion of the investigated area can be attributed to the collapse and flushing of gypsum beds in this area (Summers, 1972). This collapse was at least aided by the increased dissolution of calcite and dolomite, caused by unusually high CO_2 pressures.

Figure 7.10 - Correlation between transmissivity and pCO_2 ($=-\log_{10} CO_2$ concentration) for the northern part of the investigated area. The correlation does not hold for the southern part of the aquifer, dominated probably by gypsum.

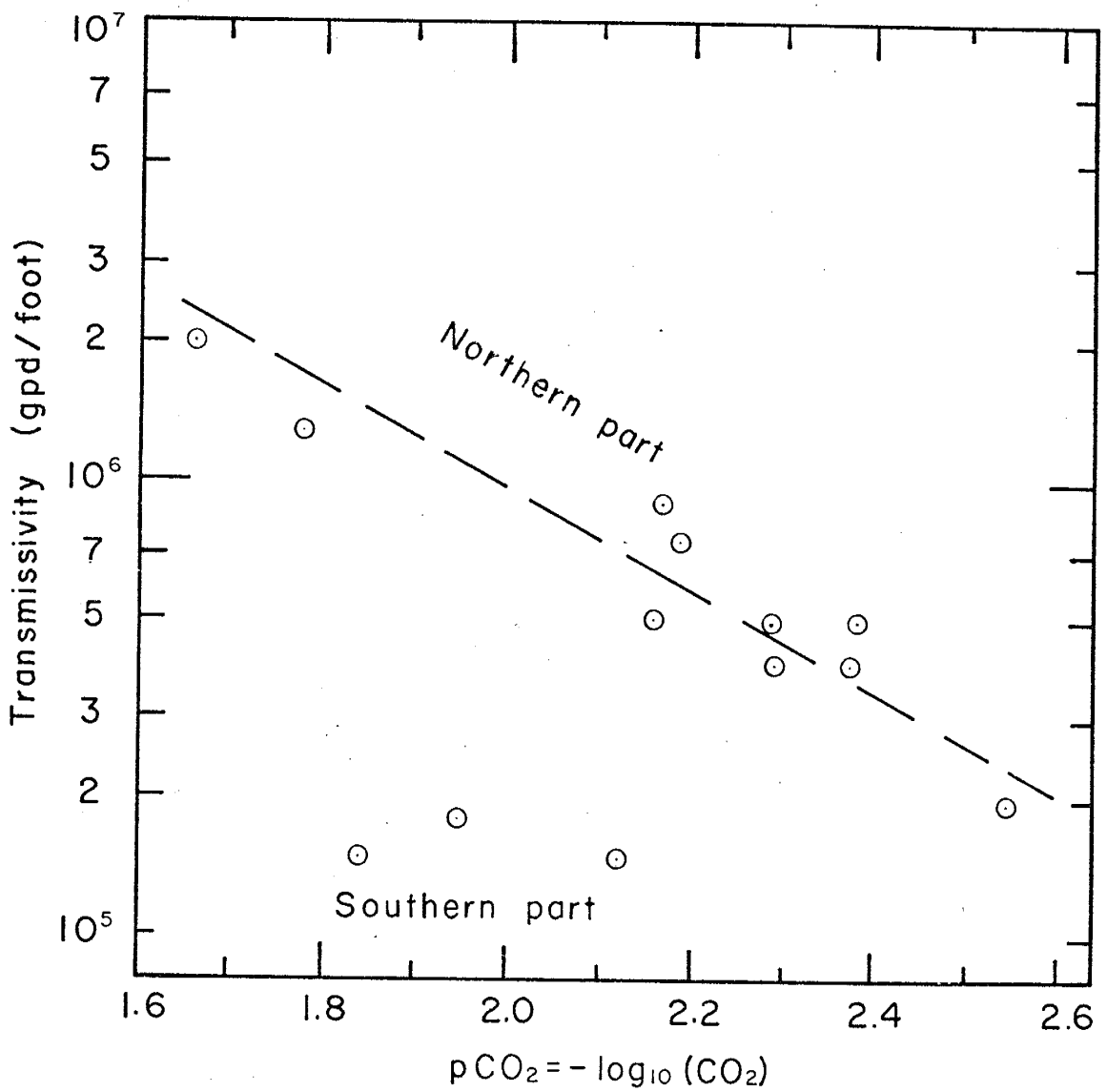
Transmissivity (gpd/foot)
10^7
7
5
3
2
10^6
7
5
3
2
10^5
Northern part
Southern part
1.6
1.8
2.0
2.2
2.4
2.6
pCO2 = - log10 (CO2)

7.3 The Hydrogeochemical Model of the Roswell Limestone Aquifer

(a) Basic Assumptions and Data - The derivation of the Roswell hydrogeochemical model, presented below, is based on the following assumptions:

1. The chemical composition of groundwater, downstream of the presumed recharge boundary, is determined by dissolution processes only. Changes in water quality, caused by the intrusion of saline water are neglected by selection of samples.

2. The major minerals forming the Roswell limestone aquifer are: calcite, dolomite, and gypsum.

3. The three minerals are homogeneously distributed in the aquifer, permitting the use of constant dissolution rate coefficients, over the whole area.

4. The chemical composition of groundwater has not changed considerably during the last 46 years (1926-1972), permitting the use of chemical analyses collected at different dates. Following this reasoning, water quality data should be a function of the flow pattern which prevailed in the early 20's (i.e., the 1926 water level map) rather than of the present flow regime.

5. Water contributed through leakage does not alter the chemical composition of the groundwater solution.

6. The flow problem to be considered is two-dimensional; leakage, from both upper and lower aquifers downstream of the recharge boundary is neglected.

7. The distribution of pCO_2, temperature, sodium, and chloride, which is determined primarily by secondary processes, will serve

here as a set of boundary conditions for the dissolution process.

(b) Calibration of the Hydrogeochemical Model - The calibration of the model was carried out in two steps, facilitating the handling of the complicated system:

1. The dissolution rate constants with respect to calcite, dolomite, and gypsum were estimated roughly with the aid of the CARMOD-B computer program (Chapter 3 and Appendix G), using chemical data of San Andres wells, except those contaminated by saline water (29, 30, 31, 32, 39). This program requires known concentration-time relationships. The residence-time corresponding to the available samples was computed with the aid of one of the options offered by the HYDCEM program (Chapter 6 and Appendix G). The hydrologic data used for determining the residence-time distribution were chosen as follows:

(1) Water levels: 1926 surface map (Saleem and Jacob, 1971).

(2) Transmissivity distribution: Summer's map (Summers, 1972).

(3) Effective Thickness (=bn): was estimated at 2 ft. (Rabinowitz, 1972) over the whole area.

The chemical boundary conditions, namely pCO_2, temperature, sodium and chloride, were regressed to the form of a third-order polynomial with respect to the estimated residence time; this is one of the input options offered by the CARMOD-B program (Appendix G).

The plot of the concentration of species against elapsed time had shown, in initial computer runs, an unexplained "jump" of concentrations, occurring after 20 to 30 years in samples 13, 20, 38. This may indicate that the actual residence-time in the southeastern part of the aquifer is longer than the computed one. In order to delineate

the concentration-time curves, the transmissivity of this part of the aquifer was slightly reduced (Fig. 7.5). Later on, this change of Summer's original map was justified by study of the permeability map prepared by Motts and Cushman (1964, Plate 5). The author was not aware of this map at the beginning, which demonstrates the interaction between hydrological and geochemical data yielding a better understanding of both systems. Figure 7.8 shows the resulting residence-time distribution in the aquifer, following the change in transmissivities.

(ii) The estimates described above, were refined with aid of the HYDCEM computer model. At this stage pCO_2, temperature, sodium and chloride distributions were discretized and used as geochemical boundary conditions, assigned for each block of the grid system used by the model (Fig. 7.2). Similarly, the appropriate hydrological data were discretized according to the grid system (Appendix F). The initial concentration along the recharge boundary was approximated by using the chemical analyses of groundwater samples collected in the vicinity of this boundary (Fig. 7.6). Chemical composition was computed along several stream lines, as indicated in Figure 7.8 .

Following several calibration runs, the best fit values of the dissolution rate coefficients were determined to be: $k_c = 4.0 \times 10^{-4}$, $k_d = 4.5 \times 10^{-5}$, and $k_g = 5.85 \times 10^{-6}$ M/yr for calcite, dolomite, and gypsum respectively. Figure 7.6 shows the resulting water quality maps as compared to the actual field data. Considering the extremely complicated geochemical and hydrogeological features of the Roswell basin, as compared to the oversimplified assumptions listed above, the hydrogeochemical model seems to be a reasonable approximation of the

field conditions, as far as the comparison between computed and measured water quality data is concerned. The model fails to reproduce, however, the relatively high concentrations of samples 1, 7, and 13 (Fig. 7.2 and Fig. 7.6). The high concentration of sample 13 can be explained by a localized low-permeability zone, which might be expected along the eastern boundary of the aquifer (Fig. 7.5). The only explanation offered for the high concentration of samples 1 and 7 is that these wells penetrate both San Andres and Grayburg units; the Grayburg groundwater is more stagnant and therefore more saline (See samples 14, 15, 17 and 18 in Appendix F). These wells have been defined, however, as tapping the San Andres formation only (Hood, 1959).

7.4 Comparison Between Computed Residence-Time and Tritium Data

Available tritium data were used by Rabinowitz (1972) to determine the transit-time of bomb-produced tritium pulses in the northern and central parts of the investigated area. The most probable range for transit-times was estimated also for the southern part of the aquifer (ibid). According to his research, the age of most groundwater samples was within the range of 3 to 10 years, with the exception of the low permeability zone below Lake Arthur (about 8 miles south of Hagerman), where the groundwater may exceed the age of 20 years (Rabinowitz, 1972).

Tritium data seem to be in reasonable agreement with the hydrologic age estimates (Fig. 7.8). The only contradiction between the two estimates is between Dexter and Lake Arthur, along the eastern part of the aquifer, where the hydrologic estimates of 20 to 60 years do not

agree with tritium measurements. This disagreement could be resolved by decreasing the calculated residence time which would require increased transmissivity in this area. Further interpretation of data may also show that the aquifer is not chemically homogeneous, as assumed above.

Generally, if reliable age-estimates (tritium or otherwise) are available, one should calibrate the transmissivity map of the aquifer and then determine the distribution of the dissolution rate constants.

8. SUMMARY AND RECOMMENDATIONS

The aim of this study was to develop quantitative relationships between hydrologic and geochemical progesses, especially in limestone aquifers, and to enhance the use of water quality data for hydrologic investigations. Some of the results and conclusions, stemming from this work, are discussed briefly below.

8.1 Kinetic Models

(a) Dissolution of Single Minerals - Two kinetic laws, representing the two extreme alternative mechanisms of the dissolution process, were considered: (i) transport-controlled kinetics, governed by a verified form of the Nernst equation, and (ii) chemically-controlled kinetics, governed by an approximate form of the mass-action law (Eq. 2.26):

$$\frac{1}{\nu_p}\frac{dC_p}{dt} = k[1 - \beta(t)]$$

Laboratory experimental results seem to satisfy both laws as far as the consistent reproduction of experimental data is considered. However, since the experimental rate constants, determined for the transport-controlled dissolution of both gypsum and calcite, were lower by 3 to 5 orders of magnitude than those predicted by diffusion theory, the transport-controlled alternative was rejected.

(b) The β Approximation - Both analytical studies and experimental evidence indicate that the reaction ratio, under certain restrictions, can serve as a tracer for practical purposes. This property of the $\beta(t)$ function can be used for deriving approximate solutions for transient-cases.

(c) Dissolution of Multi-Mineral Assemblages - The dissolution of multi-mineral assemblages in aqueous solutions was described as kinetic competition between the dissolving minerals. The variation of the concentration C_i of the i-th species, with respect to the time t, was defined as the sum of the variations of each mineral j separately (Eq. 2.44):

$$\frac{dC_i}{dt} = \sum_j [\nu_{ij} k_j (1 - \beta_j(t))]$$

The equation above explains the supersaturation of groundwater with respect to several minerals as the net result of the kinetic competition between dissolving minerals. Thus, both dissolution and precipitation of different minerals, having a common product ion, may occur simultaneously. When the dissolution rate of one mineral is higher than the rate of precipitation of other minerals, the solution will tend toward supersaturation with respect to other minerals.

The dissolution processes in carbonate aquifers, where calcite, dolomite, and gypsum may dissolve simultaneously, served as a demonstration of the kinetic competition discussed above. The solubility gap between gypsum and calcite, or gypsum and dolomite, force the dissolution of gypsum to proceed, increasing the calcium content of the solution even when the solution is supersaturated with respect to dolomite or calcite.

The simultaneous dissolution process was studied for two boundary conditions related to the carbonate equilibria: (i) the dissolving system is equilibrated with an external CO_2 source, with partial pressure either constant or varying in time or space coordinates.

(ii) the dissolving system is equilibrated originally with an external CO_2 source (say-CO_2 of the soil atmosphere), but then closed at some time $t = 0^+$. Following both laboratory and field studies, it was concluded that the first boundary condition is closer to reality.

Some of the major errors involved in the interpretation of ^{14}C data, even when corrected with the aid of $\delta^{13}C$ measurements, may be related to the precipitation of calcite and dolomite, as well as to the possible existence of petroleum-derived carbon in the aquifer.

8.2 Comparison Between Laboratory and Field Dissolution Rate Constants

Comparison between the dissolution rate constants determined in the laboratory and those determined from field data, shows that the field rate constants are significantly lower than those predicted from laboratory measurements. A comparison between the two is given in Table 8.1 . The predicted values are based on the laboratory measurements, adjusted for the assumed range (Chapter 2) of $A_s/V = 0.1$ to 100 cm^{-1}.

The large gap between laboratory and field data may be explained by the reduction of the effective surface area, available for the reaction, caused by coating by non-reacting minerals and other impurities of natural minerals. The field rate constants determined for the Roswell area are higher by 1 to 3 orders of magnitude than those determined for Florida. The reason for this gap may be the difference in groundwater velocities, permeabilities, and the difference in mineral composition. In addition, the hydrogeochemical model used for the Roswell example was simplified by assuming $C_i \frac{dv_s}{dS} << v_s \frac{dC_i}{dS}$. This is most certainly not correct for the northern portion of the aquifer. This simplification

TABLE 8.1 - COMPARISON BETWEEN LABORATORY AND FIELD DISSOLUTION RATE CONSTANTS (M/yr)

Mineral	Florida	Roswell	Predicted From Laboratory Experiments*
Calcite	6.5×10^{-7}	4.0×10^{-4}	$2 \times 10^{-3} - 2 \times 10^{-1}$
Dolomite	1.0×10^{-6}	4.5×10^{-5}	
Gypsum	2.25×10^{-7}	5.85×10^{-6}	$1.2 \times 10^{2} - 1.2 \times 10^{4}$

*Note: Based on laboratory experiments for $A_s/V = 0.1 - 100$ cm^{-1}

will affect the field rate constant and is probably reflected in the differences of the field rate constants of Florida and Roswell (see discussion, Chap. 6).

In short, the laboratory rate constants are affected by surface area in contact with the fluids, intrinsic chemical characteristics of the mineral, surface electrostatic effects, and temperature. They may also be affected by surface coating if caused by any process. This is generally more of a problem under field conditions.

Field rate constants are affected by all of these parameters. In addition, because they are derived from spatially distributed chemical analyses they are affected by hydrologic parameters such as velocity, transmissivity and porosity. They are also affected by mineralogic ratios. For example, this is the probable explanation for the observation that field rate constants for gypsum are lower than those for calcite or dolomite in some cases.

A conclusion can be drawn, therefore, that field rate constants cannot be determined from laboratory experiments, or extrapolated from other aquifers. This conclusion represents one of the most serious disadvantages of using water quality data for hydrological investigations, until such time as the effect of aquifer parameters on field rate constants can be further delineated.

8.3 Dissolution and Precipitation Processes in Carbonate Aquifers as a Tool for Groundwater Investigations

Two main courses of using groundwater quality data for hydrological investigations were shown: (i) dating of groundwater age according to a

pre-calibrated concentration-time relationship. This approach was applied in Chapter 5, where the age distribution within the Florida limestone aquifer was determined with the aid of water quality data and compared reasonably well with ^{14}C data. (ii) integrated study of both hydrological and geochemical phenomena with the aid of a hydrogeochemical model (Chapter 6). This approach was applied in Chapter 7 for the Roswell limestone aquifer and resulted in improved transmissivity data for a small part of the basin. In addition, water quality distribution as given by the model compared reasonably well with field data.

Both approaches might yield similar results; however, the second seems to be more general and thus more promising for future investigations.

8.4 Recommendations for Future Studies

(a) Geochemical Processes - The experimental part of this work deals only with the dissolution of calcite, dolomite, and gypsum in carbonate aquifers. In order to generalize the application of hydrochemical models for hydrological studies, more processes should be included in the model; among them: (i) ion exchange by clay minerals; (ii) incongruent dissolution processes, such as the dissolution of silicates; (iii) oxidation-reduction reactions, and (iv) organic geochemical processes:

(b) Hydrologic Applications - The hydrogeochemical models presented above can be used for handling a variety of specific field problems, such as: (i) verification of hydrologic boundary conditions and boundaries. (ii) transmissivity distribution in the aquifer.

(iii) recharge estimates in free-surface aquifers. (iv) intrusion of sea-water in coastal aquifers, and many others. A further study of these topics, and others, under semi-controlled field conditions, is highly recommended.

(c) Ore exploration - The emphasis in this work was on the application of geochemical processes for hydrologic studies. Hydrogeochemical models can be used, however, to predict geochemical distribution based on hydrologic parameters. Ore exploration is probably one of the most promising applications. For a given hydrologic system the distribution of the respective rate constants can be determined from water quality data with the aid of hydrochemical models and rationalize the selection of target areas for further investigations. That is, given a source of tracer, such as a trace element, its measured spatial distribution is a function of hydrology and kinetics. Therefore, a prediction can be made of the location of the source.

(d) Geochemical "Pumping-Tests" - The major disadvantage of geochemical tracers over the radioactive environmental tracers, is that the first group should be pre-calibrated against known hydrologic data. One of the possibilities to overcome this difficulty is to develop geochemical pumping test techniques. Essentially, such tests will include the injection of water into existing pumping wells, and repumping after a certain delay-time. The injected water should be significantly different in composition from the indigeneous aquifer water. It is expected that the kinetic rate constant can be determined from the resulting changes in chemical composition of the repumped water.

(e) The Roswell Limestone Aquifer - The preliminary evaluation

of the Roswell hydrogeochemical model has demonstrated the potential application of such models for hydrologic investigations. The evaluation of this model was based on a set of oversimplified assumptions, and rather scarce chemical data. The refinement of this model calls for further investigations, which should include: (i) collection and analysis of groundwater samples; special attention should be paid to the area between the recharge boundaries and the Pecos River. The potential stratification of the vertical cross-section should be studied by collecting samples from wells penetrating different depths and sub-aquifers. (ii) integration of the hydrogeochemical data with available tritium data. Practically, the hydrologic system should be calibrated first against the residence-time distribution estimated from tritium data; the hydrogeochemical model should then be re-calibrated by using the new set of hydrologic parameters. (iii) the refinement of the hydrogeochemical model may require the extension of the HYDCEM program from two-dimensional to three-dimensional flow fields.

APPENDIX A - DERIVATION OF APPROXIMATE EXPRESSIONS FOR THE RATIO A_s/V IN POROUS MEDIA

The surface area A_s of a given porous medium can be estimated if we presume that it consists of ideal spherical grains.

Considering that the granular medium consists of a mixture of m fractions, each made of N_i identical spheres of radius R_i, then the total surface area A_s, and the volume V_s of the solid spheres are given by (Bear, 1971; Eq. 2.6.2):

$$A_s = \sum_{i=1}^{m} 4\pi R_i^2 N_i \tag{A.1}$$

$$V_s = \sum_{i=1}^{m} \frac{4}{3} \pi R_i^3 N_i = (1-n)V_b \tag{A.2}$$

where V_b is the bulk volume and n the porosity; then:

$$A_s/V_b = \sum_{k=1}^{m} 4\pi R_i^2 N_i \Big/ \left(\sum_{i=1}^{m} \frac{4}{3} \pi R_i^3 N_i/(1-n) \right) \tag{A.3}$$

Defining an harmonic mean radius $\bar{R}$, such that:

$$\frac{1}{\bar{R}} = \sum_{i=1}^{m} R_i^2 N_i \Big/ \sum_{i=1}^{m} R_i^3 N_i \tag{A.4}$$

Then:

$$A_s/V_b = 3(1-n)/\bar{R} \tag{A.5}$$

The water volume V is given by $V - nV_b$, therefore:

$$A_s/V = \frac{3}{\bar{R}} \left(\frac{1 - n}{n} \right) \tag{A.6}$$

APPENDIX B - EVALUATION OF EQUILIBRIUM CONSTANTS AS A FUNCTION OF TEMPERATURE FOR DISSOLUTION REACTIONS IN CARBONATE AQUIFERS

Equilibrium constants of the reactions in carbonate aquifers can be obtained either experimentally, or from available thermodynamic data. Table B.1 summarizes the available experimental, or acceptable data, as used by several investigators. The equilibrium constants are expressed in Table B.1 as $pK = -\log_{10}(K)$. Their experimental dependency on temperature was regressed to a quadratic interpolating polynomials, having the general form of:

$$pK(T) = a + 10^{-4}\, b(T - T_r) + 10^{-6}\, c(T - T_r)^2 \qquad (B.1)$$

The coefficients a, b and c were computed from the experimental data given in the cited references. T is the temperature and T_r is the reference temperature of the polynomial regression, both in centigrades.

Whenever experimental data does not exist for $K_{eq}(T)$, the thermodynamic relationships between enthalpy (ΔH), entropy ($S°$), free energy (ΔG), and heat capacity (c_p), may be used in order to evaluate the function $K_{eq}(T)$. Discussion is limited here to the most useful formulas for determining such functions.

The relationship of enthalpy (ΔH_r) to K_{eq} is expressed by the van't-Hoff equation (for example, Krauskopf, 1967):

$$\frac{d \ln K_{eq}}{dT} = \frac{\Delta H_r}{RT^2} \qquad (B.2)$$

Where R is the gas constant (= 1.98719 cal/mole), and T is the absolute temperature on the Kelvin scale. For small changes in the temperature,

TABLE B.1 - EXPERIMENTAL EQUILIBRIUM CONSTANTS AS A FUNCTION OF TEMPERATURE

Dissolution Reaction	pK at 25°C	Coefficient of pK expansion (eq. B.1)				Temperature Range (°C)	Error Estimate of pK**
		a	b	c	Tr (°C)		
Calcite							
Garrels & Christ (1965)	8.34	8.34	123.33	-22.22	25	10-40	
Langmuir (1971)	8.40	8.37	27.50	25.00	15	5-25	±0.02
Krauskopf (1967)	8.35						
Aragonite							
Hanshaw et al (1965)	8.14						
Krauskopf (1967)	8.22						
Dolomite							
Hanshaw et al (1965)	17.00						
Barnes & Back (1964)	16.65						±0.15
Langmuir (1971)	17.00	16.79	185.00	250.00	15	5-25	±0.30
Anhydrite							
Hanshaw et al (1965)	4.43						
Gypsum							
Hanshaw et al (1965)	4.61						
CO_2							
Garrels & Christ (1965)	1.47	1.47	123.00	-66.70	25	10-40	
H_2CO_3							
Garrels & Christ (1965)	6.35	6.35	-52.50	175.00	25	15-35	
HCO_3^-							
Garrels & Christ (1965)	10.33	10.33	-90.00	111.11	25	10-40	

Note: (*) $pK(T) = a + 10^{-4}b(T - T_r) + 10^{-6}c(T - T_r)^2$
(**) Only if such estimate was given by the cited authors

ΔH may be assumed to be constant, and the solution of eq. (B.2) yields:

$$\log_{10} K(T) = \frac{\Delta Hr}{2.3R}\left(\frac{T - T_r}{T \cdot T_r}\right) + \log_{10} K_r(T_r) \qquad (B.3)$$

where $K_r(T_r)$ is the equilibrium constant at the reference temperature T_r.

In most cases, however, ΔH is a significant function of temperature; the function $\Delta H(T)$ is evaluated from the relationships between the enthalpy and the heat capacity Δc_p:

$$\Delta H = \int \Delta c_p \, dT \qquad (B.4)$$

Δc_p is generally expressed (Kelley 1960) by a power expansion having the general form:

$$\Delta c_p = \Delta a + \Delta bT + \Delta c/T^2 \qquad (B.5)$$

Where Δa, Δb, and Δc are the differences obtained by adding up the expansion constants a, b, and c for the products, and substracting those for the reactants. Substituting (B.5) into (B.4), and integrating with respect to T;

$$\Delta H(T) = \Delta aT + \frac{\Delta b}{2} T^2 - \frac{\Delta c}{T} + A \qquad (B.6)$$

Where A is the integration constant, determined from $\Delta H(T_r)$; T_r being the reference temperature. Substituting eq.(B.6) into the van't-Hoff equation (B.2) and integrating with respect to T;

$$\log_{10} K = \frac{1}{2.303R}\left(-\frac{A}{T} + \Delta a \ln T + \frac{\Delta b}{2} T + \frac{\Delta c}{2T^2} + D\right) \qquad (B.7)$$

D being another integration constant, determined from $K(T_r)$. The

function $K_{eq}(T)$, based on equations (B.6 and B.7) was calculated by a computer program named KEQ (Appendix G).

Whenever experimental or accepted values for $K(T_r)$ are not available, the estimate of the equilibrium constants as a function of temperature, can be evaluated directly from the available thermochemical data. However, the reactions discussed herein have known values for $K(T_r)$.

The thermodynamic properties for the components participating in the reactions given above and used in this work are summarized in Table B.2 . The function pK(T) of both experimental data and computed curves for the dissolution reaction of calcite, dolomite, gypsum, aragonite and anhydrite is shown in Figure B.1 . Figure B.2 described the pK(T) function for the equilibrium relationships among carbon species and the dissociation constant of water $K_w(T)$.

The KEQ computer output for the dissolution reactions of calcite, dolomite, gypsum, aragonite, and anhydrite is given at the end of this appendix.

As can be seen from Figure B.1, there are significant differences among the various estimates. The following estimates for K(T) were chosen: For calcite, the experimental data cited by Garrels & Christ (1965) were preferred over the recent data published by Langmuir (1971) due to the wide application of the former by most investigators. For dolomite the semi-experimental data cited by Langmuir (1971) shifted downward by 0.5 pK units was chosen. It should be mentioned, however, that the estimates for pK (25°C) of dolomite are rather controversial.

TABLE B.2 - THERMOCHEMICAL DATA (25°C)

Component	H_f°	S°	Coefficients of $c_p(T)$			Source
			a	$bx10^3$	$c\ 10^{-5}$	
Ca^{++}	-129,770	-13.2	- 3.2	0.0	0.0	GC,H
$CO_3^=$	-161,840	-13.6	-83.6	0.0	0.0	H
HCO_3^-	-165,090	22.7				H,GC
H^+	0.	0.				
H_2O (liq.)	- 68,317	16.72	18.07	0.0	0.0	GC,H
$SO_4^=$	-217,320	4.8	-48.2	0.0	0.0	H
Mg^{++}	-110,410	-28.2	4.8	0.0	0.0	GC,H
Calcite	-288,442	22.15	24.98	5.24	- 6.20	GC,K
Aragonite	-288,651	21.18	20.13	10.24	- 3.34	H,K
Dolomite	-557,613	37.09	42.76	20.85	-11.53	B,K
Anhydrite	-343,320	25.5	16.78	23.60	0.0	H,B,K
Gypsum	-483,981	46.36	34.75	23.60	0.0	H,B,K

Sources: GC - Garrles & Christ (1965); H - Helgeson (1969;
K - Kelley (1960); B- Beane (Personal Communication - 1972)

Note : H-in Cal/Mole; S-in Cal/Mole/Degree

Figure B.1 - pK as a function of temperature for the dissolution of calcite, dolomite, gypsum, aragonite, and anhydrite. Full lines describe the regression of selected experimental data to a quadratic interpolating polynomial. Dashed lines represent the pK(T) function as computed by the KEQ program.

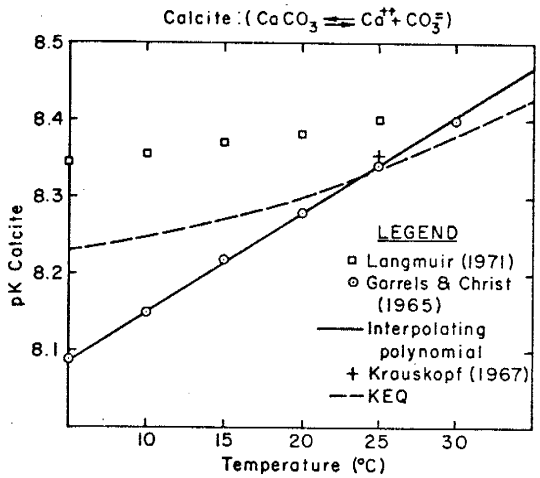
Calcite : ($CaCO_3 \rightleftharpoons Ca^{++} + CO_3^{=}$)
pK Calcite
Temperature (°C)
LEGEND
Langmuir (1971)
Garrels & Christ (1965)
Interpolating polynomial
Krauskopf (1967)
KEQ

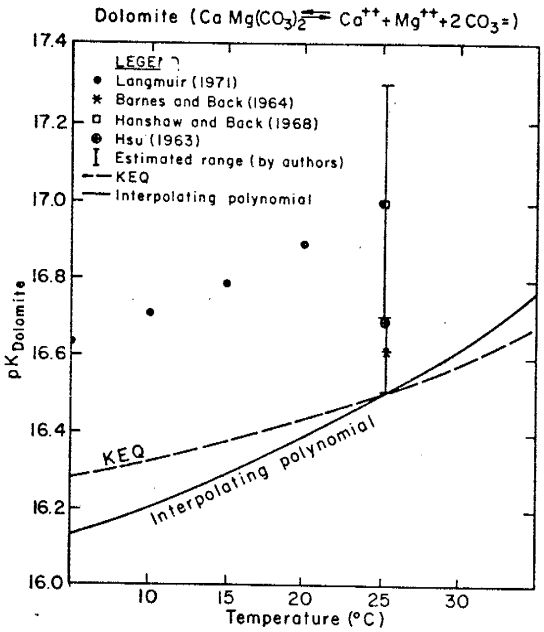
Dolomite ($CaMg(CO_3)_2 \rightleftharpoons Ca^{++} + Mg^{++} + 2CO_3^{=}$)
pK Dolomite
Temperature (°C)
LEGEND
Langmuir (1971)
Barnes and Back (1964)
Hanshaw and Back (1968)
Hsu (1963)
Estimated range (by authors)
KEQ
Interpolating polynomial
KEQ
Interpolating polynomial

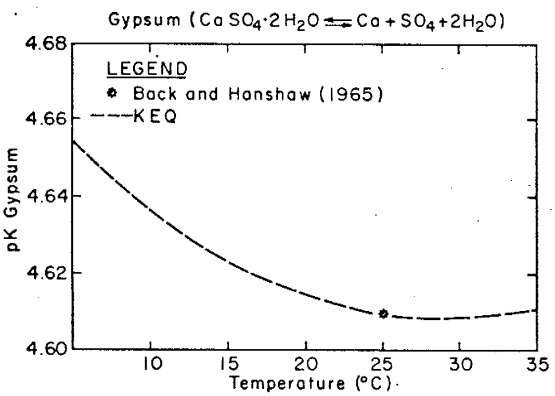
Gypsum ($CaSO_4 \cdot 2H_2O \rightleftharpoons Ca + SO_4 + 2H_2O$)
pK Gypsum
Temperature (°C)
LEGEND
Back and Hanshaw (1965)
KEQ

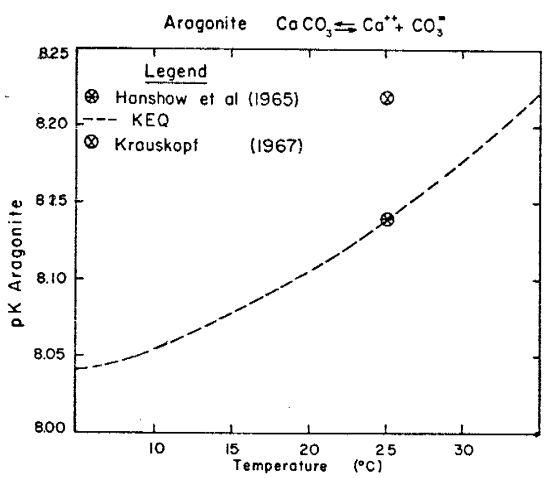
Aragonite $CaCO_3 \rightleftharpoons Ca^{++} + CO_3^{=}$
pK Aragonite
Temperature (°C)
Legend
Hanshow et al (1965)
KEQ
Krauskopf (1967)

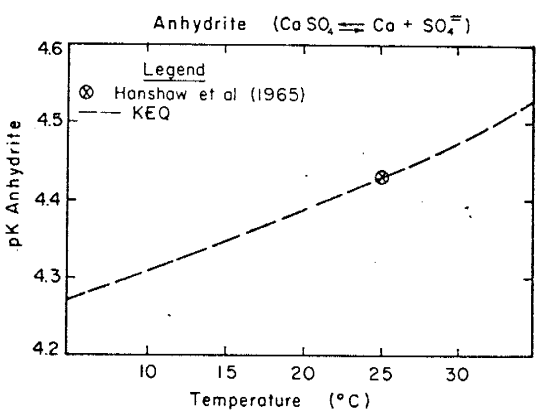
Anhydrite ($CaSO_4 \rightleftharpoons Ca + SO_4^{=}$)
pK Anhydrite
Temperature (°C)
Legend
Hanshaw et al (1965)
KEQ

Figure B.2 - pK as a function of temperature for CO_2, H_2CO_3, HCO_3^-, and water. Full lines represent the regression of data cited by Garrels and Christ (1965) to a quadratic interpolating polynomials.

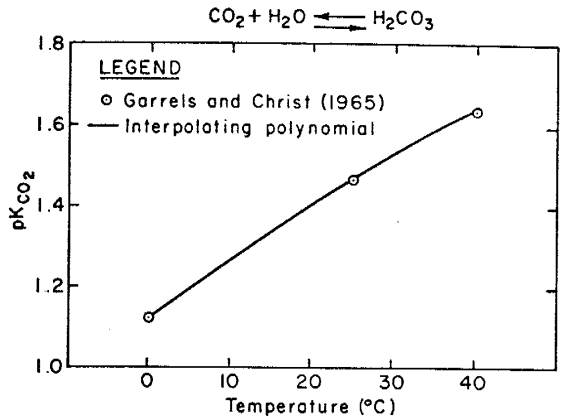
$CO_2 + H_2O \rightleftharpoons H_2CO_3$
LEGEND
Garrels and Christ (1965)
Interpolating polynomial
pK_{CO_2}
1.8
1.6
1.4
1.2
1.0
0
10
20
30
40
Temperature (°C)

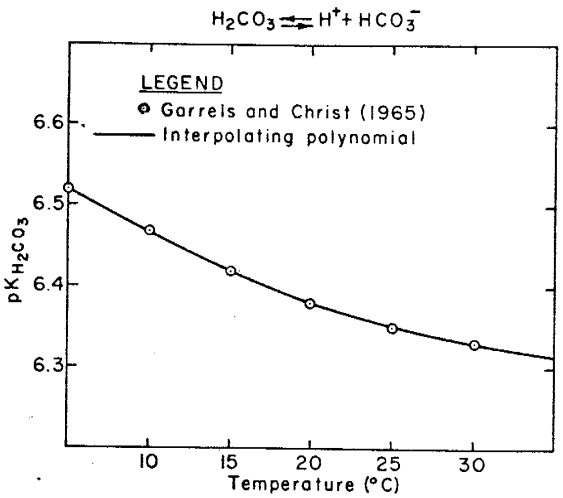
$H_2CO_3 \rightleftharpoons H^+ + HCO_3^-$
LEGEND
Garrels and Christ (1965)
Interpolating polynomial
$pK_{H_2CO_3}$
6.6
6.5
6.4
6.3
10
15
20
25
30
Temperature (°C)

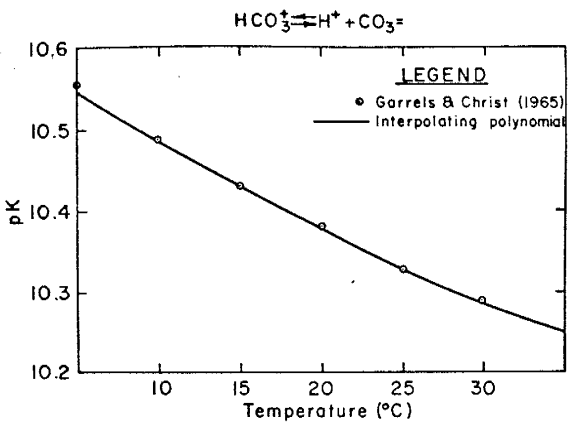
$HCO_3^- \rightleftharpoons H^+ + CO_3^=$
LEGEND
Garrels & Christ (1965)
Interpolating polynomial
pK
10.6
10.5
10.4
10.3
10.2
10
15
20
25
30
Temperature (°C)

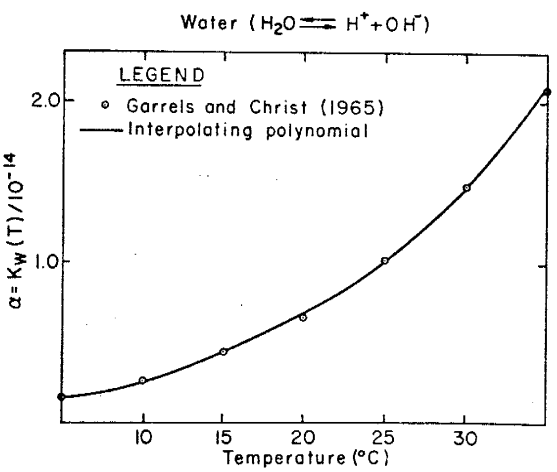
Water ($H_2O \rightleftharpoons H^+ + OH^-$)
LEGEND
Garrels and Christ (1965)
Interpolating polynomial
$\alpha = K_W(T)/10^{-14}$
2.0
1.0
10
15
20
25
30
Temperature (°C)

as they vary between 16.5 and 19.5 (Stumm and Morgan, 1970). For the dissociation of bicarbonates the experimental data cited by Garrels and Christ (1965) are used. For the dissolution reactions of gypsum, aragonite and anhydrite the KEQ program based on equations (B.6 and B.7), was used, along with the pK (25°C) values cited by Hanshaw, et al., (1965) and the thermochemical data given in Table B.2 .

TABLE B.3

****
DISSOLUTION OF GYPSUM
****

BASIC DATA FOR 25. CG
****

	COMPONENT	STOCH. COEFF.	ENTHALPY	COEFFICIENTS OF CP=CP(T) A	B	C
1	GYPSUM	-1.	-0.483981E 06	0.348E 02	0.236E-01	0.0
2	CA++	1.	-0.129770E 06	-0.320E 01	0.0	0.0
3	SO4--	1.	-0.217320E 06	-0.482E 02	0.0	0.0
4	H2O (LIQ)	2.	-0.683150E 05	0.181E 02	0.0	0.0

REACTION DATA FOR 25. CG
****

DELTA H= 0.261000E 03
DELTA G= 0.628938E 04
LOG10 K= -4.610

REACTION DATA AS A FUNCTION OF ABSOLUTE(KELVIN) TEMPERATURE
****

CP(T) =-0.500E 02 + -0.236E-01*T + 0.0 *T(-2)

DELTA H= 0.162E 05 + -0.500E 02*T + -0.118E-01*T(+2) - 0.0 *T(-1)

LOG10 K= 0.704E 02 - 0.355E 04*T(-1) + -0.109E 02*LN(T) + -0.258E-02*T + 0.0 *T(-2)

TABLE B.3(A)

****
DISSOLUTION OF GYPSUM
****

REACTION DATA FOR SELECTED TEMPERATURES
****

TEMP (CG)	LOG10-K	DLTA-H(CAL)	DLTA-G(CAL)
0.0	-0.4677E 01	0.1681E 04	0.5845E 04
5.0	-0.4655E 01	0.1398E 04	0.5924E 04
10.0	-0.4637E 01	0.1114E 04	0.6008E 04
15.0	-0.4624E 01	0.8306E 03	0.6097E 04
20.0	-0.4615E 01	0.5461E 03	0.6191E 04
25.0	-0.4610E 01	0.2610E 03	0.6289E 04
30.0	-0.4609E 01	-0.2468E 02	0.6393E 04
35.0	-0.4611E 01	-0.3109E 03	0.6501E 04
40.0	-0.4616E 01	-0.5978E 03	0.6614E 04

TABLE B.4

****
DISSOLUTION OF ARAGONITE
****

BASIC DATA FOR 25. CG
****

	COMPONENT	STOCH. COEFF.	ENTHALPY	COEFFICIENTS OF CP=CP(T) A	B	C
1	ARAGONITE	-1.	-0.288651E 06	0.201E 02	0.102E-01	-0.334E 06
2	CA++	1.	-0.129770E 06	-0.320E 01	0.0	0.0
3	CO3--	1.	-0.161840E 06	-0.836E 02	0.0	0.0

REACTION DATA FOR 25. CG
****

DELTA H=-0.295900E 04
DELTA G= 0.111053E 05
LOG10 K= -8.140

REACTION DATA AS A FUNCTION OF ABSOLUTE(KELVIN) TEMPERATURE
****

CP(T) =-0.107E 03 + -0.102E-01*T + 0.334E 06*T(-2)

DELTA H= 0.305E 05 + -0.107E 03*T + -0.512E-02*T(+2) - 0.334E 06*T(-1)

LOG10 K= 0.147E 03 - 0.667E 04*T(-1) + -0.234E 02*LN(T) + -0.112E-02*T + 0.365E 05*T(-2)

TABLE B.4(A)

****
DISSOLUTION OF ARAGONITE
****

REACTION DATA FOR SELECTED TEMPERATURES
****

TEMP (CG)	LOG10-K	DLTA-H(CAL)	DLTA-G(CAL)
0.0	-0.8033E 01	-0.3151E 03	0.1004E 05
5.0	-0.8041E 01	-0.8419E 03	0.1023E 05
10.0	-0.8057E 01	-0.1370E 04	0.1044E 05
15.0	-0.8078E 01	-0.1899E 04	0.1065E 05
20.0	-0.8106E 01	-0.2428E 04	0.1087E 05
25.0	-0.8140E 01	-0.2959E 04	0.1111E 05
30.0	-0.8179E 01	-0.3491E 04	0.1135E 05
35.0	-0.8223E 01	-0.4023E 04	0.1159E 05
40.0	-0.8271E 01	-0.4556E 04	0.1185E 05

TABLE B.5

****
DISSOLUTION OF ANHYDRITE
****

BASIC DATA FOR 25. CG
****

	COMPONENT	STOCH. COEFF.	ENTHALPY	COEFFICIENTS OF CP=CP(T) A	B	C
1	ANHYDRITE	-1.	-0.343328E 06	0.168E 02	0.236E-01	0.0
2	CA++	1.	-0.129770E 06	-0.320E 01	0.0	0.0
3	SO4--	1.	-0.217320E 06	-0.482E 02	0.0	0.0

REACTION DATA FOR 25. CG
****

DELTA H=-0.376200E 04
DELTA G= 0.604381E 04
LOG10 K= -4.430

REACTION DATA AS A FUNCTION OF ABSOLUTE(KELVIN) TEMPERATURE
****

CP(T) =-0.682E 02 + -0.236E-01*T + 0.0 *T(-2)

DELTA H= 0.176E 05 + -0.682E 02*T + -0.118E-01*T(+2) - 0.0 *T(-1)

LOG10 K= 0.941E 02 - 0.385E 04*T(-1) + -0.149E 02*LN(T) + -0.258E-02*T + 0.0 *T(-2)

TABLE B .5(A)

****
DISSOLUTION OF ANHYDRITE
****

REACTION DATA FOR SELECTED TEMPERATURES
****

TEMP (CG)	LOG10-K	DLTA-H(CAL)	DLTA-G(CAL)
0.0	-0.4242E 01	-0.1869E 04	0.5303E 04
5.0	-0.4272E 01	-0.2262E 04	0.5438E 04
10.0	-0.4306E 01	-0.2636E 04	0.5579E 04
15.0	-0.4344E 01	-0.3011E 04	0.5728E 04
20.0	-0.4385E 01	-0.3386E 04	0.5883E 04
25.0	-0.4430E 01	-0.3762E 04	0.6044E 04
30.0	-0.4476E 01	-0.4138E 04	0.6212E 04
35.0	-0.4528E 01	-0.4515E 04	0.6385E 04
40.0	-0.4582E 01	-0.4893E 04	0.6565E 04

APPENDIX C - THE DISSOLUTION OF CALCITE IN PURE WATER UNDER VARIOUS CO_2 PRESSURES

Garrels and Christ (1965) have treated the dissolution of calcite under five sets of specified conditions, of which two are considered to be of importance for the interpretation of the single cell experiments (Chapter 4). The two cases are: (i) the dissolution reaction of calcite in pure water, with the system opened to a CO_2 reservoir in which a constant CO_2 pressure is maintained; and (ii) the dissolution of calcite in pure water, originally opened to the same CO_2 reservoir, but closed before the addition of $CaCO_3$.

Garrels and Christ (1965) have studied these two cases, assuming the ionic strength of the solution can be neglected and for equilibrium conditions only. In this appendix the activities and concentrations of the various aqueous species are determined for various reaction ratios (β) with respect to calcite, without neglecting the ionic strength of the solution, which appears to play a significant role in these computations.

An assumption is made that although the system is not in equilibrium with respect to calcite, an equilibrium is attained among the carbonate species in the solution.

(i) Calcium Carbonate-Water, With Externally Fixed CO_2 Pressure: As shown by Garrels and Christ (1965) this system can be described with the aid of the electrical neutrality equation, and the equilibrium relationships between the carbonate species.

Since the equilibrium between CO_2 and H_2CO_3 is pH independent, the activity of H_2CO_3 is governed by the concentration of dissolved

CO_2 only; which in turn is a function of P_{CO_2}:

$$\alpha_{H_2CO_3} = m_{H_2CO_3} = K_{CO_2}(T) \cdot m_{CO_2} = A \qquad (C.1)$$

where $K_{CO_2}(T)$ is the temperature (T) dependent equilibrium constant for the reaction $CO_2 + H_2O \rightleftarrows H_2CO_3$; α and m denoted activity and molarity respectively. Thermodynamic constants are given in Appendix B.

Equilibrium between the carbonate species require:

$$m_{HCO_3^-} = \frac{1}{\alpha_{HCO_3^-}} \left(\frac{K_{H_2CO_3}(T) \cdot m_{H_2CO_3}}{\alpha_{H^+} \, m_{H^+}} \right)$$

or:

$$m_{HCO_3^-} = A \cdot B/m_{H^+} \qquad (C.2)$$

where B is another constant given by:

$$B = K_{H_2CO_3}(T)/(\gamma_{HCO_3^-} \cdot \gamma_{H^+}) \qquad (C.3)$$

$\gamma_{HCO_3^-}$ and γ_{H^+} are the activity coefficients, as described from the Debye-Hückel equation (Chapter 3) for the bicarbonate and hydrogen ions respectively.

In addition:

$$m_{CO_3^=} = \frac{1}{\gamma_{CO_3^=}} \left(\frac{K_{HCO_3}(T) \cdot \gamma_{HCO_3^-} \cdot m_{HCO_3^-}}{\gamma_{H^+} \cdot m_{H^+}} \right)$$

or:

$$m_{CO_3^=} = A \cdot B \cdot C/(M_{H^+})^2 \qquad (C.4)$$

where the constant C is given by:

$$C = K_{HCO_3^-}(T) \cdot \gamma_{HCO_3^-}/\gamma_{CO_3^=} \cdot \gamma_{H^+} \qquad (C.5)$$

$\gamma_{CO_3^=}$ is the activity coefficient of the $CO_3^=$ ions.

For a given reaction ratio β the molarity of the Ca^{++} ions is determined from:

$$m_{Ca^{++}} = \frac{1}{\gamma_{Ca^{++}}} \left(\frac{\beta \quad K_{Ca^{++}}(T)}{\gamma_{CO_3^=} \; m_{CO_3^=}} \right)$$

or:

$$m_{Ca^{++}} = \frac{D}{A \cdot B \cdot C} (m_{H^+})^2 \qquad (C.6)$$

where the constant D is given here by:

$$D = \beta K_{Ca^{++}}(T)/\gamma_{Ca^{++}} \cdot \gamma_{CO_3^=} \qquad (C.7)$$

The molar concentration of the OH^- ions is determined from the dissociation constant of water $K_w(T)$:

$$m_{OH^-} = \frac{1}{\gamma_{OH^-}} \cdot \frac{K_w(T)}{\gamma_{H^+} \cdot m_{H^+}} \qquad (C.8)$$

or:

$$m_{OH^-} = E/m_{H^+} \qquad (C.8)$$

where E is given by:

$$E = K_w(T)/\gamma_{OH^-} \cdot \gamma_{H^+} \qquad (C.9)$$

From electrical neutrality relationships:

$$2m_{Ca^{++}} + m_{H^+} = m_{HCO_3^-} + 2m_{CO_3^=} + m_{OH^-} \qquad (C.10)$$

Substituting equations (C.2), (C.4), (C.6), and (C.8) into the equation above:

$$2\frac{D}{A \cdot B \cdot C}(m_{H^+})^2 + m_{H^+} - \frac{A \cdot B}{m_{H^+}} - 2\frac{A \cdot B \cdot C}{(m_{H^+})^2} - \frac{E}{m_{H^+}} = 0 \qquad (C.11)$$

Which is a non-linear equation in m_{H^+}. For a given set of initial molarities, the coefficients, A, B, C, D and E are computed and equation (C.11) is solved by applying the secant method for solving non-linear equations (Conte, 1965). The molarities of the various species are computed then from equations (C.2), (C.4), (C.6), and (C.8); activity coefficients and the A, B, C, D, and E constants are recomputed, and the value of m_{H^+} is determined again by solving equation (C.11). The iteration terminates when:

$$\left| \frac{(m_{H^+})_n}{(m_{H^+})_o} - 1. \right| < TOL \qquad (C.12)$$

where TOL is the tolerance of the numerical solution for m_{H^+}; the indices n and o stand for the new and old values of m_{H^+} respectively.

(ii) Dissolution of Calcite in Pure Water, Originally Open to a CO_2 Reservoir, Then Closed Before the Addition of $CaCO_3$ - This system corresponds to case 5, discussed by Garrels and Christ (1965, p. 86). Since $m_{H_2CO_3}$ is not a constant for this situation, the mass balance equation should be considered in addition to the equations given above. The mass balance requires:

$$m_{Ca^{++}} + (m_c)_o = m_{H_2CO_3} + m_{HCO_3^-} + m_{CO_3^=} \tag{C.13}$$

$(m_c)_o$ is the total carbonates in the pure water before adding the calcite:

$$(m_c)_o = (m_{H_2CO_3})_o + (m_{HCO_3^-})_o + (m_{CO_3^=})_o \tag{C.14}$$

Multiplying both sides of equation (C.13) by 2, and subtracting equation (C.10) from the resulting equation yields:

$$2m_{Ca^{++}} + 2(m_c)_o = 2m_{H_2CO_3} + 2m_{HCO_3^-} + 2mCO_3^=$$

$$-\quad 2m_{Ca^{++}} + m_{H^+} = m_{OH^-} + m_{HCO_3^-} + 2mCO_3^=$$

$$2(m_c)_o - m_{H^+} = 2m_{H_2CO_3} + m_{HCO_3^-} - m_{OH^-}$$

Because the resulting pH will be well above 9 (Garrels and Christ 1965) both m_{H^+} and $m_{H_2CO_3}$ may be neglected, and as a result:

$$m_{HCO_3^-} \cong 2(m_c)_o + m_{OH^-} \tag{C.15}$$

Using a similar procedure, and the same coefficients, as described for the previous case:

$$m_{OH^-} = E/m_{H^+} \tag{C.8}$$

$$m_{HCO_3^-} = 2(m_c)_o + E/m_{H^+} \tag{C.16}$$

$$m_{CO_3^=} = C[2(m_c)_o + E/m_{H^+}]/m_{H^+} \tag{C.17}$$

$$m_{Ca^{++}} = \frac{D \cdot m_{H^+}}{C[2(m_c)_o + E/m_{H^+}]} \tag{C.18}$$

$$m_{H_2CO_3} = \frac{\gamma_{H^+} \cdot m_{H^+} \cdot \gamma_{HCO_3^-} \cdot m_{HCO_3^-}}{K_{H_2CO_3}(T)}$$

or:

$$m_{H_2CO_3} = \frac{m_{H^+}}{B} [2(m_c)_o + E/m_{H^+}] \qquad (C.19)$$

where B is given by eq (C.3).

Substituting equations (C.16), (C.17), (C.18), and (C.19) into the mass balance equation (C.13), results in a non-linear equation for m_{H^+}:

$$\frac{Dm_{H^+}}{C[2(m_c)_o + E/m_{H^+}]} + (m_c)_o - \frac{m_{H^+}}{B} [2(m_c)_o + E/m_{H^+}] -$$

$$[2(m_c)_o + E/m_{H^+}] - \frac{C}{m_{H^+}} [2(m_c)_o + E/m_{H^+}] = 0 \qquad (C.20)$$

Equation (C.20) is solved, and the molarities of the various species are determined by using the same procedure, as described above.

For determining $(m_c)_o$ equations (C.2), (C.4), and the electrical neutrality condition are used:

$$m_{H^+} \cong m_{HCO_3^-} + 2m_{CO_3^=}; \quad (ph<<8) \qquad (C.21)$$

Substituting equations (C.2) and (C.4) into the equation above:

$$m_{H^+} - \frac{A \cdot B}{m_{H^+}} - 2\frac{A \cdot B \cdot C}{(m_{H^+})^2} = 0 \qquad (C.22)$$

Equation (C.22) is solved, and the molarities of the H^+, HCO_3^-, and $CO_3^=$

ions are determined as described before.

A computer program, named CALDIS, was developed for evaluating numerically the two cases discussed above.

The resulting concentrations of the various species at equilibrium ($\beta = 1$) as a function of the external CO_2 pressure, for both open and closed systems, are plotted in Figures C.1 and C.2 respectively. The pH of pure water as a function of CO_2 pressure is plotted in Figure C.3.

The atmospheric partial pressure of CO_2 at sea level is about $10^{-3.5}$ atm. (Garrels and Christ, 1965). The barometric pressure at sea level is 760 mm Hg, whereas at Socorro, N.M. the barometric pressure is about 650 mm Hg. Assuming that CO_2 behaves as an ideal gas, the partial pressure of CO_2 at Socorro will be:

$$(PCO_2)_{Socorro} \cong \frac{650}{760} \times 10^{-3.50} = 10^{-3.57} \text{ atm.}$$

The computed pH of pure water, corresponding to this CO_2 pressure is 5.69, which agrees with observed average values (Gross, 1972). The range of observed pH values in the ice laboratory of NMT is 5.6-5.8 (Fig. C.3).

Using the P_{CO_2} at Socorro the equilibrium concentrations of Ca^{++}, and HCO_3^- ions will be 21 and 61 ppm, respectively, for open systems, and 5.4 and 6.3 ppm for closed systems. The computed pH, at equilibrium with respect to calcite is 8.37 and 9.90 for open and closed systems respectively. The computer printout for the chemical composition of the solution as a function of β for $PCO_2 = 10^{-3.57}$, and $PCO_2 = 10^{-3.5}$ is given in Tables C.1 and C.4.

Figure C.1 - Calcium, bicarbonate, and pH as a function of pCO_2 ($=-\log_{10}CO_2$ concentration) under equilibrium conditions and at 25°C. The system is open to the atmosphere.

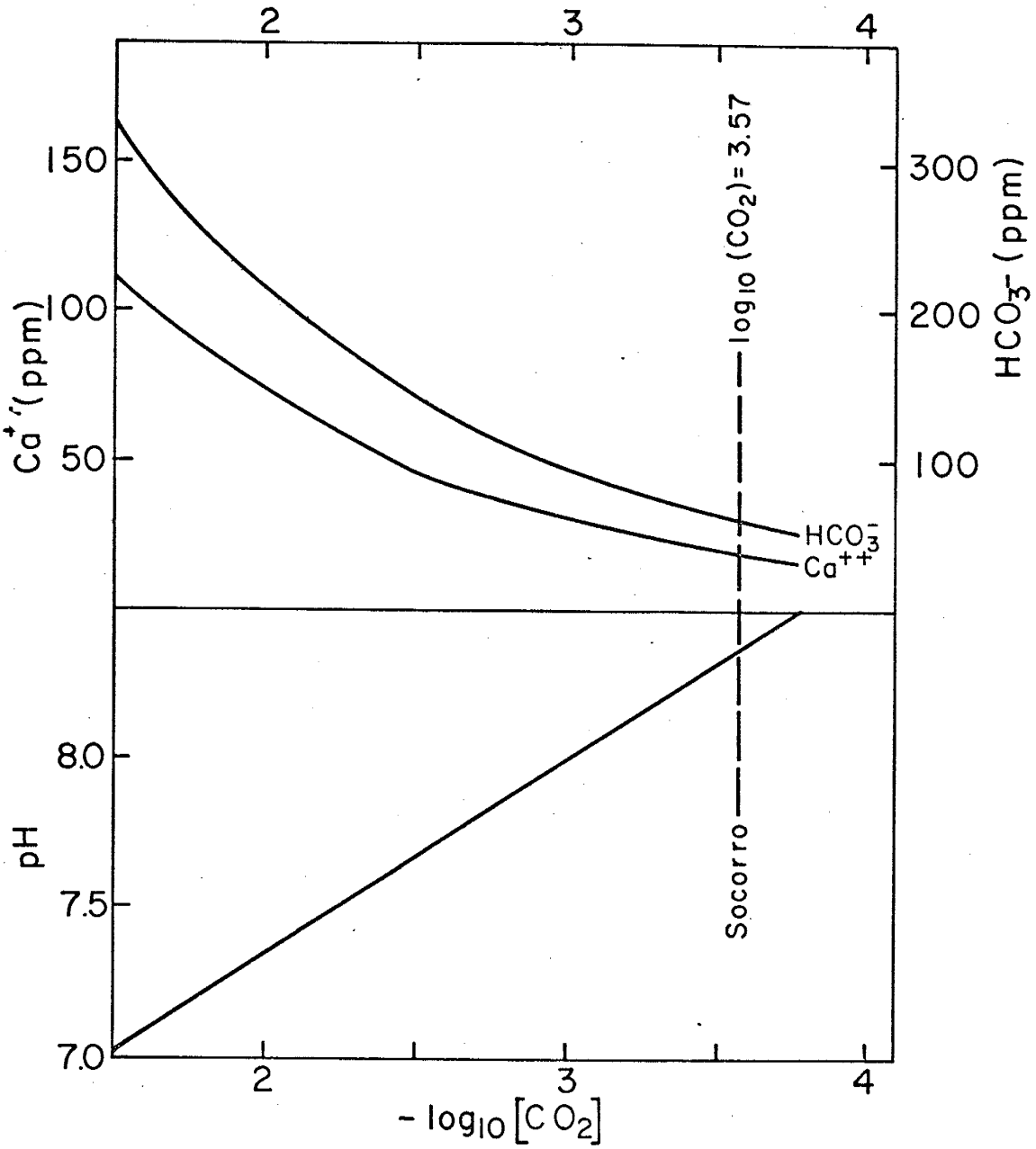
2
3
4
150
100
50
300
200
100
Ca^{++} (ppm)
HCO_3^- (ppm)
$\log_{10}(CO_2) = 3.57$
HCO_3^-
Ca^{++}
8.0
7.5
7.0
pH
Socorro
2
3
4
$-\log_{10}[CO_2]$

Figure C.2 - Calcium, bicarbonate, and pH as a function of CO_2 pressure at time - 0, before the addition of calcite. Concentrations and pH are computed for equilibrium conditions, and at 25°C. The system is disconnected from the atmosphere after the calcite is added.

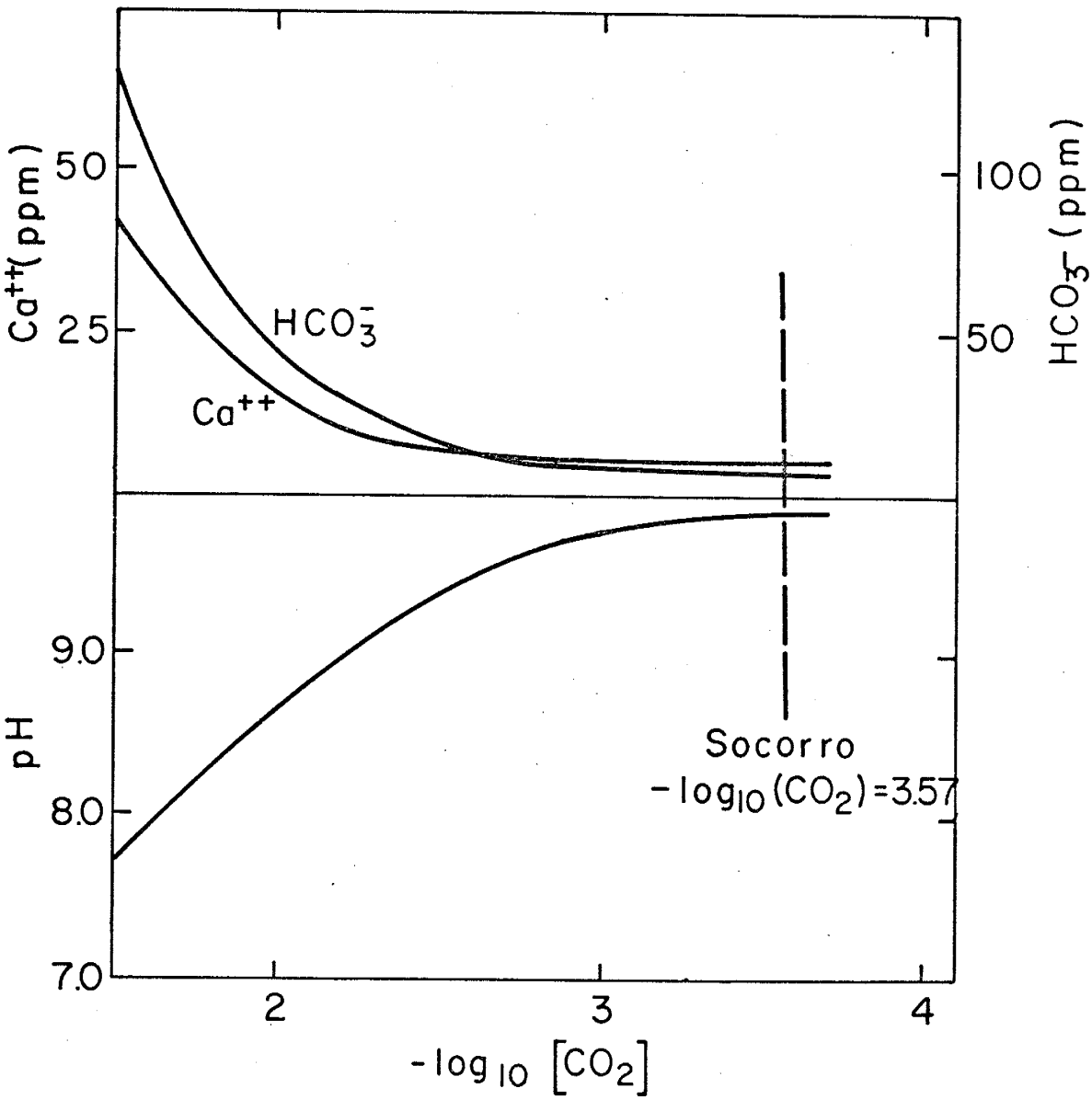
Ca++(ppm)
50
25
HCO3-
Ca++
100
50
HCO3- (ppm)
pH
9.0
8.0
7.0
Socorro
-log10(CO2)=3.57
2
3
4
-log10 [CO2]

Figure C.3 - pH of distilled water as a function of partial pressure of CO_2 at 25°C. The dashed line represents the computed CO_2 pressure in Socorro, assuming CO_2 behaves as an ideal gas.

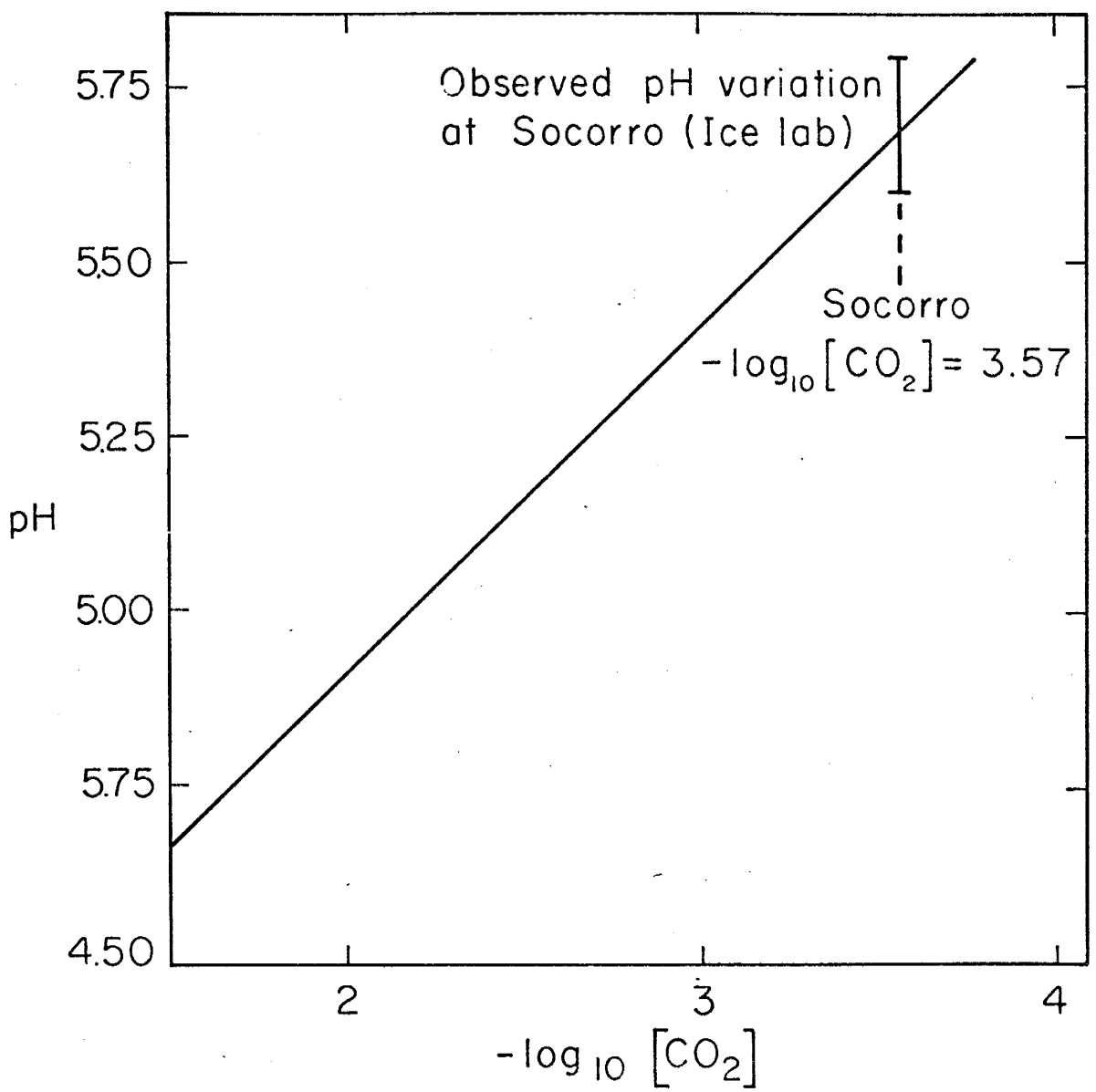
Observed pH variation
at Socorro (Ice lab)
Socorro
$-\log_{10}[CO_2] = 3.57$
5.75
5.50
5.25
5.00
5.75
4.50
pH
2
3
4
$-\log_{10}[CO_2]$

TABLE C.1 - DISSOLUTION OF CALCITE UNDER CONSTANT CO_2 PRESSURE (SOCORRO)

CHEMICAL COMPOSITION AS A FUNCTION OF REACTION RATIO

LOG10(PCO2)=CONST=-3.57
TEMPERATURE=25.0 CG

BETA	P CA	P M HCO3	PH	POH	LOG10(MOLE/LITER) CO2	H2CO3	CO3
0.0	0.0	0.1	5.69	8.30	-3.57	-5.04	-10.33
0.0500	7.4	21.8	7.93	6.06	-3.57	-5.04	-5.81
0.1000	9.4	27.7	8.03	5.96	-3.57	-5.04	-5.60
0.1500	10.8	31.8	8.09	5.90	-3.57	-5.04	-5.48
0.2000	11.9	35.1	8.14	5.86	-3.57	-5.04	-5.39
0.2500	12.9	37.8	8.17	5.83	-3.57	-5.04	-5.33
0.3000	13.8	40.3	8.19	5.80	-3.57	-5.04	-5.27
0.3500	14.6	42.4	8.22	5.78	-3.57	-5.04	-5.22
0.4000	15.3	44.4	8.24	5.76	-3.57	-5.04	-5.18
0.4500	15.9	46.3	8.25	5.74	-3.57	-5.04	-5.15
0.5000	16.5	48.0	8.27	5.73	-3.57	-5.04	-5.12
0.5500	17.1	49.6	8.28	5.71	-3.57	-5.04	-5.09
0.6000	17.6	51.1	8.30	5.70	-3.57	-5.04	-5.06
0.6500	18.1	52.5	8.31	5.69	-3.57	-5.04	-5.04
0.7000	18.6	53.9	8.32	5.68	-3.57	-5.04	-5.01
0.7500	19.0	55.2	8.33	5.67	-3.57	-5.04	-4.99
0.8000	19.4	56.4	8.34	5.66	-3.57	-5.04	-4.97
0.8500	19.8	57.6	8.35	5.65	-3.57	-5.04	-4.95
0.9000	20.2	58.8	8.36	5.64	-3.57	-5.04	-4.94
0.9500	20.6	59.9	8.36	5.63	-3.57	-5.04	-4.92
1.0000	21.0	61.0	8.37	5.63	-3.57	-5.04	-4.90

TABLE C.2 - DISSOLUTION OF CALCITE IN A CLOSED SYSTEM (SOCORRO)

CHEMICAL COMPOSITION AS A FUNCTION OF REACTION RATIO

LOG10(PCO2)-(T=0)=-3.57
TEMPERATURE=25.0 CG

BETA	P CA	P M HCO3	PH	POH	LOG10(MOLE/LITER) CO2	H2CO3	CO3
0.0	0.0	0.1	5.69	8.30	-3.57	-5.04	-10.33
0.0500	1.8	2.9	9.40	4.60	-5.91	-7.38	-5.23
0.1000	2.2	3.5	9.53	4.47	-5.96	-7.43	-5.03
0.1500	2.6	3.8	9.60	4.40	-5.99	-7.46	-4.91
0.2000	2.9	4.1	9.65	4.35	-6.00	-7.47	-4.83
0.2500	3.2	4.4	9.68	4.31	-6.01	-7.48	-4.77
0.3000	3.4	4.6	9.71	4.28	-6.02	-7.49	-4.72
0.3500	3.6	4.8	9.74	4.26	-6.03	-7.50	-4.68
0.4000	3.8	4.9	9.76	4.24	-6.04	-7.51	-4.64
0.4500	4.0	5.1	9.78	4.22	-6.04	-7.51	-4.61
0.5000	4.2	5.2	9.79	4.21	-6.05	-7.52	-4.58
0.5500	4.3	5.4	9.80	4.19	-6.05	-7.52	-4.55
0.6000	4.5	5.5	9.82	4.18	-6.05	-7.52	-4.53
0.6500	4.6	5.6	9.83	4.16	-6.06	-7.53	-4.50
0.7000	4.7	5.7	9.84	4.15	-6.06	-7.53	-4.48
0.7500	4.8	5.9	9.85	4.14	-6.06	-7.53	-4.46
0.8000	5.0	6.0	9.86	4.13	-6.06	-7.53	-4.45
0.8500	5.1	6.1	9.87	4.12	-6.07	-7.54	-4.43
0.9000	5.2	6.2	9.88	4.11	-6.07	-7.54	-4.41
0.9500	5.3	6.3	9.89	4.11	-6.07	-7.54	-4.40
1.0000	5.4	6.3	9.90	4.10	-6.07	-7.54	-4.38

TABLE C.3 - DISSOLUTION OF CALCITE UNDER CONSTANT CO_2 PRESSURE (SEA-LEVEL)

CHEMICAL COMPOSITIONS AS A FUNCTION OF REACTION RATIO

LOG10(PCO2)=CONST=-3.50
TEMPERATURE=25.0 CG

BETA	P CA	P HCO3	PH	POH	LOG10(MOLE/LITER) CO2	H2CO3	CO3
0.0	0.0	0.1	5.66	8.34	-3.50	-4.97	-10.33
0.0500	7.8	23.1	7.89	6.11	-3.50	-4.97	-5.83
0.1000	9.9	29.3	7.99	6.01	-3.50	-4.97	-5.62
0.1500	11.4	33.7	8.05	5.95	-3.50	-4.97	-5.50
0.2000	12.6	37.2	8.09	5.91	-3.50	-4.97	-5.41
0.2500	13.6	40.1	8.12	5.87	-3.50	-4.97	-5.34
0.3000	14.5	42.6	8.15	5.85	-3.50	-4.97	-5.29
0.3500	15.3	44.9	8.17	5.83	-3.50	-4.97	-5.24
0.4000	16.1	47.0	8.19	5.81	-3.50	-4.97	-5.20
0.4500	16.8	49.0	8.21	5.79	-3.50	-4.97	-5.17
0.5000	17.4	50.8	8.22	5.77	-3.50	-4.97	-5.14
0.5500	18.0	52.4	8.24	5.76	-3.50	-4.97	-5.11
0.6000	18.6	54.0	8.25	5.75	-3.50	-4.97	-5.08
0.6500	19.1	55.5	8.26	5.74	-3.50	-4.97	-5.06
0.7000	19.6	57.0	8.27	5.72	-3.50	-4.97	-5.03
0.7500	20.1	58.4	8.28	5.71	-3.50	-4.97	-5.01
0.8000	20.5	59.7	8.29	5.70	-3.50	-4.97	-4.99
0.8500	21.0	60.9	8.30	5.70	-3.50	-4.97	-4.97
0.9000	21.4	62.2	8.31	5.69	-3.50	-4.97	-4.96
0.9500	21.8	63.4	8.32	5.68	-3.50	-4.97	-4.94
1.0000	22.2	64.5	8.32	5.67	-3.50	-4.97	-4.92

TABLE C.4 - DISSOLUTION OF CALCITE IN A CLOSED SYSTEM (SEA-LEVEL)

CHEMICAL COMPOSITION AS A FUNCTION OF REACTION RATIO

LOG10(PCO2)-(T=0)=-3.50
TEMPERATURE=25.0 CG

BETA	P CA	P HCO3	PH	POH	LOG10(MOLE/LITER) CO2	H2CO3	CO3
0.0	0.0	0.1	5.66	8.34	-3.50	-4.97	-10.33
0.0500	1.8	3.1	9.38	4.62	-5.86	-7.33	-5.24
0.1000	2.3	3.6	9.51	4.49	-5.93	-7.40	-5.03
0.1500	2.6	4.0	9.58	4.42	-5.96	-7.43	-4.92
0.2000	2.9	4.3	9.63	4.37	-5.98	-7.45	-4.83
0.2500	3.2	4.5	9.67	4.33	-5.99	-7.46	-4.77
0.3000	3.4	4.7	9.70	4.30	-6.00	-7.47	-4.72
0.3500	3.6	4.9	9.72	4.27	-6.01	-7.48	-4.68
0.4000	3.8	5.1	9.75	4.25	-6.01	-7.48	-4.64
0.4500	4.0	5.2	9.76	4.23	-6.02	-7.49	-4.61
0.5000	4.1	5.4	9.78	4.21	-6.03	-7.50	-4.58
0.5500	4.4	5.5	9.79	4.20	-6.03	-7.50	-4.56
0.6000	4.5	5.6	9.81	4.19	-6.03	-7.50	-4.53
0.6500	4.6	5.7	9.82	4.18	-6.04	-7.51	-4.51
0.7000	4.8	5.9	9.83	4.16	-6.04	-7.51	-4.49
0.7500	4.9	6.0	9.84	4.15	-6.04	-7.51	-4.47
0.8000	5.0	6.1	9.85	4.14	-6.05	-7.52	-4.45
0.8500	5.1	6.2	9.86	4.13	-6.05	-7.52	-4.43
0.9000	5.2	6.3	9.87	4.12	-6.05	-7.52	-4.41
0.9500	5.3	6.4	9.88	4.11	-6.05	-7.52	-4.40
1.0000	5.4	6.5	9.89	4.11	-6.06	-7.53	-4.38

A P P E N D I X D

LABORATORY EXPERIMENTAL DATA

SINGLE CELL MEASUREMENTS OF REACTION RATE COEFFICIENTS

****

RUN B1 (CALCITE+DIST. WATER) - JUNE 7-10 1971

CELL VOLUME	875.0 CC
CALCITE WEIGHT	17.6 GRAM
MESH SIZE	200-270
GYPSUM WEIGHT	0.0 GRAM
MESH SIZE	0- 0
TEMPERATURE	23.8-25.7 CENTG
AVERAGE TEMP.	24.6 CENTG

****

A. EXPERIMENTAL RESULTS

TIME (MIN.)	COND (25CG)	PH	TEMP (CG)	HCO3- (PPM)	CA++ (PPM)	SO4-- (PPM)	PCO2	R. RATIOS (%) CALC	GYPS
0.	17.	8.83	24.2	2.7	1.1	0.0	5.38	0.7	0.0
610.	41.	9.01	25.1	23.5	7.1	0.0	4.61	63.2	0.0
1386.	56.	8.96	23.9	29.9	8.7	0.0	4.47	80.9	0.0
2075.	74.	8.76	25.3	37.9	12.2	0.0	4.16	95.0	0.0
2812.	83.	8.68	24.1	42.6	13.1	0.0	4.04	89.2	0.0
3360.	91.	8.64	25.6	45.9	13.9	0.0	3.96	99.9	0.0
4715.	100.	8.53	25.7	54.5	15.7	0.0	3.77	103.3	0.0
5010.	97.	8.44	24.8	59.8	16.6	0.0	3.65	92.8	0.0
6030.	110.	8.42	25.6	62.3	17.1	0.0	3.60	98.7	0.0

SINGLE CELL MEASUREMENTS OF REACTION RATE COEFFICIENTS

****

RUN B2 (CALCITE+DIST. WATER) - JUNE 10-11 1971

CELL VOLUME	1025.0 CC
FLOW RATE	3.7 CC/MIN
CALCITE WEIGHT	17.6 GRAM
MESH SIZE	200-270
TEMPERATURE	23.7-26.2 CENTG
AVERAGE TEMP.	25.2 CENTG

****

A. EXPERIMENTAL RESULTS

TIME (MIN.)	SPECIFIC CONDUCT. (MICROMHOS AT 25 CG)	PH	HCO3- (PPM)	COMP. CO3-- (PPM)	CA++ (PPM)	REAC. RATIO (PCT)
0.0	94.	8.66	49.4	0.11E 01	12.70	103.04
14.0	92.	8.78	41.6	0.12E 01	11.05	100.83
57.0	83.	8.87	33.8	0.12E 01	9.14	84.83
112.0	71.	9.07	22.7	0.13E 01	6.83	69.64
276.0	50.	9.21	16.2	0.12E 01	5.41	55.65
504.0	34.	9.56	8.0	0.14E 01	3.24	37.98
806.0	31.	9.58	6.8	0.12E 01	2.86	29.18
1146.0	28.	9.63	6.5	0.12E 01	2.68	26.86
1617.0	26.	9.62	5.8	0.11E 01	2.79	26.25
2010.0	27.	9.64	6.2	0.12E 01	2.74	28.26
2460.0	29.	9.61	6.5	0.12E 01	2.72	26.38

SINGLE CELL MEASUREMENTS OF REACTION RATE COEFFICIENTS

****

RUN B3 (CALCITE+DIST. WATER) - JUNE 11-13 1971

CELL VOLUME	875.0	CC
CALCITE WEIGHT	17.6	GRAM
MESH SIZE	200-270	
GYPSUM WEIGHT	0.0	GRAM
MESH SIZE	0- 0	
TEMPERATURE	24.8-26.5	CENTG
AVERAGE TEMP.	25.5	CENTG

****

A. EXPERIMENTAL RESULTS

TIME (MIN.)	COND (25CG)	PH	TEMP (CG)	HCO3- (PPM)	CA++ (PPM)	SO4-- (PPM)	PCO2	R. RATIOS (%) CALC	GYPS
0.	24.	9.62	24.8	3.7	0.8	0.0	6.03	4.8	0.0
49.	30.	9.60	24.9	6.3	1.4	0.0	5.77	13.1	0.0
108.	31.	9.56	25.4	6.2	2.2	0.0	5.74	19.1	0.0
325.	45.	9.44	26.5	10.5	3.4	0.0	5.38	40.0	0.0
476.	65.	9.27	26.2	15.1	5.2	0.0	5.06	57.3	0.0
1027.	81.	8.85	24.8	34.6	8.1	0.0	4.29	70.7	0.0
1376.	90.	8.76	25.4	36.7	10.8	0.0	4.17	82.8	0.0
2110.	95.	8.70	26.6	43.0	12.4	0.0	4.04	101.3	0.0
2601.	104.	8.60	24.8	47.9	13.2	0.0	3.90	86.9	0.0
2980.	98.	8.54	25.1	48.7	14.1	0.0	3.83	83.1	0.0
3150.	99.	8.48	24.9	46.9	15.7	0.0	3.79	76.6	0.0
3376.	102.	8.45	24.8	47.9	15.9	0.0	3.75	73.5	0.0

SINGLE CELL MEASUREMENTS OF REACTION RATE COEFFICIENTS

****

RUN B4 (CALCITE+DIST. WATER) - JUNE 13-15 1971

CELL VOLUME	1025.0 CC
FLOW RATE	16.1 CC/MIN
CALCITE WEIGHT	17.6 GRAM
MESH SIZE	200-270
TEMPERATURE	24.3-26.4 CENTG
AVERAGE TEMP.	25.3 CENTG

****

A. EXPERIMENTAL RESULTS

TIME (MIN.)	SPECIFIC CONDUCT. (MICROMHOS AT 25 CG)	PH	HCO3- (PPM)	COMP. CO3-- (PPM)	CA++ (PPM)	REAC. RATIO (PCT)
0.0	61.	8.92	23.1	0.88E 00	9.70	66.90
3.0	59.	8.94	22.6	0.90E 00	9.13	64.69
7.0	56.	8.99	23.2	0.10E 01	8.64	70.60
25.0	49.	9.00	16.4	0.75E 00	6.45	39.08
52.0	37.	9.14	14.1	0.90E 00	5.24	38.44
78.0	31.	9.21	10.3	0.77E 00	4.16	26.57
172.0	23.	9.29	7.7	0.71E 00	3.24	19.53
246.0	18.	9.36	5.6	0.60E 00	2.18	11.50
521.0	15.	9.46	3.8	0.51E 00	2.14	9.35
1074.0	17.	9.42	3.6	0.43E 00	2.06	7.34
1610.0	16.	9.45	3.9	0.51E 00	2.12	9.25
1943.0	14.	9.40	3.8	0.45E 00	2.08	8.15
2570.0	18.	9.41	3.7	0.44E 00	2.10	7.84
3009.0	15.	9.43	3.8	0.47E 00	2.04	8.17

SINGLE CELL MEASUREMENTS OF REACTION RATE COEFFICIENTS

****

RUN 0-1(CALCITE+DIST. WATER) - JUNE 19-28,1971

CELL VOLUME	875.0	CC
CALCITE WEIGHT	14.8	GRAM
MESH SIZE	65-100	
GYPSUM WEIGHT	0.0	GRAM
MESH SIZE	0- 0	
TEMPERATURE	23.2-26.7	CENTG
AVERAGE TEMP.	24.8	CENTG

****

A. EXPERIMENTAL RESULTS

TIME (MIN.)	COND (25CG)	PH	TEMP (CG)	HCO3- (PPM)	CA++ (PPM)	SO4-- (PPM)	PCO2	R. RATIOS (%) CALC	GYPS
0.	44.	9.07	24.6	24.9	5.7	0.0	4.65	60.2	0.0
210.	48.	8.98	23.2	27.7	6.0	0.0	4.53	53.1	0.0
753.	47.	8.94	26.4	30.1	6.7	0.0	4.43	68.3	0.0
1796.	60.	8.71	23.4	38.1	9.5	0.0	4.12	61.0	0.0
2938.	68.	8.64	23.7	42.7	10.8	0.0	4.00	66.7	0.0
5310.	83.	8.62	24.8	47.9	12.6	0.0	3.92	87.1	0.0
6220.	84.	8.54	26.1	52.4	13.9	0.0	3.79	92.6	0.0
8610.	93.	8.52	26.5	54.1	14.4	0.0	3.76	96.0	0.0
10750.	97.	8.44	24.9	58.0	16.5	0.0	3.66	90.1	0.0
12988.	102.	8.41	24.6	59.4	16.7	0.0	3.62	85.7	0.0

SINGLE CELL MEASUREMENTS OF REACTION RATE COEFFICIENTS

****

RUN D2 (CALCITE+DIST. WATER) - JUNE 28-29 1971

CELL VOLUME	1025.0 CC
FLOW RATE	11.5 CC/MIN
CALCITE WEIGHT	14.8 GRAM
MESH SIZE	65-100
TEMPERATURE	23.9-26.7 CENTG
AVERAGE TEMP.	24.8 CENTG

****

A. EXPERIMENTAL RESULTS

TIME (MIN.)	SPECIFIC CONDUCT. (MICRUMHOS AT 25 CG)	PH	HCO3- (PPM)	COMP. CO3-- (PPM)	CA++ (PPM)	REAC. RATIO (PCT)
0.0	53.	8.69	27.7	0.62E 00	7.90	37.87
4.0	48.	8.73	25.4	0.62E 00	7.14	34.86
50.0	41.	8.74	19.9	0.50E 00	5.43	21.91
84.0	41.	8.73	20.5	0.51E 00	5.71	23.59
175.0	32.	8.71	12.9	0.31E 00	4.01	10.65
312.0	25.	8.68	8.3	0.19E 00	2.92	4.81
591.0	22.	8.84	6.3	0.20E 00	1.71	3.05
956.0	19.	9.12	3.8	0.23E 00	1.44	2.69
1330.0	13.	9.10	4.0	0.23E 00	1.51	2.86

SINGLE CELL MEASUREMENTS OF REACTION RATE COEFFICIENTS

****

RUN 03(CALCITE+DIST. WATER) - JUNE 29-30,1971

CELL VOLUME	875.0	CC
CALCITE WEIGHT	14.8	GRAM
MESH SIZE	65-100	
GYPSUM WEIGHT	0.0	GRAM
MESH SIZE	0- 0	
TEMPERATURE	23.7-26.8	CENTG
AVERAGE TEMP.	25.3	CENTG

****

A. EXPERIMENTAL RESULTS

TIME (MIN.)	COND (25CG)	PH	TEMP (CG)	HCO3- (PPM)	CA++ (PPM)	SO4-- (PPM)	PCO2	R. RATIOS (%) CALC	GYPS
0.	12.	9.09	24.1	4.0	0.9	0.0	5.47	1.7	0.0
102.	31.	9.14	24.5	6.7	1.4	0.0	5.29	5.0	0.0
226.	36.	9.05	25.2	8.8	2.1	0.0	5.07	8.2	0.0
398.	42.	8.93	26.7	12.2	3.3	0.0	4.81	14.3	0.0
579.	42.	8.84	26.0	16.2	4.6	0.0	4.60	20.3	0.0
1165.	47.	8.75	23.7	22.0	6.7	0.0	4.39	28.4	0.0
1629.	51.	8.68	26.8	29.0	7.7	0.0	4.18	42.5	0.0

SINGLE CELL MEASUREMENTS OF REACTION RATE COEFFICIENTS

****

RUN D4(CALCITE+DIST. WATER) JUNE 30-JULY 2,1971

CELL VOLUME	1025.0	CC
FLOW RATE	6.4	CC/MIN
CALCITE WEIGHT	14.8	GRAM
MESH SIZE	65-100	
TEMPERATURE	23.6-28.4	CENTG
AVERAGE TEMP.	26.2	CENTG

****

A. EXPERIMENTAL RESULTS

TIME (MIN.)	SPECIFIC CONDUCT. (MICROMHOS AT 25 CG)	PH	HCO3- (PPM)	COMP. CO3-- (PPM)	CA++ (PPM)	REAC. RATIO (PCT)
0.0	38.	9.12	23.1	0.15E 01	6.58	83.43
16.0	37.	9.23	18.5	0.15E 01	5.93	79.53
57.0	35.	9.27	16.0	0.15E 01	5.10	66.33
210.0	28.	9.22	11.0	0.88E 00	3.10	23.93
408.0	25.	9.18	7.4	0.54E 00	2.32	10.91
702.0	24.	9.17	6.2	0.42E 00	2.26	7.88
914.0	23.	9.19	6.6	0.46E 00	2.12	7.88
1336.0	22.	9.21	6.2	0.46E 00	2.05	8.14
1828.0	23.	9.17	4.7	0.33E 00	1.86	5.43
2234.0	21.	9.14	5.6	0.36E 00	1.81	5.58
2623.0	21.	9.13	5.0	0.30E 00	1.73	4.35
2968.0	23.	9.16	4.5	0.30E 00	1.98	5.10

SINGLE CELL MEASUREMENTS OF REACTION RATE COEFFICIENTS

****

RUN D5(CALCITE+DIST. WATER) - JULY 2-6, 1971

CELL VOLUME	875.0	CC
CALCITE WEIGHT	14.8	GRAM
MESH SIZE	65-100	
GYPSUM WEIGHT	0.0	GRAM
MESH SIZE	0- 0	
TEMPERATURE	23.2-28.7	CENTG
AVERAGE TEMP.	26.3	CENTG

****

A. EXPERIMENTAL RESULTS

TIME (MIN.)	COND (25CG)	PH	TEMP (CG)	HCO3- (PPM)	CA++ (PPM)	SO4-- (PPM)	PCO2	R. RATIOS (%) CALC	GYPS
0.	20.	8.89	25.5	4.6	2.0	0.0	5.20	2.8	0.0
247.	28.	9.08	26.7	10.5	2.4	0.0	5.02	12.7	0.0
516.	34.	8.67	25.6	17.8	5.3	0.0	4.39	1o.9	0.0
1530.	48.	8.71	24.2	26.2	8.0	0.0	4.28	37.7	0.0
2020.	52.	8.67	26.1	30.0	9.0	0.0	4.16	48.1	0.0
3132.	57.	8.68	25.3	32.3	10.4	0.0	4.15	58.1	0.0
3720.	64.	8.55	24.2	38.2	12.1	0.0	3.95	55.9	0.0
4528.	70.	8.48	28.6	48.7	14.0	0.0	3.75	84.8	0.0
5385.	76.	8.43	26.6	54.2	14.6	0.0	3.67	79.4	0.0

SINGLE CELL MEASUREMENTS OF REACTION RATE COEFFICIENTS

****

RUN D6 (CALCITE+DIST. WATER) - JULY 7-11 1971

CELL VOLUME	875.0 CC
CALCITE WEIGHT	67.8 GRAM
MESH SIZE	65-100
GYPSUM WEIGHT	0.0 GRAM
MESH SIZE	0- 0
TEMPERATURE	23.4-28.5 CENTG
AVERAGE TEMP.	26.3 CENTG

****

A. EXPERIMENTAL RESULTS

TIME (MIN.)	COND (25CG)	PH	TEMP (CG)	HCO3- (PPM)	CA++ (PPM)	SO4-- (PPM)	PCO2	R. RATIOS (%) CALC	GYPS
0.	24.	9.64	24.9	3.6	0.8	0.0	6.06	4.8	0.0
47.	31.	9.58	25.1	5.6	1.2	0.0	5.81	9.7	0.0
102.	29.	9.51	25.2	5.5	1.6	0.0	5.74	11.5	0.0
346.	46.	9.42	27.4	10.8	3.4	0.0	5.34	40.6	0.0
512.	63.	9.17	27.2	15.6	5.3	0.0	4.94	50.4	0.0
1056.	80.	8.85	23.4	34.6	8.1	0.0	4.30	66.2	0.0
1413.	84.	8.82	25.4	33.1	9.9	0.0	4.28	79.2	0.0
2215.	85.	8.65	24.5	42.9	11.2	0.0	4.00	73.9	0.0
2980.	91.	8.58	28.5	48.5	13.1	0.0	3.85	99.3	0.0
3206.	96.	8.54	27.3	48.3	14.1	0.0	3.82	91.8	0.0
3610.	102.	8.49	26.2	47.7	15.1	0.0	3.79	81.9	0.0
4012.	100.	8.51	26.2	49.8	15.7	0.0	3.79	92.8	0.0
4920.	102.	8.53	27.6	48.3	16.2	0.0	3.81	103.8	0.0

SINGLE CELL MEASUREMENTS OF REACTION RATE COEFFICIENTS

****

RUN D7 (CALCITE+DIST. WATER) - JULY 12-16 1971

CELL VOLUME	1025.0 CC
FLOW RATE	7.2 CC/MIN
CALCITE WEIGHT	67.8 GRAM
MESH SIZE	65-100
TEMPERATURE	23.8-28.9 CENTG
AVERAGE TEMP.	26.4 CENTG

****

A. EXPERIMENTAL RESULTS

TIME (MIN.)	SPECIFIC CONDUCT. (MICROMHOS AT 25 CG)	PH	HCO3- (PPM)	COMP. CO3-- (PPM)	CA++ (PPM)	REAC. RATIO (PCT)
0.0	42.	9.12	22.5	0.13E 01	6.42	66.87
15.0	39.	9.09	21.7	0.12E 01	5.62	53.05
48.0	36.	9.16	17.0	0.11E 01	5.29	47.06
104.0	34.	9.15	13.8	0.89E 00	4.60	33.47
195.0	29.	9.19	11.5	0.83E 00	4.43	30.56
412.0	28.	9.22	9.9	0.81E 00	3.47	25.46
710.0	26.	9.20	9.2	0.69E 00	3.06	18.04
960.0	26.	9.23	8.1	0.64E 00	2.52	13.66
1235.0	24.	9.18	7.9	0.54E 00	2.76	12.02
1506.0	25.	9.16	8.5	0.56E 00	2.74	12.71
1812.0	25.	9.21	8.6	0.69E 00	2.87	17.90
2155.0	26.	9.09	8.5	0.50E 00	2.94	13.08
2620.0	24.	9.13	8.4	0.51E 00	2.91	11.98
3048.0	26.	9.15	8.7	0.57E 00	3.01	14.37

SINGLE CELL MEASUREMENTS OF REACTION RATE COEFFICIENTS

****

RUN E1 (CALCITE+DIST. WATER) - JULY 17-20 1971

CELL VOLUME	875.0	CC
CALCITE WEIGHT	31.4	GRAM
MESH SIZE	100-150	
GYPSUM WEIGHT	0.0	GRAM
MESH SIZE	0- 0	
TEMPERATURE	23.5-27.1	CENTG
AVERAGE TEMP.	25.8	CENTG

****

A. EXPERIMENTAL RESULTS

TIME (MIN.)	COND (25CG)	PH	TEMP (CG)	HCO3- (PPM)	CA++ (PPM)	SO4-- (PPM)	PCO2	R. RATIOS (%) CALC	GYPS
0.	18.	9.68	26.6	2.1	0.6	0.0	6.32	2.6	0.0
45.	25.	9.61	26.7	5.4	0.9	0.0	5.84	8.7	0.0
109.	31.	9.47	26.9	6.7	1.7	0.0	5.60	14.4	0.0
186.	36.	9.40	27.1	7.8	2.4	0.0	5.46	20.2	0.0
487.	47.	9.22	25.8	14.3	4.1	0.0	5.03	37.6	0.0
951.	53.	9.07	23.6	21.7	5.9	0.0	4.72	51.7	0.0
1734.	61.	8.81	26.9	40.2	9.1	0.0	4.17	92.5	0.0
2620.	95.	8.54	25.1	49.9	14.5	0.0	3.82	87.5	0.0
3194.	98.	8.42	23.8	61.4	15.3	0.0	3.62	80.0	0.0

SINGLE CELL MEASUREMENTS OF REACTION RATE COEFFICIENTS

****

RUN E2 (CALCITE+DIST. WATER) - JULY 20-22 1971

CELL VOLUME	1025.0 CC
FLOW RATE	5.4 CC/MIN
CALCITE WEIGHT	31.4 GRAM
MESH SIZE	100-150
TEMPERATURE	23.8-26.9 CENTG
AVERAGE TEMP.	25.7 CENTG

****

A. EXPERIMENTAL RESULTS

TIME (MIN.)	SPECIFIC CONDUCT. (MICROMHOS AT 25 CG)	PH	HCO3- (PPM)	COMP. CO3-- (PPM)	CA++ (PPM)	REAC. RATIO (PCT)
0.0	88.	8.62	48.6	0.91E 00	12.30	82.34
62.0	72.	8.69	37.7	0.83E 00	10.14	63.24
91.0	53.	8.81	31.2	0.91E 00	8.17	56.69
186.0	39.	9.19	17.6	0.12E 01	4.13	41.49
412.0	34.	9.53	7.5	0.12E 01	2.46	25.35
678.0	32.	9.54	6.1	0.10E 01	2.18	18.94
920.0	33.	9.49	6.2	0.88E 00	2.04	15.31
1387.0	32.	9.53	5.6	0.85E 00	1.88	13.14
1916.0	29.	9.52	5.8	0.92E 00	1.91	15.33
2871.0	32.	9.54	5.7	0.89E 00	1.94	14.21

SINGLE CELL MEASUREMENTS OF REACTION RATE COEFFICIENTS

****

RUN H1 (GYPSUM + DIST. WATER) - JUNE 6 1972

CELL VOLUME	1750.0 CC
CALCITE WEIGHT	0.0 GRAM
MESH SIZE	0- 0
GYPSUM WEIGHT	15.0 GRAM
MESH SIZE	150-270
TEMPERATURE	24.4-25.1 CENTG
AVERAGE TEMP.	24.7 CENTG

****

A. EXPERIMENTAL RESULTS

TIME (MIN.)	CCND (25CG)	PH	TEMP (CG)	HCO3- (PPM)	CA++ (PPM)	SO4-- (PPM)	PCO2	R. RATIOS (%) CALC	GYPS
0.	6.	6.05	24.4	0.0	0.0	0.0	0.0	0.0	0.0
1.	350.	6.51	24.4	0.0	115.0	220.0	0.0	0.0	8.8
3.	460.	6.60	24.4	0.0	165.0	270.0	0.0	0.0	13.2
5.	470.	6.75	24.5	0.0	170.0	280.0	0.0	0.0	13.9
10.	900.	6.74	24.4	0.0	265.0	630.0	0.0	0.0	34.3
20.	1380.	6.85	24.9	0.0	390.0	990.0	0.0	0.0	60.1
30.	1600.	6.82	25.0	0.0	475.0	1150.0	0.0	0.0	75.3
45.	2010.	6.83	25.1	0.0	560.0	1375.0	0.0	0.0	94.1
60.	2070.	6.85	24.9	0.0	603.0	1450.0	0.0	0.0	102.3

SINGLE CELL MEASUREMENTS OF REACTION RATE COEFFICIENTS

****

RUN 11 (CALC.+GYPS.+DIST. WATER) JUNE 7-12 1972

CELL VOLUME	1750.0	CC
CALCITE WEIGHT	155.0	GRAM
MESH SIZE	100-150	
GYPSUM WEIGHT	15.0	GRAM
MESH SIZE	150-270	
TEMPERATURE	22.6-28.6	CENTG
AVERAGE TEMP.	27.4	CENTG

****

A. EXPERIMENTAL RESULTS

TIME (MIN.)	COND (25CG)	PH	TEMP (CG)	HCO3- (PPM)	CA++ (PPM)	SO4-- (PPM)	PCO2	R. RATIOS (%) CALC	GYPS
0.	580.	8.86	22.6	12.0	170.0	400.0	4.82	248.5	18.4
6.	870.	8.76	22.8	10.3	245.0	625.0	4.80	211.5	32.5
15.	1400.	8.63	23.1	8.0	410.0	950.0	4.79	177.4	61.1
28.	1800.	8.57	23.4	7.1	520.0	1310.0	4.78	155.6	87.9
45.	1950.	8.51	24.2	6.5	565.0	1325.0	4.76	140.3	92.9
75.	2000.	8.43	24.9	7.0	593.0	1375.0	4.65	133.2	97.6
115.	2050.	8.45	25.3	7.0	593.0	1395.0	4.66	140.9	98.2
265.	2070.	8.40	26.2	6.4	602.0	1425.0	4.65	120.7	99.9
645.	2080.	8.32	27.3	8.6	605.0	1450.0	4.43	141.1	100.8
1405.	2100.	8.26	27.5	10.4	615.0	1405.0	4.29	155.2	99.6
2105.	2050.	8.16	28.5	10.9	607.0	1405.0	4.16	133.4	98.2
2835.	2040.	8.07	25.0	11.2	598.0	1420.0	4.08	93.0	100.3
4565.	2070.	7.99	28.6	12.3	601.0	1450.0	3.93	99.4	99.3
6880.	2050.	7.93	28.1	13.6	650.0	1450.0	3.83	102.0	104.6

A P P E N D I X E

COMPILATION OF FIELD DATA

THE ROSWELL ARTESIAN AQUIFER - COMPILATION OF AVAILABLE DATA (MARCH 1972)
(SOURCES: (1) HOOD-U.S.G.S. SALINITY SURVEY 58/9; (2) NMT-MERCADO'S SURVEY)

1. SAMPLES AND WELL DATA

NO	LOCATION	NAME	RA-NO.	DATE	S.L.	W.D.	C.D.	SOURCE	REMARKS
1	09.24.05.311	SHORTRIDGE	------	17-05-50	----	365	----	HOOD	ESTIMATED TEMP.
2	10.23.34.432	ROSW. CITY	------	11-05-51	----	568	----	HOOD	CITY WELL #10 ESTIMATED TEMP.
3	10.23.34.432	ROSW. CITY	------	30-11-57	----	568	----	HOOD	REPEAT ANALYSIS
4	10.23.34.432A	ROSW. CITY	------	30-11-57	----	561	----	HOOD	CITY WELL #11
5	11.25.15.343	CLARDY	------	10-05-28	----	843	643	HOOD	FLOWING-5500 GPM
6	12.25.35.411	STONE A.C	------	13-09-56	----	937	----	HOOD	
7	13.25.10.430	----------	------	10-05-28	----	922	----	HOOD	
8	13.26.07.313	----------	------	10-05-28	----	945	----	HOOD	
9	13.26.17.333	DEXTER T.	------	06-04-56	----	975	940	HOOD	ESTIMATED TEMP.
10	13.26.28.114	GREENFIELD	------	04-04-56	----	1000	889	HOOD	ESTIMATED TEMP.
11	13.26.31.113	----------	------	05-10-28	----	1025	----	HOOD	
12	13.26.31.113	----------	------	08-02-39	----	1025	----	HOOD	REPEAT ANALYSIS ESTIMATED TEMP.
13	14.26.10.413	HAGERMAN T	------	14-04-39	----	1236	----	HOOD	ESTIMATED TEMP.
14	15.25.24.120	HAL BOGLE	------	19-01-44	----	----	----	HOOD	ESTIMATED TEMP.
15	15.25.35.213	----------	------	05-09-55	----	----	----	HOOD	

1. SAMPLES AND WELL DATA
(CONTINUED-2)

NO	LOCATION	NAME	RA-NO.	DATE	S.L.	W.D.	C.D.	SOURCE	REMARKS
36	11.16.12.	ANDERSON T	------	29-10-71	----	----	----	NMT	HARDEST WATER IN TINNIE
37	10.16.28.	"SOFT" SP.	------	29-10-71	----	----	----	NMT	ON HWY 380 1.8 MI W. JCT 70 PH(12/1/72)
38	19.26.05.323	POWELL LF	749	11-01-72	----	905	567	NMT	PUMPING
39	09.23.15.334	MARLEY	4317	12-01-72	----	386	----	NMT	STOCK WELL
40	10.21.25.111	WHITNEY R.	------	12-01-72	----	703	60	NMT	SUBMERGED PUMP
41		MCGEE D.	------	12-01-72	----	----	----	NMT	STOCK WELL
42	11.22.22.111	WRIGHT R.	------	12-01-72	----	414+	----	NMT	STOCK WELL
43	14.23.08.144	MADE TANK	------	13-01-72	----	460	----	NMT	STOCK WELL ESTIMATED TEMPERATU.
44	15.22.09.122	RUNYON F	------	13-01-72	----	520	----	NMT	STOCK WELL; SAMPLE FROM TANK EST. TEMP.
45	17.23.30.123	HOPE VILL.	------	13-01-72	----	600	498	NMT	MUNICIPAL WELL PERF.: 498-558 FT
46	11.24.20.333	----------	------	12-01-72	----	----	----	NMT	SHALLOW AQUIFER NO CONFINEMENT

1. SAMPLES AND WELL DATA
(CONTINUED-1)

NO	LOCATION	NAME	RA-NO.	DATE	S.L.	w.D.	C.D.	SOURCE	R E M A R K S
16	15.26.32.	----------	------	30-05-40	----	1000	----	HOOD	ESTIMATED TEMP.
17	16.25.03.114	----------	------	21-05-28	----	841	----	HOOD	
18	16.25.03.114	----------	------	08-02-39	----	841	----	HOOD	ESTIMATED TEMP.
19	16.26.33.211	COLEMAN R.	------	07-06-57	----	1168	----	HOOD	ESTIMATED TEMP.
20	16.26.35.113A	FULTON	------	30-04-57	----	1238	1012	HOOD	
21	17.26.08.442	ARTESIA C.	------	10-05-51	----	----	----	HOOD	ESTIMATED TEMP.
22	17.26.10.433	SULLIVAN D	------	21-05-28	----	1007	----	HOOD	
23	17.26.10.433	SULLIVAN D	------	14-03-40	----	1007	----	HOOD	REPEAT ANALYSIS
24	17.26.14.133	----------	------	22-07-40	----	961	----	HOOD	ESTIMATED TEMP.
25	17.26.21.311	----------	------	23-07-40	----	821	----	HOOD	ESTIMATED TEMP.
26	17.26.33.111	ZELERY	------	20-01-44	----	----	----	HOOD	ESTIMATED TEMP.
27	11.22.09.	WOODS HOME	------	26-10-71	----	----	----	NMT	BETWEEN WOODS WEST AND WRIGHT RANCH
28	12.23.06.214	PETERSON P	2888	26-10-71	----	----	----	NMT	
29	11.25.15.343	OASIS 1	1102	26-10-71	----	----	----	NMT	INTRUSION OF SALINE WATER; CLARDY'S WELL
30	11.25.15.343A	OASIS 2	------	26-10-71	----	----	----	NMT	100 M W. OF OASIS 1 SALINE WATER INTR.
31	11.25.23.111	----------	62	26-10-71	----	----	----	NMT	SALINE WATER INTR.
32		ELK 2	------	26-10-71	----	----	----	NMT	SALINE WATER INTRUS.
33	11.22.18.211	WOODS-WEST	------	29-10-71	----	550+	----	NMT	LAB. PH(17 HRS) ESTIMATED TEMP.
34	11.21.01.	WHITNEY	------	29-10-71	----	----	----	NMT	LAB. PH(17 HRS)
35	11.17.22.	KIMBELL-P.	------	29-10-71	----	80	----	NMT	PICACHIO VILLAGE

2. MEASURED DATA

SAMPLE	TEMP (CC)	PH	COND	TDS	CONSTITUENTS (PPM) CA	MG	NA	CL	SO4	HCO3	SIO2
1	20.0	0.0	2950	2440	512.	86.	124.	218.	1410.	150.	16.0
2	20.0	7.90	1250	943	168.	41.	54.	58.	421.	237.	0.0
3	20.0	7.70	1460	1070	186.	60.	59.	111.	472.	224.	16.0
4	20.0	7.50	1400	1040	183.	53.	62.	96.	461.	228.	16.0
5	20.0	0.0	0	666	133.	41.	17.	22.	291.	242.	16.0
6	19.4	7.40	1070	0	0.	0.	0.	22.	385.	226.	0.0
7	21.7	0.0	0	1680	358.	91.	27.	37.	1040.	224.	0.0
8	23.3	0.0	0	836	158.	51.	16.	18.	401.	239.	0.0
9	22.0	7.80	965	715	137.	48.	6.	16.	322.	236.	0.0
10	22.0	7.15	997	754	142.	50.	0.	15.	343.	234.	0.0
11	21.7	0.0	0	690	134.	45.	12.	12.	303.	241.	0.0
12	22.0	0.0	985	764	152.	48.	0.	16.	384.	0.	0.0
13	22.0	0.0	3320	2860	634.	111.	75.	172.	1780.	126.	0.0
14	22.0	0.0	2780	2630	603.	120.	24.	31.	1730.	252.	0.0
15	22.7	7.90	2430	0	0.	0.	28.	29.	1460.	182.	0.0
16	20.0	0.0	1350	1000	197.	69.	23.	28.	576.	226.	0.0
17	18.9	0.0	0	2160	434.	137.	17.	20.	1420.	230.	0.0
18	20.0	0.0	2040	1890	418.	75.	0.	15.	1100.	0.	0.0
19	20.0	7.70	1190	0	0.	0.	0.	17.	490.	235.	0.0
20	17.8	7.20	2130	0	0.	0.	0.	48.	1140.	182.	0.0
21	20.0	7.30	1090	842	162.	43.	16.	8.	400.	240.	0.0
22	22.7	0.0	0	965	162.	67.	15.	17.	531.	156.	0.0
23	22.7	0.0	1250	1010	187.	67.	9.	17.	527.	230.	0.0
24	22.0	0.0	1120	854	152.	55.	22.	15.	481.	160.	0.0

2. MEASURED DATA

(CONTINUED-1)

SAMPLE	TEMP (CG)	PH	COND	TDS	CONSTITUENTS (PPM) CA	MG	NA	CL	SO4	HCO3	SIO2
25	22.0	0.0	981	770	130.	46.	23.	14.	382.	176.	0.0
26	22.0	0.0	1150	832	182.	54.	8.	16.	452.	242.	0.0
27	19.9	7.40	1370	0	150.	46.	62.	88.	434.	190.	19.0
28	20.3	7.10	1080	0	144.	49.	64.	41.	315.	236.	17.2
29	20.3	6.90	2090	0	192.	57.	193.	321.	410.	203.	15.5
30	20.3	7.00	2170	0	194.	54.	199.	316.	418.	199.	17.2
31	20.4	7.50	3290	0	245.	65.	406.	683.	540.	197.	17.5
32	18.3	7.85	0	0	380.	160.	2376.	0.	1420.	227.	0.2
33	20.4	7.60	1470	0	184.	54.	88.	103.	545.	195.	18.8
34	20.0	7.49	1090	0	144.	42.	37.	72.	335.	180.	19.2
35	20.0	7.03	2680	0	379.	114.	56.	135.	1280.	205.	21.0
36	20.0	7.11	2420	0	359.	108.	59.	87.	1350.	336.	24.5
37	17.5	7.35	830	0	114.	34.	22.	33.	278.	217.	19.2
38	22.1	7.17	1380	0	200.	66.	73.	13.	690.	245.	16.2
39	19.9	7.65	1850	0	151.	46.	240.	298.	480.	175.	15.4
40	21.5	7.80	975	0	141.	41.	81.	29.	470.	190.	15.0
41	18.5	7.85	660	0	87.	23.	68.	15.	257.	235.	11.2
42	19.1	7.70	1240	0	179.	45.	92.	51.	420.	397.	11.4
43	20.0	7.49	745	0	108.	29.	73.	14.	315.	245.	11.2
44	20.0	7.45	650	0	78.	22.	63.	14.	112.	354.	11.2
45	20.2	7.41	850	0	127.	28.	66.	16.	355.	223.	12.0
46	20.0	7.28	1260	0	170.	44.	103.	88.	540.	204.	12.4

3. COMPUTED DATA (CHEMICAL PROFILE)

	ANIONS (%)		CATIONS(%)	
SAMPLE	HCO3 + CO3	SO4 + CL	CA + MG	NA + K
1	6.5	93.5	85.8	14.2
2	27.2	72.8	83.3	16.7
3	22.1	77.9	84.7	15.3
4	23.3	76.7	83.3	16.7
5	37.3	62.7	93.1	6.9
6	74.2	25.8	94.3	5.7
7	13.9	86.1	95.6	4.4
8	30.7	69.3	94.6	5.4
9	35.1	64.9	97.5	2.5
10	33.6	66.4	100.0	0.0
11	37.3	62.7	95.2	4.8
12	0.0	100.0	100.0	0.0
13	4.7	95.3	92.6	7.4
14	10.1	89.9	97.5	2.5
15	8.7	91.3	0.0	100.0
16	22.5	77.5	93.9	6.1
17	11.1	88.9	97.8	2.2
18	0.0	100.0	100.0	0.0
19	12.9	87.1	55.9	44.1
20	9.4	90.6	50.2	49.8
21	31.5	68.5	94.3	5.7
22	18.1	81.9	95.4	4.6
23	24.8	75.2	97.5	2.5
24	20.1	79.9	92.7	7.3

3. COMPUTED DATA (CHEMICAL PROFILE)

(CONTINUED-1)

SAMPLE	ANIONS (%) HCO3 + CO3	ANIONS (%) SO4 + CL	CATIONS (%) CA + MG	CATIONS (%) NA + K
25	25.7	74.3	91.1	8.9
26	28.7	71.3	97.6	2.4
27	21.3	78.7	80.7	19.3
28	33.4	66.6	80.1	19.9
29	15.9	84.1	63.0	37.0
30	15.6	84.4	62.0	38.0
31	9.6	90.4	49.9	50.1
32	11.2	88.8	23.7	76.3
33	18.3	81.7	78.1	21.9
34	24.7	75.3	86.9	13.1
35	9.9	90.1	92.1	7.9
36	15.3	84.7	91.3	8.7
37	34.6	65.4	89.9	10.1
38	21.7	78.3	82.9	17.1
39	13.5	86.5	52.0	48.0
40	22.7	77.3	74.7	25.3
41	40.0	60.0	67.8	32.2
42	39.0	61.0	75.9	24.1
43	36.6	63.4	71.0	29.0
44	68.0	32.0	65.8	34.2
45	31.8	68.2	75.1	24.9
46	19.6	80.4	73.0	27.0

4. COMPUTED DATA (COMPLEXING ESTIMATES)

SAMPLE	COMPLEXED IONS (PCNT) CA	MG	SO4	HCO3
1	30.20	32.42	33.91	1.10
2	18.30	20.40	24.71	0.73
3	18.66	20.73	27.25	1.04
4	18.68	20.76	26.48	0.93
5	14.73	16.87	24.48	0.80
6	14.73	16.87	0.0	0.0
7	27.88	30.84	33.24	1.27
8	18.05	21.14	26.81	0.91
9	15.86	18.51	26.03	0.91
10	16.53	19.19	26.45	0.94
11	15.24	17.82	25.52	0.87
12	18.26	19.53	26.97	0.87
13	32.96	36.10	36.89	1.29
14	32.96	36.40	37.19	1.41
15	32.96	36.40	0.0	0.0
16	21.51	23.57	28.07	1.15
17	31.06	33.01	34.89	1.77
18	26.65	30.00	34.17	1.77
19	28.65	30.00	0.0	0.0
20	28.65	30.00	0.0	0.0
21	18.05	20.15	25.34	0.79
22	21.67	24.28	27.43	1.13
23	20.76	23.73	28.80	1.13
24	20.93	23.29	25.87	0.96

4. COMPUTED DATA (COMPLEXING ESTIMATES)

(CONTINUED-1)

SAMPLE	COMPLEXED IONS (PCNT) CA	MG	SO4	HCO3
25	18.53	20.89	24.44	0.85
26	19.12	21.89	27.98	0.95
27	18.93	20.73	23.80	0.82
28	14.84	17.03	25.62	0.93
29	15.48	17.52	26.23	0.99
30	15.79	17.81	25.95	0.93
31	16.61	18.81	26.42	1.03
32	24.26	26.57	26.91	1.90
33	21.12	23.19	25.66	0.91
34	16.01	17.77	24.63	0.80
35	30.28	32.59	32.58	1.50
36	31.88	34.65	30.73	1.37
37	14.68	16.63	21.34	0.68
38	24.42	27.42	27.14	1.03
39	18.85	20.68	21.60	0.78
40	20.87	23.20	22.55	0.71
41	14.95	16.68	17.35	0.47
42	17.30	20.06	24.93	0.79
43	16.53	18.67	19.70	0.55
44	7.36	10.46	18.01	0.48
45	17.71	19.75	20.82	0.52
46	21.54	23.48	23.37	0.74

5. COMPUTED DATA (REACTION RATIOS)

SAMPLE	LOG10 (CO2)	REACTION RATIOS (%) CALC.	ARAG.	DOLOM.	GYPS.	ANHYD.
1	0.0	0.0	0.0	0.0	82.0	48.3
2	-2.59	433.4	292.1	519.0	16.3	9.6
3	-2.42	273.7	184.5	275.0	18.4	10.8
4	-2.21	174.7	117.7	100.4	18.1	10.7
5	0.0	0.0	0.0	0.0	10.4	6.1
6	-2.09	0.0	0.0	0.0	0.0	0.0
7	0.0	0.0	0.0	0.0	51.8	31.7
8	0.0	0.0	0.0	0.0	14.5	9.2
9	-2.47	336.5	220.5	437.6	11.2	6.9
10	-1.83	76.4	50.0	22.7	12.1	7.5
11	0.0	0.0	0.0	0.0	10.6	6.5
12	0.0	0.0	0.0	0.0	14.3	8.8
13	0.0	0.0	0.0	0.0	107.9	66.6
14	0.0	0.0	0.0	0.0	102.7	63.3
15	-2.70	0.0	0.0	0.0	0.0	0.0
16	0.0	0.0	0.0	0.0	22.5	13.2
17	0.0	0.0	0.0	0.0	72.6	41.7
18	0.0	0.0	0.0	0.0	63.5	37.4
19	-2.38	0.0	0.0	0.0	0.0	0.0
20	-2.02	0.0	0.0	0.0	0.0	0.0
21	-1.98	109.4	73.8	35.9	15.5	9.1
22	0.0	0.0	0.0	0.0	18.0	11.3
23	0.0	0.0	0.0	0.0	19.9	12.5
24	0.0	0.0	0.0	0.0	16.4	10.1

5. COMPUTED DATA (REACTION RATIOS)

(CONTINUED-1)

SAMPLE	LOG10 (CO2)	REACTION RATIOS (%) CALC.	ARAG.	DOLOM.	GYPS.	ANHYD.
25	0.0	0.0	0.0	0.0	12.4	7.7
26	0.0	0.0	0.0	0.0	18.0	11.1
27	-2.18	96.7	65.3	32.6	15.1	8.9
28	-1.79	63.7	42.7	15.5	11.3	6.7
29	-1.66	40.3	27.1	5.5	15.7	9.3
30	-1.77	50.1	33.6	8.0	16.2	9.6
31	-2.29	174.8	117.1	93.8	21.5	12.8
32	-2.62	423.3	292.7	925.3	50.0	28.3
33	-2.37	184.0	123.3	112.7	20.5	12.2
34	-2.29	117.2	79.0	45.5	12.2	7.2
35	-1.80	78.1	52.7	21.2	60.8	35.8
36	-1.67	142.2	95.8	69.6	60.7	35.7
37	-2.08	75.5	52.9	19.8	9.2	5.1
38	-1.84	95.7	62.6	33.4	25.2	15.6
39	-2.48	146.7	99.0	75.3	15.1	8.9
40	-2.37	153.9	101.5	76.6	15.3	9.3
41	-2.54	212.6	146.5	137.0	7.0	4.0
42	-2.17	455.6	311.2	593.4	16.6	9.6
43	-2.16	122.2	82.4	45.1	9.5	5.6
44	-1.95	137.8	92.9	59.4	3.0	1.8
45	-2.12	106.9	71.8	28.3	11.9	7.0
46	-2.04	83.6	56.3	20.6	19.4	11.4

THE FLORIDA LIMESTONE AQUIFER - COMPILATION OF PUBLISHED DATA (1970)

(SOURCES: H-B-R=HANSHAW, BACK AND RUBIN-1965,1965A,1970)

1. SAMPLES AND WELL DATA

NO	LOCATION	NAME	RA-NO.	DATE	S.L.	W.D.	C.D.	SOURCE	REMARKS
01	1	POLK CITY		15-03-62		180	40	H-B-R	1965: SIO2=0.2 PPM 1970: SIO2=12 PPM ??
02	2N	GROVELAND		13-03-62				H-B-R	
03	3N	CLERMONT		20-03-62				H-B-R	
04	4N	LEESBURG		12-03-62				H-B-R	
05	5N	WILDWOOD 2		09-03-62		82	39	H-B-R	
06	6N	BELLEVIEW		09-03-62				H-B-R	
07	7N	OCALA 3		08-03-62				H-B-R	
08	7N	OCALA 4				115	30	H-B-R	
09	2W	LAKELAND		16-03-62				H-B-R	
10	3W	PLANT CITY		11-05-62				H-B-R	
11	4W	LITHIA SP.		11-05-62				H-B-R	
12	5W	ELLENTON		10-05-62				H-B-R	
13	2F	KISSIMMEE		07-05-62				H-B-R	
14	3E	ST CLOUD		07-05-62				H-B-R	
15	4F	CHRISTMAS		07-05-62				H-B-R	SEA WATER INTRUSION

1. SAMPLES AND WELL DATA
(CONTINUED-1)

NO	LOCATION	NAME	RA-NO.	DATE	S.L.	W.D.	C.D.	SOURCE	REMARKS
16	2S	FT MEADE		14-03-62		291	127	H-B-R	
17	3S	WAUCHULA		10-05-62		245	114	H-B-R	
18	4S	ARCADIA		10-05-62		151	100	H-B-R	
19	5S	VENUS		23-03-62				H-B-R	MIXTURE WITH SEA WATER
20	6S	CLEVELAND				152	39	H-B-R	SEA WATER INTRUSION

2. MEASURED DATA

SAMPLE	TEMP (CG)	PH	CONC	TDS	CONSTITUENTS (PPM) CA	MG	NA	CL	SO4	HCO3	SIO2
1	23.8	8.00	218	138	34.	6.	3.	5.	2.	124.	12.0
2	23.7	7.80	255	148	42.	4.	4.	7.	2.	143.	11.0
3	24.7	7.89	192	112	25.	6.	5.	10.	3.	92.	11.0
4	23.6	7.62	290	172	46.	7.	6.	10.	3.	168.	15.0
5	23.8	7.59	290	158	51.	3.	5.	8.	3.	150.	10.0
6	22.9	7.59	380	248	58.	9.	5.	8.	36.	171.	11.0
7	24.9	7.50	610	420	100.	15.	8.	12.	153.	197.	11.0
8	24.5	7.50	0	420	96.	15.	8.	11.	148.	175.	10.0
9	26.3	7.62	395	238	54.	14.	7.	9.	4.	253.	18.0
10	26.3	7.62	430	238	66.	11.	12.	12.	0.	244.	24.0
11	24.5	7.79	440	266	61.	9.	12.	18.	66.	128.	15.0
12	26.2	7.58	1200	874	140.	68.	19.	25.	458.	178.	22.0
13	24.9	8.10	228	115	33.	2.	4.	4.	3.	116.	12.0
14	25.9	7.89	370	209	51.	8.	8.	9.	38.	155.	14.0
15	23.8	7.33	2600	1770	146.	51.	340.	620.	254.	247.	18.0
16	26.6	7.75	428	272	58.	17.	6.	9.	71.	163.	16.0
17	25.4	7.69	600	392	66.	29.	8.	10.	155.	168.	18.0
18	26.3	7.44	1000	726	106.	60.	21.	28.	344.	206.	31.0
19	30.8	7.83	1300	780	80.	44.	138.	275.	202.	108.	0.0
20	26.7	7.51	0	1600	114.	82.	283.	655.	216.	145.	18.0

3. COMPUTED DATA (CHEMICAL PROFILE)

SAMPLE	ANIONS (%) HCO3 + CO3	ANIONS (%) SO4 + CL	CATIONS (%) CA + MG	CATIONS (%) NA + K
1	92.0	8.0	93.9	6.1
2	91.5	8.5	94.0	6.0
3	81.8	18.2	88.2	11.8
4	89.0	11.0	91.6	8.4
5	89.4	10.6	93.1	6.9
6	74.2	25.8	94.3	5.7
7	47.8	52.2	94.8	5.2
8	45.8	54.2	94.7	5.3
9	92.9	7.1	92.8	7.2
10	92.2	7.8	88.9	11.1
11	52.7	47.3	87.8	12.2
12	22.2	77.8	93.8	6.2
13	91.7	8.3	91.5	8.5
14	70.9	29.1	90.5	9.5
15	15.1	84.9	43.7	56.3
16	60.7	39.3	94.2	5.8
17	44.0	56.0	94.0	6.0
18	29.8	70.2	91.8	8.2
19	12.9	87.1	55.9	44.1
20	9.4	90.6	50.2	49.8

4. COMPUTED DATA (COMPLEXING ESTIMATES)

	COMPLEXED IONS (PCNT)			
SAMPLE	CA	MG	SO4	HCO3
1	0.31	1.77	13.63	0.16
2	0.20	1.85	14.80	0.12
3	0.43	1.57	11.50	0.17
4	0.33	2.25	16.66	0.19
5	0.39	2.12	16.25	0.07
6	3.31	5.29	16.10	0.22
7	10.47	13.32	20.90	0.33
8	10.30	12.89	20.56	0.33
9	0.32	2.98	16.89	0.36
10	0.0	2.53	16.89	0.29
11	5.86	7.75	16.31	0.21
12	20.08	23.92	28.03	1.16
13	0.37	1.78	11.91	0.07
14	3.69	5.78	15.13	0.19
15	10.27	13.18	23.22	0.91
16	6.13	8.62	18.65	0.42
17	10.77	13.47	19.87	0.63
18	17.14	20.90	26.03	1.10
19	11.27	14.90	22.80	0.85
20	8.80	11.45	26.74	1.49

5. COMPUTED DATA (REACTION RATIOS)

		REACTION RATIOS (%)				
SAMPLE	LOG10 (CO2)	CALC.	ARAG.	DOLOM.	GYPS.	ANHYD.
1	-2.91	122.5	78.4	27.2	0.1	0.0
2	-2.65	107.6	69.0	12.5	0.0	0.0
3	-2.92	55.6	35.2	7.7	0.1	0.0
4	-2.40	88.6	56.9	12.6	0.1	0.0
5	-2.42	83.5	53.4	3.9	0.1	0.1
6	-2.37	95.4	61.8	14.7	1.0	0.6
7	-2.22	141.4	89.3	32.3	5.2	3.4
8	-2.27	119.6	75.9	24.2	5.0	3.2
9	-2.21	168.3	104.7	78.7	0.1	0.1
10	-2.23	197.2	122.6	69.6	0.0	0.0
11	-2.69	123.8	78.6	23.5	1.8	1.2
12	-2.35	174.2	108.4	157.5	13.8	9.4
13	-3.03	150.1	94.8	17.2	0.1	0.0
14	-2.69	177.5	110.9	49.9	0.9	0.6
15	-1.99	122.5	78.4	58.3	7.6	4.9
16	-2.53	148.4	92.0	69.5	1.7	1.2
17	-2.47	126.6	79.5	75.6	3.5	2.3
18	-2.14	119.9	74.6	86.9	8.9	6.1
19	-2.78	150.4	89.5	135.0	4.2	3.2
20	-2.38	99.8	61.8	79.2	4.9	3.4

A P P E N D I X F

GRID DATA USED FOR THE CALIBRATION OF THE ROSWELL HYDROGEOCHEMICAL MODEL

ROSWELL ISOCHRONES AND COMPUTED WATER QUALITY MAPS
****
(W.L.-1926; TRANSM.-SUMMERS 1972; BN-RABINOVITZ 1972; WATER QUALITY APP. "F")

HYDCEM/ROSWELL-FINAL CALIBRATION (AUG. 23, 1972)
****

PRINTOUT OF INPUT DATA

DX= 3.000 MILES
DY= 6.000 MILES

LEGEND

BN =EFFECTIVE THICKNESS (FT)
H =HYDRAULIC POTENTIAL (FT)
TRANSM=TRANSMISSIVITY(GPD/FT)
FKC =CALCITE RATE CONSTANT(MOLE/YR)
FKD =DOLOMITE RATE CONSTANT(MOLE/YR)
FKG =GYPSUM RATE CONSTANT(MOLE/YR)
CL =CHLORIDE CONTENT(PPM)
NA =SODIUM CONTENT(PPM)
PCO2 =-LOG10(CO2)
TEMP =TEMPERATURE(CG)

PRINTOUT OF INPUT DATA (CONTN-D)

I	J	H	TRANSM.	BN	PCO2	TEMP	CL	NA	FKC	FKD	FKG
1	1	3680.0	0.0	2.0	0.0	0.0	0.	0.	0.4000E-03	0.4500E-04	0.5850E-04
2	1	3645.0	0.0	2.0	0.0	0.0	0.	0.	0.4000E-03	0.4500E-04	0.5850E-04
3	1	3610.0	0.0	2.0	0.0	0.0	0.	0.	0.4000E-03	0.4500E-04	0.5850E-04
4	1	3575.0	0.0	2.0	0.0	0.0	0.	0.	0.4000E-03	0.4500E-04	0.5850E-04
5	1	3525.0	0.0	2.0	0.0	0.0	0.	0.	0.4000E-03	0.4500E-04	0.5850E-04
6	1	3472.0	0.0	2.0	0.0	0.0	0.	0.	0.4000E-03	0.4500E-04	0.5850E-04
7	1	3432.0	0.0	2.0	0.0	0.0	0.	0.	0.4000E-03	0.4500E-04	0.5850E-04
8	1	3415.0	0.0	2.0	0.0	0.0	0.	0.	0.4000E-03	0.4500E-04	0.5850E-04
9	1	3392.0	0.0	2.0	0.0	0.0	0.	0.	0.4000E-03	0.4500E-04	0.5850E-04
10	1	3365.0	0.0	2.0	0.0	0.0	0.	0.	0.4000E-03	0.4500E-04	0.5850E-04
11	1	3340.0	0.0	2.0	0.0	0.0	0.	0.	0.4000E-03	0.4500E-04	0.5850E-04
12	1	3315.0	0.0	2.0	0.0	0.0	0.	0.	0.4000E-03	0.4500E-04	0.5850E-04
13	1	3290.0	0.0	2.0	0.0	0.0	0.	0.	0.4000E-03	0.4500E-04	0.5850E-04
1	2	3680.0	0.1000E 05	2.0	2.20	20.0	15.	70.	0.4000E-03	0.4500E-04	0.5850E-04
2	2	3645.0	0.1000E 05	2.0	2.20	20.0	15.	70.	0.4000E-03	0.4500E-04	0.5850E-04
3	2	3610.0	0.1000E 05	2.0	2.15	20.0	15.	70.	0.4000E-03	0.4500E-04	0.5850E-04
4	2	3575.0	0.1000E 05	2.0	2.10	20.0	15.	70.	0.4000E-03	0.4500E-04	0.5850E-04
5	2	3525.0	0.1000E 06	2.0	2.00	20.0	15.	70.	0.4000E-03	0.4500E-04	0.5850E-04
6	2	3472.0	0.5000E 05	2.0	2.30	20.0	15.	70.	0.4000E-03	0.4500E-04	0.5850E-04
7	2	3432.0	0.5000E 05	2.0	1.90	20.0	15.	70.	0.4000E-03	0.4500E-04	0.5850E-04
8	2	3415.0	0.1000E 05	2.0	1.90	20.0	15.	75.	0.4000E-03	0.4500E-04	0.5850E-04
9	2	3392.0	0.5000E 04	2.0	1.85	22.1	15.	75.	0.4000E-03	0.4500E-04	0.5850E-04
10	2	3365.0	0.3000E 04	2.0	1.85	22.0	15.	75.	0.4000E-03	0.4500E-04	0.5850E-04
11	2	3340.0	0.2000E 04	2.0	1.80	22.0	15.	70.	0.4000E-03	0.4500E-04	0.5850E-04
12	2	3315.0	0.1000E 04	2.0	1.78	22.0	15.	60.	0.4000E-03	0.4500E-04	0.5850E-04
13	2	3290.0	0.0	2.0	1.75	22.0	15.	60.	0.4000E-03	0.4500E-04	0.5850E-04

PRINTOUT OF INPUT DATA (CONTN-D)

I	J	H	TRANSM.	BN	PCO2	TEMP	CL	NA	FKC	FKD	FKG
1	3	3680.0	0.1000E 05	2.0	2.20	20.0	15.	70.	0.4000E-03	0.4500E-04	0.5850E-04
2	3	3645.0	0.1000E 05	2.0	2.20	20.0	15.	70.	0.4000E-03	0.4500E-04	0.5850E-04
3	3	3610.0	0.7500E 05	2.0	2.15	20.0	15.	70.	0.4000E-03	0.4500E-04	0.5850E-04
4	3	3575.0	0.1000E 06	2.0	2.10	20.0	15.	70.	0.4000E-03	0.4500E-04	0.5850E-04
5	3	3535.0	0.1000E 06	2.0	2.00	20.0	15.	70.	0.4000E-03	0.4500E-04	0.5850E-04
6	3	3485.0	0.5000E 05	2.0	1.90	20.0	15.	70.	0.4000E-03	0.4500E-04	0.5850E-04
7	3	3435.0	0.5000E 05	2.0	1.90	20.0	15.	70.	0.4000E-03	0.4500E-04	0.5850E-04
8	3	3412.0	0.1000E 05	2.0	1.90	20.0	15.	60.	0.4000E-03	0.4500E-04	0.5850E-04
9	3	3395.0	0.5000E 04	2.0	1.85	22.1	15.	60.	0.4000E-03	0.4500E-04	0.5850E-04
10	3	3382.0	0.5000E 04	2.0	1.85	22.0	15.	40.	0.4000E-03	0.4500E-04	0.5850E-04
11	3	3350.0	0.3000E 04	2.0	1.80	22.0	15.	30.	0.4000E-03	0.4500E-04	0.5850E-04
12	3	3318.0	0.2000E 04	2.0	1.78	22.0	15.	30.	0.4000E-03	0.4500E-04	0.5850E-04
13	3	3288.0	0.0	2.0	1.75	22.0	15.	30.	0.4000E-03	0.4500E-04	0.5850E-04
1	4	3665.0	0.1000E 05	2.0	2.20	20.0	15.	65.	0.4000E-03	0.4500E-04	0.5850E-04
2	4	3640.0	0.7500E 05	2.0	2.20	20.1	5.	65.	0.4000E-03	0.4500E-04	0.5850E-04
3	4	3615.0	0.1200E 06	2.0	2.10	20.0	15.	70.	0.4000E-03	0.4500E-04	0.5850E-04
4	4	3590.0	0.1200E 06	2.0	2.00	20.0	15.	70.	0.4000E-03	0.4500E-04	0.5850E-04
5	4	3575.0	0.1500E 06	2.0	2.15	20.0	15.	70.	0.4000E-03	0.4500E-04	0.5850E-04
6	4	3535.0	0.1500E 06	2.0	2.15	20.0	15.	60.	0.4000E-03	0.4500E-04	0.5850E-04
7	4	3475.0	0.1500E 06	2.0	1.95	20.0	15.	30.	0.4000E-03	0.4500E-04	0.5850E-04
8	4	3425.0	0.1500E 06	2.0	1.90	20.0	15.	40.	0.4000E-03	0.4500E-04	0.5850E-04
9	4	3405.0	0.1500E 06	2.0	1.90	20.0	15.	30.	0.4000E-03	0.4500E-04	0.5850E-04
10	4	3385.0	0.1500E 06	2.0	1.80	20.0	25.	30.	0.4000E-03	0.4500E-04	0.5850E-04
11	4	3355.0	0.1000E 05	2.0	1.80	21.0	75.	50.	0.4000E-03	0.4500E-04	0.5850E-04
12	4	3325.0	0.5000E 04	2.0	1.80	22.0	172.	75.	0.4000E-03	0.4500E-04	0.5850E-04
13	4	3295.0	0.0	2.0	1.80	22.0	172.	75.	0.4000E-03	0.4500E-04	0.5850E-04

PRINTOUT OF INPUT DATA (CONTN-D)

I	J	H	TRANSM.	BN	PCO2	TEMP	CL	NA	FKC	FKD	FKG
1	5	3650.0	0.5000E 05	2.0	2.20	20.0	15.	70.	0.4000E-03	0.4500E-04	0.5850E-04
2	5	3635.0	0.1000E 06	2.0	2.20	20.0	15.	70.	0.4000E-03	0.4500E-04	0.5850E-04
3	5	3620.0	0.1300E 06	2.0	2.15	20.0	15.	70.	0.4000E-03	0.4500E-04	0.5850E-04
4	5	3605.0	0.1300E 06	2.0	2.10	20.0	15.	70.	0.4000E-03	0.4500E-04	0.5850E-04
5	5	3595.0	0.1300E 06	2.0	2.05	20.0	15.	50.	0.4000E-03	0.4500E-04	0.5850E-04
6	5	3582.0	0.1000E 06	2.0	2.00	20.0	15.	40.	0.4000E-03	0.4500E-04	0.5850E-04
7	5	3537.0	0.1000E 06	2.0	1.90	20.0	15.	30.	0.4000E-03	0.4500E-04	0.5850E-04
8	5	3467.0	0.1000E 06	2.0	1.80	20.0	15.	25.	0.4000E-03	0.4500E-04	0.5850E-04
9	5	3422.0	0.2500E 05	2.0	1.85	20.1	5.	15.	0.4000E-03	0.4500E-04	0.5850E-04
10	5	3395.0	0.1500E 05	2.0	1.80	20.0	25.	15.	0.4000E-03	0.4500E-04	0.5850E-04
11	5	3375.0	0.1000E 04	2.0	1.80	22.0	50.	25.	0.4000E-03	0.4500E-04	0.5850E-04
12	5	3355.0	0.1000E 04	2.0	1.80	22.0	60.	30.	0.4000E-03	0.4500E-04	0.5850E-04
13	5	3335.0	0.0	2.0	1.80	22.0	150.	70.	0.4000E-03	0.4500E-04	0.5850E-04
1	6	3650.0	0.1000E 06	2.0	2.25	20.0	15.	70.	0.4000E-03	0.4500E-04	0.5850E-04
2	6	3640.0	0.1500E 06	2.0	2.00	20.0	15.	70.	0.4000E-03	0.4500E-04	0.5850E-04
3	6	3630.0	0.1500E 06	2.0	2.00	20.0	15.	70.	0.4000E-03	0.4500E-04	0.5850E-04
4	6	3620.0	0.1500E 06	2.0	2.00	20.0	15.	70.	0.4000E-03	0.4500E-04	0.5850E-04
5	6	3603.0	0.1500E 06	2.0	2.15	20.0	15.	70.	0.4000E-03	0.4500E-04	0.5850E-04
6	6	3581.0	0.1000E 06	2.0	2.10	20.0	15.	50.	0.4000E-03	0.4500E-04	0.5850E-04
7	6	3550.0	0.1000E 06	2.0	2.00	20.0	15.	45.	0.4000E-03	0.4500E-04	0.5850E-04
8	6	3507.0	0.1000E 06	2.0	2.00	20.0	15.	40.	0.4000E-03	0.4500E-04	0.5850E-04
9	6	3462.0	0.5000E 05	2.0	1.90	20.0	15.	30.	0.4000E-03	0.4500E-04	0.5850E-04
10	6	3420.0	0.2500E 05	2.0	1.80	22.5	20.	30.	0.4000E-03	0.4500E-04	0.5850E-04
11	6	3392.0	0.1000E 05	2.0	1.80	22.3	0.	50.	0.4000E-03	0.4500E-04	0.5850E-04
12	6	3364.0	0.5000E 04	2.0	1.80	22.0	100.	60.	0.4000E-03	0.4500E-04	0.5850E-04
13	6	3336.0	0.0	2.0	1.80	22.0	150.	70.	0.4000E-03	0.4500E-04	0.5850E-04

PRINTOUT OF INPUT DATA (CONTN-D)

I	J	H	TRANSM.	BN	PCO2	TEMP	CL	NA	FKC	FKD	FKG
1	7	3740.0	0.1500E 06	2.0	2.50	19.5	15.	65.	0.4000E-03	0.4500E-04	0.5850E-04
2	7	3705.0	0.1500E 06	2.0	2.40	20.0	15.	68.	0.4000E-03	0.4500E-04	0.5850E-04
3	7	3670.0	0.2000E 06	2.0	2.00	20.0	15.	70.	0.4000E-03	0.4500E-04	0.5850E-04
4	7	3625.0	0.3500E 06	2.0	2.00	20.0	15.	70.	0.4000E-03	0.4500E-04	0.5850E-04
5	7	3605.0	0.4000E 06	2.0	2.10	20.0	15.	70.	0.4000E-03	0.4500E-04	0.5850E-04
6	7	3582.0	0.4000E 06	2.0	2.15	20.0	15.	60.	0.4000E-03	0.4500E-04	0.5850E-04
7	7	3557.0	0.2500E 06	2.0	2.05	20.0	15.	50.	0.4000E-03	0.4500E-04	0.5850E-04
8	7	3532.0	0.1000E 06	2.0	2.00	20.0	15.	40.	0.4000E-03	0.4500E-04	0.5850E-04
9	7	3515.0	0.2500E 05	2.0	1.90	20.0	15.	30.	0.4000E-03	0.4500E-04	0.5850E-04
10	7	3482.0	0.1000E 05	2.0	1.80	20.0	25.	30.	0.4000E-03	0.4500E-04	0.5850E-04
11	7	3440.0	0.2500E 04	2.0	1.80	21.0	75.	50.	0.4000E-03	0.4500E-04	0.5850E-04
12	7	3402.0	0.2500E 04	2.0	1.80	22.0	172.	75.	0.4000E-03	0.4500E-04	0.5850E-04
13	7	3364.0	0.0	2.0	1.80	22.0	172.	75.	0.4000E-03	0.4500E-04	0.5850E-04
1	8	3800.0	0.1000E 06	2.0	2.60	18.0	15.	68.	0.4000E-03	0.4500E-04	0.5850E-04
2	8	3750.0	0.2500E 06	2.0	2.55	18.5	15.	68.	0.4000E-03	0.4500E-04	0.5850E-04
3	8	3700.0	0.5000E 06	2.0	2.50	18.7	15.	70.	0.4000E-03	0.4500E-04	0.5850E-04
4	8	3650.0	0.7500E 06	2.0	2.40	19.0	15.	70.	0.4000E-03	0.4500E-04	0.5850E-04
5	8	3615.0	0.8000E 06	2.0	2.15	20.0	15.	70.	0.4000E-03	0.4500E-04	0.5850E-04
6	8	3603.0	0.7500E 06	2.0	2.10	20.0	15.	60.	0.4000E-03	0.4500E-04	0.5850E-04
7	8	3592.0	0.6500E 06	2.0	2.00	20.0	15.	50.	0.4000E-03	0.4500E-04	0.5850E-04
8	8	3557.0	0.3000E 06	2.0	1.95	20.0	15.	40.	0.4000E-03	0.4500E-04	0.5850E-04
9	8	3545.0	0.2000E 06	2.0	1.90	21.7	15.	30.	0.4000E-03	0.4500E-04	0.5850E-04
10	8	3515.0	0.2500E 05	2.0	1.80	22.5	15.	30.	0.4000E-03	0.4500E-04	0.5850E-04
11	8	3490.0	0.1000E 05	2.0	1.80	22.2	5.	50.	0.4000E-03	0.4500E-04	0.5850E-04
12	8	3465.0	0.2500E 04	2.0	1.80	22.0	50.	75.	0.4000E-03	0.4500E-04	0.5850E-04
13	8	3440.0	0.0	2.0	1.80	22.0	60.	50.	0.4000E-03	0.4500E-04	0.5850E-04

PRINTOUT OF INPUT DATA (CONTN-D)

I	J	H	TRANSM.	BN	PCO2	TEMP	CL	NA	FKC	FKD	FKG
1	9	3644.0	0.1000E 06	2.0	2.50	19.0	30.	65.	0.4000E-03	0.4500E-04	0.5850E-04
2	9	3632.0	0.3500E 06	2.0	2.50	19.0	30.	65.	0.4000E-03	0.4500E-04	0.5850E-04
3	9	3620.0	0.7000E 06	2.0	2.25	19.0	30.	65.	0.4000E-03	0.4500E-04	0.5850E-04
4	9	3608.0	0.1000E 07	2.0	2.00	19.0	30.	65.	0.4000E-03	0.4500E-04	0.5850E-04
5	9	3597.0	0.1000E 07	2.0	1.85	20.0	40.	60.	0.4000E-03	0.4500E-04	0.5850E-04
6	9	3585.0	0.1000E 07	2.0	1.85	20.0	35.	50.	0.4000E-03	0.4500E-04	0.5850E-04
7	9	3575.0	0.1000E 07	2.0	1.80	20.0	30.	40.	0.4000E-03	0.4500E-04	0.5850E-04
8	9	3563.0	0.1500E 07	2.0	1.80	20.0	25.	40.	0.4000E-03	0.4500E-04	0.5850E-04
9	9	3547.0	0.1000E 07	2.0	1.75	20.5	25.	30.	0.4000E-03	0.4500E-04	0.5850E-04
10	9	3530.0	0.5000E 06	2.0	1.70	22.0	20.	25.	0.4000E-03	0.4500E-04	0.5850E-04
11	9	3510.0	0.1000E 06	2.0	1.70	23.0	20.	30.	0.4000E-03	0.4500E-04	0.5850E-04
12	9	3490.0	0.1000E 05	2.0	1.70	23.0	20.	40.	0.4000E-03	0.4500E-04	0.5850E-04
13	9	3470.0	0.0	2.0	1.70	23.0	20.	40.	0.4000E-03	0.4500E-04	0.5850E-04
1	10	3646.0	0.2500E 06	2.0	2.50	20.0	70.	50.	0.4000E-03	0.4500E-04	0.5850E-04
2	10	3628.0	0.4300E 06	2.0	2.40	20.0	70.	75.	0.4000E-03	0.4500E-04	0.5850E-04
3	10	3610.0	0.7500E 06	2.0	2.20	19.0	70.	80.	0.4000E-03	0.4500E-04	0.5850E-04
4	10	3592.0	0.1000E 07	2.0	2.10	19.5	60.	80.	0.4000E-03	0.4500E-04	0.5850E-04
5	10	3587.0	0.1000E 07	2.0	1.85	20.0	60.	60.	0.4000E-03	0.4500E-04	0.5850E-04
6	10	3578.0	0.1000E 07	2.0	1.80	20.0	60.	50.	0.4000E-03	0.4500E-04	0.5850E-04
7	10	3571.0	0.1500E 07	2.0	1.80	20.0	50.	40.	0.4000E-03	0.4500E-04	0.5850E-04
8	10	3565.0	0.2000E 07	2.0	1.80	20.0	40.	30.	0.4000E-03	0.4500E-04	0.5850E-04
9	10	3557.0	0.2000E 07	2.0	1.75	20.0	30.	25.	0.4000E-03	0.4500E-04	0.5850E-04
10	10	3545.0	0.1500E 07	2.0	1.65	20.0	25.	15.	0.4000E-03	0.4500E-04	0.5850E-04
11	10	3535.0	0.2000E 06	2.0	1.65	20.5	20.	25.	0.4000E-03	0.4500E-04	0.5850E-04
12	10	3525.0	0.1000E 06	2.0	1.65	21.0	20.	30.	0.4000E-03	0.4500E-04	0.5850E-04
13	10	3515.0	0.0	2.0	1.65	21.0	20.	30.	0.4000E-03	0.4500E-04	0.5850E-04

PRINTOUT OF INPUT DATA (CONTN-D)

I	J	H	TRANSM.	BN	PCO2	TEMP	CL	NA	FKC	FKD	FKG
1	11	3614.0	0.2500E 06	2.0	2.50	20.0	30.	75.	0.4000E-03	0.4500E-04	0.5850E-04
2	11	3607.0	0.4500E 06	2.0	2.40	21.0	30.	80.	0.4000E-03	0.4500E-04	0.5850E-04
3	11	3600.0	0.7500E 06	2.0	2.20	20.0	80.	80.	0.4000E-03	0.4500E-04	0.5850E-04
4	11	3592.0	0.1000E 07	2.0	2.20	20.0	150.	90.	0.4000E-03	0.4500E-04	0.5850E-04
5	11	3585.0	0.1000E 07	2.0	2.40	20.0	150.	100.	0.4000E-03	0.4500E-04	0.5850E-04
6	11	3580.0	0.1000E 07	2.0	2.20	20.0	150.	80.	0.4000E-03	0.4500E-04	0.5850E-04
7	11	3573.0	0.1000E 07	2.0	2.05	20.0	120.	60.	0.4000E-03	0.4500E-04	0.5850E-04
8	11	3557.0	0.1500E 07	2.0	2.00	20.0	80.	50.	0.4000E-03	0.4500E-04	0.5850E-04
9	11	3550.0	0.1250E 07	2.0	1.85	20.0	50.	40.	0.4000E-03	0.4500E-04	0.5850E-04
10	11	3540.0	0.1000E 07	2.0	1.75	20.0	40.	30.	0.4000E-03	0.4500E-04	0.5850E-04
11	11	3532.0	0.2000E 06	2.0	1.70	20.0	30.	40.	0.4000E-03	0.4500E-04	0.5850E-04
12	11	3524.0	0.1000E 06	2.0	1.70	20.0	30.	40.	0.4000E-03	0.4500E-04	0.5850E-04
13	11	3516.0	0.0	2.0	1.70	20.0	30.	40.	0.4000E-03	0.4500E-04	0.5850E-04
1	12	3614.0	0.2500E 06	2.0	2.60	20.0	30.	100.	0.4000E-03	0.4500E-04	0.5850E-04
2	12	3606.0	0.4500E 06	2.0	2.60	21.0	50.	100.	0.4000E-03	0.4500E-04	0.5850E-04
3	12	3598.0	0.8000E 06	2.0	2.50	20.0	100.	100.	0.4000E-03	0.4500E-04	0.5850E-04
4	12	3590.0	0.1000E 07	2.0	2.50	20.0	200.	150.	0.4000E-03	0.4500E-04	0.5850E-04
5	12	3583.0	0.1000E 07	2.0	2.50	20.0	250.	150.	0.4000E-03	0.4500E-04	0.5850E-04
6	12	3577.0	0.1000E 07	2.0	2.50	20.0	250.	150.	0.4000E-03	0.4500E-04	0.5850E-04
7	12	3570.0	0.1000E 07	2.0	2.40	20.0	200.	100.	0.4000E-03	0.4500E-04	0.5850E-04
8	12	3555.0	0.1000E 07	2.0	2.30	20.0	150.	75.	0.4000E-03	0.4500E-04	0.5850E-04
9	12	3548.0	0.8500E 06	2.0	2.00	20.0	80.	60.	0.4000E-03	0.4500E-04	0.5850E-04
10	12	3535.0	0.6000E 06	2.0	2.00	20.0	50.	50.	0.4000E-03	0.4500E-04	0.5850E-04
11	12	3525.0	0.1500E 06	2.0	2.00	20.0	40.	50.	0.4000E-03	0.4500E-04	0.5850E-04
12	12	3515.0	0.5000E 05	2.0	1.90	20.0	30.	50.	0.4000E-03	0.4500E-04	0.5850E-04
13	12	3505.0	0.0	2.0	1.90	20.0	30.	50.	0.4000E-03	0.4500E-04	0.5850E-04

PRINTOUT OF INPUT DATA (CONTN-D)

I	J	H	TRANSM.	BN	PCO2	TEMP	CL	NA	FKC	FKD	FKG
1	13	3614.0	0.0	2.0	0.0	0.0	0.	0.	0.4000E-03	0.4500E-04	0.5850E-04
2	13	3606.0	0.0	2.0	0.0	0.0	0.	0.	0.4000E-03	0.4500E-04	0.5850E-04
3	13	3598.0	0.0	2.0	0.0	0.0	0.	0.	0.4000E-03	0.4500E-04	0.5850E-04
4	13	3590.0	0.0	2.0	0.0	0.0	0.	0.	0.4000E-03	0.4500E-04	0.5850E-04
5	13	3583.0	0.0	2.0	0.0	0.0	0.	0.	0.4000E-03	0.4500E-04	0.5850E-04
6	13	3577.0	0.0	2.0	0.0	0.0	0.	0.	0.4000E-03	0.4500E-04	0.5850E-04
7	13	3590.0	0.0	2.0	0.0	0.0	0.	0.	0.4000E-03	0.4500E-04	0.5850E-04
8	13	3555.0	0.0	2.0	0.0	0.0	0.	0.	0.4000E-03	0.4500E-04	0.5850E-04
9	13	3548.0	0.0	2.0	0.0	0.0	0.	0.	0.4000E-03	0.4500E-04	0.5850E-04
10	13	3535.0	0.0	2.0	0.0	0.0	0.	0.	0.4000E-03	0.4500E-04	0.5850E-04
11	13	3525.0	0.0	2.0	0.0	0.0	0.	0.	0.4000E-03	0.4500E-04	0.5850E-04
12	13	3515.0	0.0	2.0	0.0	0.0	0.	0.	0.4000E-03	0.4500E-04	0.5850E-04
13	13	3505.0	0.0	2.0	0.0	0.0	0.	0.	0.4000E-03	0.4500E-04	0.5850E-04

APPENDIX G - COMPUTER PROGRAMS

The following programs have been prepared, and applied here, as a tool for laboratory and field hydrogeochemical studies. The printout of programs and subroutines, listed below, is available on request from the: Geoscience Dept., New Mexico Institute of Mining & Technology, Socorro, N.M. 87801.

1. FILDAT

   Purpose: Compilation, and preliminary evaluation of field data.

   Subroutine Package: EQCON1, BETA, COMLX1, ACTCF2

2. CARMOD-B

   Purpose: Determination of concentration-time relationships with respect to calcium, magnesium, sulphate, bicarbonate, and hydrogen ions in carbonate aquifers. This program can be used also for determining the dissolution rate constant of calcite, dolomite, and gypsum, from available field data. The field rate constants can be determined here for both chemically and transport controlled processes.

   Subroutine Package: COMLX1, ACTCF2, SINTG2, BETA1, PPMOL, CONML1, EQCON2, FIELD, SATCON, DISTRD

3. HYDCEM

   Purpose: Integrated simulation of both hydrological and geochemical processes in a given carbonate aquifer. For a given set of hydrological and geochemical data, the program computes and plots the maps of groundwater residence-time and groundwater quality. The resulted water quality maps represents the steady-state, non-

equilibrium distribution of aqueous species in the aquifer. In this program, only a chemically-controlled dissolution is considered. The comparison between computed and measured groundwater quality data, enables the calibration of either geochemical constants, hydrological parameters, or both.

Subroutine Package: WELOC, LINEZ, PGOUT, PMOVE, PLOC, BALANC, CARMOD, BETA1, PPMOL, COMNL2, EQCON2, SINTG3, COMLX1, ACTCF2.

4. KEQ

Purpose: Evaluation of equilibrium constants as a function of temperature. Computations are based on the acceptable, or experimental, equilibrium constant for certain reference temperature, and related thermochemical properties of both reactants and products.

5. CALDIS

Purpose: Determination of the distribution of species in aqueous solution as a function of the equilibrium ratio with respect to a dissolving calcite mineral. Two boundary conditions, with respect to the CO_2 gaseous phase are considered: (i) Constant CO_2 partial pressure. (ii) The distilled water solution is equilibrated initially with a given external CO_2 partial pressure, and then closed immediately after introducing the calcite.

Subroutine Package: ACTCF, EQCON, CONMOL, DISTRA, DISTRB, DISTRC.

6. SCEL1

Purpose: Evaluation of laboratory stagnant dissolution experiments of calcite, gypsum, and calcite + gypsum, under variable temperature and CO_2 pressure. Rate constants, for both chemically and transport controlled dissolution reactions, can be

determined by scanning for the minimum deviation between observed and computed concentrations.

Subroutine Package: CONML1, EQCON2, PPMOL, BETA1, ACTCF1, COMPLX, SINTG1, SATCON

7. SCELEX

Purpose: Evaluation of laboratory dissolution experiments, both flow and stagnant, of calcite. Observed reaction ratios are compared to theoretical curves, based on the $\beta(t)$ approximation. The program compares also experimental results with the parabolic and logarithmic rate laws. Rate constants can be determined by scanning for the minimum deviation between observed and computed data.

REFERENCES CITED

Bachmat, Y. and J. Bear (1964), The general equation of dispersion in homogeneous, isotropic porous mediums, JGR 69, pp. 2561-2567.

Back, W. and B. B. Hanshaw (1965), Chemical geohydrology, in Advances in Hydroscience, Vol. 2, edited by van te Chow, Academic Press.

Back, W. and B. B. Hanshaw (1970), Comparison of chemical hydrology of the carbonate peninsulas of Florida and Yucatan, Jour. of Hydrology, 10, pp. 330-368.

Back, W. and B. B. Hanshaw (1971), Rates of physical and chemical processes in carbonate aquifers, preprint.

Barnes, I. and W. Back (1964), Dolomite solubility in groundwater, Art. 160 in U.S.G.S. Prof. Paper 475-D, pp. D179-D180.

Bear, J. and D. K. Todd (1960), The transition zone between fresh and salt waters in coastal aquifers, Contr. #29, WRC, Univ. of California at Berkeley, 156 p.

Bear, J. (1965), Hydrodynamic dispersion, Lectures delivered during a summer program at the Princeton Univ., Aug. 1965, Technion-Israel Institute of Technology, Haifa, Israel, 112 p.

Bear, J. (1971), Dynamics of Fluids in Porous Media (Draft).

Benson, S. W. (1968), Thermochemical Kinetics, John Wiley & Sons Inc., 223 p.

Buttlar, Haro von (1959), Groundwater studies in New Mexico using tritium as a tracer, JGR 64, pp. 1031-1038.

Carnahan, B., H. A. Luther and J. O. Wilkes (1969), Applied Numerical Methods, John Wiley & Sons Inc., 604 p.

Conte, S. D. (1965), Elementary Numerical Analysis, McGraw-Hill, 278 p.

Day, P. R. (1956), Dispersion of a moving salt boundary advancing through a saturated sand, Trans. Am. Geoph. Union, 37, pp. 591-601.

de Josselin de Jong, G. (1958), Longitudinal and transverse diffusion in granular deposits, Trans. AGU, 39, pp. 67-74.

Deju, R., R. B. Bhappu and C. E. Jacob (1969), A kinetic study of flow through porous media, ASME 98th Ann. meeting (abstract).

Deju, R. A. (1971), A model of chemical weathering of silicates, Geol. Soc. of Amer. Bull., 82, pp. 1055-1062.

Denbigh, K. (1955), The Principles of Chemical Equilibrium, Cambridge University Press, 491 p.

Feely, H. W. (1961), The potential application of radioisotope technology to water resources investigations and utilization, AEC Contract AT(30-1)-2477, Isotope Inc., Westwood, N. J.

Frank-Kamenitskii, D. A. (1955), Diffusion and Heat Exchange in Chemical Kinetics, (Translated from Russian), Princeton Univ. Press, 370 p.

Gardiner, W. C., Jr. (1969), Rates and Mechanisms of Chemical Reactions, W. A. Benjamin Inc., 284 p.

Garrels, R. M. and C. L. Christ (1965), Solutions, Minerals, and Equilibria, Harper & Row, 450 p.

Garrels, R. M., R. M. Dreyer and A. L. Howland (1949), Diffusion of ions through intergranular spaces in water-saturated rocks, Bull. Geol. Soc. of Amer., 60, pp. 1809-1828.

Garrels, R. M. and M. E. Thompson (1962), A chemical model of sea water at 25°C and one atmosphere total pressure, Am. J. Sci., 260, pp. 57-66.

Gat, R. J., E. Mazor and A. Mercado (1971), The application of tracer techniques and geochemical methods in groundwater hydrology, draft of Ch. 6 in "Evaluation and management of groundwater resources", edited by J. Bear.

Gisser, M. and A. Mercado (1972), An integration of the agricultural demand function for water and the hydrological model of the Pecos basin, Southeastern New Mexico, accepted for publication by Water Resources Research.

Golterman, H. L. (1969), Methods for Chemical Analysis of Fresh Waters, IBP Handbook No. 8, Blackwell Scientific Publ., 172 p.

Gross, G. W. (1972), Personal communication.

Halevy, E. and A. Nir (1962), The determination of aquifer parameters with the aid of radioactive tracers, JGR 67, pp. 2403-2409.

Hanshaw, B. B., W. Back and M. Rubin (1965a), Carbonate equilibria and radioacrbon distribution related to groundwater flow in the Florida limestone aquifer, IASH, Proc. of the symposium of Dubrovnik (Yugoslavia).

Hanshaw, B. B., W. Back and M. Rubin (1965b), Radiocarbon determinations for estimating the groundwater flow velocities in central Florida, Science, 148, pp. 494-495.

Hanshaw, B. B., W. Back, M. Rubin and R. W. Wait (1965c), Relation of carbon-14 concentration to saline water contamination of coastal aquifers, Water Resources Res., 1, pp. 109-114.

Hanshaw, B. B., M. Rubin, W. Back and I. Friedman (1967), Radiocarbon determination applied to groundwater hydrology, Isotope Techniques in the Hydrological Cycle, AGU, Geoph. Monograph Series #11, pp. 117-118.

Hantush, M. S. (1955), Preliminary quantitative study of the Roswell groundwater reservoir, N. M. Tech, Socorro, N. M., 118 p.

Helgeson, H. C. (1967), Solutions chemistry and metamorphism, in Researches in Geochemistry, edited by P. H. Ableson, Vol. II, John-Wiley, pp. 362-404.

Helgeson, H. C. (1968), Evaluation of irreversible reactions in geochemical processes involving minerals and aqueous solutions-(I) Thermodynamic relations, Geoch. Cosmoch. Acta, 32, pp. 853-877.

Helgeson, H. C. (1969), Thermodynamics of hydrothermal systems at elevated pressures and temperatures, Amer. J. of Sci., 267, pp. 729-804.

Helgeson, H. C., R. M. Garrels and F. T. Mckenzie (1969), Evaluation of irreversible reactions in geochemical processes involving minerals and aqueous solutions-(II) Applications, Geoch. Cosmoch. Acta, 33, pp. 455-481.

Helgeson, H. C. (1970), Reaction rates in hydrothermal flow systems, Econ. Geol., 65, pp. 293-303.

Helgeson, H. C., T. H. Brown, A. Nigrini and T. A. Jones (1970), Calculation of mass-transfer in geochemical processes involving aqueous solutions, Geoch. Cosmoch. Acta, 34, pp. 569-592.

Helgeson, H. C. (1971), Kinetics of mass-transfer among silicates and aqueous solutions, Geoch. Cosmoch. Acta, 35, pp. 421-469.

Hem, J. D. (1970), Study and Interpretation of the Chemical Characteristics of Natural Water, U.S.G.S. Water Supply Paper 1473, 2nd edition, 363 p.

Henninghausen, F. H. (1970), Change of chloride content of water in response to pumping in the artesian aquifer in the Roswell-East Grand Plains area, Chaves County, New Mexico, Contr. #13, Comm. on Desert and Arid-Zones Res., Southwestern and Rocky Mountains Div., A.A.A.S.

Hood, J. W. (1963), Saline groundwater in the Roswell basin-Chaves and Eddy Counties, N.M. (1958-59), U.S.G.S. Water Supply Paper, 1593M, 46 p.

Hostetler, P. B. (1964), The degree of saturation of magnesium and calcium carbonate minerals in natural waters, IASH publ. #64, pp. 34-49.

Hsu, K. Jinghwa (1963), Solubility of dolomite and composition of Florida groundwaters, J. of Hydrology, 1, pp. 288-310.

Kelley, K. K. (1960), Contribution to the Data of Theoretical Metallurgy, (XIII)-High Temperature Heat Content, Heat Capacity, and Entropy Data for the Elements and Inorganic Compounds, U.S.B.M. Bull. 584, 232 p.

Kelley, V. C. (1971), Geology of Pecos Country, Southeastern N. M., N. M. State Bureau of Mines, Mem. #24, 75 p.

Krauskopf, K. B. (1967), Introduction to Geochemistry, McGraw-Hill, 721 p.

Langmuir, D. (1971), The geochemistry of some carbonate groundwater in central Pennsylvania, Geoch. Cosmoch. Acta, 35, pp. 1023-1045.

Lau, L. K., W. J. Kaufman and D. K. Todd (1959), Dispersion of water tracer in radial laminar flow through homogeneous porous media, Prog. Rep. No. 5, 93 p., Univ. of California, Berkeley.

McKee, Chester (1972), Personal Communication.

Mercado, A. and J. Bear (1965), Dilution of labeled water through recharge and pumping in a single well, (in Hebrew), 146 p., 40 drawings, UWSS Tech. Rep. Tahal-Water Planning for Israel, P.M. 511, Tel-Aviv, Israel.

Mercado, A. (1967), The spreading pattern of injected water in a permeability stratified aquifer, Proc. of the intern. symp, on Artificial Recharge and Related Problems, IASH Publ., No. 72, pp. 23-36.

Moelwyn-Hughes, E. A. (1947), The Kinetics of Reactions in Solutions, Oxford Univ. Press. 2nd edition, 423 p.

Morgan, J. J. (1967), Applications and limitations of thermodynamics in natural water systems, Ch. 1 in Equilibrium Concepts in Natural Systems, edited by W. Stumm, pp. 1-29, Amer. Chem. Soc.

Motts, W. S. and R. L. Cushman (1964), An appraisal of the possibilities of artificial recharge to groundwater supplies in part of the Roswell basin, N. M., U.S.G.S. Water Supply Paper 1785, 85 p.

Nalluswami, M. (1971), Numerical solution of general hydrodynamic dispersion in porous media, Ph.D. diss., Colorado State Univ., Fort Collins, 138 p.

Nernst, W. (1904), Theorie der reaktionsgeschwindigkeit in heterogenen systemen, Z. Physik. Chem., 47, pp. 52-55.

Nir, A. (1964), On the interpretation of tritium age measurements of groundwater, JGR 69, pp. 2589-2595.

Nir, A. (1965), Development of isotope methods applied to groundwater hydrology, Isotope Techniques in the Hydrological Cycle, AGU, Geoph. Monograph Series, #11, pp. 109-116.

Ogata, A. (1958), Dispersion in porous media, Ph.D. diss., Northwestern Univ., 121 p.

Ogata, A. and R. B. Banks (1961), A solution of the differential equation for longitudinal dispersion in porous media, U.S.G.S. Prof. Paper No. 411-A, 7 p.

Ogata, A. (1970), Theory of dispersion in granular media, U.S.G.S. Prof. Pager No. 411-I, 34 p.

Passioura, J. B. (1971), Hydrodynamic dispersion in aggregated media, Soil Science, 111, pp. 339-344.

Pearson, F. J. (1965), Use of $^{13}C/^{12}C$ ratio to correct ages of materials initially dilluted by limestone, Proc. of the 6th Intern. Conf. on Radiocarbon and Tritium Dating, Pullman, Washington, pp. 357-366.

Pearson, F. J. and B. B. Hanshaw (1970), Sources of dissolved carbonate species and their effects on ^{14}C dating, Proc. of the Vienna Symposium on Isotope Hydrology (IAEA), pp. 271-286.

Plummer, L. N. (1972), Rates of mineral-aqueous solution reactions, Ph.D. diss., Northwestern Univ., 144 p.

Rabinowitz, D. (1972), Personal communication.

Rankama, K. (1954), Isotope Geology, Pergamon Press, 535 p.

Reddell, D. L. (1969), Dispersion in groundwater systems, Ph.D. diss., Colorado State Univ., Fort Collins, 225 p.

Rifai, M. N. E., W. J. Kaufman and D. K. Todd (1956), Dispersion phenomena in laminar flow through porous media, Rep. No. 3, I.E.R. Series, No. 90, Univ. of California, Berkeley, 157 p.

Saleem, Z. A., and C. E. Jacob (1971), Dynamic programming model and quantitative analysis-Roswell basin, New Mexico. NMSU, WRRI, Rep. #10, 180 p.

Schoeller, H., (1962), Les Eaux Souterraines, Massio and Cie, Paris, 642 p.

Shamir, U.Y., and D. R. F. Harteman, (1967), Numerical solutions for dispersion in porous media, WWR, 3, pp. 557 - 581.

Stumm, W. J., and J. J. Morgan (1970), Aquatic Chemistry, Wiley-Interscience, 583 p.

Summers, K. (1972), Personal communication.

Sung-Tsuen, Liu, and G. H. Nancollas (1971), The kinetics of dissolution of calcium sulphate dihydrate, J. Inorg. Nucl. Chem., 33, pp 2311 - 2316.

Walas, S. M. (1959), Reaction Kinetics for Chemical Engineers, McGraw-Hill, 338 p.

Wendt, I., W. Stahl, M. Geyh and F. Fauth (1966), Model experiments for ^{14}C age determination, Proc. of the Vienna Symp. on Isotopes in Hydrology, IAEA, pp 32. - 337.

Welder, E. (1972), Personal communication.

Weyl, P.K. (1958), The solution kinetics of calcite, J. of Geol. 66, pp 163 - 176.

This dissertation is accepted on behalf of the faculty of the Institute by the following committee:

Dale K. Billings
Adviser

Richard C. Beane

Willem Bruinsma

Gerardo Wolfgang Gross

Oct. 26, 72
Date